CRANFIELD UNIVERSITY

BABA MUSA ABBAGONI

Experimental Investigations of Two-Phase Flow Measurement Using Ultrasonic Sensors

SCHOOL OF ENERGY, ENVIRONMENT AND AGRIFOOD
Oil and Gas Engineering Centre
PhD in Energy

Academic Year: 2015 - 2016

Supervisor: Professor Hoi Yeung
May 2016

i

CRANFIELD UNIVERSITY

SCHOOL OF ENERGY, ENVIRONMENT AND AGRIFOOD

Oil and Gas Engineering Centre

PhD

Academic Year 2012 - 2016

BABA MUSA ABBAGONI

Experimental Investigations of Two-Phase Flow Measurement Using Ultrasonic Sensors

Supervisor: Professor Hoi Yeung
May 2016

This thesis is submitted in partial fulfilment of the requirements for the degree of Doctor of Philosophy in Energy

ABSTRACT

This thesis presents the investigations conducted in the use of ultrasonic technology to measure two-phase flow in both horizontal and vertical pipe flows which is important for the petroleum industry. However, there are still key challenges to measure parameters of the multiphase flow accurately. Four methods of ultrasonic technologies were explored.

The Hilbert-Huang transform (HHT) was first applied to the ultrasound signals of air-water flow on horizontal flow for measurement of the parameters of the two-phase slug flow. The use of the HHT technique is sensitive enough to detect the hydrodynamics of the slug flow. The results of the experiments are compared with correlations in the literature and are in good agreement.

Next, experimental data of air-water two-phase flow under slug, elongated bubble, stratified-wavy and stratified flow regimes were used to develop an objective flow regime classification of two-phase flow using the ultrasonic Doppler sensor and artificial neural network (ANN). The classifications using the power spectral density (PSD) and discrete wavelet transform (DWT) features have accuracies of 87% and 95.6% respectively. This is considerably more promising as it uses non-invasive and non-radioactive sensors.

Moreover, ultrasonic pulse wave transducers with centre frequencies of 1MHz and 7.5MHz were used to measure two-phase flow both in horizontal and vertical flow pipes. The liquid level measurement was compared with the conductivity probes technique and agreed qualitatively. However, in the vertical with a gas volume fraction (GVF) higher than 20%, the ultrasound signals were attenuated.

Furthermore, gas-liquid and oil-water two-phase flow rates in a vertical upward flow were measured using a combination of an ultrasound Doppler sensor and gamma densitometer. The results showed that the flow gas and liquid flow rates measured are within ±10% for low void fraction tests, water-cut measurements are within ±10%, densities within ±5%, and void fractions within ±10%. These findings are good results for a relatively fast flowing multiphase flow.

Keywords: Continuous wave Ultrasound Doppler, pulse-wave ultrasound, Hilbert-Huang transform, neural network

ACKNOWLEDGEMENTS

TABLE OF CONTENTS

LIST OF FIGURES

xv

LIST OF TABLES

LIST OF EQUATIONS

LIST OF ABBREVIATIONS

ANN	Artificial Neural Network
AR	Auto Regression
ARMA	Autoregressive Moving Average
CW	Continuous Wave
DWT	Discrete Wavelet Transform
EM	Electromagnetic
ERT	Electrical Resistance Tomography
FFT	Fast Fourier Transform
GVF	Gas Volume Fraction
ICA	Internal Carotid Arterial
IEEE	Institute of Electrical and Electronics Engineers
MAE	Mean Averaged Error
MATLAB	Matrix Laboratory (A Software for Computing)
MFM	Multiphase Flow Meter
MLPNN	Multilayer Perceptron Neural Networks
MSE	Mean Squared Error
NI	National Instrument
NN	Neural Networks
OA	Ophthalmic Arterial
PC	Personal Computer
PDF	Probability Density Function
PRF	Pulse Repetition Frequency
PSD	Power Spectral Density
PVC	Polyvinylchloride (A Pipe Material)
PW	Pulsed Wave
R	Linear Correlation Coefficient
RF	Radio Frequency
US	Ultrasonic Sensor
UTDC	Ultrasonic Time-Domain Cross-Correlation
Z	Acoustic Impedance

NOMENCLATURE

Symbol	Description
A_G	Cross-sectional area occupied by the gas
A_L	Cross-sectional area occupied by the liquid
C_W	Sound velocity in water
E_L	Average liquid holdup in pipe
E_{LS}	Liquid holdup in the slug body
H_{LLS}	Liquid holdup in the slug body
H_{LTB}	Liquid holdup in film
L_F	Liquid film length
L_S	Liquid slug length
L_U	Liquid slug unit
P_x	Power spectral density
Q_G	Volumetric gas flow rate
Q_L	Volumetric liquid flow rate
R_τ	Autocorrelation function.
U_g	Weighted mean drift velocity.
V_{LLS}	Liquid velocity in slug body
V_M	Mixture velocity (sum of superficial velocities)
V_{SG}	Superficial gas velocity
V_{SL}	Superficial liquid velocity
V_{TB}	Translational velocity,
X_L	Liquid volume fraction (V_{SL}/V_M)
V_{GLS}	Gas bubble velocity in slug
ρ_G	Gas density
ρ_L	Liquid density
G	Gravitational acceleration
α	Void fraction
γ	Attenuation constant
λ	Wave length

1 Introduction

1.1 Background

Demand for fossil fuel continues to increase and large amounts of oil products are expected to be provided by deep water reservoirs for the foreseeable future (Vedapuri, 2001). So, towards the end of the twentieth century, oil and gas production has been focused on exploration in the deep water and marginal fields which span a large surface area. Oil exploration in those areas are characterised by the requirement for satellite wells for extraction of the product, low production rates and high water content of the product. Oil and gas production from subsea wells must flow through jumpers, manifolds, flow lines and risers to reach the processing plants. As a result, the development of deep water reservoirs and marginal fields is expensive and may not be economically viable due to the cost of extending tieback distances of several kilometres (Amin et al., 2005).

As oil prices are fluctuating day by day and known reserves are diminishing, there is considerable motivation worldwide to develop cheaper, lighter and more flexible methods of oil production to meet the world's relentless demand for oil and gas (Thorn et al., 2013). The developments, evaluations, use and assessments of multiphase flow meters (MFMs) have shown that use of this technology is a valuable aid in exploiting marginal fields. Consequently, several research projects into multiphase metering have been carried out since the early 1980s (Falcone et al., 2008). However, accurate prediction of well production using traditional multiphase testing and metering is still being hampered by many factors such as changes in the well fluids, and lack of infrastructure, including space and weight limitations, especially in the deep water platforms (Afanasyev et al., 2009).

To optimise return on investment in the development of these reservoirs is to produce manifold pipelines from several wells and transport the products through commingled facilities. This forms the basis for including multiphase flow metering for both subsea and marginal field production systems' development (Vedapuri, 2001). So, oil and gas from the reservoirs to the processing plant requires the continuous development of production technologies. Key

technologies being developed for efficient oil and production are multiphase pumping, separation, fluid mechanics and multiphase metering (Vedapuri, 2001).

Traditionally, test separators are used in conjunction with single phase flow meters, such as orifice or venture meters to measure multiphase flow meters. However, test separators are not a good choice for operations such as well testing because they take a long time to stabilise to provide the needed information on flow performance, and are expensive and bulky. As a result, their use in deep water is economically prohibitive, where very long flow lines are required for each well head and production from each well would require a dedicated test separator. In contrast, a multiphase flow meter removes the need for a dedicated test separator for well testing application (Falcone et al., 2001).

For instance, the flow at the oil-gas well head is a multiphase flow which can vary greatly depending on its age and location. As a result, it is important to measure the fluids produced from these oil wells accurately for efficient oil exploitation and production (Thorn et al., 2013). Also, real time measurement of flow rate of the mixture, individual flow rate and fractional phase volumes without prior separation is a well-established approach in the process control. Multiphase flow metering is becoming increasingly common in many areas of oil and gas production, such as flow assurance, deep water development, down hole/sea separation systems and wet gas fields. The first commercial flow metering was introduced in the late 1980s (Falcone et al., 2009). Since then, many commercial multiphase flows have been developed for example: the Agar Corporation Inc. MPFM 50; Petroleum Software Ltd. ESMER; Medeng Ltd. MD 04; Weatherford International Inc. Red Eye MMS; and Neftemer Ltd. (Thorn et al., 2013). A multiphase flow meter allows operators to capture representative fluids without separation equipment (Afanasyev et al., 2009).

1.2 Motivation

Multiphase flow meters (MPFMs) are being developed to meet the demand for a compact and cost-effective metering solution for production and monitoring for developing smaller and marginal fields (Whitaker, 1996). Determination of these phase fractions and phase velocities create problems for multiphase flow measurement (MFM) as a result of the increased number of parameters, which

are used to characterise a two/three phase flow, relative to those of single phase flows (Rajan et al., 1993). This problem is the main contrasting aspect of multiphase flow measurement and single phase flow measurement. Measurements of this complex flow are by a correlation of the measurement of phase fractions at a flow cross section and the measurement of phase flow velocities (Rajan et al., 1993). However, the task of obtaining accurate measurements of oil-gas-water overall and individual phase flow rates without prior separation still needs improvement (Thorn et al., 2013).

In order to acquire data on the conditions and flow rates of the individual flow rates of the multiphase flow, there is a need for instrumentation of the multiphase flow lines. The instrumentation approaches are data acquisition of flow regimes identification, line holdup estimation, slug flow characterisation, reservoir management, production allocation and fiscal measurement. These parameters of the multiphase flow are required to be measured using appropriate techniques that can be referenced (Exploration, 1994). Many techniques have been applied to measure the phase fraction of multiphase flows, such as capacitance, gamma radiation attenuation, neutron attenuation etc. (Rajan et al., 1993). The most popular method is commercial three phase flow meters are electrical impedance and gamma ray attenuation, followed by microwave and infrared absorption (Thorn et al., 2013).

Although there are many advanced multiphase flow meters commercially available, many issues still need to be resolved because of the complexity of the multiphase flow. Wuqiang Yang, (2011) mentioned that commercially available multiphase flow meters have some problems that need to be addressed: (1) Safety concerns for radioactive meters; (2) Flow regime dependency which limits the capability of most meters to homogeneous flows to achieve an acceptable accuracy of homogenisation of the flow and interferes with the flow by causing pressure drops; (3) Need for calibration-calibration of MFM is a difficult problem to solve as test separators cannot be as a standard for calibrating an MFM because the uncertainty of the test separator is similar to MFM (Whitaker, 1996).

Ultrasound for flow measurement is well-known and can be employed non-intrusively and non-invasively onto a pipe flow. The ultrasonic technology can be applied for flow measurement in three ways: transit time flowmeters, Doppler ultrasonic flowmeters and cross-correlation flowmeters. Excellent reviews on ultrasonic flowmeters are presented in Lynnworth and Liu (2006) and Sanderson and Yeung (2002). Key advantages of the ultrasound over other sensors are suitability of the clamp-on flowmeter, low cost and low power. However, ultrasound methods have yet to be applied in commercial three phase flowmeters. There are issues hampering the widespread application of ultrasound to multiphase flow measurement that have to be overcome.

In multiphase flow, the ultrasonic meters' performance is affected by factors such as the number of scatterers per unit volume, the distribution of scatterers and their velocity profile across the pipe. Also, the ultrasonic attenuation is greatly dependent on the flow regime of multiphase flows and the input signal frequency of the transducer (Rajan et al., 1993). However, ultrasonic techniques have the potential for both phase velocity and phase fraction measurement, although they have not been applied to commercial three-phase flowmeters yet (Thorn et al., 2013). Recent developments in other ultrasonic techniques for multiphase flow measurement have progressed considerably. Besides, ultrasonic tomography, or imaging for two-phase flow, has been studied by many authors (Morriss and Hill, 1991; Rahim et al., 2007; Supardan et al., 2007; Xu et al., 1997).

This research was undertaken as part of the PTDF OSS_PhD project: Petroleum Technology Development Fund (http://www.ptdf.gov.ng/) undertaken at the Centre for Oil and Gas Research of Cranfield University. The overall project aims are to develop a clamp-on multiphase flow measurement using ultrasound techniques and auxiliary techniques for the deployment of the oil-gas industry.

The primary aim of this project is to measure multiphase flow using an ultrasonic technique in conjunction with advanced digital signal processing methods. The objective of this study is to improve the accuracy and extend the capability of ultrasonic flow meters. This work started with the following:

1.3 Aims and Objectives

The demand for two-phase flow meters comes from the oil and gas industry for monitoring of production at the well head (Oddie and Pearson, 2004). This project is about the development of the preceding work carried out by a team in the field of multiphase flow measurement. The ultimate aim of conducting this research project is to develop a clamp-on multiphase flow metering system using ultrasonic sensors, a gamma densitometer and appropriate auxiliary techniques for application in the oil and gas industry. Advanced digital signal processing techniques were developed to utilise ultrasonic and gamma densitometer signals for the measurement of constituent phases of two-phase flow. The measurement system consists of experimental two-phase flow rigs in both horizontal and vertical orientation. The primary fluids utilised in this study are air-water, air-oil and oil-water. The thesis comprises developments of the four distinct tasks summarised in the following list.

1. Development of new gas-liquid slug flow hydrodynamics parameters determination using an ultrasonic Doppler sensor of 500kHz to collect the frequency shift from the flow and processing of the signals via HHTs.

2. Development of an ultrasonic Doppler sensor and neural network for non-invasive classification flow regimes and prediction of gas-liquid two-phase flow.

3. Development of a high frequency ultrasonic pulse-echo system for two-phase flow parameter measurement.

4. Investigation of the feasibility of multiphase flow metering using a combination of ultrasound Doppler sensor and gamma densitometer to estimate the phase flow rates and phase fractions, and also the mean velocity measurement using time averaged maximum frequency of Doppler ultrasound waveforms.

1.4 Summary

Obviously, the oil and gas industry will benefit greatly from implementing multiphase flow metering systems. The flow measurement of each phase of a multiphase flow is important for the reservoir engineer to be able to calibrate the models of production of the wells and maximize the retrievable volume of oil.

Furthermore, the identification of water in the fluid allows optimised maintenance operations to limit mineral deposits (Jannier et al., 2013). It is apparent from the literature surveyed that the measurement of volumetric flow rate and composition volume fractions in multiphase flow is very difficult. Even though some devices have been developed which measure flow rates in a two-phase flow, their range and accuracy are limited and none has been successfully used for the fiscal metering of multiphase flows (Rajan et al., 1993; Thorn et al., 2013). As a result, an improvement in the existing multiphase flow models through development of new techniques, such as ultrasonic, would go a long way towards the development of more reliable and efficient equipment for handling multiphase flows. To conclude, important requirements for ideal multiphase flow meters include: accurate enough to fit the purpose of its design, able measure full range of each phase in the multiphase flow and finally, it is expected to be flow regime independent (Thorn et al., 2013). The remainder of this thesis is arranged as follows.

1.5 Thesis Structure

In Chapter 2, the focus is on the literature reviewed. It comprises four subsections: an overview of multiphase flow measurement, review of multiphase flow measurement techniques' ultrasonic technology, review of ultrasonic techniques for measurement of gas/liquid two-phase flows, and signal processing methods. In Chapter 3, the continuous wave ultrasound Doppler sensor is used to compare the effectiveness of the traditional signal process based on Fourier transform and the modern adaptive of the HHTs to measure liquid flow velocity and characterise four two-phase flow regimes in horizontal. Chapter 4 describes the aim of investigating the application of an ultrasonic Doppler flow meter for two-phase liquid-gas flow measurement using pattern recognition techniques with ANNs. The ultrasonic Doppler signal of the two-phase flow is recorded and processed to generate feature vectors. The feature vectors are utilised as inputs to the neural networks. Chapter 5, develops the pulse-wave ultrasound system that detects moving interfaces in gas-liquid two-phase flow by detecting the instantaneous positions of the interface from the time of flight of the pulsed ultrasound. Detection of the gas-liquid interface is very important for developing models that predict the unsteady behaviour of

two-phase flows. Chapter 6 presents use a combination of gamma densitometer and ultrasound Doppler sensor to measure the volume fraction and flow rates of air-water flow, air-oil flow and oil-water flow in a 50mm diameter vertical pipe and analyses all the results obtained in this research study. Chapter 7 gives the conclusions of the research and further work that could be done in this area.

2 Literature Review

2.1 Multiphase flows fundamentals

The petroleum industry is increasingly operated in physically challenging environments and is consistently seeking efficient production and reduced costs. As a result, there is a growing need to develop low-price, compact and safe multiphase flow metering systems for the oil industry worldwide (Meribout et al., 2010). Multiphase flow meters (MPFM) are being developed to meet the demand for a compact and cost-effective metering solution for production and monitoring for the development of smaller and marginal fields (Whitaker, 1996). However, the task of obtaining accurate measurements of oil-gas-water overall and individual phase flow rates without prior separation still needs improvement (Thorn et al., 2013). In the petroleum industry, multiphase flow meters (MFM) were originally developed to meet the demand for a compact and cost-effective metering solution for production and monitoring for the development of smaller and marginal fields (Whitaker, 1996). Metering of this complex flow is by a correlation of the measurement of phase fractions at a flow cross section and the measurement of phase flow velocities (Rajan et al., 1993). Determination of these phase fractions and phase velocities creates problems for multiphase flow measurement (MFM) as a result of the increased number of parameters, which are used to characterise a two/three phase flow, about those of single phase flows (Rajan et al., 1993). This problem is the main contrasting aspect between multiphase flow measurement and single phase flow measurement.

In the oil and gas sector, use of multiphase flow meters is in well testing, production monitoring, and reservoir management, for making marginal fields cost-effective, facilitation of production in difficult terrains, and energy efficiency of new fields (Thorn et al., 2013).

2.1.1 Multiphase flow regimes

Although flow regimes depend on the geometry, orientation and flow properties, it is possible to categories the flow regimes (Falcone et al., 2009). Dong et al. (2001) stated that there are currently two methods of flow regime identification: visualisation or eyeballing, and statistical method or fingerprint. The statistical method of flow regime identification in a pipeline can be verified with image

reconstruction or visual observation. These flow pattern regimes may or may not be wanted in different multiphase phase flow applications.

However, to obtain optimal design parameters and operating conditions, it is vital to understand multiphase phase flow regimes and the boundaries between them. Falcone et al. (2009) emphasised that a flow regime is not in itself a complete specification of the two-phase flows. It is also noted that the factors influencing flow regimes could change gradually with phase flow rates and transition from one flow regime to another but are not sharply defined.

In addition to the classification of multiphase flow according to the flow regimes, the GVF is also use to classify the flow. The GVF method is important to multiphase metering in that meters measuring predominantly liquid with a few percentages of gas are clearly not the same as meters designed to measure larger gas fractions, such as wet gas (Cornelissen et al., 2005). Various types of instrument have been used to measure two phase flows, such as the impedance method (Andreussi et al., 1988), and capacitance method (Da Silva et al., 2007). Others are the tomographic scanner using γ-ray (Kumara et al., 1997), hot-film anemometer (Serizawa et al., 1975); (Vince and Lahey, 1982) also employed an X-ray system on an air-water system.

2.1.2 Multiphase Flow Regimes Maps

Information on multiphase flow regimes is vital for determining volumetric fractions of individual phases when using phase fractions measuring instruments. Flow regimes and their transitions are not measured directly with an instrument but are deduced from other measurements. One important tool for discriminating flow regimes is flow regime maps (Babelli, 2002). Also, Thorn et al. (1999) mentioned that identification of the flow regime of a two-phase flow is vital for not only the determination of the phase fraction but the safety of operation and reliability of process systems. Açikgöz et al. (1992) produced the first three-phase flow regime map. Three-phase flow for air/water/oil systems presents a rich variety of flow regimes. However, many flow regime maps have been produced to express the two-phase flow pattern regarding superficial liquid and gas velocities. Mandhane et al. (1974) carried out a systematic

9

investigation of two-phase flow patterns and produced a flow map using a superficial gas velocity versus the superficial liquid velocity.

2.1.1 Horizontal flow

In horizontal flows, the transition from one flow regime to another is a function of pipe diameter, interfacial tension and density of the phases as well as the superficial gas and liquid superficial velocities. At low gas and liquid superficial velocities the flow regime would be a smooth or wavy stratified flow. For high gas velocity with low liquid velocity, the flow would be dispersed or misty, but on the other hand with low gas velocity and high liquid below, the flow regime would be a bubby flow.

If the pipeline is perfectly horizontal, the six flow patterns shown in Figure 2-1 would be observed. However, only three typical flow patterns appear at the cross section of the pipe: bubbly, stratified and annular. Slug flow can be viewed as the combination of stratified flow and bubbly flow. Rajan et al. (1993) reported that a downward or upward inclination of the pipeline has an effect on the flow patterns – an upward inclination enhances slug flow and a downward inclination enhances stratified flow.
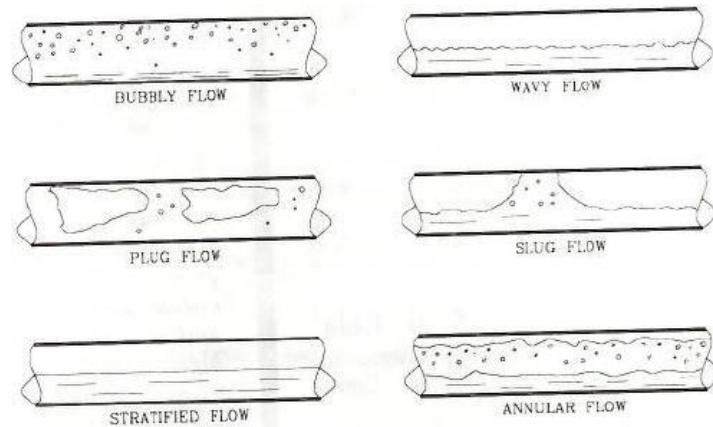
Figure 2-1 Typical flow regimes in horizontal gas/liquid flows (Rajan et al., 1993)

Even so, only three typical flow patterns feature at the cross section of the pipe: bubbly, stratified and annular. Slug flow can be viewed as a combination of stratified flow and bubbly flow. However, in industrial applications the two-phase flow regimes present in the horizontal pipe mainly include bubbly flow, stratified flow, slug flow and annular flow (Meng et al., 2010).

2.1.2 Vertical flow

In vertical flows, for example at the end of the vertical pipeline from the reservoir to the well head, the flow regimes that could be observed in vertical two-phase flow are shown in Figure 2-2. For high liquid superficial velocities, bubbly flow is the prominent flow regime. However, as superficial gas velocity increases, the multiphase flow regime will change from bubbly-slug-churn-annular (Cornelissen et al., 2005; Rajan et al., 1993).

BUBBLY FLOW   SLUG FLOW   CHURN FLOW   ANNULAR FLOW
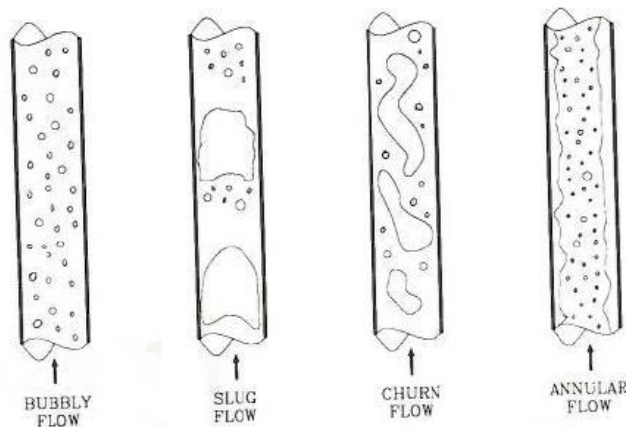
Figure 2-2 Typical flow regimes in vertical gas/liquid flows (Rajan et al., 1993)

2.1.3 Modelling of Multiphase flows

The multiphase flow is a complex phenomenon and this has made developing of multiphase models a very difficult task. The modelling techniques employ mathematical models, and correlations for calculating the properties of the two-phase flow are available in Mandhane et al. (1974), Rajan et al. (1993) and Taitel and Dukler (1976). These models are often integrated into the hardware of commercial MFMs to predict the occurrence of slip between phases of the two-phase flows. There are four different types of multiphase model: (1) Empirical – these models relate the data for pressure gradient and void fraction to the two phase flow variables. Empirical models are simple and fast to run. However, applications of these models are limited and require a large of number of experiments. (2) Phenomenological – this refers to the models constructed out of observation of flow patterns and closure laws. (3) Multifluid-multiphase flow modelling by multifluid involves solving of partial difference equations characterising the multi-dimensional and time-dependent multiphase flows. This method varies greatly, depending on the physical quantity of

interest, nature of the fluid and the interactions between them. It is important to note that numerical modelling still requires empirical models and its success relies on the availability quality of experimental data. Moreover, (4) Interface tracking employs either a free surface method or a free volume method to model the multiphase flow. Application of interface tracking is limited to simple flow set ups (Falcone et al., 2009).

2.1.4 Phase Fraction Measurement

Multiphase flow measurement could be described as a product of the measurement of the flow phase fraction and the measurement of the phase flow velocity. Many techniques have been applied to measure the phase fraction of multiphase flows, such as capacitance, gamma radiation attenuation, neutron attenuation etc. (Rajan et al., 1993). If the single phase flow meter were to be combined with a void fraction meter, then the multiphase flow measurement would be complete (Manus et al., 2013). Traditionally, void fraction in two-phase flows is measured using an optical method with image processing, electrical probing, or other methods such as X-ray and electrical capacitance tomography. An optical method is not possible for existing pipelines, but ultrasound sensors can be used to monitor and control these facilities (Murai et al., 2009). Phase fraction measurement in changing flow regime is a very difficult task to execute for multiphase flow measurement systems. The most popular method is commercial three phase flow meters which are are electrical impedance and gamma ray attenuation to determine the phase fractions, followed by microwave and infrared absorption (Thorn et al., 2013).

The basic principles of the operation of the electrical impedance method of phase concentration are described in Thorn et al. (2013). Electrical impedance methods are simple, robust, a phase fraction sensor with fast response and not radioactive. Nevertheless, it has three limitations that can affect the performances of the sensor. The first is the sensitivity to changes in fluid properties that are either water continuous to oil continuous, or vice versa. The effect of this challenge can be annulled by homogenisation of the flow which makes the flow passing through the sensors stable and known. An application of this strategy has been reported in Yang et al., (2011). The second constraint

to the electrical impedance sensor is change in the regime of the flow. The sensor is normally not suitable where flow regime is unknown. This effect can be neutralised to reduce the flow regime dependence by the use of helical electrode designs (Yang et al., 2011). However, helical sensors are often larger than the simpler surface plate ones. The last difficulty with using the electrical impedance sensor is the determination of the phase inversion point. This is the point at which an oil-water mixture changes from oil continuous to water continuous and its electrical properties change accordingly (Falcone et al., 2009). An arrangement of many sensors covering the different regions of the pipe cross section and through correct flow regime change can enhance the determination of the inversion point (Tjugum et al., 2002).

Energy from radioactive sources such as $\chi-ray$ and $\gamma-ray$ are applied to gas fraction measurement in multiphase flows due to the large difference in attenuation between liquid and gas. Gamma ray measurement is commonly known as gamma ray densitometry. In a typical example, i.e. an air-water flow, the liquid phase scatters the radiation and it changes at a rate that is equivalent to the amount of water contained in the flow. The energy detected provides data which can be used to reconstruct the void distribution(Dyakowski, 1996). Thorn et al. (1997) describe the operation of a γ-ray densitometer for metering the gas, water and oil components of multiphase flow. Two independent measurements are required to determine the values of the components' fractions in three phase flows. This could be accomplished either by a second measurement, using the same technique, or with another one such as the capacitive technique. The gamma densitometry can be single or double beam, both have applications in multiphase flow measurement.

A single beam gamma densitometer is often used for measuring the void fraction of gas-liquid flows in a pipe. The measurement of the void fraction is by correlation between loss of radiation intensity of the test volume and the void fraction of the fluid. The occurring flow regime in the pipe can be determined from the void fraction and that makes the gamma technique a non-flow regime dependent method (Stahl and von Rohr 2004). Thorn et al. (2013) reported that the use of a dual energy gamma ray for water fraction measurement requires

energy sensitive detectors, which means the beam intensity has to be lower. An effective instrument, which is based on essentially similar principles to the multi-beam gamma densitometer, is the scanning X-ray void fraction meter described by Falcone et al. (2009).
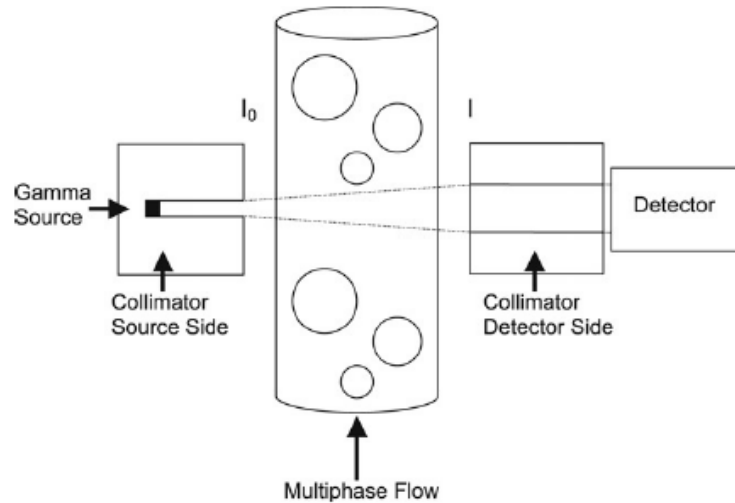
Figure 2-3 A single beam gamma densitometer (Blaney and Yeung, 2008)

The gamma-ray for phase component measurement technique is very effective in void fraction. In particular, the multi-beam gamma densitometer has a proven and successful record in measuring mean density in transient two-phase flows but it is susceptible to high attenuation of salinity which might be present in the flow. Besides, the multi-beam gamma measurement has problems with counting statistics and of phase distribution in time and space (Falcone et al., 2009; Thorn et al., 2013).

In addition to the electrical impedance and gamma-ray radiation, there are another two methods of measuring phase fractions: application of infrared absorption and microwave attenuation principles which have been used in commercial multiphase flowmeters (Thorn et al., 2013). Similarly, in the X-ray method the intensity of the source attenuate is directly proportional to the density of the fluid through which the radiation is passed. Cross-sectional process information of individual processes can be an image (tomography) or mere process parameters characterising the phase distribution of the process. Measurement or imaging of multi-component systems can be made with one measurement principle at several wavelengths or by using two or more sensors.

In multiphase flow metering systems, process tomography instruments are incorporated in the multiphase flow test loops to measure accurately the flow regime present in the flow as reference/validation instrumentation (Thorn et al., 2013). Computerised tomography or imaging of multiphase flow using the signal from standard sensors has been reported, such as microwave electrical capacitance tomography, (Ismail et al., 2005) and gamma ray, ultrasonic (Xu and Xu, 1998).

In the same way, other techniques, such as capacitive wire mesh and inductive sensors, have been applied to measure phase fraction in multiphase flow as either an alternative sensor or to complement major sensors, such as gamma ray or ECT. Yang (2006) mentioned that the ABB had developed an inductive level monitoring for multi-interface level measurement. This device has been tested experimentally and can detect water continuous emulsion easily. Above all, it has been found that scales and wax in the fluid have no effect on the inductive (magnetic) measurement technique. However, it cannot be used to detect levels of oil and gas! Also, Da Silva et al. (2007, 2010) have shown a new method of visualising gas-liquid two phase flow based on a capacitive wire mesh technique.

2.1.5 Phase Velocity Measurements

Conventional single phase flow meters have been applied for measuring fluid velocities of multiphase flows in a mixed, stable and partially separated system (Rajan et al., 1993). For instance, a Venturi meter has been used to measure mixed multiphase flow where the flow is assumed to be 'single phase flow' (Thorn et al., 2013). Also, both vortex shedding and Coriolis meters have been used to measure separated gas-stream and separated oil-water streams respectively (Thorn et al., 2013). If the single phase flow meter were to be combined with a void fraction meter, then the multiphase flow measurement would be complete (Manus et al., 2013). Another approach that eases the measurement of multiphase flow with a single phase meter is homogenisation. Homogenisation eliminates the effect of slippage between flow phases. Homogenised flows can be measured with meters such as orifice, venture, or cross-correlation, using ultrasonic or conductance signals (Rajan et al., 1993). A

mixer with a twin-cell rotational principle has obtained good homogenisation over a velocity range of 2-6 m/s. However, in intrusive meters, the homogenisation produces pressure drop and causes difficulty in pipeline pigging (Thorn et al., 1997).

2.1.5.1 Intrusive techniques

Measurement of flow by detecting a disturbance in the flow is a well-known technique. The disturbance could be naturally occurring or introduced into the flow. Hot-film anemometers and other heat probe instruments, such as thermistors, are known and accepted for single phase flow measurement (Rajan et al., 1993). Abel and Resch (1978) have developed a method of applying a hot-film anemometer for the identification of large vapour slugs and small bubbles in two-phase gas-liquid flow and proposed an extension of the method to two-phase containing both large and small bubbles. However, hot-film probe data might be very crudely processed.

Kendall and Smerek (1981) presented a single phase flowmeter based on the bending of a slender spring steel beam in a fluid stream. Strain gauges were used to detect the pressure exerted by the fluid on the spring. Turbine and positive displacement flowmeters operate with the same principle to measure volumetric flow. Both these two instruments have been used in measurement two-phase flows. Their primary drawbacks are a highly intrusive, large pressure drop, and a change in the nature of the flow. A Pitot tube is used to measure local velocity in single phase flow (Rajan et al., 1993). An application of the Pitot tube for the measurement of wet gas flow has been patented by Benton and Seay (1985). The system consists of two pressure sensors interconnected through pressure transmitting lines. The first sensor measures the total pressure at the upstream of the gas flow while the second measures the static pressure at the downstream.

These are momentum sensing devices and have been used for measuring two-phase flow by many researchers (Venturi: (Huang et al., 2005) these are in-line flow meters which operate on the differential pressure loss and their intrusiveness could change the nature of the flow. This property aids in homogenising the two-phase flow, thereby making the meter suitable for

multiphase flow metering (Rajan et al., 1993). However, these meters have a few drawbacks in two-phase flow measurement: they are affected by the flow pattern, and assumptions are often made for the ratio of the gas mass flow rate to the total mass flow rate of the two-phase flow is known. However, this is difficult to obtain (Meng et al., 2010).

2.1.5.2 Non-intrusive techniques

An electromagnetic flowmeter, or magmeter, works on Faraday's induction principle which states that a conductor moving in a magnetic field induces an electrical voltage the flowing fluid is the moving conductor (Fitzpatrick, 2012). The voltage measured between the electrodes is directly proportional to the flow rate in the pipe (Baker, 2001). The method has a good accuracy, is obstruction-free, requires low maintenance and is reliable. However, it is sensitive to velocity profile and suitable for multiphase flow measurement provided the continuous phase is conducting (Rajan et al., 1993 and Baker, 2001). In addition, an electromagnetic meter's reading for two-phase flow is sensitive to magnetic susceptibilities, velocities of both phases, geometrical distribution and the wetting characteristics of the electrodes for two-phase flow measurement use (Oddie and Pearson, 2004).

Ultrasonic technology for flow measurement is well-known and can be employed non-intrusively and non-invasively onto a pipe flow. There are three ways in which ultrasonic technology can be applied for flow measurement: transit time flowmeters, Doppler ultrasonic flowmeters and cross-correlation flowmeters. In multiphase flow, the ultrasonic meters' performance is affected by factors such as the number of scatterers per unit volume, the distribution of scatterers, and their velocity profile across the pipe. Also, ultrasonic attenuation is greatly dependent on the flow regime of multiphase flows and on the input signal frequency of the transducer (Rajan et al., 1993). However, ultrasonic techniques have the potential both for phase velocity and phase fraction measurement, although they have not been applied to commercial three-phase flowmeters yet (Thorn et al., 2013). Recent developments in other ultrasonic techniques for multiphase flow measurement have progressed considerably. Besides, ultrasonic tomography or imaging for two-phase flow has been studied

by many authors (Morriss and Hill, 1991; Rahim et al., 2007; Supardan et al., 2007; Xu et al., 1997).

Mass flow meters or Coriolis mass flow meters use Newton's second law of motion and need no probes. Specifically, this is an indirect method where a velocity meter in combination with a densitometer is used to measure the mass flow of the fluid (Rajan et al., 1993. There are various types of configuration of the commercial Coriolis mass flow meter. The first design was by Micromotion which is made up of a U-tube vibrating about a fixed axis. The flows going out and coming into the tube have equal and opposite forces turning the tube. The force is related to the mass flow rate.

Measurement of flow velocity by cross-correlation is a standard signal processing method (Cornelissen et al., 2005). Cross-correlation involves correlating any property of the flow method between two identical sensors placed at two different positions separated by a known distance. The flow passes along the sensors, the fluctuation of the measure by the first sensor will be repeated by the second sensor after a period of time t. This time is the time it takes the flow to travel between sensor positions (Falcone et al, 2009; Rajan et al., 1993). Most of the common sensors used for cross-correlation are: ultrasonic (Xu et al., 1988), capacitance (Yang and Liu, 2000) and impedance (Etuke and Bonnecaze, 1998). If the multiphase flow is homogenised, important average velocity measurement can be made and in combination with a densitometer, an accuracy of ±5% has been reported (Rajan et al., 1993). The accuracy of the method is dependent on the validity of the technique used to estimate the velocity from the correlation function's peak point to represent the mean velocity of the flow (Thorn et al., 1997). However, there are constraints to fully utilising this in three phase flows, such as slip effect on the flow velocity, in situ calibration, combination of different sensor architectures, etc. More research is needed before this technique can be applied to measure the phase velocity of multiphase flow at any point along the pipeline (Thorn et al., 2013).

2.1.6 Pattern Recognition Technique
The characteristics used to describe single phase flow, such as turbulence, velocity profile and boundary layer, are not suitable for describing the nature of

multiphase flows (Cornelissen et al., 2005). Multiphase flows are categorised into flow regimes. These flows occur both in horizontal and vertical orientations. The flow regimes are developed based on flow-line geometry and orientation, individual phase flow rates, and component transport properties (density, viscosity and surface tension (Rajan et al., 1993; Thorn et al., 2013). Identification of the flow regimes in multiphase flow is essential to both the efficient operation of the multiphase flow systems and the determination of phase fractions (Arvoh et al., 2012). To group flow regimes according to their topological similarities, several mechanisms of flow regimes classifiers or flow regimes descriptors have been developed over the years. Typical flow regimes in the horizontal pipe flow are: slug, stratified, wavy, elongated bubble and annular flow patterns and in the vertical gas-liquid flow are: bubbly, slug, churn and annular flows (Falcone et al., 2009). The process of the objective flow regimes' identification from the sensor signals of the flow requires the use of a pattern recognition technique.

The application of pressure fluctuations of the two-phase flow signals and statistical analyses for objective characterisation was pioneered by Drahoš and Čermák (1989). The two-phase flow signals from several pressures transducers have been analysed for features extraction using PSD for generating input variables for the neural network (Kv and Roy, 2012; Sun and Zhang, 2008; Xie et al., 2004). Other sensor signals have been used for flow regime classification using the statistical moment of the analysis, such as conductance probe, (Hernández et al., 2006), and radioactive images (Sunde et al., 2005). It has been found that the pattern recognition of flow regimes using pressure signals is fast enough to be used for online flow regime identification (Kv and Roy, 2012; Xie et al., 2004). However, these transducers are invasive sensors. Hence there is need for a non-invasive method of flow regime classification for two-phase flow, such as ultrasound or gamma. In addition, the review of methods of objective flow regime classification showed that the early methods used mechanistic models or empirical models. The flow patterns of the multiphase flow were identified using equations governing the physics of the fluid that were developed from the mechanistic models derived from the physics of the fluid.

The process of identifying flow patterns using these models has disadvantages in that each flow regime has to be examined independently (Ozbayoglu and Ozbayoglu, 2009).

Flow regime identification using ANN pattern recognition can be implemented for using both supervised neural networks (SNNs) and unsupervised neural networks (UNNs) or self-organising networks. The SNN uses Feed-forward networks such as multilayer perceptron and Radial-Basis Function networks for pattern recognition in which the back propagation error of the training algorithm together with information of predefined classes is used to classify the input variables into the specific classes and it does not need. However, the UNN uses the Kohonen-Network or self-organising map (SOM) for data feature mapping and it does not need information on the classes as it uses a network clustering method to group the input variable into several classes that contain similar characteristics (Mi et al., 2001a). The Kohonen self-organising neural network has been implemented for flow regime classification using measurement data points of distinct flow regimes (Cai et al., 1994).

2.2 Principles of Doppler Ultrasound

This section provides descriptions of ultrasound measurement systems for multiphase flow measurement. The ultrasonic waves, sensors, theories on generation, and propagation of the ultrasonic signal are discussed in this section. The principle of ultrasonic sensors is quite simple: they transmit acoustic waves and receive them after interaction of the ultrasonic wave and the quantity that is being investigated – the multiphase flow in this case. The received ultrasound signal carries the information about the parameters to be measured (Hauptmann et al., 2002). Ultrasonic Doppler technology for multiphase measurement flow is implemented by either using a continuous wave Doppler system or pulsed wave Doppler system.

2.2.1 Ultrasound Wave parameter measurement and process parameters

In solids there are many types of ultrasonic waves that can be used to measure physical properties, whereas in fluids usually longitudinal waves are the main

waves to be employed when measuring physical properties. The following are the types of waves used in solids media: longitudinal/compressive transverse/shear, extensional, torsional, Rayleigh and Rayleigh-like, Lamb and Lamb-like etc.; on the other hand longitudinal waves and a few others, e.g. head lateral, sezawa-like are used in fluids. Importantly, the focus here is on longitudinal/compression as it is the wave related to the measurement of physical properties of fluid (Lynnworth, 1989). Often a longitudinal wave is used for an ultrasound measurement system. This is the wave that is produced by the push-pull (backwards and forwards) action of sources on the propagating medium in the direction along which the wave is travelling.

The propagation of an ultrasonic wave can be described by the ultrasonic pressure *P:*

$$P_{(x,t)} = P_0 e^{j\omega(t-\frac{x}{c})} e^{-\alpha x} \tag{2-1}$$

where $\omega = 2\pi f$ the frequency, c the speed of sound and α the attenuation of sound. The parameters c, and α are specific for a particular substance unlike the Z and Δf. However, they are all related to the parameters of the process under investigation. Consequently, determination of the speed of sound and absorption can be realised using equations (2-2) and (2-3) (Hauptmann et al., 2002).

$$\alpha = \frac{1}{\Delta x} \ln\left(\frac{P_0}{P}\right) = \frac{1}{\Delta x} \ln(\frac{V}{V_0}) \tag{2-2}$$

$$c = \lambda f = \frac{\Delta x}{\Delta t} \tag{2-3}$$

where V, V_0 are electrical voltages proportional to the sinusoidal sound pressures P_0 and P, Δx is the path length and Δt is the transit time. Consequently the absorption measurement is reduced to an amplitude measurement (Hauptmann et al., 2002).

The viscosity causes both the attenuation losses α_V, and the thermal conductivity of liquids α_T. The attenuation coefficient can be expressed as (Kočiš and Figura, 1996):

$$\alpha = \alpha_V + \alpha_T = \frac{2\pi^2}{\rho^3}\left[\frac{4}{3}\eta + \lambda_T\left(\frac{1}{c_V} - \frac{1}{c_p}\right)\right]f^2 = af^2 \tag{2-4}$$

Where ρ = density [$kg.m^{-3}$]; c = velocity of ultrasound [$m.s^{-1}$]; η = dynamic viscosity [Pa.s]; λ_T = thermal conductivity of medium [$W.m^{-1}.K^{-1}$]; c_V, c_p = specific heats at constant volume and constant pressure respectively [$J.kg^{-1}.K^{-1}$]

The attenuation shows a square functional dependence on frequency. This is important for applications at very high frequencies.

Sound speeds: c is the speed of sound wave propagation in the medium. It is also known as acoustic velocity and depends on density, compressibility and affects by temperature.

$$c = \sqrt{\frac{E}{\rho}} \; or = f\lambda \tag{2-5}$$

where E is the bulk modulus; ρ is density of the medium f is frequency λ wave length.

Bulk modulus is a reciprocal of compressibility of the medium. This implies that liquids have higher sound speeds than gasses (Hedrick et al., 1995).

Acoustic impendence: The acoustic impedance of a medium can be expressed as:

$$Z = \rho c. \tag{2-6}$$

where Z is the acoustic impedance, ρ is the density of the media and c the sound speed.

The unit of acoustic impedance is $Kgm^{-2}s^{-1}$, or Rayl (Asher, 1997a).

Intensity: Intensity I of an ultrasound beam is the amount of acoustic energy flowing through a cross-sectional area per second.

$$I = \frac{p^2}{2\rho c} \tag{2-7}$$

where I is the intensity, ρ the density and c the sound speed.

It is often measured in decibels. Intensity variation or level is expressed in Intensity (dB) (Hedrick et al., 1995)

$$= 10log_{10}(I/I_o) \tag{2-8}$$

Ultrasonic waves: Longitudinal or compression waves used for measurement of the physical properties of a fluid. The wave is being produced by the push-

pull (backwards and forwards) action of sources on the propagating medium in the direction along which the wave is travelling (Lynnworth, 1989). Ultrasonic waves can be classified according to the manner in which the ultrasonic techniques are generated and excited, such as continuous wave (CW) and pulsed wave (PW) types (Xu et al., 1988).
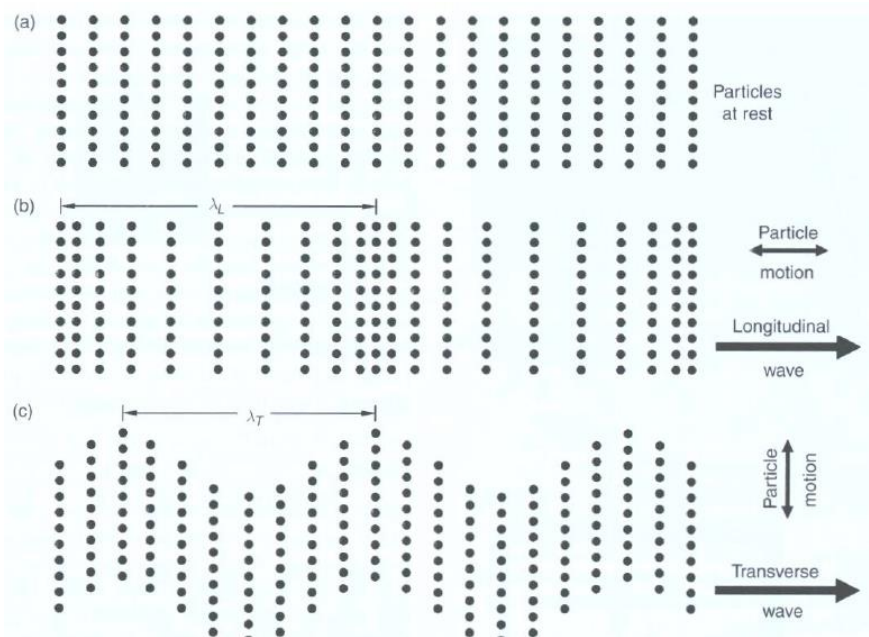
Figure 2-4 Particles in motion in ultrasonic bulk wave showing (a) particles of solid medium at rest and particles' motions for (b) longitudinal wave (c) shear or compressive wave (Wright, 2011)

Ultrasonic Transducer: In ultrasonic measurement systems, the generation and detection of ultrasound depend on the piezoelectric effect, in which mechanical energy is converted into electrical energy and vice versa (Messer, 2005). The piezoelectric unit is in the transducer, which is the heart of an ultrasonic measurement system; it generates the ultrasonic energy and converts electrical energy into acoustic energy in the transmission but converts acoustic energy into electrical energy during reception. The beam pattern of the transducer determines the velocity profile resolution (Kossoff, 2000). The sensitivity of the flow velocity measurement to weak echoes, the spatial resolution achievable and the ultrasound frequencies used depend on the transducer. The application of ultrasound in fluid velocity measurement, and the

generation and detection of ultrasound, depend on the piezoelectric effect, in which mechanical energy is converted into electrical energy and vice versa (Messer, 2005). Most transducers are made up of piezoelectric crystals which have been made with several materials such as the naturally occurring material called quartz, piezoelectric (PZT) and polyvinyl den difluoride (PVDF). PZT ceramics are superior to quartz when the combined transmission/reception performances are considered and the polymer PVDF has intermediate performance. However, PZT is widely used. The basic structure of a PZT transducer is shown in Figure 2-5 (Evans, 2002). There are various types, sizes and shapes of transducers, some are clamp-on and others are for retrofitting.
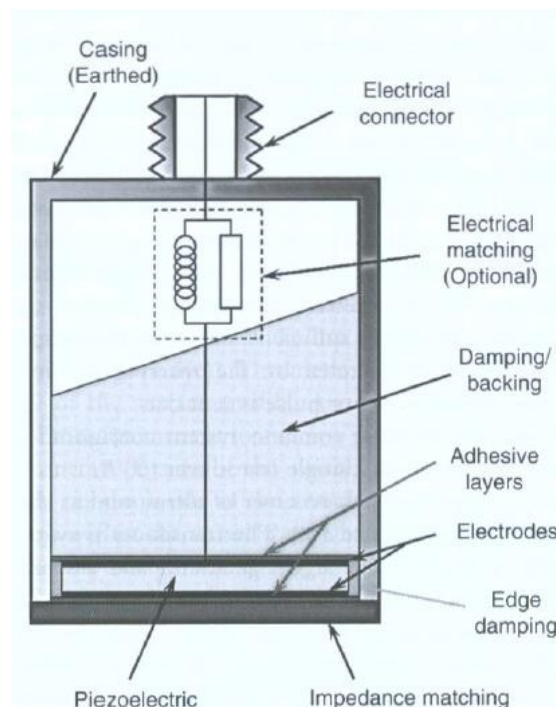
Figure 2-5 Single-element Transducer (Wright, 2011)

Single element transducers are found in Doppler devices; even though this is not the best method of generating a low noise ultrasound, it is very suitable and provides good spatial resolution (Evans and McDicken 2000). The ultrasonic wave emanates propagates in the form for a certain distance known as the near-field. The near-field is proportional to the square of the diameter of the transducer and inversely proportional to the frequency. Beyond the near-field, the beam changes from a cylinder into a cone and diverges into the far-field at a

constant angle that is proportional to the diameter of the transducer and inversely proportional to the frequency (Kossoff, 2000).

The Doppler Effect: The Doppler Effect is the change in frequency of an acoustic or electromagnetic wave resulting from the physical movement of either the emitter or receptor (Messer, 2005).The frequency *f* of the harmonic ultrasonic wave is changed by the Doppler Effect when the wave is reflected by a reflector that is moving towards the source of the wave with speed *v*. Then the frequency shift Δf between the incident and reflected waves is

$$\Delta f \approx 2f_0 \frac{v}{c} \qquad \text{(2-9)}$$

for $v \ll c$ in which the frequency of the incident wave is f_0. This effect is widely used in flow measurement when particles in a liquid are used as moved reflectors (Hauptmann et al., 2002).
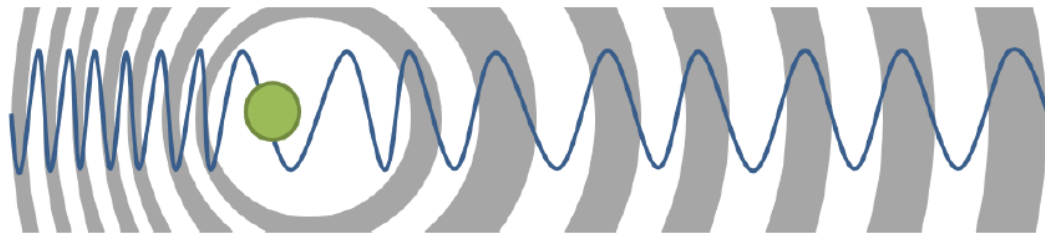
Figure 2-6 the Doppler Effect (Case et al., 2013)**.**

2.2.2 Continuous-Wave Doppler Ultrasound (CWDU) System

The Doppler ultrasound system was first invented for medical application using the continuous wave type by Satomura (1957). The early developments of the CWDU for flow velocity measurement was started with the presentation made by Satomura (1957) on the principles of operation and composition equipment for the clinical examination of blood flow in the body using a CWDU measurement of blood flow in the body. Since then, several applications of the equipment have emerged. The ultrasound Doppler principles can be implemented using either the PW or CW ultrasound systems (Brody et al., 1974; Cobbold et al., 1983; Evans and McDicken, 2000).

The CWDU system comprises the following main components: the master oscillator, the transmitter, the demodulator and the filters (Evans and McDicken,

2000). The basic principle of the continuous Doppler is shown in Figure 2-7. The master oscillator produces the frequency of the transducer and is amplified by the transmitting amplifier. The output of the transmitting amplifier is used to derive the transmitting crystal (transducer) which sends an acoustic energy (longitudinal wave) into the measuring system. The energy is reflected and scattered by particles or bubbles within the ultrasound beam and some portion of this returns to the receiving crystal (transducer) and re-converts into electrical energy which has the form. This returns a radio frequency amplifier signal and mixes with the reference signal from the master oscillator. The process of the mixing produces both the sum of the transmitted and received frequencies and the required difference frequency or Doppler shift frequency. A combination of low and high pass filters removes all signals outside the range and leaves only the Doppler difference frequency which is then amplified for further processing (Evans and McDicken, 2000).

CWDU can be designed to be operated in a bi-directional or unidirectional mode. However, in most flow measurement applications of the Doppler system, a single sideband generator is included to produce a unidirectional flow measurement – the measurement of the flow moving backwards is neglected (Smallwood and Dixon, 1986). An illustration of the main parts of the CWDU system and its use for flow measurement in a pipe flow is shown in Figure 2-7. The Doppler ultrasound for flow measurement is set up with the assumption that there are scatters in the flow and the Doppler Effect can be applied to ultrasound waves (Christopher et al., 1996). The operation of the CWDU starts with the sending of a single frequency wave continuously to drive the piezoelectric crystals of the probe by the master oscillator and the transmitted signal is reflected back continuously. The returned is detected by another piezoelectric crystal in the probe. The received ultrasound signal is the sum of the transmitted signal and echoes from the scatters, whilst the difference between the received and transmitted ultrasound beams is the Doppler frequency shift (Smallwood and Dixon, 1986) .

In the CWDU system, the continuous wave optimises the design and construction of the electronics and the transducer but impedes the use of one

26

piezoelectric transducer to be used for both reception and transmission of the ultrasound wave. As a result, the two piezoelectric crystals, one for transmission and the other for reception, are incorporated into one transducer housing. The dual-piezoelectric crystals arrangement creates the detection of the ultrasound reflection from a small area called the sample volume (Christopher et al., 1996).
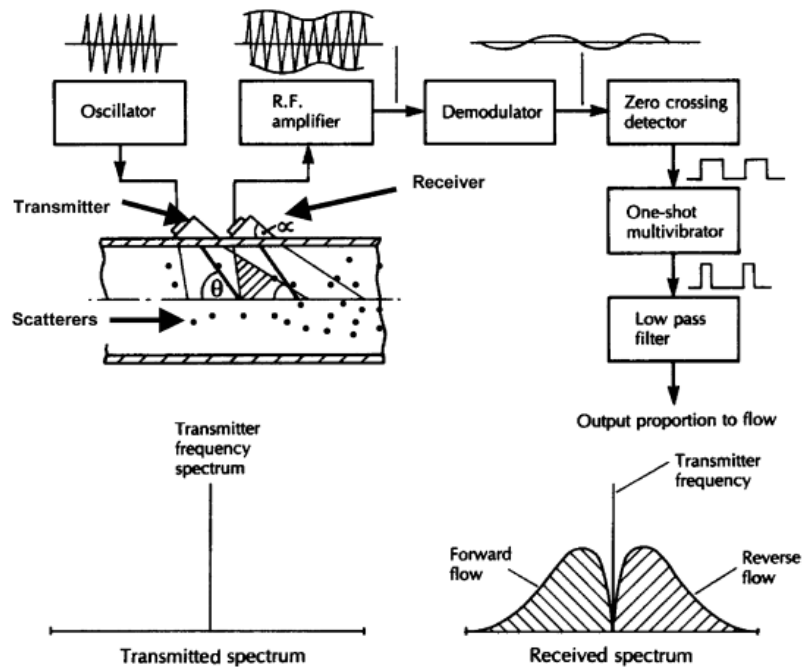
Figure 2-7 Basics of CW Doppler ultrasonic flow meter (Sanderson and Yeung, 2002)

Several developmental studies have been undertaken by researchers to improve the CWDU systems since the method was first invented in 1957 (Samaturra, 1957). In 1974, Brody and James described their theoretical analysis using mathematical model analysis of the CWDU flowmeter. The model was based on stochastic considerations of the scattering of the ultrasound by the scatters in the flow. The analysis demonstrated that the flow velocity estimation using CW can be reduced to the spectral estimation. Another study of the CWDU using model on the influence of ultrasound beam profile and degree of insonation, as applied to mean velocity, was explained by Cobbold et al. (1983). The model was based on an axisymmetric flow velocity profile and

symmetric response of the ultrasound probe. It was found that the mean velocity could be small, provided the ultrasound beam diameter was approximately the same size as the pipe diameter (Cobbold et al., 1983).

The Doppler frequency shift is given by the relationship between the velocity of the scatters v and the Doppler shift f_d is given in equation (2-10) (Sanderson and Yeung 2002).

$$f_d = f_t - f_r = (\frac{2f_t v \cos \theta}{c})$$

(2-10)

where: f_t, f_r are transmitted and received ultrasound frequencies, the velocity of the target, c is the velocity of the sound of the flow in the pipe and θ is the relative angle between the transmitted ultrasonic beam and axial direction of the flow. Usually two transducers are required for Doppler flow meters; however, these two transducers can be made into separate units or one compact unit.

As a result the power spectrum of the Doppler signal is computed to estimate the average frequency shift which is proportional to the mean velocity of the flow (Brody and James, 1974). The mean velocity may be calculated from the mean Doppler frequency shift using the standard Doppler equation, i.e.

$$\bar{v}(t) = \bar{f}_d(t)c/2f_t(t) \cos \theta$$

(2-11)

where $\bar{f}_d(t)$ is the instantaneous mean Doppler shift, f_t the transmitted frequency and θ the angle between the ultrasound beam and flow direction.

The volumetric flow is a product of the cross-sectional area of pipe A and the spatial mean velocity of the flow within the pipe (Evans and McDicken, 2000). Therefore,

$$\bar{Q} = \frac{1}{T} \int_{t=0}^{T} A(t)\bar{v}(t)dt$$

(2-12)

Substituting equation (2-11) into (2-12)

$$\bar{Q} = \left[\frac{c}{2f_t(t) \cos \theta} \int_{t=0}^{T} \frac{(A(t)\bar{f}_d(t))dt}{T} \right]$$

(2-13)

Measurable quantities are $\bar{f}_d$, A and θ.

The average frequency is calculated from the power spectrum using this equation (Morriss and Hill, 1991).

$$\overline{f_d} = \frac{\int_0^{f_{max}} P(f)fdf}{\int_0^{f_{max}} P(f)df} \qquad\qquad (2\text{-}14)$$

where $\overline{f_d}$ = average frequency, f_{max} = maximum Doppler frequency, $P(f)$ = Doppler power spectrum, f = frequency.

Importantly, in Doppler ultrasound flow measurement, a compromise has to be made between velocity resolution and temporal resolution in the spectral mode. The resolutions are dependent on the Doppler frequency shifts. For instance, increasing the temporal resolution will reduce the velocity resolution. So a low frequency is better at velocity resolution but at the cost of temporal resolution and vice versa. Moreover, an increase in the operating frequency of the Doppler system provides the following advantages: (a) a proportional increase in Doppler frequency shift, (b) a broader spectrum of Doppler frequency shifts, and (c) an increase in transducer spatial resolution. However, an increase in the operating frequency would lead to higher attenuation and lack of availability of the higher frequency transducer (Christopher, 1995).

2.2.3 Pulsed-Wave (PW) Doppler Ultrasound System

One of the disadvantages of the CWDU system is that it detects the movement of all scatters in the sample volume. Therein lies its problem of not being able to determine the range of the moving scatters. The PWDU can overcome this limitation, because, in the PWDU systems, each of the Doppler shift frequency of the echoes returns to the transducer. Also, the pulsed ultrasound Doppler (PUD) can be applied to measure flow velocity and its profile which has made it a versatile sensor (Baker, 1970). In the pulse wave Doppler system, the length of the pulses is gated. This allows the distance to the moving interfaces as well as their velocity with respect to the beam to be measured (Sleutjes, 2006). Consequently, since the invention of the PWDU systems it has become the principal ultrasound Doppler system employed (Christopher et al., 1996). A simple two-phase flow measurement application of PW Doppler and its components is illustrated in Figure 2-8. The pulse Doppler can be implemented either as a single or dual transducer for the transmission and receiving of the

echoes (Sleutjes, 2006) The example shown in the figure is the dual transducer type (Huang et al., 2013).

The pulse wave operation starts with a signal from the master oscillator which is gated under the control of the pulse repetition frequency (PRF) generator. The length of time the transmission gate remains open is dependent on the required length of sample volume. The returning pulses to the RF amplifier are used to derive the transducer. This sensor sends the bust of the ultrasound into the measuring system. The echoes of the ultrasound pulse convert into electrical energy the same transducer and this signal is mixed with a reference signal from the master oscillator before the low pass filter (LPF). The filtered signal goes to the hold circuit. The output of the sample and hold circuit is filtered to remove both the sampling frequency and unwanted low frequency component. Then the filtered signals are amplified and sent for further processing (Evans and McDicken, 2000).
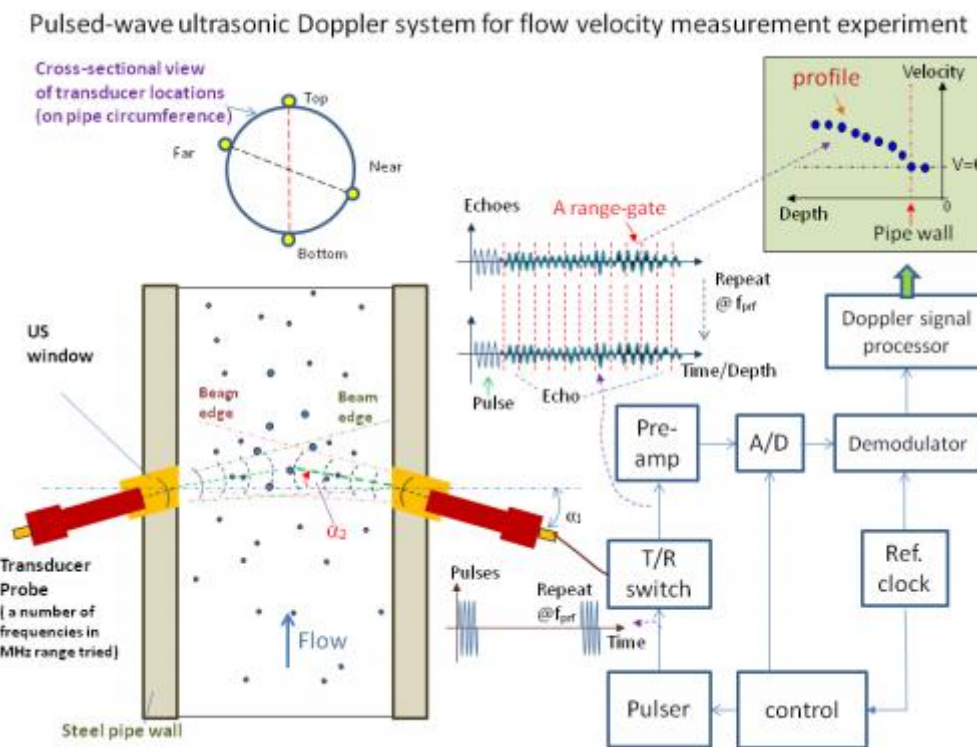
Figure 2-8 Schematic diagram of a PW ultrasonic Doppler flow measurement system (Huang et al., 2013)

In Figure 2-8, the operation of the PW ultrasound Doppler system is used for determining liquid flow velocity in an oil and water mixture. The PWDU Doppler is often operated at a constant PRF using an identical tone-burst so that the echoes from a stationary scatter or the interface will be a series of signals with a uniform time of flight, whereas, those echoes from moving scatters will produce signals with incremented times of flight. As indicated in the figure, only the scatters in the sample volume will be involved in the measurement.

The PWDU system is used to calculate the distance between two successive echoes by determining the times of flight Δt, of the two consecutive echoes (Christopher et al., 1996). The time of flight is directly proportional to the distance h between the transducer and the scatter. Also, the time between successive transmissions of the pulses is the pulse-repetition-interval ($T_{PR} = \frac{1}{f_{PR}}$ or PRI).

$$\frac{\Delta t}{T_{PR}} = \frac{2}{c} \frac{h}{T_{PR}} \tag{2-15}$$

where c is the speed sound in the flow, and the velocity of the flow along the axis of the is equal to the ratio of $\frac{h}{T_{PR}}$ and so equation (2-15) will be written as beam is $v_{flow} \cos\theta$ which

$$\frac{\Delta t}{T_{PR}} = \frac{2}{c} v_{flow} \cos\theta \tag{2-16}$$

The total phase, $\emptyset_n$, between an echo and transmitted pulse is the product of the total number of echoes received and the total transmissions frequency, f_0, of the master oscillator of an echo in which the period is 360°. Therefore, the phase difference between successive echoes of the same scatter is given by

$$\Delta\emptyset = f_0 \Delta t \tag{2-17}$$

Hence, equation (2-16) can written as:

$$\frac{\Delta\emptyset}{T_{PR}} = \frac{2f_0}{c} v_{flow} \cos\theta \tag{2-18}$$

Since frequency can be defined as the rate change of a phase then, $\frac{\Delta\emptyset}{T_{PR}}$ is the discrete measurement of a continuous frequency, f_d

where

$$f_d = \frac{2f_0}{c}\, v_{flow} \cos\theta.$$ (2-19)

Similarly to the CWDU system, the velocity of the flow will be

$$v_{flow} = \frac{f_d c}{2f_0 \cos\theta}$$ (2-20)

Therefore equations (2-18) and (2-11) are the same and are the exact form of the volume flow velocity and the frequency shift relationship.

The fact is that in the PWDU, the time of flight and the phase difference between the echoes are the representation of the continuous Doppler signal and the Doppler shift, which creates a problem on how to measure them, because the Doppler signals received at the transducer are a combination of echoes from both moving scatters and stationary scatters as well (Christopher et al., 1996). As a result, there are two types of PW architectures: non-coherent pulse Doppler and coherent pulse Doppler systems (Baker, 1970). The former uses a range gating to select the echo coming from a predetermined depth by sending a signal at an appropriate ultrasonic frequency amplifier to retain the amplitude components, whereas, the latter uses a replica of the transmitted signal to compare it with incoming echoes from the moving scatters since the moving scatters are both pulse and amplitude modulated. Most PWDU systems are of the coherent type and use the same coherent demodulation and signal processing in the same way as the CWDU systems but with the addition of sampling and filtering stages (Christopher et al., 1996). The PW Doppler schematic structure illustrated in the figure is of the coherent type.
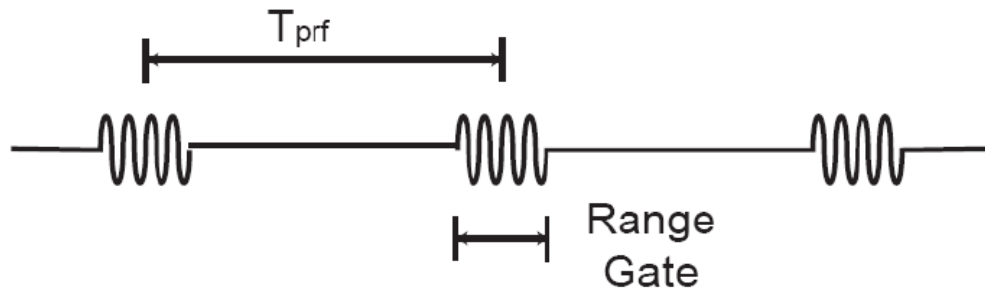
Figure 2-9 Short burst of transmitted ultrasound (Sleutjes, 2006)

Despite the PWDU having some advantages over the CWDU in that it is able to detect the range of the scatter, the benefit of measuring the range of scatters comes at the price of limitation on the maximum velocity that can be measured due to the Nyquist limit. The maximum velocity that can be measured from the frequency shift, $f_{d,max}$, is given by

$T_{prf} = \frac{1}{f_{prf}} \geq \frac{2.h}{c}$ and $\frac{f_{prf}}{2} \geq f_{d,max}$

Substituting, $\frac{f_{prf}}{2} \geq f_{d,max}$ into equation nnn

The maximum velocity is

$$v_{max} = \frac{f_{prf}c}{4f_0 \cos\theta}$$ **(2-21)**

Weaknesses of the PUD are:

1. Maximum measurable velocity is limited by pulse repetition frequency and the angle between the transducer and direction of the flow.
2. Velocity measurement may be underestimated if the angle is higher than 15 degrees even though the higher angle improves the sensitivity of the measurement system.

2.2.4 Difference between the CW and PW Doppler shift frequency

The fundamental difference between CW and PW systems is in the frequency attenuation of the Doppler signal. In CW systems, the signal returning from the target is a modified version of the transmitted signal and is being multiplied by the master oscillator; as a result it has become the difference between the transmitted frequency and returning frequency. However, in PW the received signal is affected by two events: first, it is either an incremented or decremented

version of the transmitted signal. Second, the fact that the target has moved either close to or far away from the transducer, means the consecutive received signal has experienced a time shift with respect to the change. As a result, there is a progressive change in the phase relationship between the ultrasound from the sample volume and the master oscillator. Certainly this is change that the demodulator detects.

On the other hand, there is a similarity between the CW and PW Doppler which shows that the spectrum of both signal systems is treated in the same way, because the basic Doppler equation applies to both CW and PW (Evans and McDicken, 2000).

$$f_d = f_t - f_r = (2f_t V cos\theta)/c \qquad \textbf{(2-22)}$$

The CW has an advantage over the PW in that it has limitless measurable velocity, even though it is not possible to detect the position of the scatterers with this method. On the other hand, the PW allows the determination of the position and velocity of the scatterers. However, the downside of the PW is the limitation of the measurable velocity by Nyquist's sampling theorem (Yamanaka et al., 2002).

2.3 Ultrasonic two-phase flow measurement methods

Ultrasonic flowmeters can be found in various shapes, sizes and methods of operation such as: clamp-on and wetted transducers, single and multiple paths, paths on and off the diameter, passive and active principles, contrapropagating transmission, reflection (Doppler), tag correlation, vortex shedding, liquid level sensing of open channel flow or flow in partially full pipes etc. Ultrasonic transmitters and transducers are commercially available.

The main aim of this section is to review the applications of ultrasonic techniques for the measurement of gas/liquid two-phase flow. Ultrasonic measurement of two-phase flow is an effective method and it is becoming increasingly common as researchers want to make use of its advantages, such as non-intrusiveness, clamp-on device on pipes and low power. The three ultrasonic techniques for flow for obtaining the two-phase flow parameters that have been reported are: transmission, ultrasonic reflection technique (pulse-echo and the Doppler shift) methods, and ultrasonic tomography.

2.3.1 Ultrasonic transit time method

Ultrasonic transmission techniques could be applied to multiphase flow measurements as pulse wave transmission types. Ux et al. (1985) developed an ultrasonic pulse transmission system to measure the volume fraction in air-water two-phase flow using a pair of pulsed transducers placed opposite to each other. They emphasised that the pulsed ultrasonic sensors have an advantage over their continuous counterpart, because the pulsed sensor is not affected by the harmful effects of standing waves and also pulsed ultrasonic sensors can effectively detect low gas concentration. Bonnet and Tavlarides (1987) presented an approach to determine the dispersed phase holdup of liquid-liquid dispersion by measuring the velocity of the ultrasound in suspensions, and emulsions (Xylene-water) using an ultrasonic pulse transmission time. Then, they suggested a time-averaged model that allows the estimation of the phase holdup from the total transmission time of the ultrasound pulses.

Moreover, Stolojanu and Prakash (1997) found in a multiphase flow comprising a solid phase (32 µm glass particles), a gas phase (compressed air) and a liquid phase (tap water) system, that both the transmission time and amplitude ratio vary proportionally with the solid concentrations. However, the gas bubbles have made the transmission time irregular while the relationship between the attenuation and phase volume remained proportional. Also, Mahadeva et al. (2008) studied the accuracy of ultrasonic transit time single phase flowmeters to determine factors affecting uncertainty. They found the relationship between the flow signal and separation distance between the transducers to be independent of the flow rates but dependent on pipe wall thickness and transducer frequency. Carvalho et al. (2009) explained an application of transit time ultrasound for measurement of gas-illiquid two-phase flow by using ultrasonic attenuation and experimental data. They found that attenuation can be related to the void fraction and between 4-6% of void fractions the bubble distribution was uniform. Eren (1998) presented an evaluation of the parameters affecting the accuracy of transit time ultrasonic flowmeters. The findings are that scatters or impurities in the flow affect the operation of the transit time flowmeter, and

then Eren recommended that the flowmeter should have multiple transmitters and receivers to be accurate. Therefore, in two-phase flow measurement, the transit time flowmeter operation would be hampered by the presence of the later phase or bubbles in the flow.

2.3.2 Ultrasonic cross-correlation

Ultrasonic cross-correlation methods can be implemented with either continuous wave or pulse wave ultrasound systems. Xu et al. (1988) applied pulse echoed ultrasound waves to implement a cross-correlation flow measurement system by amplitude modulation of the pulse echoed ultrasound wave passing through a gas bubble/liquid mixture. Schneider et al. (2005) demonstrated the principle of an ultrasonic cross-correlation flow meter using a continuous wave and developed an analytical model where they related the time delay measured by the meter to the mean velocity profile and statistical properties of turbulent pipe flow. The model was produced to predict the correlation and spectrum functions of the fluctuating velocity in a turbulent flow.
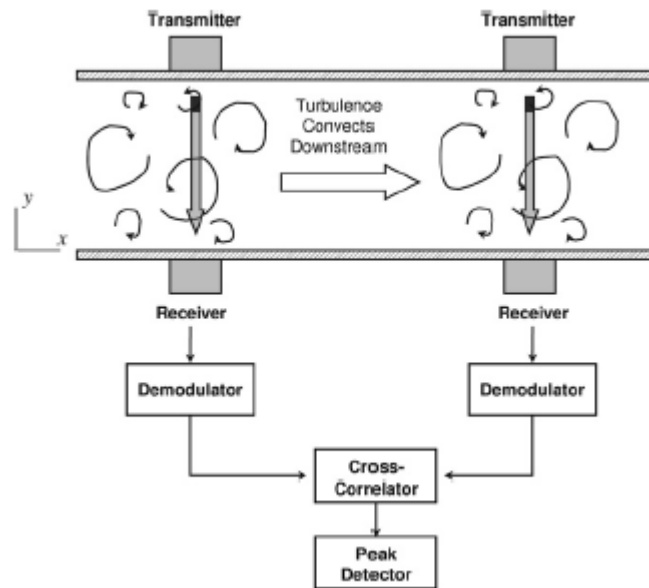
Figure 2-10 Schematic view of a cross-correlation ultrasonic flow meter applied to pipe flow with the volumetric flow rate (Schneider et al., 2005)

The procedure is based on the cross-correlation function, R, given by

$$R = \frac{1}{\Delta t} \int_0^{\Delta t} (x_{t-\tau} y_t dt)$$

(2-23)

36

where *tau* is the time delay, y_t is the downstream signal at time t, $x_{t-\tau}$ is the upstream signal at time $t - \tau$ and Δt is the time over which the integration is carried out (period during which the data are collected) (Asher 1997, Schneider et al., 2005). The flow velocity can be found by $V = L/\tau$ where L is the axial distance between the two sensing positions. That is to determine t_m is the time delay or interval required for the tags or footprint to travel along the flow for one sensing point to the second sensing position. Cross-correlation is best suited to monitoring two-phase flow where the phase component velocity and component distribution have an effect on the process performance (Xu et al., 1988).

2.3.3 Ultrasonic Doppler Shift Method flow measurements

In order to enhance the application of the ultrasonic technique for flow measurement, Brody et al. (1974) described the theoretical analysis of the CW Doppler flowmeter and the significance of the mathematical model to PSD of the ultrasound waveform. In addition, Cobbold et al. (1983) described, using a theoretical model of the CW flowmeter, the possible errors that could occur in the spectrum of the ultrasound wave as well as in the mean velocity measurement. By measurement of blood microcirculation using a high frequency Doppler system, Christopher et al. (1996) found that increasing the ultrasound frequency would lead to significant improvements in the Doppler flow measurement, such as an increase in Doppler frequency shift, a wider spectrum and better spatial resolution. However, these improvements come at the price of higher attenuation and availability of the high frequency transducers.

There are several applications of the CW Doppler ultrasound for multiphase flow measurement. Kouame et al. (2003) presented an application continuous wave ultrasound Doppler velocity measurement to two phase flow in pipes and proposed the use of high resolution frequency techniques to overcome the problem of coloured noise. Dong et al. (2015) developed a method of analysing the superficial velocity measurement of oil-water two-phase flow using a CW Doppler ultrasound model. The model is a generalised one for the flow velocity measurement; however, there is a need for hybrid sensors so that phase fraction measurement can be included in the flow velocity measurement (Dong et al., 2015). Fan et al. (2013) presented an application of CW Doppler

ultrasound velocity determination of the temporal liquid distribution in gas-liquid flow using short time Fourier transform (STFT) and autoregressive spectral analysis of the frequency shifts signal. Importantly, the CW Doppler flowmeter, if operated in the average velocity or volume flow, is similar to the electromagnetic flow meter which requires full illumination (Brody et al., 1974).

An early application of the PUD for flow measurement was described by Baker (1970) as the detection of the frequency shift of the reflected signals, which is representative of the mean velocity of the flow over a small area. The area is a function of the transducer bandwidth, ultrasonic beam dimensions, and transmitted pulse duration. The flow signal of the pulsed ultrasound can be manipulated by using a comb-type gate and sequential sampling to produce a flow velocity profile. The PUD flow measurement can be directly derived from other parameters of the flow, such as volume flow, stroke volume, and flow acceleration (Baker, 1970).

Morriss and Hill (1993) conducted experimental air-water measurements and a theoretical investigation of the potentials of using PUD for multiphase flow measurement. They described the PUD as an important instrument for production logging. However, they found that the PUD instruments were able to measure single phase flow with accuracy but for the air-water churn flow, the PUD did not represent the flow velocity and they recommended further studies.

In 2005, an innovative pulsed ultrasound system was applied for the measurement of gas-liquid two-phase flow using the ultrasound Doppler method by Murakwa. The new technique employed a multi-wave transducer which is basically two-in-one transducers (2 MHz and 8 MHz) in single sensor. The technology was used to measure flow velocity as well as positions of the scatters in the flow. However, there is need for further investigation to develop a method to separate the liquid velocity and bubble rise velocities.

Meanwhile, a commercial Doppler ultrasound velocimetry DOP2000 (Model 2030, signal processing S.A.) has been modified to measure multiphase flow. Both solid-liquid and gas-liquid have been measured in the experiment. The measurement application was first on the correction of the determination angle and measurement location by considering the effects of refraction and velocity

differences of the two phases. There is a need for further studies on the liquid-solid and gas-liquid with a high gas void fraction.

Rahammohan et al. (2014) presented two ultrasound Doppler transducers for multiphase flow measurement by placing the transducer diametrically on either side of the pipe flow. A complete velocity profile of the flow was obtained by adding two velocity profiles. In addition, the scatter velocities in the flow were estimated and used for flow regime identification.

Weaknesses of the PUD are:

1. Maximum measurable velocity is limited by pulse repetition frequency and the angle between the transducer and direction of the flow.

2. Velocity measurement may be underestimated if the angle is higher than 15 degrees even though the higher angle improves the sensitivity of the measurement system.

3. The optimum flow regime to be measured by the PW Doppler ultrasound is the bubbly flow as it is conductive for the Doppler system.

2.3.4 Ultrasound pulse echo technique

The ultrasonic method of measuring the film thickness, void fraction profile or liquid level measurement can only be done with the pulse wave ultrasound system as the continuous wave cannot be used to measure a range (Baker, 1970). Several pulse-echo ultrasonic techniques of two-phase measurement have been reported. A determination of the gas-liquid interface is one of the fundamental aspects in the measurement of both the liquid flow rate and the void fraction of two-phase flows which has been tried by Chang and Morala (1990). The pulse-echo technique uses a mismatch in the characteristic impedance of the ultrasound at the surrounding of the interface to detect the interface, as in equation (2-24)

$$a_r = a_i \times \left[\frac{\rho_2 c_2 - \rho_1 c_1}{\rho_2 c_2 + \rho_1 c_1} \right] \qquad (2\text{-}24)$$

This equation is the basis of the application of an ultrasonic technique to determine the location of a gas-liquid interface. Characteristics of the reflected wave are being influenced by the shape and size of the interface relative to the ultrasound wave length (Murai et al., 2010). Importantly, by error analysis it has

been found that the accuracy of a two-phase flow meter depends on the accuracy of the interface detection (Gonzalez et al., 2009).
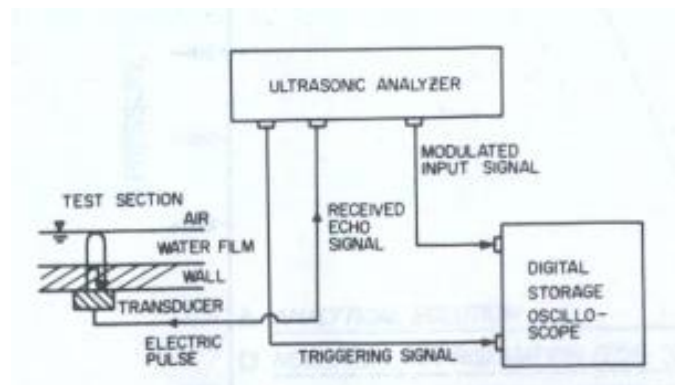
Figure 2-11 Basic Ultrasonic film thickness measurement setup (Chun et al., 1984)

Murai et al. (2010) have developed three categories of signal processing techniques used for analysing the echo signals received after pulses are reflected off the interfaces in air-water two-phase flows of a 40-mm plastic pipe. First, in the pulse echo ultrasonic technique for liquid-gas interface detection, which uses the reflection coefficient and in water-air interface, almost 99.9% of the incident wave reflected back.

Second, the interface can be detected at a layer with nearly zero-Doppler velocity along the measuring line; this situation occurs when there is 100% reflection (Murai et al.. 2010). Consequently, ultrasound reflectors (particles or others) in the standing wave produce no Doppler shift in spite of the velocity of the flow. This method is called the local Doppler velocity technique and has the following advantages: the detection efficiency is not dependent on the distance between the transducer and the interface and it is also quite a robust method due to the frequency domain used. But its disadvantages are: it can be difficult to separate the interface from the velocity distribution, due to the effects of small bubbles with curvature interfaces. However, these problems can be dealt with by signal processing filters. It is a suitable method for detecting ultrasound waves reflected off smooth interface and bubbles. In Figure 2-12, a standing wave has been created at the point of meeting of the incident and the reflected ultrasound wave. This property was used in interface detection by a local Doppler velocity technique (Gonzalez et al., 2009).

40
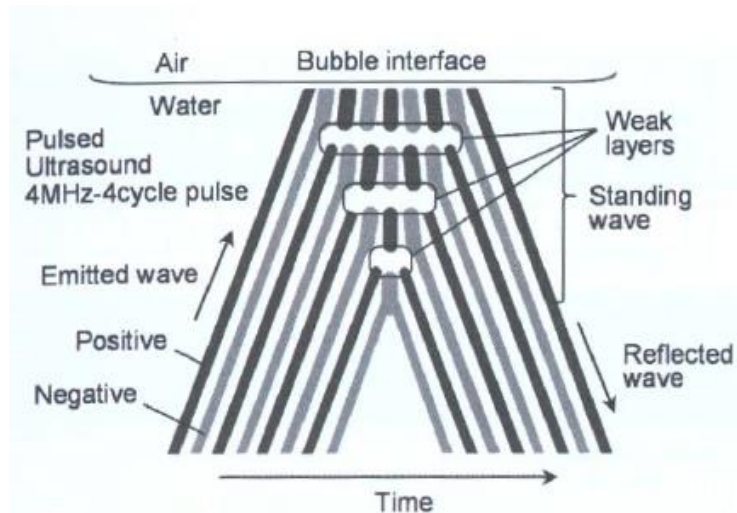
Figure 2-12 Schematic representation of ultrasound beam reflected at interface (Gonzalez et al., 2009).

The third method is based on the fluid kinematics, and the relationship between the interface S position on the measuring line, flow velocity v normal to the measurement line and flow velocity component u in the direction of measurement line is governed by this equation:

$$\frac{\partial S}{\partial t} + v\frac{\partial S}{\partial y} = u \qquad (2\text{-}25)$$

Where y represents the spatial coordinate in the direction normal to the measurement line. If one single ultrasonic transducer were to be used then the interface could not be determined, because one velocity component profile u is obtained. Alternative the variance of u in time can be used instead (Murai et al., 2010).

More importantly, an ultrasonic interface detection technique which uses a single transducer has the advantage that the cost of mounting arrangement is halved and transducer alignment is eliminated (Matikainen et al., 1986). However, a study conducted by Schmitt et al. (2012) found that reflection on the air-water boundary layer has some challenges depending on the size, shape and motion of the interface. For instance, for a smooth and steady air-water interface, the ultrasonic wave reflects symmetrically to the plane perpendicular boundary layer. No signal from the interface returns to the transducer for non-perpendicular at steady state, but a non-perpendicular disturbed air-water

41

boundary layer allows scattering of the ultrasonic waves which can be received by the transducer. These studies of the interface show that the single-sensing principle is not enough to capture the interface in all gas-liquid two-phase flows. Traditionally, the void fraction in two-phase flows is measured using an optical method with image processing or electrical probing, or other methods such as X-ray and electrical capacitance tomography. An optical method is not possible for existing pipelines, but ultrasound sensors can be used to monitor and control these facilities (Murai et al., 2009). Void fraction profiling is the ultrasonic measurement distribution of void fraction in a bubbly two phase flow using signal processing of the ultrasonic pulse scattering on bubbles. Chakraborty et al. (2009) introduced a new ultrasonic method for measuring the void fraction of two-phase flow using an ultrasonic sensor and twin signal processing methods based on a time series analysis technique: symbolic dynamic filtering and analytical signal space partitioning for void fraction measurements and identification of flow regimes. An algorithm was built on the method of symbolic dynamic filtering to analyse the ultrasonic pulse echoes reflected off the bubbles. The experiment was conducted using laboratory instruments and results were in agreement with the void fraction measurement derived for spatial measurement using conductivity probes.

Murai et al. (2009) developed two methods for determining the spatial distributions or void fraction profile in a two-phase bubbly flow. One of the methods of detecting the bubble interface was by applying two signal processing techniques: the echo intensity method and Doppler method. The second approach is a mathematical relationship which enables the reconstruction of the true void fraction along the path of the ultrasound pulse. Both of these two methods of determining the void fraction profile were applied to four different settings of bubbly flows. Zhai et al. (2013) studied the response of an ultrasonic pulsed sensor on oil-water two-phase in a vertical upward pipe. By using finite element calculation they found that ultrasonic levels are very sensitive to the concentration of the dispersed oil phase and the oil droplets can affect the transmission-type ultrasonic field.

2.3.5 Ultrasonic velocity profiling (UVP)

An accurate measurement of flow rate requires the velocity profile to be taken into consideration. Pitot tubes have traditionally been used to measure flow rates and fluid velocity profiles in power plants, but their installation requires plant shut down and system drain out in order to insert the Pitot tube (Tezuka et al., 2008). UVP is a non-invasive ultrasonic flow velocity measurement technique using pulse echoed ultrasound. It has its roots in medical application, as an external blood flow meter (Histand et al., 1973; Takeda, 1986). The UVP monitor was developed at the *Paul Scherrer Institut* (PSI) for both engineering and academic demands (Yamanaka et al., 2002). The UVP uses a pulsed ultrasonic echography which can be done with both an in frequency domain, by applying the Doppler principle, or time domain by using time domain cross-correlation (Sato et al., 2002; Takeda, 1991).

Takeda (1986) developed the UVP for general fluid to assess the suitability of the method with two configurations. A UVP consisting of an ultrasonic transducer placed on the external wall of the pipe at an angle (θ) transmits pulses and their echoes reflected from the particles of the flow are observed. The frequency of the reflected wave at any point is the Doppler frequency shift (f_{iD}) for the flow. The relationship between the Doppler shift and instantaneous fluid velocity is given by:

$$V_i = \frac{c f_{iD}}{2 f_0 \cos \theta}$$ 2-4

where V_i is the velocity value at instant I; c is the speed of the ultrasound in the fluid; f_0 is the basic ultrasound frequency; f_{iD} is the Doppler frequency shift for channel I; θ is the angle between the transducer and flow direction. It was found that UVP can measure instantaneous velocity profiles on a diameter of a pipe directly. So, the flow rate is calculated using the integration over space of the averaging velocity profiles.

Wada et al. (2013) have proposed a new method to determine the number of transducers in a multi-transducer UVP for accurate flow measurement. The multi-transducer UVP is particularly required for UVP at the downstream of a double elbow pipe. This method employed Fast Fourier transforms (FFTs) on the wave number of the profiles to estimate the number of transducers and it

43

has been verified with computational fluid dynamics (CFD) with a standard deviation of less than ±2%.
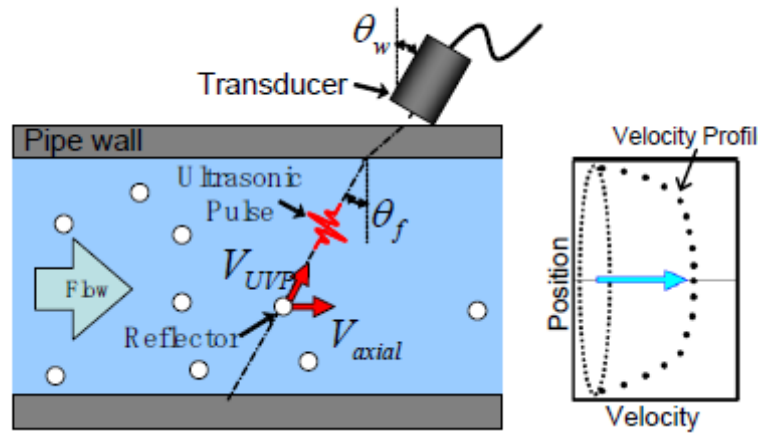
Figure 2-13 Ultrasonic propagation in the UVP method (Wada et al., 2013)

Importantly, an obvious a problem with the current method of UVP is that the maximum detectable velocity is based on the Nyquist sampling theorem (Takeda, 1991). There is another constraint for UVP in larger pipe diameter as maximum velocity decreases as the measurable depth increases. On the other hand, UVP is applicable to opaque fluids and is also a non-invasive technique. In addition, Sato et al. (2002) have presented a cross-correlation technique to determine the time difference between the echo signals of a two pulse emission. This technique improved the signal processing by allowing control over the echo repetition and reception, which would give high time resolution velocity profile measurements. So, an important extension of the pulse–echo technique is the development of the UVP technique as it can measure instantaneous velocity profile in time and position. The Nyquist sampling theorem which limited the maximum measurable velocity has been resolved through a signal processing technique known as ultrasound time-domain cross-correlation (UTDC). Therefore, a high time resolution velocity measurement could be obtained by the application of UTDC to the UVP method to obtain the velocity profile, which could readily be integrated into the flow velocity (Yamanaka et al., 2002). It was found that UVP can measure instantaneous

velocity profiles on a diameter of a pipe directly. So, the flow rate is calculated using the integration over space of the averaging velocity profiles.

2.3.6 Ultrasound and neural network

The ultrasonic technique, based on the principle of pulse-echo intensity, is widely used in gas/liquid interface detection and often the location of the interface is determined by measuring the time of flight of the reflected wave (Chang and Morala, 1990). Wada et al. (2006) presented an ultrasonic method of two-phase flow pattern recognition based on the measurement of the instantaneous echo intensity profile along the ultrasonic beam. They comment that the echo intensity of the flow is measured by the integral of the difference in energy of single phase flow and two-phase flow over the pipe diameter. The flow patterns from single phase flow to annular flow are identified by the statistical distribution of the echo intensity. Murai et al. (2010) developed a pulse-echo ultrasonic technique to determine instantaneous liquid-gas interface detection.

The pulse-echo technique of flow pattern identification is not completely a flow regime classification technique but an identification of the flow pattern itself (Jha et al. (2013). However, the authors recommended that more research work on the computational and experimental work will be required before the method can be deploying for industrial use. Another issue is that the ultrasound method applied is not intrusive but it is an invasive set up. Jha et al. (2013) extended the work of Chakraborty et al. (2009) and propose that the concept of the ultrasonic pulse echo to be implemented in a clamp-on set up, together with the symbolic dynamic filtering for industrial application. Wada et al. (2006) reported an application of flow pattern recognition based on the delay time strength of the echo signal of pulse echoed ultrasound under two phase flow. The pattern recognition was used to obtain instantaneous echo intensity profiles along the ultrasonic beam.

Despite the feasibilities of using the pulse-echo ultrasound for flow regime identification, the flow regime's identification is based on computational models. The computational methods for flow regime identification has employed sets of non-linear equations but often the equations are simplified. For practical

applications, the simplified equations are infrequently used because they require prior knowledge of several flow properties, such as pipe diameter and pipe thickness, which degrade over time (Meribout et al., 2010). The method of the pulse-echo ultrasound is limited in liquid flow velocity information due to the restriction on the maximum measurable velocity using pulse wave ultrasound by the Nyquist criterion (Evans and McDicken, 2000).

Ultrasound Doppler flow sensors which use a continuous wave of ultrasound signals also have a great potential for achieving non-invasive flow velocity measurement. The techniques for using continuous wave ultrasound have existed in the medical ultrasound system. The techniques use frequency shift representing the flow velocities to develop methods to predict multiphase flow regimes (Übeyli and Güler 2005). In multiphase flow measurement, Kouame et al. (2003) presented an application of CWDU velocity measurement to two phase flow in pipes. They proposed the use of frequency resolution techniques to overcome the hindrance to the velocity profile measurement by the presence of coloured noise which introduces a significant obstacle to classical frequency estimators. Pulse echo ultrasound techniques for two-phase flow measurement have limited liquid velocity information due to the restriction on the maximum measurable velocity using pulse wave ultrasound by the Nyquist criterion (Evans and McDicken, 2000). Also, the characteristics of the reflected wave are being influenced by the shape and size of the interface about the ultrasound wave length (Murai et al., 2010).

Yeh et al. (2001) reported on an advanced ultrasonic flow meter which comprises multi-path transducer with pattern recognition to predict the presence and chances of flow fields. Data from CFD and experimental results were used to train the flow pattern algorithm of the flow field recogniser. The algorithm was fed into the ultrasonic flow meter. In addition, it was claimed that flow patterns of various flow can be identified using this technique.

2.3.7 Hybrid systems (Ultrasound and another sensor combination)

In multiphase flow, ultrasonic techniques have the potential for both phase velocity and phase fraction measurement, although they have not been applied to commercial three-phase flowmeters yet (Thorn et al., 2013). However, the

ultrasonic meters' performance is affected by factors such as the number of scatters per unit volume, the distribution of scatters and their velocity profile across the pipe. Also, the ultrasonic attenuation is greatly dependent on the flow regime of multiphase flows and the input signal frequency of the transducer (Rajan et al., 1993). Recent developments in other ultrasonic techniques for multiphase flow measurement have progressed considerably.

Usually, the phase fraction and phase velocity measurement are measured by at least two devices or two independent measurements of one device. This approach is achieved by separately metering the phase flow rate and the phase fraction (Tan et al., 2015). Several combinations of two sensors for gas liquid flow measurement have been reported in the literature. Xing et al. (2014) used a combination of ultrasonic gas flow meter and Coriolis flowmeter for metering the gas-liquid two phase flow of low liquid loading. Various models to represent the gas and liquid flow rate, density of mixture flow are used to obtain the coupling models for the two instruments. A theoretical method of data fusion of an electromagnetic (EM) flow meter, electrical resistance tomography (ERT) and two-phase flow models has been developed to improve the accuracy of the EM meter for the measurement of gas-liquid slug flow in a vertical pipe. The feasibility of a two-phase flowmeter was achieved by using simulation measurements of the averaged velocity, liquid flow rates and gas void fraction. Obviously, this approach requires invasive sensors and relies on the electrical conductance of the fluid (Deng et al., 2011; Xing et al., 2014). Similarly, Meng et al. (2010) presented an experimental combination of a liquid (Venturi) flowmeter and ERT sensor for air-water two-phase flow measurement. Three aspects of the flow measurement techniques were acquired with the ERT sensor: the flow regime identification, the void fraction using the conductance signal and void fraction model, and lastly, establishing a mass quality-void fraction correlation from the void fraction results. The gas-liquid mass flow rate is measured with the Venturi differential pressure across the tube and the mass quality. Experimental results show the method developed has been accurate within the data tested but both mass quality and fluid flow rate measurement rely on correlations. A chapter of this thesis is on two-phase flow measurements

with ultrasound sensors and gamma densitometer techniques and an overview of those methods is given in that chapter.

2.3.8 Ultrasonic Tomography for Two-Phase Flow

In most industrial processes involving two phase flow, ultrasonic tomography is preferred over other techniques such as electrical resistance/capacitance tomography. Ultrasonic tomography is primarily concerned with reconstruction of the distribution of gas/liquid over a cross section of a pipe based on the arrival or non-arrival of the transmitted pulse at a fixed time. It is often used for flow regime identification and the measurement of void fraction cross section on multiphase flow. Ultrasonic tomography is non-invasive, non-intrusive and it allows measurement of real-time data without interruption. There are three principles for implementing ultrasonic tomography: (i) transmission mode, (ii) reflection mode and (iii) diffraction mode.

Xu and Xu (1998) have developed an ultrasound tomography for gas-liquid two-phase flow based on binary logic operation and a method of time-probation along a straight line for flow regime identification. The identification requires a real time measurement which involves electronics and a fast image reconstruction algorithm. Rahim et al. (2007) have developed a UT that uses an image processing technique for executing real time image reconstruction at 10 frame/seconds. It is an application of the transmission-mode tomography; i.e. a non-invasive UT using 16 transducers placed round the pipe and a reconstruction algorithm with fan-shaped beam for scanning geometry.

Ultrasonic tomography has a few limitations as there is a tendency that the acoustic wave propagating in gas/liquid interface could be lost because of acoustic wave inability to penetrate the gas/liquid interface in the transmission mode. Also maximum speed to capture an image is limited by the depth of the beam, i.e. the system sensitivity and resolutions are determined by the number of transducers and signal processing used. The spatial imaging error would be reduced with increased number of transducers which can measure the void fraction and identify the flow regime but it was tested on static experiment to gauge performance. Therefore, further investigation is required to extend its application to industry standards (Rahim et al., 2007).

2.4 Ultrasound Signal processing methods

The Doppler signals contain the velocity information and they are a stochastic process that is not stationary signals. So, the velocity related information is extracted from the Doppler signals by determining their frequency contents (spectrum). The Doppler signals were digitized for predetermined intervals at a fixed rate and stored on disk. This discrete record is transformed from the time domain to display time varying frequency (spectrum) of the Doppler signal which enables the assessment of velocity waves and detection of spectral broadening associated with lesion-induced flow disturbance (Fish et al., 1997). Methods of extracting the required frequency from the sampled digitised Doppler signals are discussed below (Morriss and Hill, 1991).

2.4.1 Spectral estimations and signal analysis

The objective of the processing is to evaluate those waveforms of the reflected signal using spectral analyses techniques to determine the shape and speed of the flow. It is difficult to separate the ultrasound Doppler signals into the flow regimes using the values of the standard waveform indices, because there are noticeable overlaps in their sonographs. Whenever there is a need to extract a power spectrum for a Doppler signal, it has to be transformed into a frequency domain so as to produce a spectrum estimator and FFT is the most popular spectrum estimator (Evans and McDicken, 2000). The FFT method has an advantage in the manner in which the spectrum is produced for the Doppler signal. Especially, the real time Fourier analysis is able to visualise the complete Doppler spectrum rather than extract a single numerical parameter (Jones, 1993).

Bergland (1969) has summarised the merits and demerits of using an FFT for signal analysis. The advantages are 1- computing a power spectrum as a function of time, 2- digital filtering by convolution of two time series, and 3- correlation between two signals. On the other hand, some drawbacks of the FFT are 1- aliasing: this problem arises when signals of the high frequency component of the time domain pass on as low frequencies when the sampling rate is low. However, this problem can be remedied by adhering to the Nyquist's criterion. 2- leakage: windowing manifests itself as "leakage" in the spectral

domain, i.e., energy in the main lobe of a spectral response "leaks" into the side lobes, obscuring and distorting other spectral responses that *are* present. These drawbacks of the FFT have prompted an examination of alternative techniques of analysis (Fish et al., 1997).

Time-frequency representation of a signal using STFT is known as a spectrogram. It is created by dividing the signal into small segments and then FFT is applied to each of these segments. These segments are further multiplied by window frame so that the transformed signal is zero outside the window; however, this limits the resolution of the spectrogram. As a result, alternative methods of spectral analysis are to be explored. The Welch's method, which is based on the FFT, was used for the spectral analysis of the two-phase flow Doppler signals. The signals are divided into overlapping segments; each data segment is windowed to compute the periodgrams and then the average of the periodograms is plotted.

Wavelet Transforms (WTs) Methods

In the STFT method, the type and width of the analysis window are fixed in the entire time-frequency representation; the resolutions are unchangeable. However, the time and frequency resolution of the wavelet is not fixed over the entire time-frequency representation. Therefore, the time resolution becomes better at higher frequencies and the frequency resolution becomes at low frequencies. The time-frequency resolution depends on the choice of the mother wavelet (Zhang et al., 2003). The Doppler signal from the ultrasound analysis is highly non-stationary and STFT is not the appropriate tool to do the analysis (Keeton and Schlindwein, 1997).

WTs represent the signals in terms of both scale and space at once so as to view fluctuations in various patterns of two-phase flow. This representation shows the measure of the energy contribution of each spectrum (Farge, 1992). WTs have been successfully utilised in the study of two-phase flow classification (Nguyen et al., 2010). Kulkarni et al. (2001) applied wavelet to measure the fraction of gas in a bubbly vertical flow. Wu et al. (2001) used a wavelet theory for filtering and analysing the signals of pressure in an oil–gas–

50

water multi-phase flow, and Shang et al., (2004) used a wavelet signal extraction technique to investigate the instability of two-phase flow.

The idea of signal decomposition using the DWT is well established. However, its usefulness lies in its ability to manipulate the wavelet coefficients to identify the characteristics of the signal as distinct from the original time signal (Soltani, 2002). In this work, decomposition of the ultrasound Doppler signal from the two-phase flow was carried out using the DWT. It is important to choose an appropriate wavelet and the number of decomposition levels in the analysis of the signal using the WTs (Übeyli and Güler, 2005). The Doppler signals of the flow were decomposed continually until all the dominant frequency ranges were viewed. The computation of the DWT of the coefficient was done using the MATLAB software package (Misiti *et* al., 1996). In this thesis, wavelet transform is used to analyse the two-phase flow Doppler signal to generate features which are then used as inputs into the neural network models.

Alternative ("Modern") Spectral Analysis Methods

The most prominent limitation of FFT is that of frequency resolution, i.e. the ability to distinguish the spectral responses of two or more signals. The fact that some defects of FFT are quite obvious has meant searching for and application of alternative methods to spectral analysis. Modern methods of spectral analyses use a digital filter to model whose input is white noise. The characteristic of the filter (estimated coefficients) is adjusted to obtain a match with the autocorrelation of the function of the signal of interest and filter output. The signal spectrum will have the same shape as the frequency response of the signal**.** Modern spectral analysis techniques are named according to the filter used and the order, such as AR (autoregression), MA (moving average), and ARMA (autoregressive moving average) etc. (Fish et al., 1997).
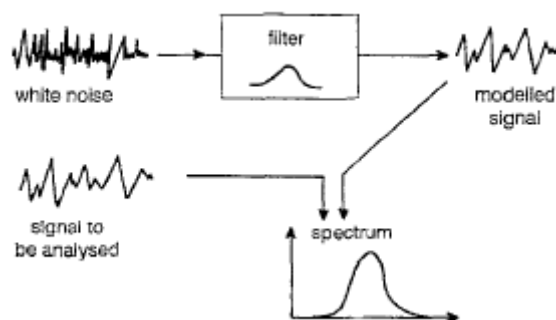
Figure 2-14 Concept behind parametric or model-based spectral estimator (Fish et al., 1997)

The Doppler signal from the ultrasound analysis is highly non-stationary. So an appropriate tool is necessary to undertake the analysis (Keeton and Schlindwein, 1997). More importantly, in order to increase the resolution of the frequency shift, which is proportional to the flow velocity, a longer time duration is needed. Besides, the signal duration is inversely proportional to the frequency of the resolution, and thus the resolution of the velocity measurement (Morriss and Hill, 1991). This means that the stationary time domain methods such as FFT or STFT may not be valid. The spectral components resulting from a large interval will be stretched as a result, a reduced time resolution. The alternative method, model-based technique, autoregressive AR is better than the STFT, but its own drawbacks are that the length of the stationary interval determines the time and frequency resolution of the time-frequency representation, and also lower model orders are selected for reduced time interval (Zhang et al., 2003).

The accuracy of Doppler shift estimation is governed by the uncertainty principle about the product of time duration and frequency bandwidth, as:

$$\Delta t \Delta f \geq 1/(4\pi)$$

(2-26)

In a time-frequency resolution, the time-frequency is defined as a rectangle which has an area as $\Delta t \Delta f$ which satisfies Heisenberg's uncertainty principle-equation (3-3), i.e. the smaller the value of the $\Delta t \Delta f$ product, the higher the time-frequency resolution (Matani et al., 1996), where: Δt = time duration or radius of the time-domain window and Δf = bandwidth of a generic function or radius of the frequency domain.

Previously, in (Fan et al., 2013) a continuous wave ultrasound Doppler flowmeter was used to determine the liquid distribution in slug flow. The frequency shift of the ultrasound signal was estimated using AR and STFT to obtain the velocity distribution in both liquid slug and film velocities. However, in order to increase the resolution of the frequency shift, a longer time duration is

needed. This means that the stationary time domain methods such as FFT or STFT may not be valid. An alternative is a model-based technique that is better than the STFT. But this has its own drawbacks, because the length of the stationary interval determines the time and frequency resolution of the time-frequency representation.

The HHT is adaptive and can provide better time and frequency resolution to the ultrasonic measurement. The HHT has been applied to the processing of two-phase flow signals such as in: differential pressures (Ding et al., 2007), Doppler signal (Ye et al., 2008). Ding et al. (2007) used the HHT method to determine the energy distribution of gas-liquid two-phase flow from pressure fluctuation signals.

In this study, the application of the HHT has allowed decomposition of the ultrasonic signals into their intrinsic mode components (IMFs) (Huang et al., 1998). Therefore, as an alternative way to estimate the slug flow parameters, from the ultrasound signal, the IMFs are further analysed for the measurement of mean flow velocities and to obtain distinct signal characteristics of the slug flow.   The performance of the ultrasonic method of determining the slug parameters is assessed against reference conductivity probes slug parameter measurements.

2.4.2 Time domain estimations

Time domain signal processing is a major technique for estimating the displacement of scatterers in flow measurement processes such as time domain correlation in flow velocity measurement. To illustrate, 'at time $t = t_0$ a scatterer is located in position X and at time $t = t_0 + T$ that scatterer has moved to a new position Y. Therefore the speed is $(Y - X)/T$ where Y is the time difference between the change in position by the scatterers (Foster et al., 1990b). This is a key feature that distinguishes it from the Doppler technique which estimates the velocity of the scatterers (Hein and O'Brien, 1993).

Autocorrelation techniques have also been suggested to estimate the mean frequency of the Doppler spectrum (Allam and Greenleaf, 1996). Spectral Doppler and autocorrelation are called *narrow-band* techniques. Similarly, Foster et al. (1990a) have developed a method of blood flow velocity profile

measurement using time domain cross-correlation of parallel ultrasound echoes. Cross-correlation was used to obtain the time difference between the transmissions of two parallel pulses. Subsequently, the difference was used in calculating the velocity profile of blood flow. This technique was extended by Yamanaka et al. (2002) to calculate a novel velocity profile measuring technique by using ultrasonic time domain cross-correlation.

In multiphase flow measurement, time-domain is either used for time delay analysis or time series analysis. Roosnek (2000) developed a novel digital signal processing method for the determination of pulses' transit times in ultrasonic gas flow measurement using an application of least square method recorded on received ultrasonic pulses. In addition, an effective algorithm for reduction or elimination of cross-talk between transducers across the pipe is presented. Jin et al. (2003)(Jin et al. 2003) have used non-linear time series analyses for conductance signals obtained from monitoring conditions, such as chaos, fractal and Kolmogorov entropy to characterise flow pattern in a vertical upward flow. They concluded that non-linear time series analysis is a valuable tool for flow enhancing, flow pattern identification.

Cross-correlation methods can be implemented with either continuous wave or pulse echoed ultrasound based. Schneider et al. (2005) demonstrated the principle of ultrasonic cross-correlation using continuous wave. Also, Xu et al., (1988) applied a pulse echoed ultrasound wave to implement a cross-correlation flow measurement system by amplitude modulation of the pulse echoed ultrasound wave passing through a gas bubble /liquid mixture.

2.4.2.1 Echo intensity measurement for pulse echo ultrasound

An echo intensity technique is applied to the echo signals to measure the distances of the two-phase flow interfaces and then converted into liquid level measurement. However, the received echo signals contain the desired interface signal, noises and multiple reflections. Therefore, the echo intensity technique signal processing must include a mechanism for allowing only the signals from the interface by limiting the computed to the pipe and all other repetition echo signals are ignored (Masala, 2004). This study investigates the technique of

using of a single beam pulse-echo ultrasonic system to measure the liquid layer thickness of a gas-liquid two-phase flow in a horizontal pipe.

2.4.3 Neural Networks

Liu et al. (2001) suggested that the Neural Network (NN) has become an investigative tool in pattern recognition, identification, classification, speech recognition and also the application of a multi-layer perceptron and a radial basis function model for mass flow error in Coriolis mass flowmeters under two phase flow.   Also, Luntta and Halttunen (1999) have applied NNs to investigate the velocity profile dependence of ultrasonic transit time flow meters. Specifically, feed-forward NNs can provide a non-parametric framework for representing non-linear functions, while single layer NNs with linear neurons have been used for the computation of errors in piping configurations.

ANNs' attactiveness come from their information processing characteristics, such as the ablity to model non-linear relationships between input variables and required ouput by function approximation methods, and also in their capabilties to identify complicated relationships for non-linear mapping using pattern recognition algorithms (Basheer and Hajmeer, 2000; Hernández et al., 2006). In multiphase flow measurement, pattern recognition is used for flow regime identification/classification in which input variables are classified as a member of a predifined flow regime. In order to obtain objective flow regimes identification, ANNs are often preferred over statistical methods because of their fast responses and simplification (Mi et al., 2001a).

Also, ANNs have good performance on pattern recognition due to their efficiency and available learning algorithms (Jain et al., 2000). With regard to flow regime classification, the ANN has advantages over other analytical tools such as Expert System and Clustering. The former requires prior information on the flow regime which could be affecting its objectivity; similarly, the latter may not affect performance accurately due to its poor handling of transitional data points (Hu et al., 2011). Usually, the process of NN development is by training the network to recognise the measurement error in training data and then the network tests on another set data. If the trained network is accurate enough then it is implemented for online measurement for prediction error correction

(Liu et al., 2001). More importantly, NNs would offer a non-linear mapping between the ultrasound input signals and the predicted flow regimes. So the use of the ANN avoids the need for calibration of the multiphase flowmeter (Figueiredo et al., 2016).

Seleghim (2010) developed a numerical simulation measurement of interfacial area and volumetric fraction in two-phase flow using an acoustic signal and ANN to investigate the feasibility of the application of the ultrasound system for a clamp-on flow measuring system. They found that the trained ANN models were able to estimate the values of the volumetric fraction and the interfacial area. Similarly, Figueiredo et al. (2016) employed an ultrasonic methodology based on pulse wave ultrasound transducers which operates on the principle of signal attenuation detection. The ultrasound signal attenuation was analysed and incorporated with ANN for flow pattern detection and void fraction measurement. They suggested that the flow regime's identification in the 2-in pipe was limited to bubbly flow and slug flow only. The technology presented is appropriate for the detection of the GVF and flow regime determination in multiphase flow. However, there does not appear to be any consideration of the flow regimes, except for the bubbly flow and slug flow. According to the authors, studies on the two-phase flow regimes classification using a clamp-on continuous wave Doppler ultrasound and neural network have not been reported in the open literature.

Therefore, in the ultrasound and neural network application, the waveform indices' values were not used as inputs but rather two feature extraction techniques were performed to generate the inputs to the ANN (Übeyli and Güler, 2005). Four different methods of spectral analysis of the Doppler signal were used to view the various signals of the flow: FTT, STFT, PSD and WT.

2.4.4 Models for Hybrid sensors for two-phase flow measurement

A combination of two instruments to measure two-phase flow will necessitate the use of models. Fischer (1994) explained the application of a Pitot tube single phase flow measurement model into a two-phase flow model. Subsequently, a phase slip model of unity ratio was substituted into the model to obtain a two-phase flow mixture flow model of the total mass flow. The

mixture flow model was used for the gas-liquid flow. However, the Pitot tube is an intrusive instrument and it incurs some disruption to the flow. Huang et al. (2005) showed that the single phase flow model of the Venturi flow meter and homogeneous model of gas-liquid two-phase flow can be used to obtain the parameters of the gas-liquid two-phase flow measurement. The combined models take the input of the void fraction from an ECT measurement and differential pressure measurement from the Venturi flow meter. The investigation demonstrated is on a pilot scale and further study of the methodology was recommended.

Similarly, evaluation of the no slip model to achieve a combination of two sensors' measurements to obtain two-phase flow is interesting. A combination of a Venturi flow meter and vortex flow meter measurement of gas-liquid two-phase flow was achieved at low void fraction for the no slip model. The methodology assumed that the mixture density was the sum of the fractional densities of the constituent phases which was then substituted into the mas flow measurement equation of the Venturi flow meter. The approach was able to provide measurement with reasonable accuracy but it is limited to the low void fraction.

An experimental application of the combination of the two instruments in which the effect of flow regime was taken into the consideration was described by (Meng et al., 2010). A Venturi flow meter and ERT sensor for the measurement of gas-liquid two-phase flow was achieved and real time identification of the flow regimes with the ERT was incorporated into the models of the two-phase flow. They found that the Butterworth void-fraction-mass quality and Collins Correlation for two-phase flow are the best performing models.

Interestingly, there are other applications of the hybrid sensor which do not include pressure based sensors. A simulation based fusion model of measurements from electromagnetic flow meter and ERT was explained by Deng et al. (2011). The result of the simulation was verified by theoretical analysis of slug flow measurement. This investigation has laid a good foundation for further studies to test the methodology experimentally as both of the sensors are non-intrusive. Another, non-pressure sensors-based

combination of ultrasonic gas flowmeter and Coriolis flow meter for two-phase flow measurement for experimental measurement of horizontal wet gas flow was described by Xing et al. (2014). A coupling model which uses the measurements of the ultrasound flow and the Coriolis flow meter as input was developed with the use of two sub-models from the Coriolis flow meter for mass flow measurement. It has been found that the method achieved has a very high accuracy under the conditions tested but it was tested on single pressure data. So there is a need for further investigation and further study for validation.

2.5 Summary

Gas/liquid two-phase flow is a very complex process and yet it is widely being encountered in a variety of processing industries, e.g. petroleum, chemical, nuclear reactors, etc. Two phase flow measurement is important for predicting liquid holdup, pressure gradient and flow patterns. For instance, changes in the flow rates of wells producing into a flow line could change the liquid holdup. The effect is overloading of the processing equipment. Other phenomena that hamper two-phase flow metering are slippage between phases, change of flow regime and gas-liquid interface characteristics – smooth or wavy (Beggs and Brill, 1973).

In multiphase flow, the ultrasonic meters' performance is affected by factors such as the number of scatterers per unit volume, the distribution of scatterers and their velocity profile across the pipe. Also, the ultrasonic attenuation is greatly dependent on the flow regime of multiphase flows and on the input signal frequency of the transducer (Rajan et al., 1993). However, ultrasonic techniques have the potential for both phase velocity and phase fraction measurement, although they have not been applied to commercial three-phase flowmeters yet (Thorn et al., 2013). Recent developments in other ultrasonic techniques for multiphase flow measurement have progressed considerably.

Neural networks application is based on real time analyses and it could be effective in recognising and removing or reducing common ultrasonic flow measurement problems: cross talk between transmitting and receiving transducers. Waveform analysis is indispensable in ultrasonic flow

58

measurement systems and pattern recognition processes can be used to complement it.

Multiphase flow rates measurement using ANNs is often implemented using a multilayer perceptron network by training the network to establish a relationship between inputs and output to estimate each phase flow rate. ANNs are popular for pattern recognition due to their efficiency and available learning algorithms (Jain et al., 2000).

3 Application of CW Doppler Ultrasonic technique

3.1 Introduction

Two-phase slug flow is the most common flow regime in a horizontal flow pipe. It is intermittent, transient and its hydrodynamic parameters are difficult to predict. Determinations of the hydrodynamic parameters are required for many design calculations in pipes and downstream equipment (Romero et al., 2012). Both non-contact and contact types of sensor are being used to measure parameters of the two-phase flow. The contact instruments include conductivity probes and hot-wire film measurement both of which have the ability to identify flow patterns and liquid holdup measurement. But the contacts measure requires the sensor to contact the fluid and non-contact techniques employ sensors such as ultrasonic, optical and radiation techniques. The optical methods, such as PIV and Laser Doppler sensor, have good capabilities to determine the flow structure in terms of spatio-temporal resolutions but they have the disadvantage of requiring a transparent measurement section and are also expensive (Rajan et al., 1993).

The HHT has been applied to the processing of two-phase flow signals of many sensor fluctuation signals, such as differential pressures (Ding et al., 2007), electrostatic (Hu et al., 2011), Doppler signal etc., and is considered to be potentially viable for non-stationary signal analysis. Besides, the HHT, unlike the other Fourier based method, is not affected by the uncertainty principle which limits the time and frequency resolution. Thus, it can be applied to provide high time and frequency resolution (Ye et al., 2008).

In this chapter the continuous wave ultrasound Doppler sensor is utilised to compare the effectiveness of the traditional signal process based on Fourier transform and the modern adaptive of the HHTs to measure liquid flow velocity and characterise four two-phase flow regimes in horizontal flow.

The velocity information of the flow is measured by the Continuous Wave Ultrasonic Doppler (CWUD) using the HHT method of signal processing. The Doppler ultrasound signals were obtained from experiment two-phase flow measurement system. The flows tested were single phase water flow and two-phase gas-liquid flow, including flow regimes such as slug, stratified wavy,

stratified smooth and bubbly flows. The application of the HHT has allowed decomposition of the ultrasonic signals into its intrinsic mode components (Huang et al., 1998). These components were further analysed for mean frequencies of the flow. Distinct signal characteristics for each of the four flow regimes investigated were obtained, which can be used for flow regime identification (Ding et al., 2007), and estimation of two-phase flow parameters such as slug frequency and bubble lengths. The HHT is reported to be considerably more promising than the Fourier based methods of signal analysis. It is adaptive and can provide better time and frequency resolution.

3.2 Experimental Setup and Procedures

3.2.1 Air-water supplies

Air supply into the rig is provided by a compressor of a Free Air Delivery system to a receiver tank of 2.5m^3. The provision of the receiver tank between the rig air supply and the air compressor stabilises the air supply system (Al-Lababidi, 2006). The flow rates of the air are controlled by hand operated valves and they are measured at the inlet of the pipe air supply pipeline using a gas turbine flow meter (QFG 25B/B/EP1, Quadrina) before the injection point of the rig where the air is mixing with water. Pressure and temperature gauges are attached near the air flow meter so as to compute the standard volumetric flow rate of the air.

The water is pumped into the loop from a storage tank of $2m^3$ capacity using a Worthington Simpson centrifugal pump with a maximum flow rate of $40m^3/hr$ and discharge pressure of 5bar(g). The flow rate water is controlled by regulating hand operated manifold valves (V-3 and V-4). The regulation of the manifold valves allow some portion of the water flow to return to the tank and sends the desired flow rate into the rig and then it mixes with air at the mixing point before the test section.
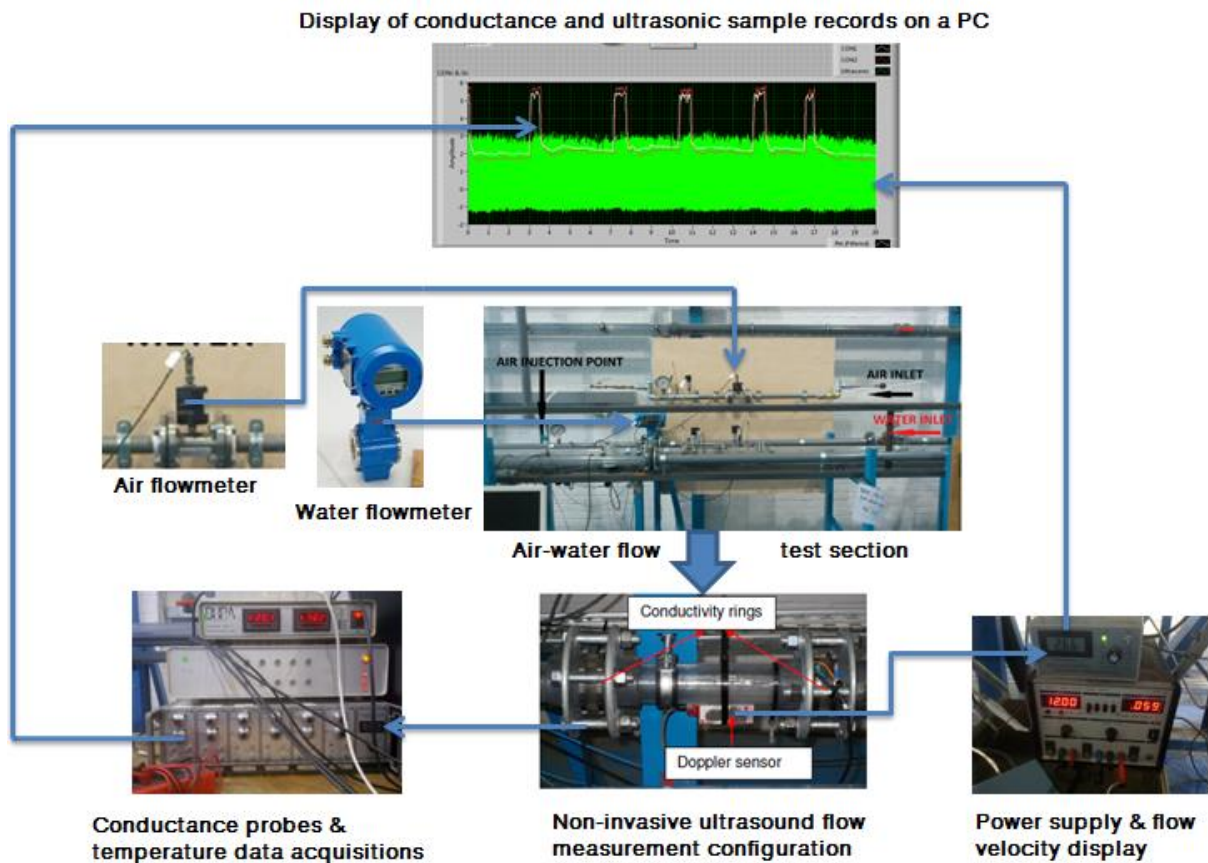
Figure 3-1 Part of air-water test rig showing the instruments used in conducting the experiment

3.2.2 The test section of the horizontal flow pipe test

The test section is made of Perspex pipe for observation and it was installed into the rig using flanges at 21m (420 hydraulic diameters, *D*) downstream from the water supply tank. The 420 *D* length available pipeline in the experimental apparatus before the test section was thus enough for guaranteeing the development of the various flow regime profiles of the horizontal two-phase flow. Two conductance probes, static pressure transducer, ultrasound Doppler sensor, ultrasound pulse echo sensor and temperature sensor (thermocouple wire) were installed in the test section.

3.2.3 Ultrasonic Doppler sensor

The ultrasound Doppler flowmeter is a non-invasive instrument which is used for making the measurement entirely from the outside of the pipe. It is a commercial ultrasound Doppler sensor (DFM2 United Automation Ltd UK) with an operating frequency of 500kHz. The transducer of the sensor has two

piezoelectric crystals: one for generating the sound wave and receiving the ultrasound reflected by the scatters in the fluids such as air bubbles or particles in the flow. The ultrasonic of the flowmeter is based on continuous ultrasound waves which propagate into and are reflected back to the sensor by scatters in the flow.

The operation of the ultrasound Doppler flowmeter is by transmission of high frequency ultrasound by the sensor through the coupling gel and pipe into the fluid. Some portion of the ultrasound waves is reflected by the scatters in the flowing fluid back into the receiving element of the sensor. This sending and receiving ultrasound causes a Doppler frequency shift of the ultrasound waveform which is directly related to the velocity of the fluid.

Therefore, the ultrasound Doppler is basically measuring the frequency shift, processing the signal and calculating the flow velocity. The flowmeter has a digital display which indicates the flow velocity measured by the flowmeter in feet per second. Doppler flow meter operation is dependent on the presence of scatters in the flow, either as gas bubbles or solid particles. The basic components of a Doppler flow meter system are shown in the Figure 3-1and the relationship between the velocity of the scatters v and the Doppler shift f_d is given in equation (3-1 (Sanderson and Yeung, 2002).

$$f_d = 2f_t \frac{v}{c} \cos \theta \qquad (3\text{-}1)$$

where v = average flow velocity, c = velocity of sound in the fluid,f_d = Doppler shift frequency,θ = angle between ultrasound beam and flow velocity and f_t = ultrasound transmitted frequency.

The sensor of the ultrasound Doppler can be easily fitted on an existing pipeline without breaking into the pipe and it is independent of the pipe thickness and fluid pressure (UAL, Ltd). It is suitable for pipes made of metal, plastic, ceramic etc. In this study the sensor was clamped onto the PVC pipe with the aid of a Jubilee Clip. The recommended sensor location is at least 10 pipe diameters away from valves, bends to prevent incorrect velocity measurement due to swirl, cavitation and turbulent eddies.

The manual supplied by the manufacturer of the ultrasound Doppler flowmeter contains a recommendation for applying a good acoustic coupling between the face of the sensor and the pipe surface at the location where the sensor would be clamped on. In the study, the ultrasound couplant is a gel containing propylene glycol and water. Figure 3-2 shows the ultrasound Doppler flowmeter sensor clamped on to a horizontal pipe with a clip at the 6 o'clock position. A poor coupling of the sensor could affect the accuracy of the measurement as the strength of the received signal will be diminished.
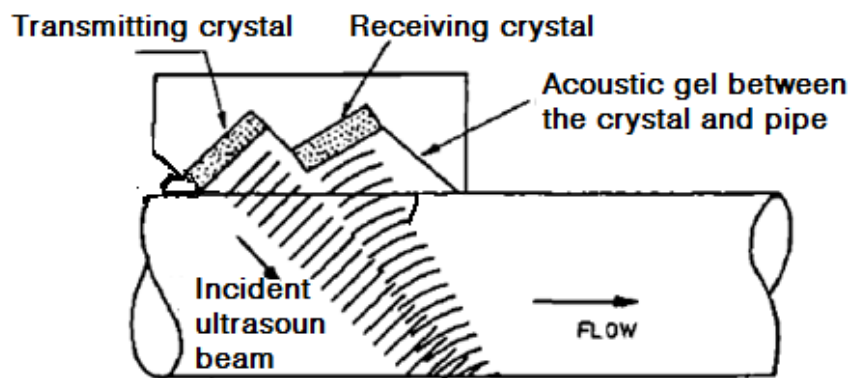
Figure 3-2 Schematic diagram of Doppler shift (Banerjee and Lahey, 1981)

The sensor has a signal processing unit with two output channels: one for flow velocity display (readout) and the other for recording the reflected ultrasound signals from the flow which are sent to the data acquisition system. The data acquisition system includes a signal conditioner (12-bit NI-card NI6040E) and a personal computer with LabVIEW software installed on it. The LabVIEW application on the PC was programmed to control the sampling frequency and record the data onto disk storage for offline processing.

3.3 Signal Processing and Frequency Shift Analyses

The objective of the processing is to evaluate those waveforms of the reflected signal using a spectral analyses technique to determine the shape and speed of the flow.

3.3.1 Fourier Transform and Wavelet Transform

Fourier transform uses frequency domain for the analysis of the Doppler signal to extract the frequency contents of the time domain Doppler signal (Barber et al., 1985). This process detects the spectral component of the signal and

assumes that the original signal is slightly periodic since the sum of the sinusoidal function is periodic (Poesio, 2008). FFT is a process of separating a waveform into a series of single frequency, sine wave components which is possible to go back and forth between the original waveform (time domain) and the frequency domain (Hedrick et al. 1995). The FFT method consists of calculating the next power of 2 (NFFT) from the length of the data sampled. The ultrasound Doppler signals obtained from the flow were analysed for flow velocity estimation using the FFT function in the MATLAB software package. The results of the FFT of the ultrasound signal are grouped and averaged to give the spectrum of the whole signal, as shown in Figure 3-3 (Poesio, 2008).
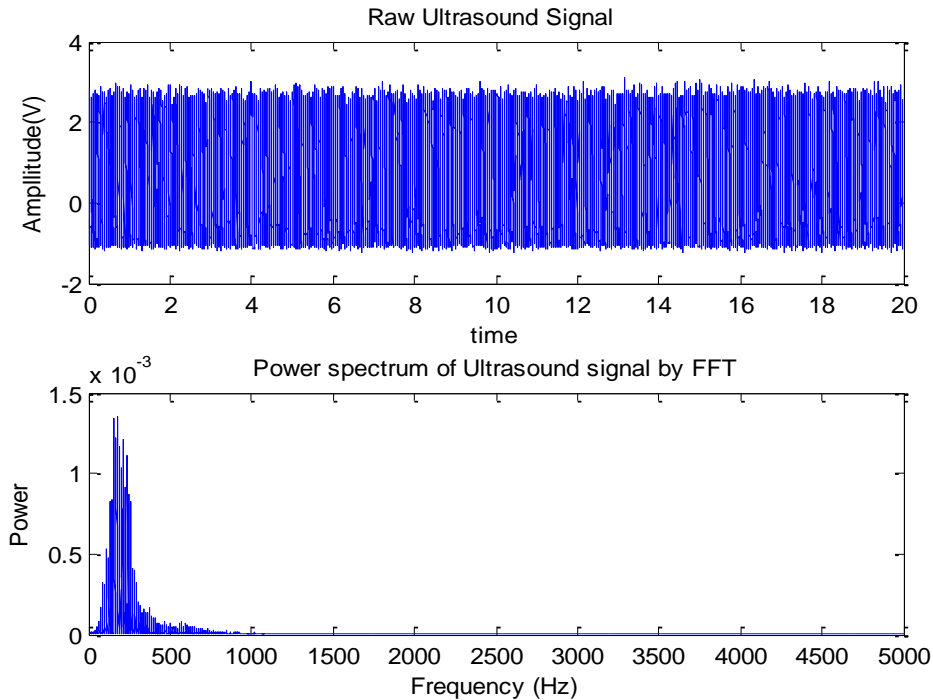
Figure 3-3 Raw ultrasound signal and the FFT of the ultrasonic signal

3.3.2 Mean Doppler shift frequency

In order to estimate the flow rate, the Doppler system determines the average frequency of the signal and often the means of deriving the Doppler frequency shift from the frequency power spectrum is to use the intensity weighted mean frequency (equation (3-2) (Christmann et al., 1990; Evans and McDicken, 2000).

$$f_a = \frac{\int_{-\infty}^{\infty} f(S_a(f) - S_t(f))df}{\int_{-\infty}^{\infty} (S_a(f) + S_t(f))df}$$ **(3-2)**

3.3.3 Resolution property of time-frequency analysis

The Doppler signal from the ultrasound analysis is highly non-stationary. So an appropriate tool is necessary to do the analysis (Keeton and Schlindwein, 1997). More importantly, in order to increase the resolution of the frequency shift, which is proportional to the flow velocity, a longer time duration is needed. Besides, the signal duration is inversely proportional to the frequency of the resolution, thus the resolution of the velocity measurement (Morriss and Hill, 1991). This means that the stationary time domain methods, such as FFT or the STFT, may not be valid. The spectral components resulting from a large interval will be stretched as a result, a reduced time resolution. The alternative method, i.e. the model-based technique AR, is better than the STFT, but its own drawbacks are that the length of the stationary interval determines the time and frequency resolution of the time-frequency representation, and also lower model orders are selected for reduced time intervals (Zhang et al., 2003).

The accuracy of Doppler shift estimation is governed by the uncertainty principle about the product of time duration and frequency bandwidth as:

$$\Delta t \Delta f \geq 1/(4\pi) \qquad\qquad \textbf{(3-3)}$$

In a time-frequency resolution, the time-frequency is defined as a rectangle which has its area as $\Delta t \Delta f$ which satisfies Heisenberg's uncertainty principle – equation (3-3), i.e. the smaller the value of $\Delta t \Delta f$ product, the higher the time-frequency resolution (Matani et al., 1996).

where Δt = time duration or radius of the time-domain window and Δf = bandwidth of a generic functions or radius of the frequency domain.

3.4 Methodology

3.4.1 Hilbert-Huang transform

The HHT is a recently developed method for analysing non-linear and non-stationary data. It comprises the empirical mode decomposition (EMD) method which allows any complex data set to be broken into small fixed units called intrinsic mode functions (IMFs) and the IMFs are then suitable for Hilbert spectrum analysis (HSA) to generate instantaneous frequencies (IFs). As a

result, the energy distribution of the signal is obtained in the time-frequency spectrum (Ding et al., 2007; Huang et al., 1998).

3.4.1.1 Empirical mode decomposition (the sifting process)

The EMD method breaks down the whole data set into a collection of the IMF and each IMF must satisfy the following two conditions:

(1) in the whole data set, the number of extrema and the number of zero-crossings must either equal or differ at most by one, and

(2) at any point, the mean value of the envelope defined by the local maxima and the envelope defined by the local minima is zero.

The first challenge of the EMD is that it requires a narrow-band for a stationary Gaussian is Fourier transforms methods. The second is to modify the global requirement to a local one and this is required for not including any unwanted fluctuations in the instantaneous frequency.

The EMD of a data series $x(t)$ is achieved by the following steps (Ding et al., 2007; Huang et al., 1998) described below:

1. Determine all the local maxima and local minima of the signal $x(t)$ and then interpolate all the local maxima to create an upper envelope $x_{max}(t)$ and lower envelope $x_{min}(t)$ to cover all the data set by using the cubic. Calculate the mean $m_1(t)$ of the upper and lower envelopes as:

$$m_1(t) = \frac{x_{max}(t) + x_{min}(t)}{2} \tag{3-4}$$

2. Subtracting the local mean $m_1(t)$ from the data series $x(t)$ gives:

$h_1(t) = x(t) - m_1(t)$. Usually, $h_1(t)$ is treated as a candidate for an IMF to be tested to see if it qualifies as an IMF. Equation **(3-4)** will be repeated k times until an IMF is generated when the mean envelope is closest to zero. Then the first component $I_1(t)$, which has the highest frequency of the signal, is generated as:

$$h_1(k-1) - m_1 k(t) = h_1 k(t), \qquad I_1(t) = h_1 k(t) \tag{3-5}$$

By generating h_1 it is anticipated to meet the requirements of an IMF. But this is often not the case, as the process of the generation or sifting the h_1 may contain new extrema. As a result, the above sifting process is usually repeated. The sifting process functions in two ways: (1) to banish all riding waves in the

background of an IMF. This is necessary for the IF to be meaningful (2) to flatten uneven wave profiles. This is also required in case the neighbouring waves have very large amplitudes to have symmetry. However, the second function of the sifting process could annihilate the physical meaning of the IMF in the extreme. Consequently, a process for stopping the sifting is suggested as applying the standard deviation (SD), computed from two consecutive sifting results (Ding et al., 2007; Huang et al., 1998)
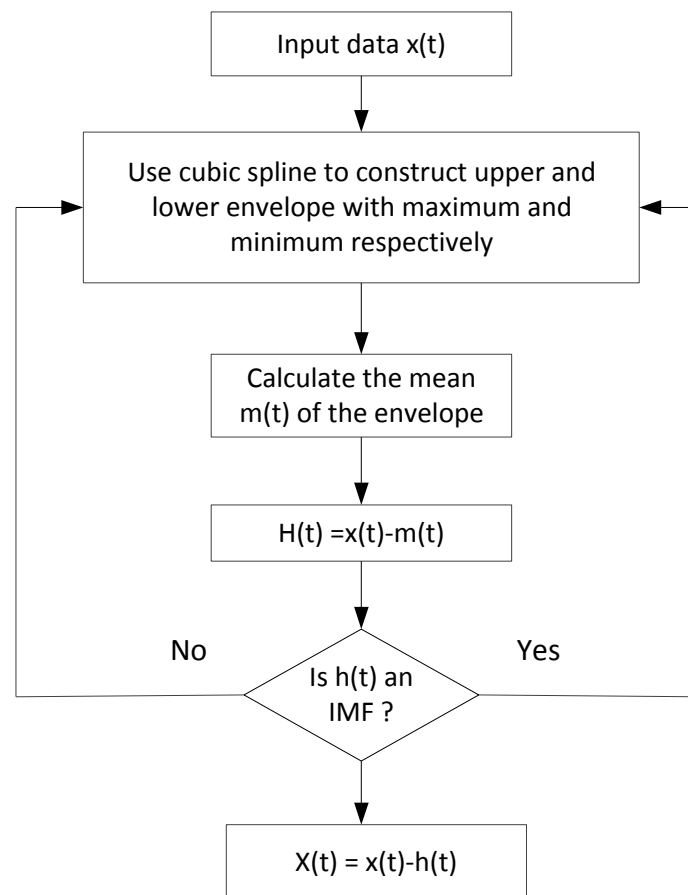
Figure 3-4 HHT process in a flow chart

1. The next step is to subtract h_1 from the remaining part of the data series $x(t)$ and the result or the residue *is* now the new the data series. The residue $r_1(t)$ is still rich in information of lower frequencies. Consequently, it would undergo the same sifting process. These procedures above will be carried out until the generated residue is smaller than the defined value, which is usually the lowest frequency, and the final result is then:

$$r_1(t) - I_2(t) = r_2(t) \dots r_n(t) - I_n(t) = r_n(t) \tag{3-6}$$

$r_n(t)$ is the characteristic of the signal which cannot produce any more IMF and In is the nth IMF. Every IMF contains a lower frequency component than the preceding one. The above procedure of the EMD can be summed up to recreate the signal $x(t)$ (Ding et al., 2007; Huang et al., 1998).

$$x(t) = \sum_{i=1}^{n} I_i(t) + r_n(t) \tag{3-7}$$

3.4.1.2 Hilbert Spectral Analysis

The sifting process of the signal using the EMD produces the IMFs. The HSA is applied to each of these IMFs to calculate the aptitudes, and instantaneous frequencies in a frequency distribution according to equation (3-8) which is called the Hilbert Spectrum (HS). The HS allows the local characteristic of the signal to be examined. For an arbitrary time series, $X(t)$, the Hilbert transform, $Y(t)$, can be expressed as (Huang et al., 1998):

$$Y(t) = \frac{1}{\pi} P \int_{-\infty}^{\infty} \frac{X(t')}{t - t'} dt' \tag{3-8}$$

where: P denotes the Cauchy principal value. The transform exists for all classes of L^p.

When the HT is applied to each of the IMFs, the data can be expressed as:

$$X(t) = \sum_{j=1}^{n} a_j(t) exp^{(i \int \omega_j(t) dt)} \tag{3-9}$$

Equation (3-9) produces the instantaneous frequencies and amplitudes of the data. According to Huang et al. (1998) if the data were to be expressed in Fourier transform they would be:

$$X(t) = \sum_{j=1}^{\infty} a_j(t) exp^{ij\omega t} \tag{3-10}$$

Both a_j and ω_j are constants. A comparison of equations (3-9) and (3-10) shows that the EMD can be thought of as a generalised Fourier transform. But the distinguishing features of equation (3-10) are that the IMF expansion, the amplitude and the frequency representation are not constants. This enables us

to represent the signal with a function whose amplitudes and frequency may vary with time Consequently, this analysis can deal with non-linear and non-stationary data (Ngo, 2013).

3.4.1.3 Instantaneous Frequency

The Hilbert transform of the equation can be expressed analytically as:

$$z_i(t) = c_i(t) + jH[c_i(t)] = a_i(t)e^{j\theta_i(t)} \tag{3-11}$$

where $a_i(t) = \sqrt{c_i^2(t) + H^2[c_i(t)]}$ (3-12)

and $\theta_i(t) = \arctan(H[c_i(t)]/c_i(t))$ (3-13)

are the instantaneous amplitude and instantaneous phases respectively. Expressing equation (3-13) with respect to time gives the instantaneous frequency (Ye et al., 2008))

$$f_i(t) = \frac{1}{\pi}\frac{d\theta_i(t)}{dt} \tag{3-14}$$

3.4.1.4 Marginal Spectrum

In the HS, the amplitude and frequency are functions of time (t) and frequency (ω), the amplitude or the energy (squared of the amplitude) in terms of a function of time and frequency $H(\omega, t)$. The marginal spectrum (MS) can be expressed as:

$$h(\omega) = \int_0^T H(\omega, t)dt \tag{3-15}$$

where, $[0, T]$ is the total time of the data. The MS depicts the collated amplitudes of the data and shows a measure of total amplitudes of each IF. It is an alternative to the traditional spectrum, such as the one from the Fourier transforms (Ngo, 2013).

Cross-fertilisation of the EMD and the HSA is given the appellation HHT. The HHT is designed particularly for analysing non-linear and non-stationary data. It is based on differentiation rather convolution (Huang and Wu, 2008).
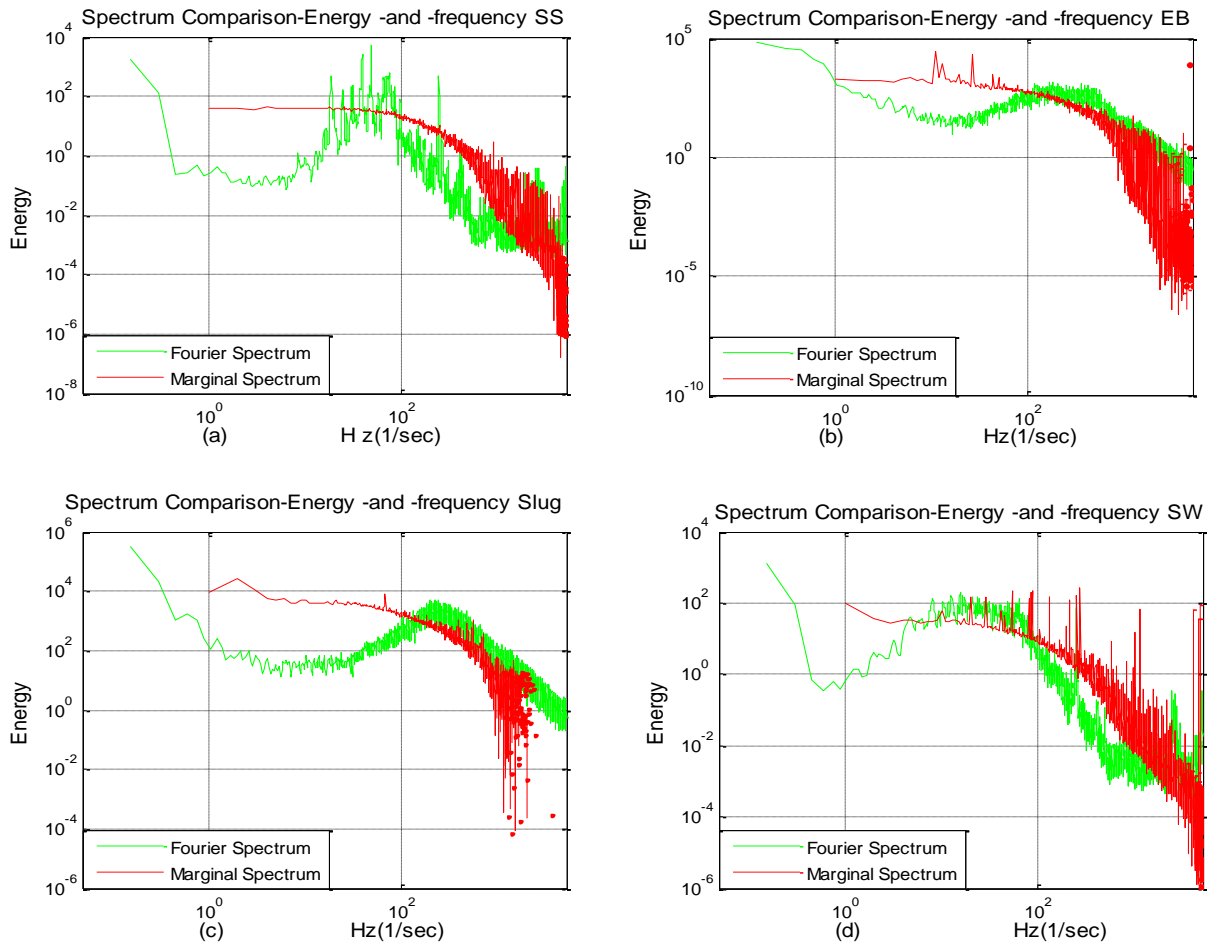
Figure 3-5 Comparison of marginal Hilbert spectrum with Fourier transform of the four ultrasonic two-phase flow data signals

3.4.1.5 Mean frequency estimation using HHT

The mean instantaneous frequency of the data is estimated from the Hilbert transforms of the IMFs and is computed as (Xie and Wang, 2006):

$$MIF(j) = \frac{\sum_{i=1}^{m} \omega_j(i) a_j^2(i)}{\sum_{i=1}^{m} a_j^2(i)} \tag{3-16}$$

where m is the size of the data point, $\omega_j(i)$ is the weighted mean frequency $a_j^2(i)$ weighted mean of the amplitudes. The mean frequency estimation using the HHT provides estimations based on each frequency which is considered to be a true representative of the signal as the mean frequencies estimated are computed based on the relative magnitude of each frequency band.

3.5 Results and discussion

The results, which are described below in sections 3.5.1 and 3.5.2, demonstrate the application of the HHT for ultrasonic signals of gas-liquid two-phase. The HHT techniques were applied both for the determination of the mean Doppler frequency shift single phase flow and further adaptive analysis of the signals of the two-phase flow.

3.5.1 Single phase flow metering

For the purpose of calibration, a single phase water flow was metered using the ultrasonic sensor and the electromagnetic flowmeter. The measurement of the water flow was recorded on the Doppler flowmeter readings, electromagnetic flowmeter (reference meter) and raw data signals of the flow for offline processing. The single phase flow records were processed for estimating the mean frequency using FFT and the HHT. The results of the flow metering are presented in Figure 3-6
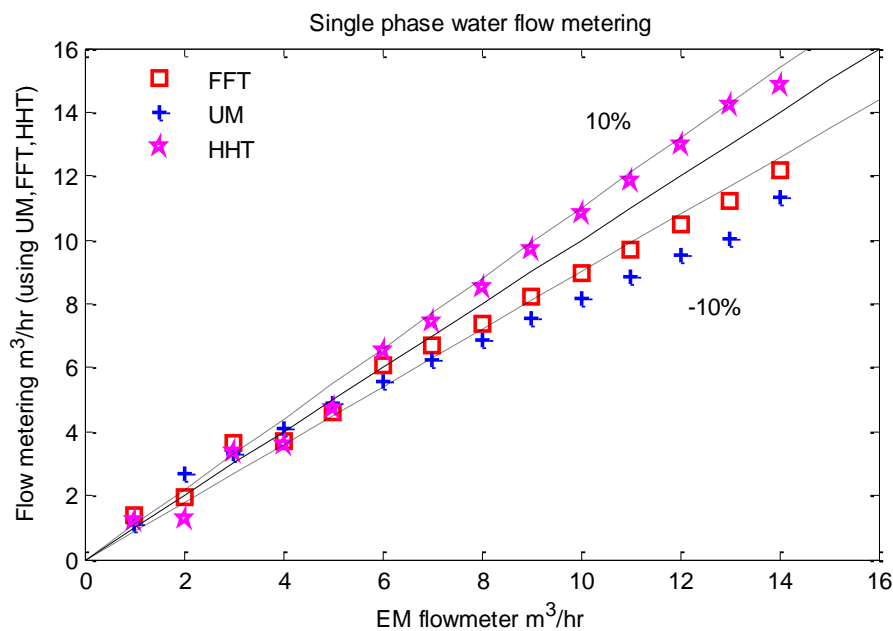
Figure 3-6 Single phase flow rates estimated using the ultrasonic Doppler flowmeter, mean frequency estimation with FFT and HHT compared with EM flowmeter measurement

It can be seen that the location of the test results for each flow data relative position on the graph are within the range $\pm 10\%$ of the reference meter readings, where UM is the ultrasonic flowmeter measurement, FFT is the

ultrasonic measurement from raw signal processed using the FFT technique and HHT refers to ultrasonic processing using the HHT method.

Figure 3-7, shows a comparison of the Fourier spectrum and Marginal Spectrum obtained from the HHT techniques of a single phase flow rate metering.
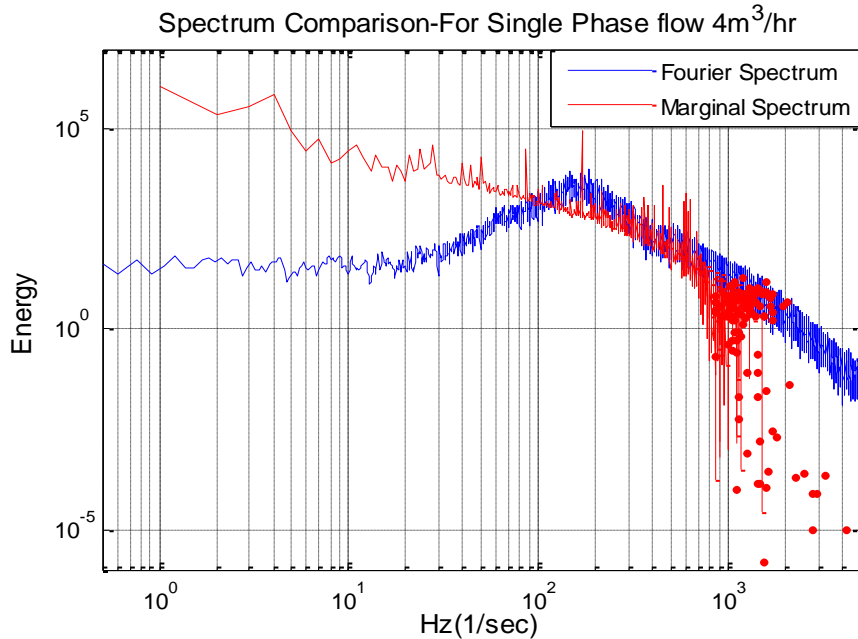
Figure 3-7 Spectrum comparison of Fourier spectrum and Marginal spectrum

3.5.2 Characterisation of air-water flow

3.5.2.1 EMD of the Doppler signals

The EMD is an adaptive, intuitive and data driven algorithm for dealing with non-stationary signals to eliminate riding waves and to make wave profiles of the signal more symmetric. The algorithm picks out the highest frequency component of the data in descending order (Huang et al., 1998). In order to adaptively decompose the raw ultrasonic signal of the two-phase into its intrinsic mode functions, the results are displayed in 17 IMFs and the original signal itself as an IMF1 at the top.

Figure 3-8, Figure 3-9, Figure 3-10 and Figure 3-101 show the decomposition of the ultrasonic signal of the two-phase flow into 17 modes: IMF2–IMF 17 for stratified smooth, bubbly flow, slug flow and stratified wavy flow respectively. From the figures it can be seen that the IMFs have different local frequencies. The process of the decomposition picks out the highest frequency component

first, followed by the component with the second highest frequency and so on until the residual R is the residual signal after the decomposition which is not an IMF (Ding et al., 2007). In addition, the decomposition shows that the higher frequency information with smaller amplitudes and low-frequency information is represented by larger amplitudes (Ding et al., 2007).
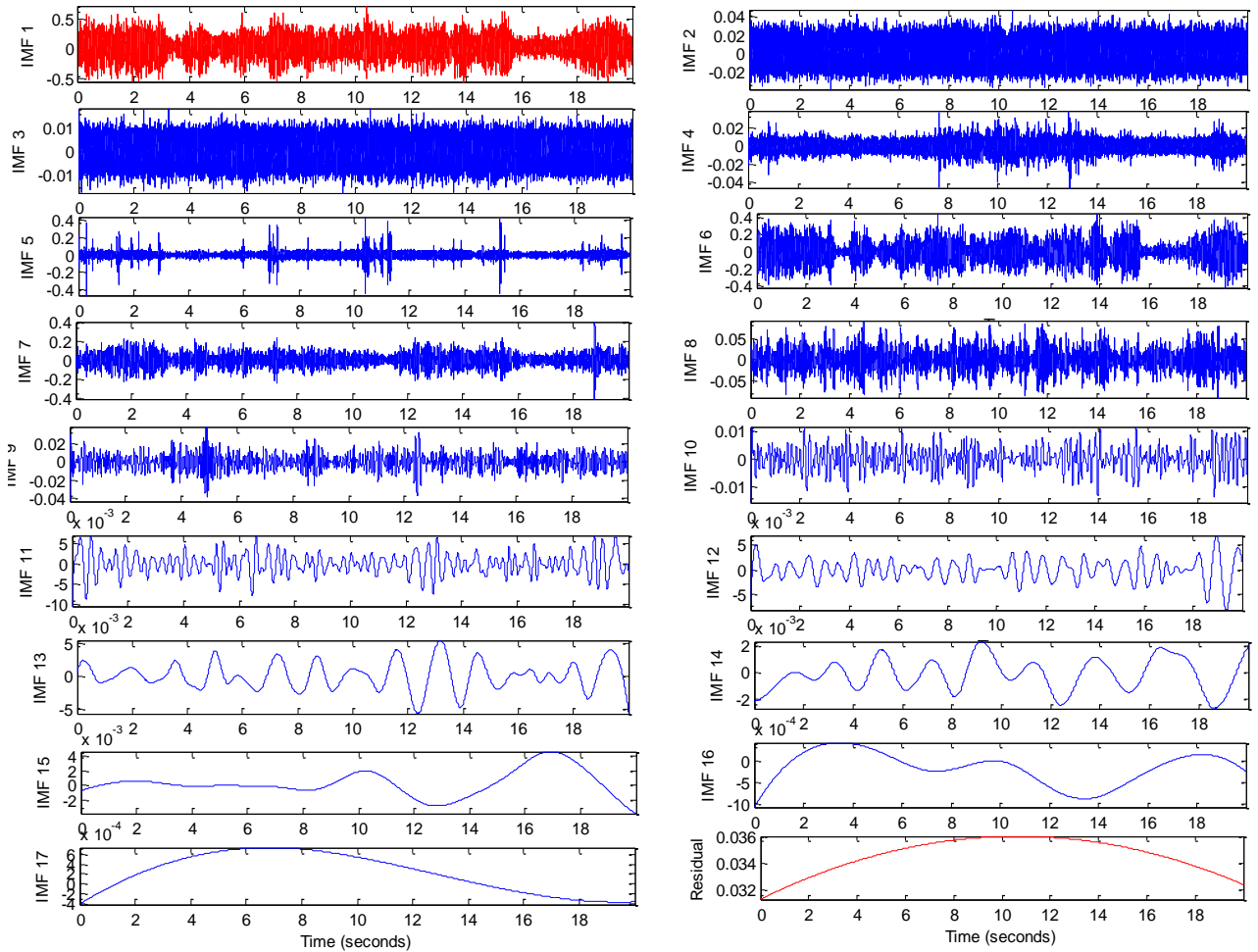
Figure 3-8 Extracted IMFs from the ultrasonic data of the air-water stratified smooth flow using the Empirical Mode Decomposition
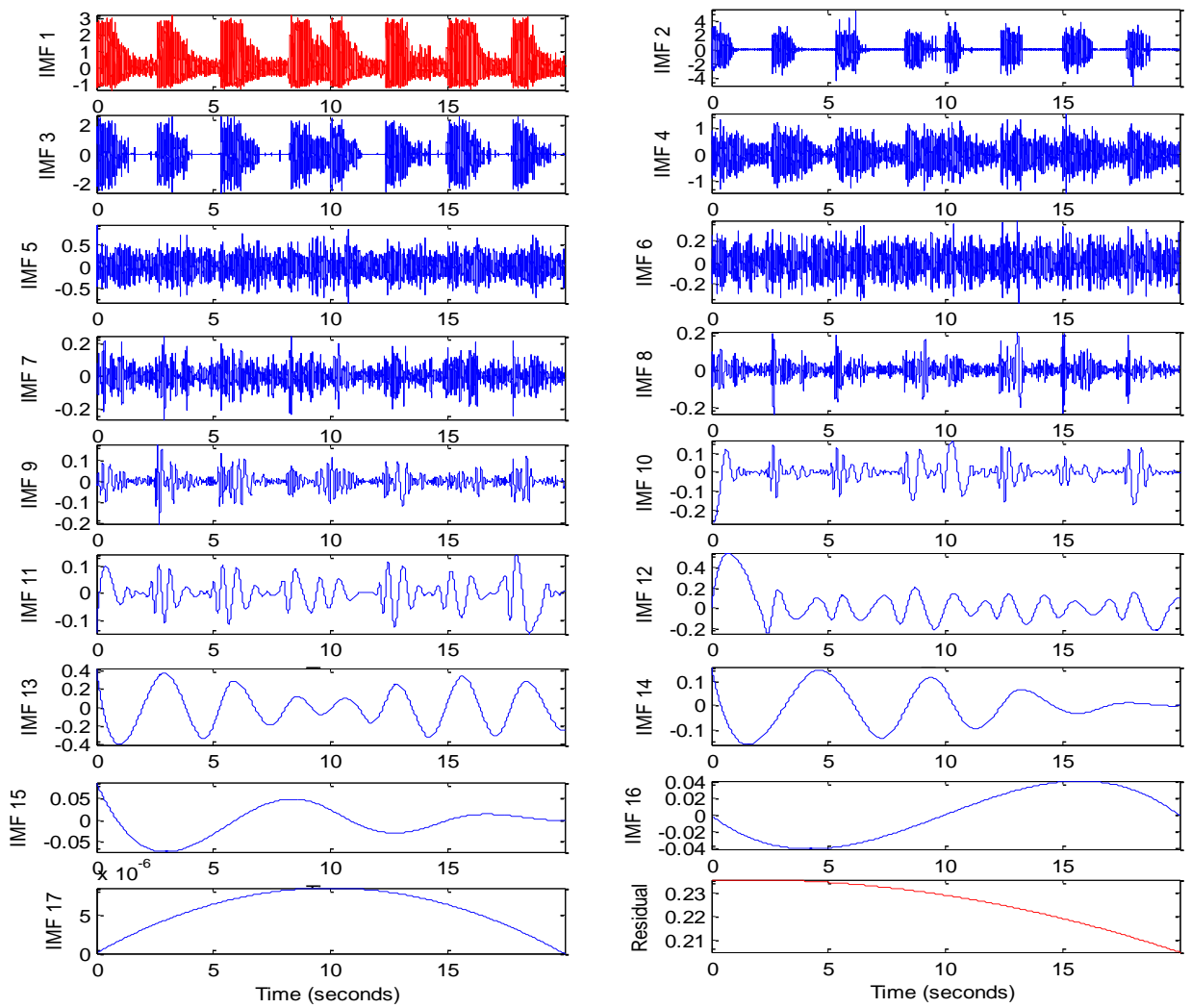
Figure 3-9 Extracted IMFs from the ultrasonic data of the air-water bubbly flow using the Empirical Mode Decomposition
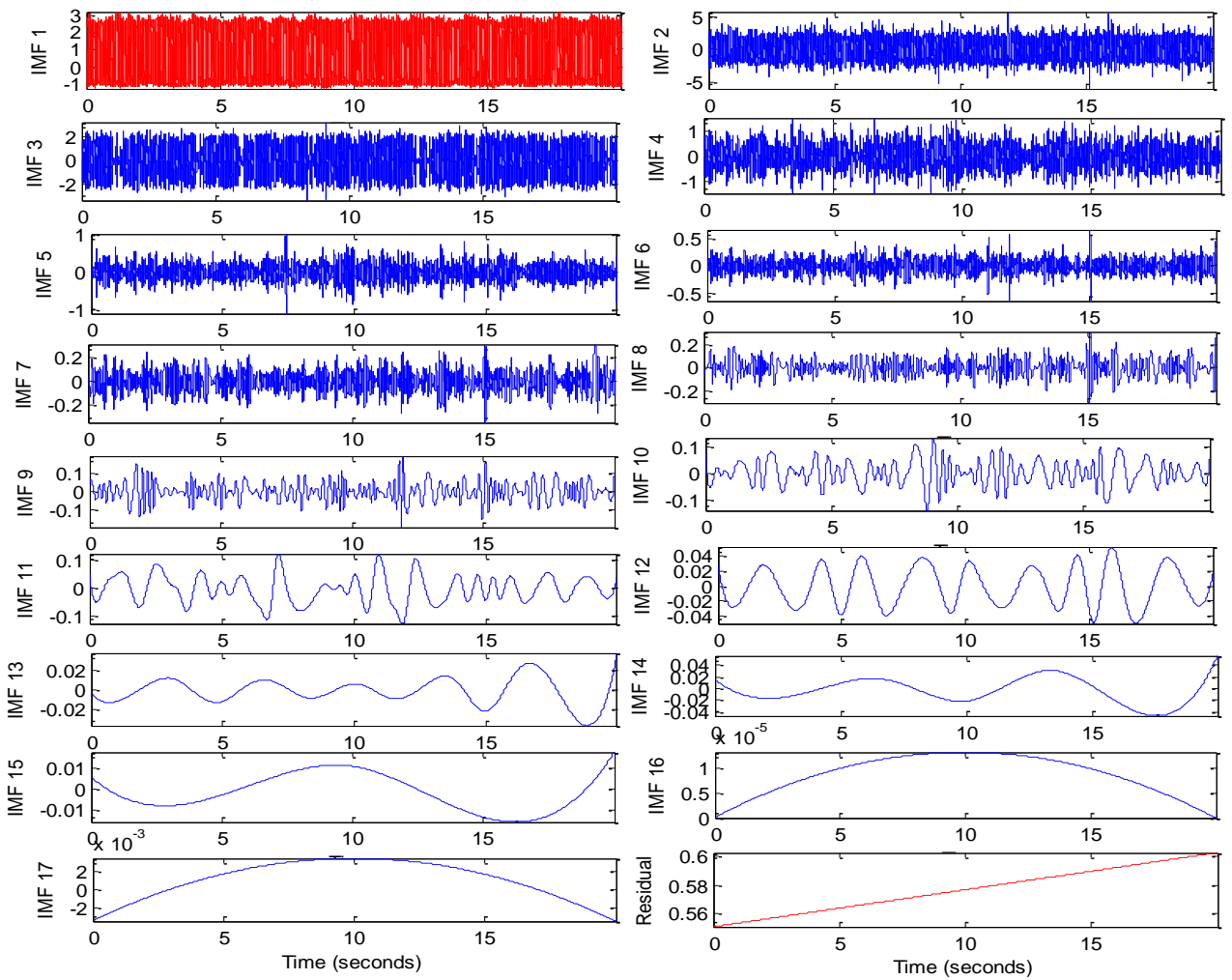
Figure 3-10 Extracted IMFs from the ultrasonic data of the air-water slug flow using the Empirical Mode Decomposition
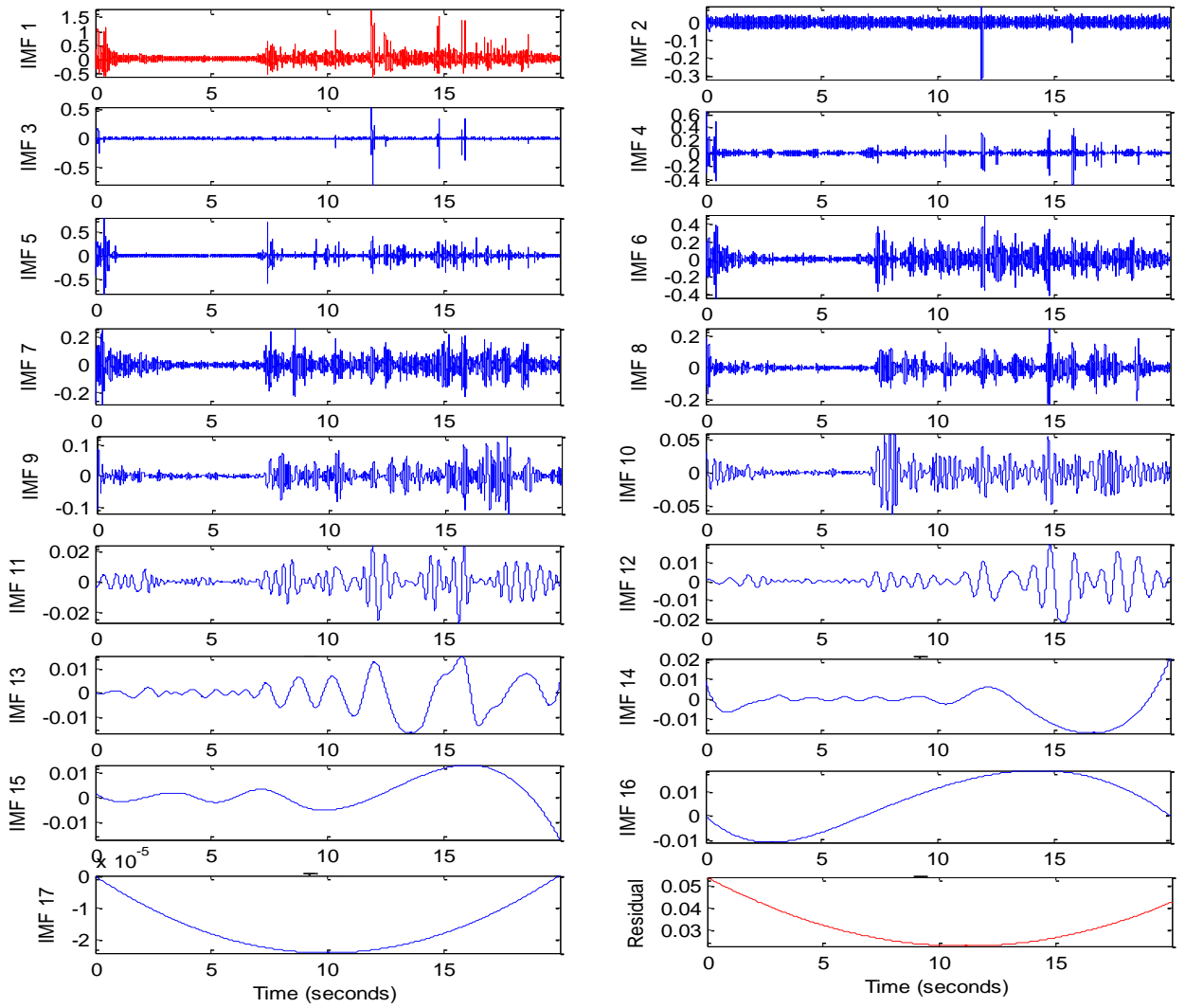
Figure 3-11 extracted IMFs from the ultrasonic data of the air-water stratified wavy flow using the Empirical Mode Decomposition

The results of the empirical decomposition are often processed by the Hilbert transform (Meng et al., 2012). Figure 3-12 and Figure 3-13 show the Hilbert Spectra and Marginal Spectra produced for the four flow regimes sample analysed with the Hilbert transform respectively.

77

3.5.2.2 Hilbert Spectrum
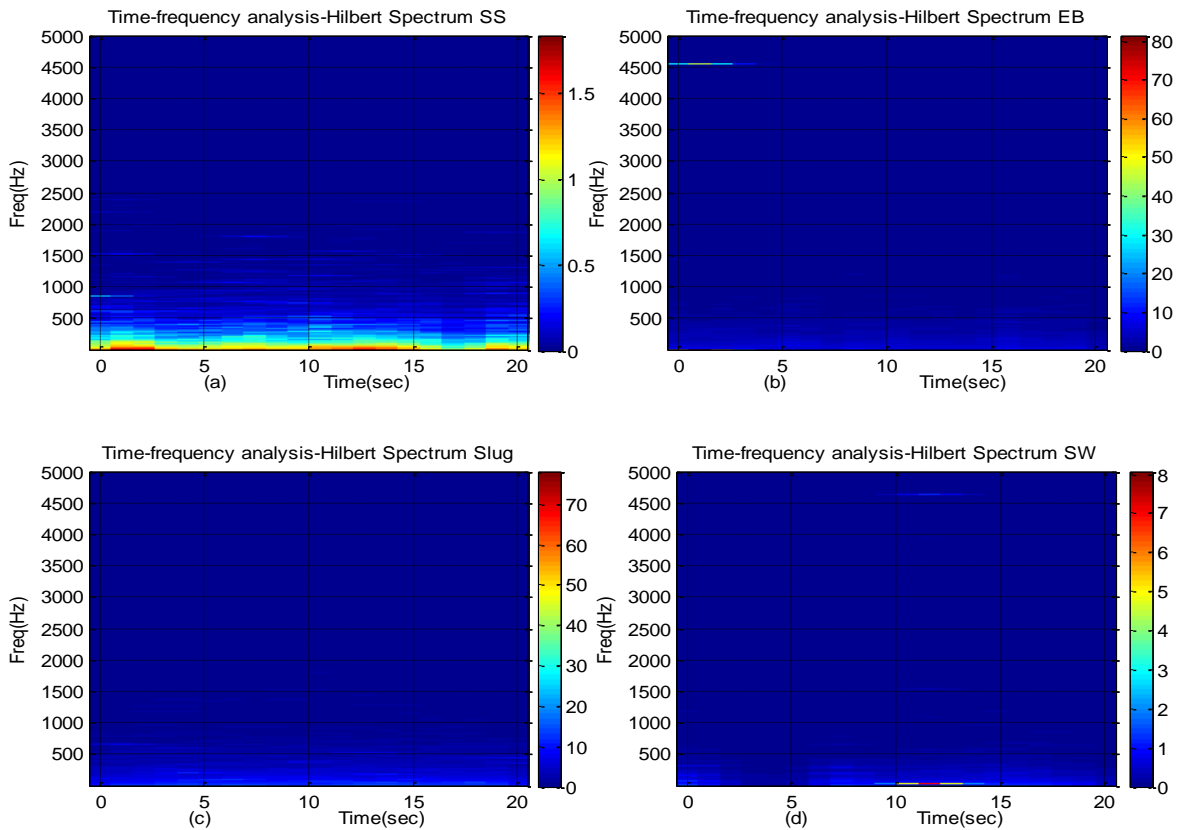
Figure 3-12 The Hilbert spectrum under different two-phase flow regimes

In the Hilbert spectrum, the horizontal axis is the instantaneous time of the signal acquired while the vertical axis shows the instantaneous frequency. The velocities of the flow measured are within the frequency range of 200Hz to 300Hz; the Hilbert Spectra are plotted on the full frequency range of the samples.

3.5.3 Marginal spectrum

Figure 3-13 shows the marginal spectrum of the four two-phase flow regimes ultrasonic which was obtained, as explained above, from the integration of the Hilbert spectrum across time. The red line show the marginal spectrum while the green lines show the plot of Fourier transforms of the four data sets.

78
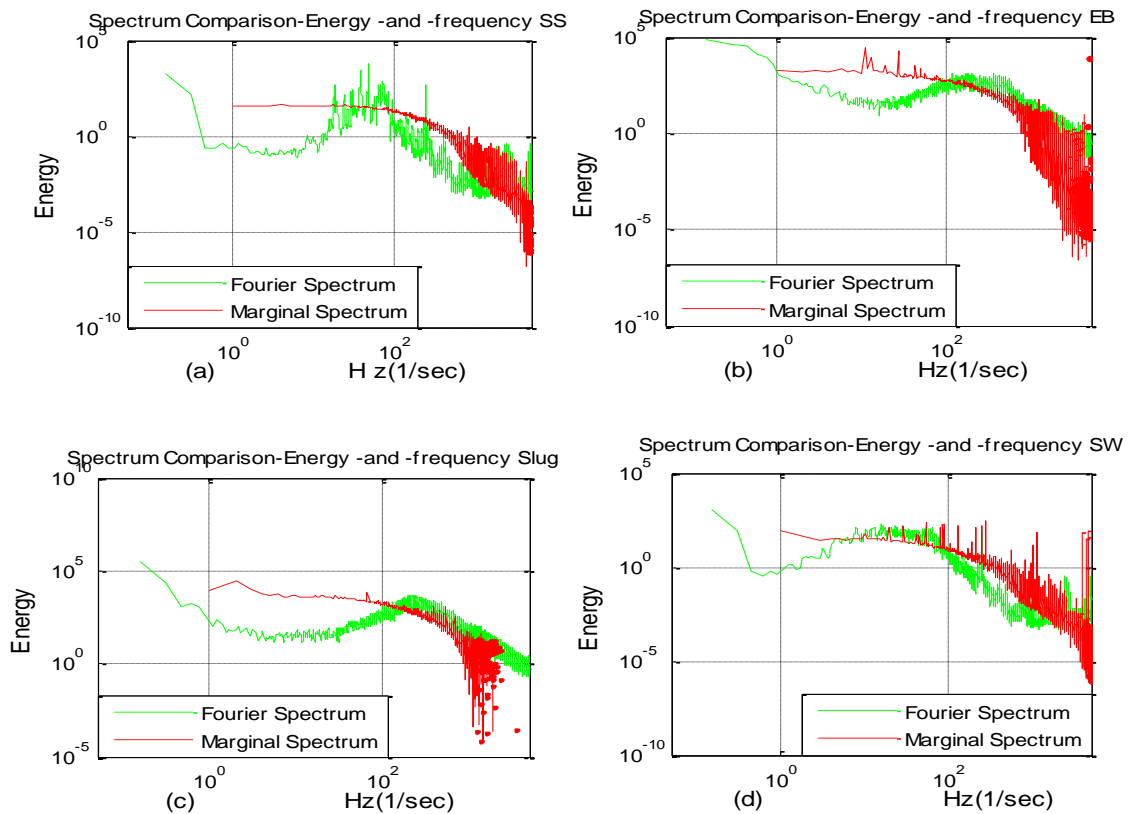
Figure 3-13 Comparison between marginal spectra and Fourier spectra

There are differences between the information displayed by the two spectra. The Fourier spectrum provides information on certain frequencies in the entire time span of the data with the energy given in squared amplitudes. But in contrast, in the marginal spectrum, the existence of energy at a given frequency means that there is the probability of a frequency with oscillation existing in that local time of the data. In Figure 3-13, the Fourier spectrum showed the form of a harmonic in the data without the analysis on the existence of the harmonic in the data. However, the marginal spectrum, which is adaptive in nature and non-harmonic, showed real properties of the signal as a decrease in energy with an increase in frequency of the signal (Molla et al., 2006)**.**

3.5.3.1 Characterisation of two-phase slug flow

In addition to the decomposition of the ultrasonic signals, clear representations of the two-phase flow signal can be obtained by summing up the totals or some of the IMFs. The result of the IMFs summed up from IMF10 down to IMF17 and residual signal R, demonstrates the intrinsic meaning of the decomposition

method. These intrinsic trends illustrate the gas-liquid profile from the ultrasonic signals of the two-phase.

In slug flow measurement, a detailed profile of the gas-liquid interface is often necessary (Mi, 1998). We plotted the partial sum of IMF10 to IMF17 and the conductivity probes signal obtained the same two-phase flow, as shown in Figure 3-14.
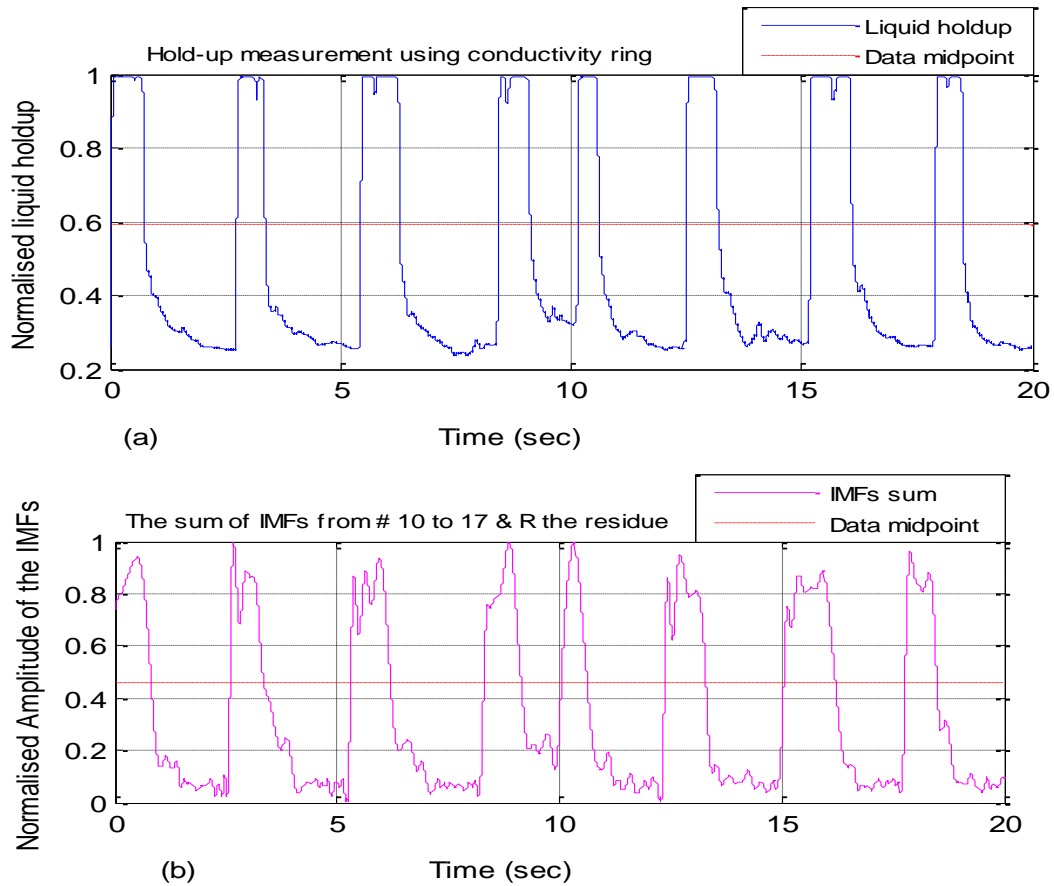
Figure 3-14 the sum of IMFs from mode 10 to R of a slug flow signal compared with results of the conductivity probe signal slug flow parameters (Gas Superficial velocity 0.70m/s and Liquid superficial velocity 0.50m/s.

Figure 3-14 shows the ultrasound signal and the response of the IMFs summed to represent a slug flow profile. Similarly, the figure shows higher amplitude signals at the presence of slug body and lower signals at the film body as in the conductivity probes measurement of slug flow profile.

3.5.3.2 Elongated bubble length

The bubble in gas-liquid two-phase flow is defined as the distance from the bubble's nose to its tail (Romero et al., 2012). Wang et al. (2007) employed a pair of conductivity probes for the experimental investigation of parameters of gas-liquid slug on horizontal flow pipe with diameter (0.05m) and proposed a correlation to estimate the bubble length. With the conductivity probes, the length of the elongated bubble (L_B) is determined as the product of the bubble's velocity estimated and time difference of the signal trace of the bubble. At the same time, the sum of the IMFs derived with HHT from the ultrasonic signal were compared with the conductivity trace and the ultrasonic method for estimates of the bubble lengths formulated, as shown in Figure 3-15.
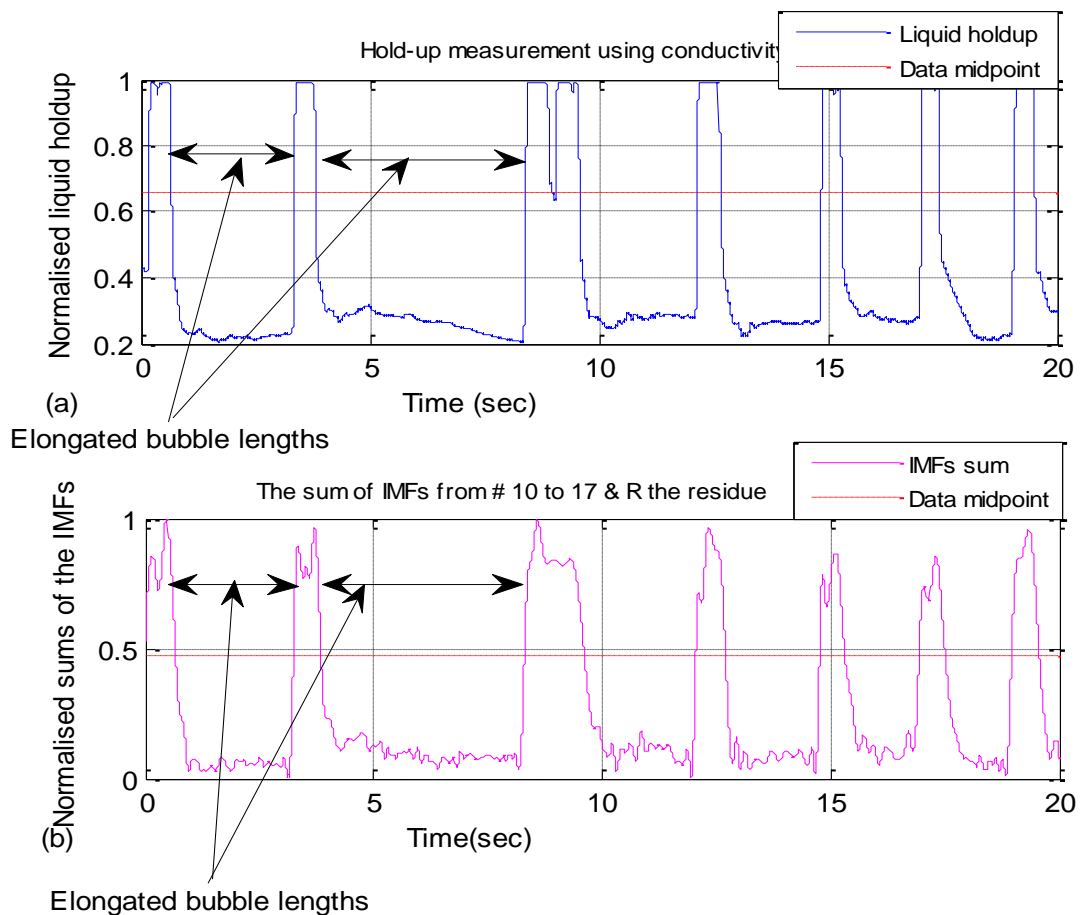
Figure 3-15 Signal trace of a slug flow from the conductivity probes and ultrasound with HHT showing the bubble lengths (Gas superficial velocity 0.70m/s and Liquid superficial velocity 0.50m/s.

Figure 3-16 shows the results of the elongated bubbles' length calculated in the present as a function of liquid superficial velocities. The present experimental result is very good and in agreement with the prediction of Wang et al. (2007), except when the gas superficial velocity is 1.5m/s. The present results were in agreement with the work of Mi et al. (2001b) which reported that the lengths of the elongated bubbles increase with increases in gas superficial velocity but decrease with increases in the liquid superficial velocity.
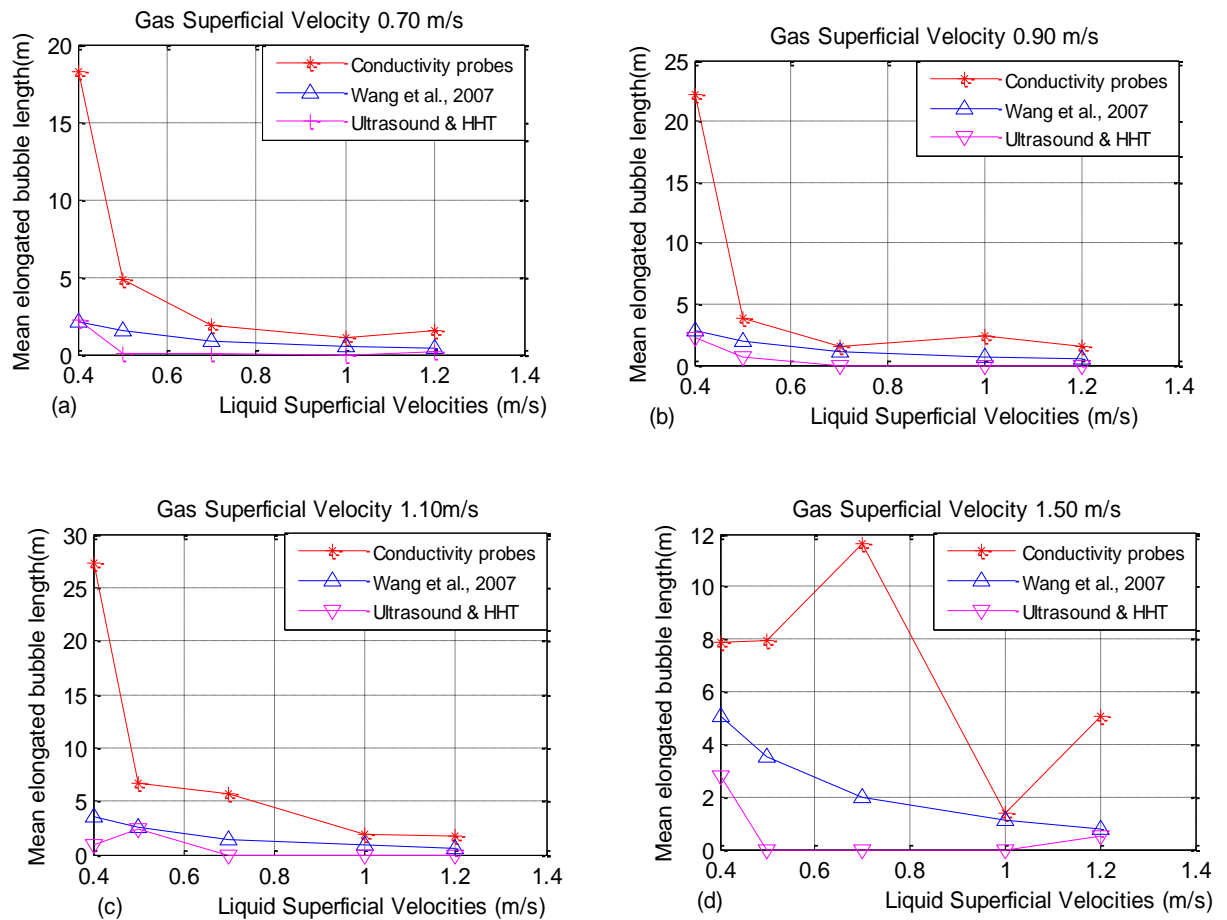
Figure 3-16 Mean elongated bubble length as a function of liquid superficial velocities

3.5.3.3 Slug frequency

Slug frequency is defined as the ratio of the number of slug units per sampling time. Based on measured values for the carbon dioxide-water system in a 0.0 19m diameter pipe, Gregory et al. (1978) suggested that the slug frequency is as follows:

$$v = 0.0226 \left[\frac{V_{SL}}{g \times d} \left(\frac{19.5}{V_{mix}} + V_{mix} \right) \right]^{1.2}$$

(3-17)
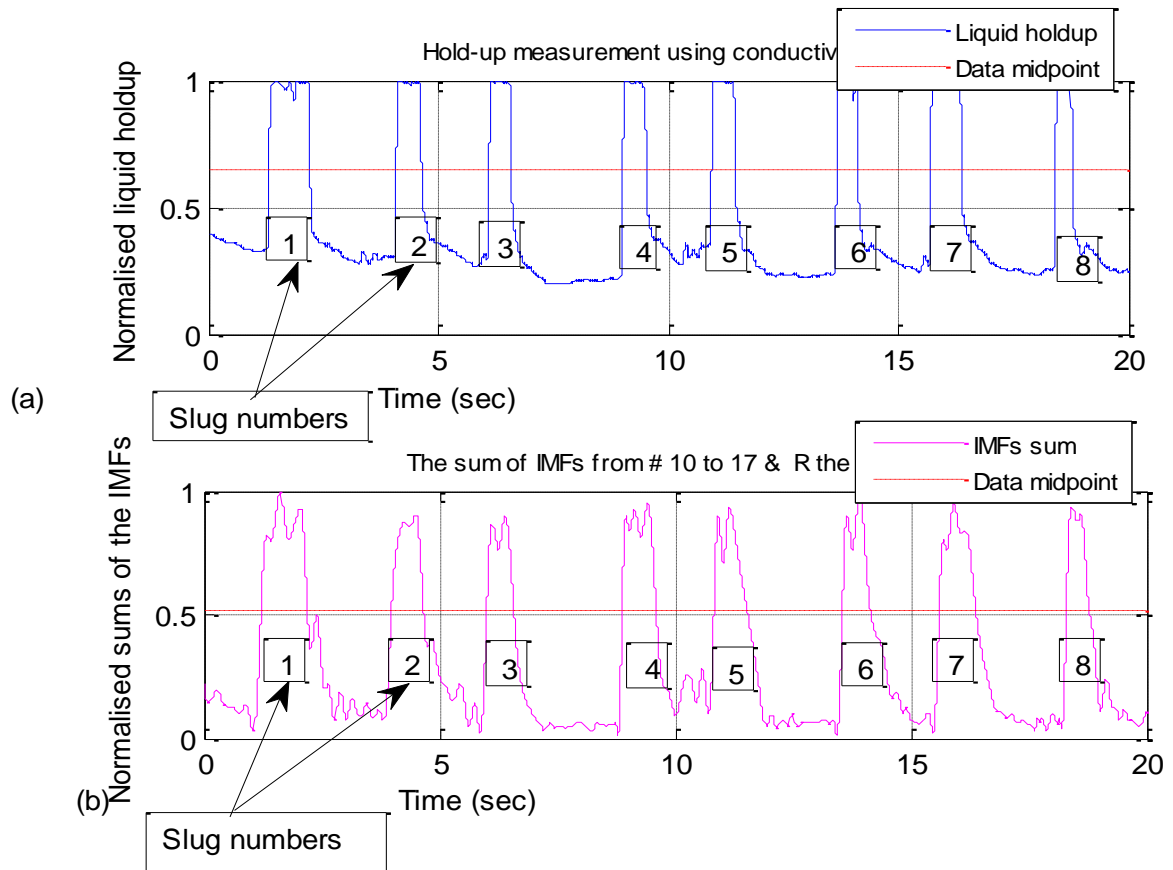
Figure 3-17 Signal trace of a slug flow from the conductivity probes and ultrasound with HHT showing the number of slugs detected

The results of the slug frequencies of the flow condition are shown in Figure 3-18 as a function of the liquid superficial velocities. The results were compared with the correlation of Gregory et al. (1978).

83
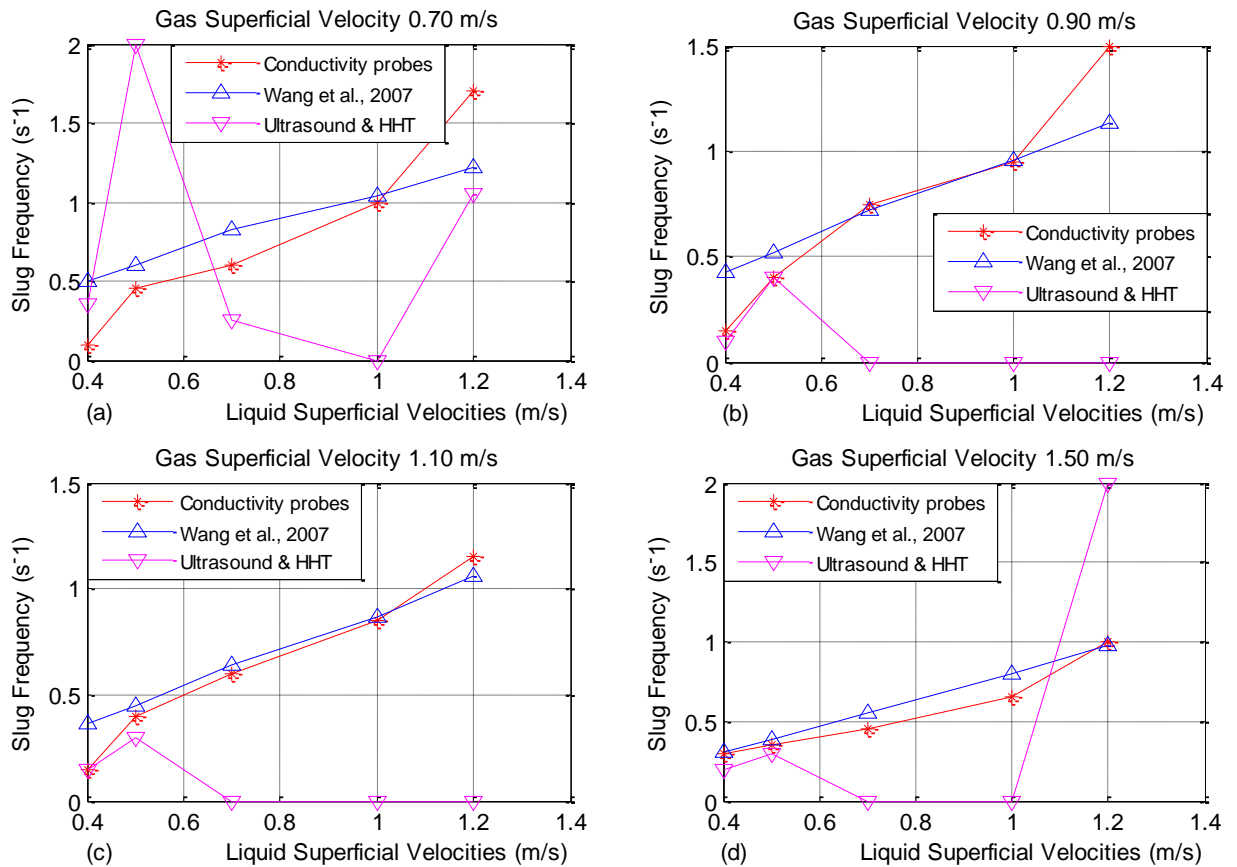
Figure 3-18 Comparison of calculated mean bubble frequency with a correlation as a function of the liquid superficial velocities at four different gas superficial velocities

Figure 3-18 shows the estimated slug flow frequencies of four sets of data points. The slug frequency estimates of ultrasonic signals, conductivity probes and the correlation (Wang et al., 2007) were compared. It can be seen that when the liquid flow rate is less than 0.6m/s, the traces of the ultrasonic could be well used for estimating the slug frequencies, which is in good agreement with Wang et al. (2007). However, the estimation of the conductivity probes generally agreed with the correlation.

3.6   Summary

An investigation of the ultrasonic Doppler sensor for single flow rates and gas-liquid flow characterised with the HHT method was conducted. First, a single phase water flow rate was carried out to determine the performance of the produced against the measurement of the reference EM flowmeter.

The Doppler shift signal, as a result, contains a spectrum of frequencies which varies in shape as the velocity distribution through the pipe changes with time. In order to estimate the flow rate from the reflected signal, the Doppler system has to first determine the average frequency of the signal. The objective of the processing is to evaluate those waveforms of the reflected signal using a spectral analyses technique to determine flow, frequency shifts, f_d and contents of the Doppler signals of the flow.

The approach of this investigation is based on an adaptive method of signal processing and the ultrasonic is non-invasive. The results of the gas-liquid characterisation using the HHT method are found to be in very good agreement with the literature at certain points, especially for the low liquid flow rates and low gas flow rates. However, at the higher liquid and gas superficial velocities, the HHT did not predict the gas-liquid properties.

4 Application of Pulse-Wave Ultrasound System

4.1 Introduction

This chapter develops a pulse-wave ultrasound system that detects moving interfaces in gas-liquid two-phase flow by detecting the instantaneous positions of the interface from the time of flight of the pulsed ultrasound. Detection of the gas-liquid interface is very important for developing models for predicting the unsteady behaviour of two-phase flows. Also, the location of the gas-liquid interface can be used to determine the liquid holdup and liquid phase velocity distribution (Gonzalez et al., 2009). Importantly, by error analysis it has been found that the accuracy of a two-phase flow meter depends on the accuracy of the interface detection (Gonzalez et al., 2009).

Different methods have been developed for the measurement of gas-liquid interface in two-phase flow (Al-Lababidi and Sanderson, 2005; Murai et al., 2010). Electrical probe methods of gas-liquid interfacial area measurement employ electrical resistivity of the fluid to measure the local instantaneous interface in the two-phase flow. The flow in the pipe sets an electrical circuit that is open or closed, depending on whether the gas or the liquid phase is flowing, and the voltage drops across the sensor vary between the two reference points. For regimes such as bubbly flow, whereby the liquid phase is continuous, the circuit is closed but the voltage drop varies, depending on how much liquid contacted the probe. The electrical probe has a disadvantage in that a cut in the pipe is required – it is an invasive technique (Fossa, 1998; Revankar and Ishii, 1992; Tan and Ishii, 1990). Another technique that has been developed to measure the gas-liquid interfacial area is the radiation technique. This is a non-invasive approach but it does have disadvantages in that it either requires thin pipes or a strong source combined with heavy shielding to operate safely and effectively (Chang and Morala, 1990).

The CW system can detect the movement of any gas bubbles, particles or scatters in the pipe, but it is impossible to detect the range of the moving target. As a result, the CW systems have no range resolution and cannot be used to determine liquid height or the cross-sectional area of the fluid (Baker, 1970).

86

4.2 Experimental procedure

4.2.1 PicoScope data acquisition system

An ultrasound pulse echo data acquisition setup is depicted in Figure 4-1. The Pulser/Receiver with a bandwidth of 25MHz (Panametrics 500PR) generates a signal to drive the ultrasound transducer. The Pulser/Receiver has a knob for selecting the PRF up to 10kHz and an adjustable gain for the transmitted signal. The reflected ultrasound signal is received by the same ultrasound transducer and is then collected by the Pulser/Receiver. The echo received is an RF signal and it under goes amplification at the Pulser/Receiver before it passes on to the PicoScope.

The PicoScope works well with the operating system without any modification. An external trigger pulse sent to the Pulser/Receiver from the PicoScope at the receipt of software triggers a signal from a control signal or at the instant an echo signal is received. This communication between the Scope and the Pulser/Receiver commences the data acquisition simultaneously. The scope captures a pre-set number of the ultrasound wave once it has been triggered and this enables the PicoScope to capture many waveforms of the ultrasound at one setting of the PRF on the Pulser/Receiver (Safvi, 1996).
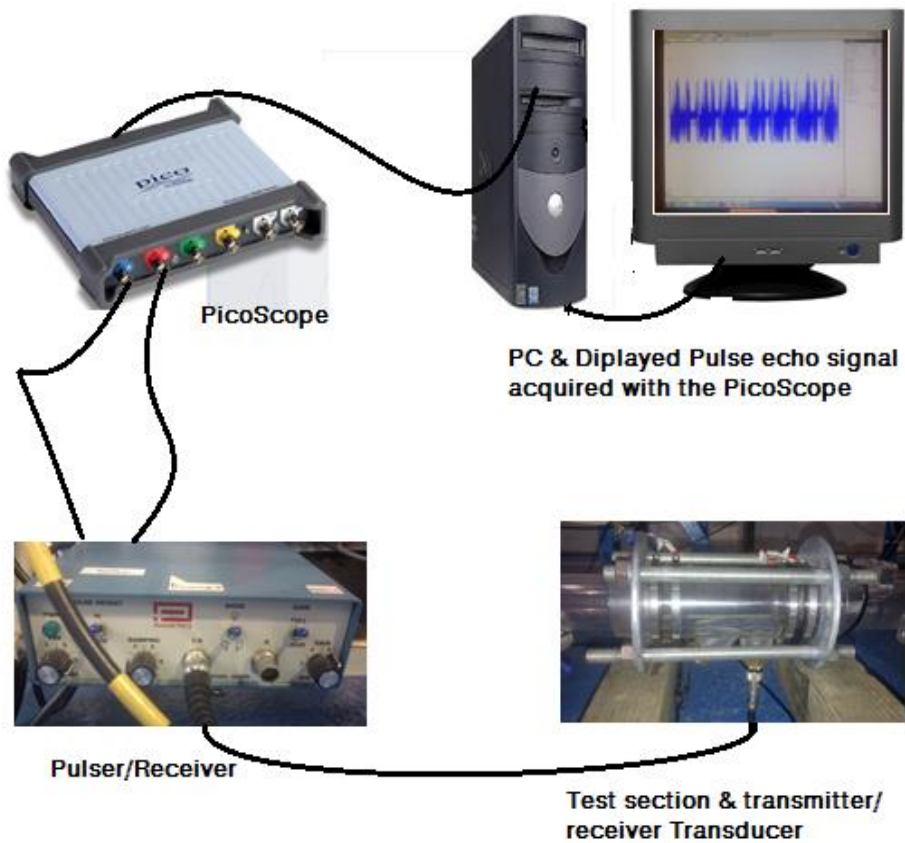
Figure 4-1 Ultrasonic experimental setup for study of liquid/gas interface in a horizontal pipe

The echo signals which are received by the Pulser/Receiver via the transducer are captured by the PicoScope. The scope will then transfer the captured waveforms to be sent to the PC as fast as the setting of the PRF on the Pulser/Receiver. On the PC, the waveforms are further processed for measurement analysis, display and storage for offline processing. If the waveform data capturing capacity of the Scope is slower for the task, some signals to be received will be missed out. The limitation of the Scope memory was the challenge we faced at the beginning of this work. The previous Scope, PicoScope 3402, could sample the data fast but for only seconds and it lacked the capability to capture data fast and transfer them to the PC hard drive. As a result, a decision was made to purchase the PicoScope 5444B.

Recording of the reflected echo signals were done at pulses of 20 Volts, peak-peak amplitude for the trigger signal, and 4 Volts, peak-peak for the echo

signals. Sampling frequencies of 42.7MS/s were used for 321 frames and continuous recording for 5 seconds for the 1MHz and 7.5MHz transducers respectively. The air-water horizontal flow test for two-phase flow measurement using the ultrasonic sensors and the axillary instruments together with advanced signal processing, was able to provide a study of slug flow parameters and liquid height measurement using non-invasive measurement techniques. However, the capacity of the rig gas flow rate was not high enough and the fluids that could be tested on the rig were only the air-water flow. As a result, the next section on the experimental setup is on the study conducted for two-phase flow measurement using a three-phase flow facility.

4.3 Pulse-Echo Ultrasound Measurement Principle

The pulse-echo ultrasonic technique uses the ultrasonic waves reflected strongly off the gas-liquid interface because of the large difference in acoustic impedance between the interfaces. The amplitude of the reflected wave depends on the relative acoustic impedance of the two fluids (Murai et al., 2010). This phenomenon was exploited using two ultrasound pulse echo transducers with a centre frequency of 1MHz and 7.5MHz to measure the gas-liquid interface in a two-phase flow pipe. The sensor signal was applied across the flow pipe to measure the instantaneous liquid or interfacial area and liquid holdup. The time of flight is the time that elapsed between the transmission of a pulse and its reception by the transducer. As a result, the distance from the transducer to the interface (h) can be calculated if the velocity of the sound (C_w) is estimated or assumed.

$$h = \frac{t C_w}{2}$$
(4-1)

where C_w is the water sound velocity =1480m/s at 20°C (Evans and McDicken, 2000) and t is the time of flight of the ultrasonic signal. There are three methods of ultrasound interface detection: echo intensity, local Doppler, and velocity variance techniques. The echo intensity technique was adopted to process the echoes for ultrasound detection in the present experiment (Murai et al., 2010).

4.4 Methodology

4.4.1 Signal processing

The method and schematic diagram designed is shown in Figure 4-2 which is modified from the work of Chang and Morala (1990). The test section is made of Perspex so as to visually observe the type of flow regime formed. With this pipe flow arrangement, three different flow regimes were observed. The liquid level in the tube can be obtained from the geometrical representation of the spool piece using equation (4-2) (Masala, 2004).

$$h_{Geometry} = r(1 - \cos\frac{\theta}{2}) \tag{4-2}$$

where $h_{Geometry}$ is the height of the liquid level in the test spool piece, r is the tube radius and θ is the angle subtended by the cross-sectional view of the liquid level at the centre of the tube, as shown in Figure 4-2. The void fraction in the test tube can be expressed as in equation (4-3):

$$\alpha = \frac{V_{total} - V_{total}}{V_{total}} = 1 - \frac{V_{liquid}}{V_{total}} \tag{4-3}$$

where $V_{total} = \pi.r^2.L$, L is the tube's length and the values of the tube dimensions are $L = 670\ mm; r = 25\ mm$ $V_{liquid} = \frac{L}{2}r^2(\theta - \sin\theta)$, while θ is calculated from the transcendental equation (4-4).

$$\theta - \sin\theta = 2\pi(1 - \alpha) \tag{4-4}$$

where α is the void fraction and is simply defined by equation (4-3).
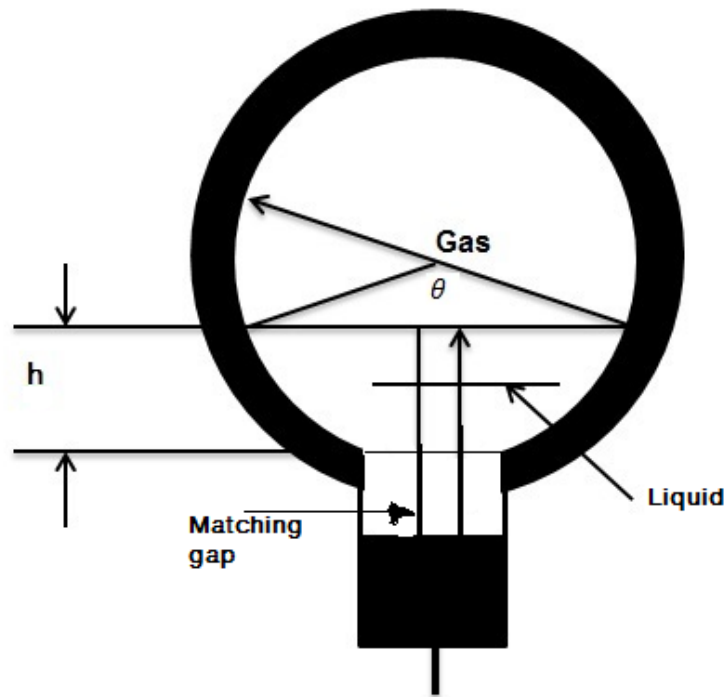
Figure 4-2 Liquid level measurements; geometrical representation in a horizontal tube

The pulse-wave ultrasound sensor system is applied for liquid height by measurements detecting the instantaneous positions of the interface from the time of flight of the pulsed ultrasound non-intrusive measurement. The 1MHz is

a wet transducer which was installed on the test section, flush mounted, while the 7.5MHz is a clamp-on and was attached to the surface of the test section with wire clips.

4.4.2 Experimental procedure

The first step in the study was to determine the feasibility of the experimental techniques for the two-phase flow. Therefore, the single phase water flow was first measured with the ultrasonic Doppler flowmeter; water liquid holdup measurement calibration was conducted using the conductivity probes by static tests. The ultrasound pulse wave sensors were tested to study the ultrasonic echo signals reflected by the gas-liquid interface of the flow. The test was a static test for determining the measurement of the accuracy of the liquid/gas interface determination technique.

Thereafter, two phase flow experimental runs were tested. The two-phase air water flow is generated by inducing individually air and water flows into the rig, thereby a two-phase flow is created at the test section of the rig. In the test, all the instruments on the rig and those at in section in particular are all used for recording the data generated for a period of 20 seconds. The two-phase flow test points investigated during this study belong to the four horizontal flow regimes: slug, elongated bubble, stratified smooth and stratified wavy flows. The superficial velocity of the liquid flow was varied between 0.004mls and 1.5mls and the superficial velocity of the gas ranged from 0.05mls to 2.0mls. The superficial velocities were calculated as the ratio between the volumetric flow rate of the phase and the cross-sectional area of the pipe. An overview of the test conditions of the horizontal two-phase flow tested in this study is given in the Appendix, in section A.1.3. All stated superficial gas velocities are at standard conditions (1 bar, average of 22°C).

The ultrasonic Doppler sensor signal of the two-phase was used for studying the non-invasive measurement of two-phase flow parameters, such as slug flow velocities and slug frequency, while the pulse echo ultrasound was used for investing ultrasound liquid height measurement which is required for liquid holdup measurement. The conductivity probes are used for measuring the slug

flow parameters and these measurements are used for validating the results of the ultrasonic measurement.

4.4.3 Detection of Δt and Liquid Level Calculation

The echo intensity technique is a signal processing approach for measuring the location of a gas-liquid interface by estimating the time duration between transmission and reception of an ultrasound signal. The waveform resulting from the pulse-echo system was analysed using a threshold algorithm for the echo intensity technique to identify the peaks' amplitude. The algorithm was written in MATLAB which reads the pulse-echo data from the storage disk and stores them as variables. The program then pre-processes the data by tapering and filtering. The tapering sets signals very low and amplitudes to zero, and the filter eliminates the DC components of the signal using a design as an LPF. The pre-processed data are then processed further to identify the location of the peaks in the signal. The maximum peak for each pulse echo signal is determined by finding a peak that has a higher amplitude than the peaks before and after it. The difference between the two peaks calculated gives the number of samples which is multiplied by sample duration to obtain the time of flight.

4.4.4 Determination of the Measurement Accuracy

A calibration experiment was conducted in a pipe section of the test rig which was plugged at both ends with flanges to form a short close pipe (length: 67cm and internal diameter: 5cm) called a spool piece. The spool piece was gradually filled up by intermittently pouring in known volumes of water (static). The liquid level was measured using the ultrasonic contact transducer. The piece was placed on a horizontal plane so that the pipe diameter was now the depth of the pipe or height of the interface. The ultrasonic measurement system was calibrated for liquid levels measurement. With each water volume introduced, the corresponding ultrasonic signal resulting from the liquid level of the volume of water was recorded for offline processing to determine the time of flight.

The instantaneous liquid level is calculated as h_l using equation (4-5)

$$h_l = \frac{C_w \times \Delta t}{2} \tag{4-5}$$

93

where C_w = speed of sound in water at 20℃ = 1480m/s, Δt = time of flight of the reflected signal from the liquid/gas interface (b), as shown in Figure 4-3.
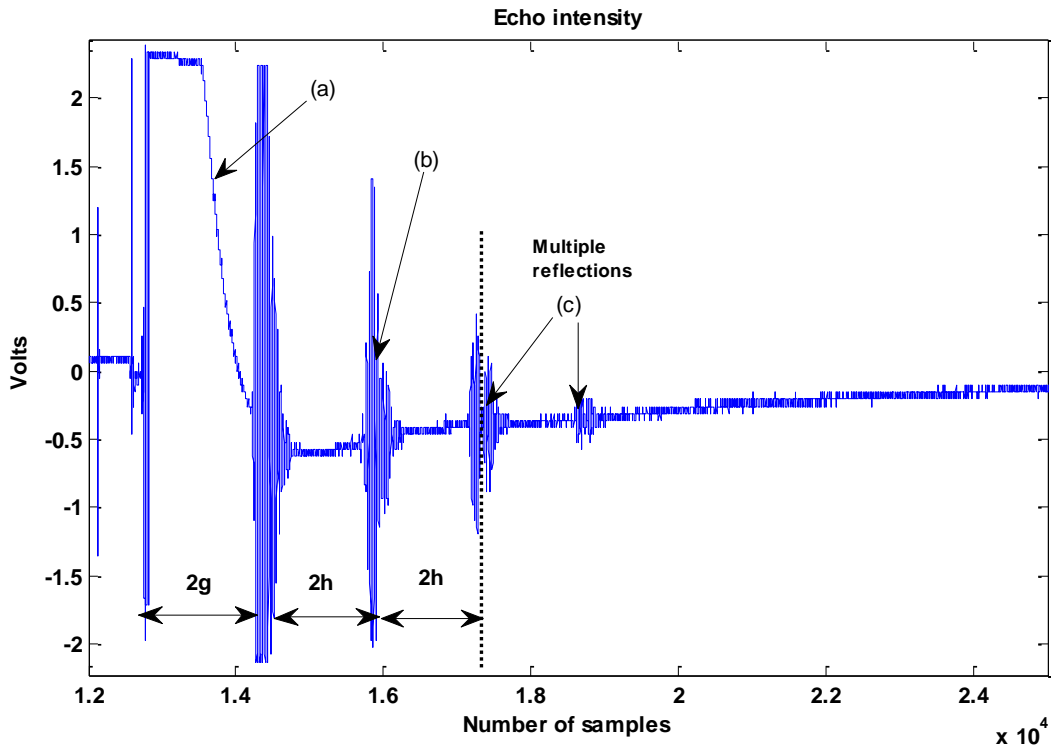
Figure 4-3 Typical representation of the wave from a pulse echo signal (A-Scan) where (a) is the initial pulse (2g), (b) is the wave reflected from the pipe/liquid interface (2h), (c) is the wave reflected from the liquid/gas interface, multiple reflection from the liquid interface.

4.4.5 Determination of Measurements Accuracy

Figure 4-4 illustrates the liquid levels measured based on the liquid volume in the test spool (h-geometry) as a function of liquid levels measured by the ultrasonic pulse echo technique (h-ultrasonic). A trendline is applied to show the accuracy of the measurements. The points are in good agreement with the linear line, with a coefficient of determination R^2 = 0.9939. The measurement error is due to a combination of the following factors: the transducer resolution, the imprecision in the determination of the height of the gap between the pipe surface and head of the transducer, and in the determination of the speed of sound in water.
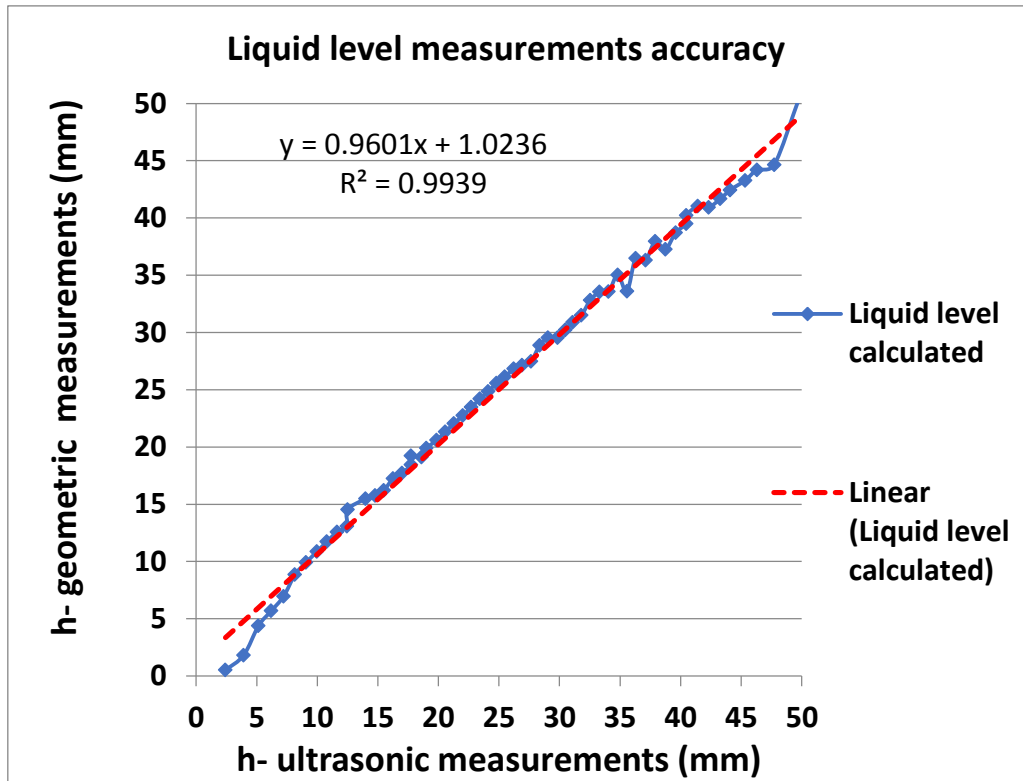
Figure 4-4 Measurement accuracy results for a 50mm internal diameter tube

4.4.6 Measurement of Time Averaged Liquid Height $\bar{\bar{H}}_L$

The objective of two-phase liquid level determination is to investigate the potential for two-phase flow regime characterisation and timed averaged liquid level, and void fraction using ultrasound systems.

The average liquid height is a summation of the values of the instantaneous liquid height sampled over the total number of sample points (Chang and Morala, 1990)**.**

$$\bar{H}_L = \frac{1}{N}\sum_{i=1}^{N} H_{Li} \tag{4-6}$$

H_{Li} is the number of instantaneous liquid heights sampled for a period

where N is the total number of liquid height points sampled

A_{Li} is the cross-sectional area of the pipe filled with water and it is calculated using:

$$A_{Li} = r^2 \left[\frac{\pi}{2} - \sin^{-1}(1 - \frac{H_{Li}}{r}) \right] - (r - H_{Li}) (2rH_{Li} - H_{Li}{}^2)^{1/2} \qquad \textbf{(4-7)}$$

These techniques are developed to study the instantaneous liquid levels, time averaged void fraction, characterisation of the two-phase flow patterns and ultrasonic velocity profile of two-phase flow.

The experiments were conducted on the horizontal air-water two-phase flow test rig which comprises an ultrasound pulse echo transmitting and receiving system, PicosScope (a PC based Oscilloscope), and a Perspex test section. The specifications are listed in Table_Apx 1. The test rig consists of a water circulation system whereby the water is circulated by a centrifugal pump from a tank into the flow pipe. The flow rate is regulated using a hand controlled valve and monitored with an EM flow meter with a capacity of 0 - 40m^3/hr.

4.4.7 Ultrasound echo signals from the vertical flow
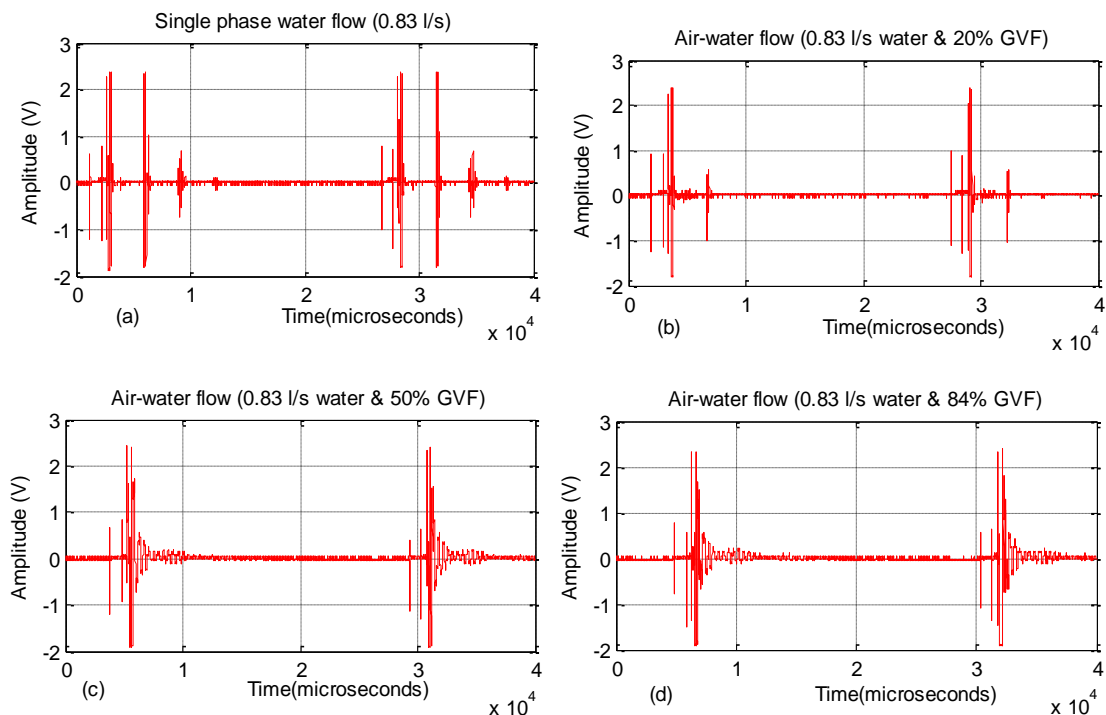
Figure 4-5 Typical examples of reflected echo signals from air-water flow

96
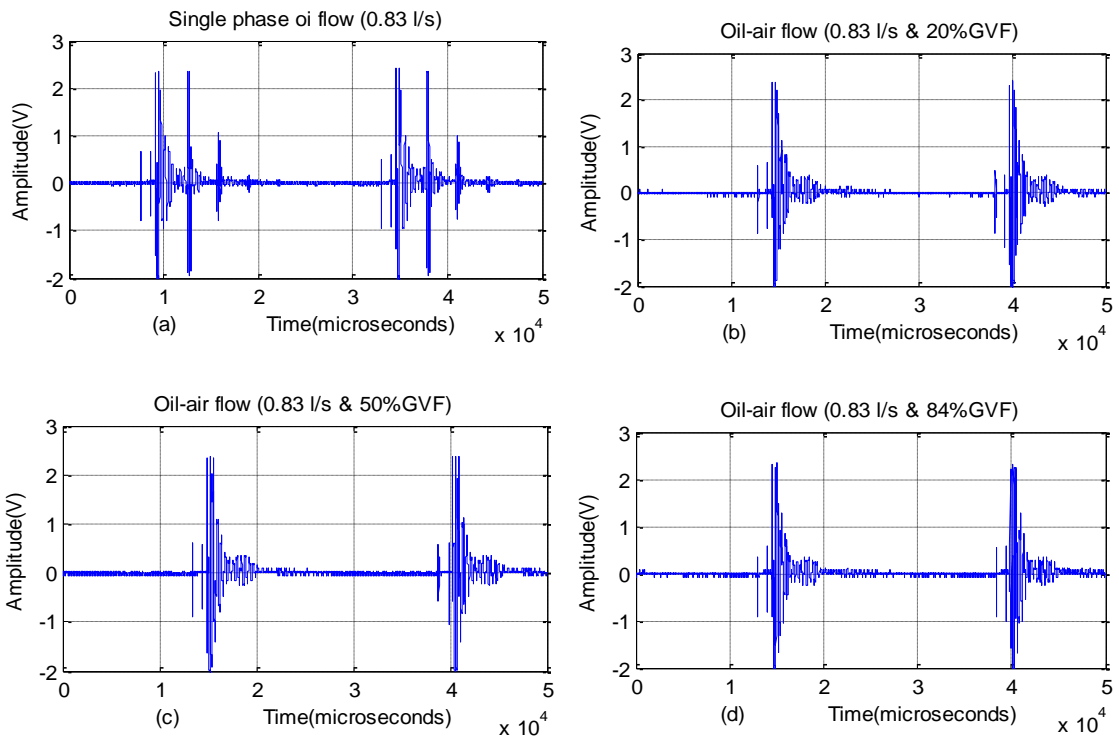
Figure 4-6 Typical examples of reflected echo signals from oil-air flow
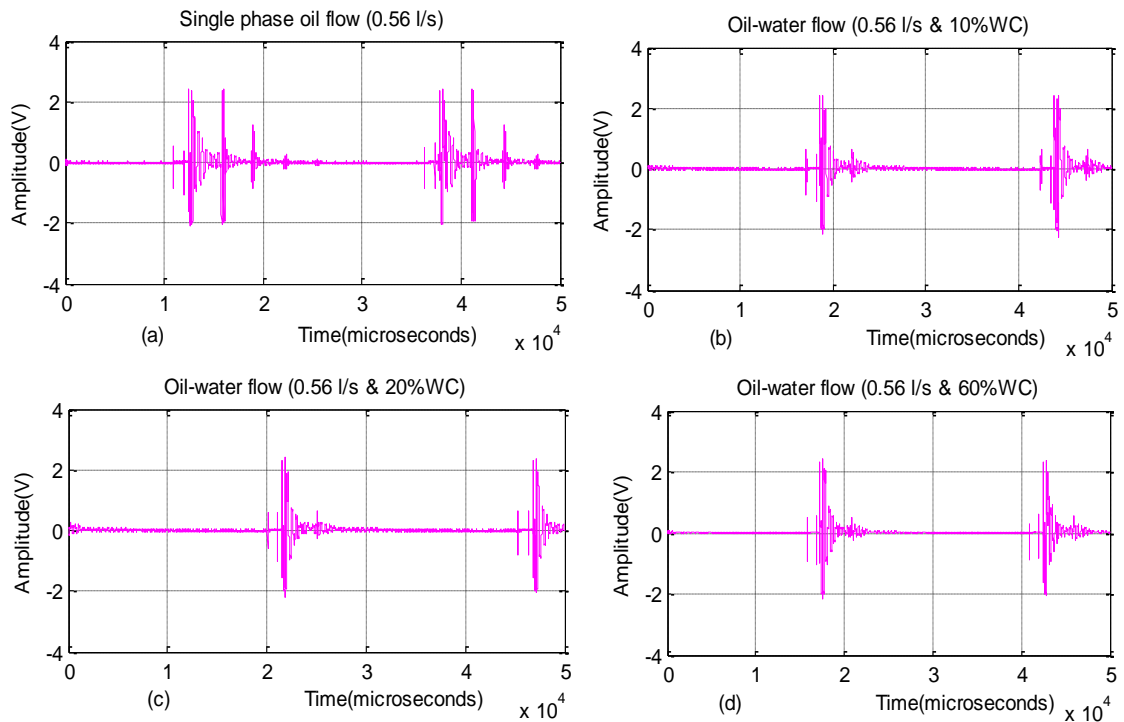
Figure 4-7 Typical examples of reflected echo signals from oil-water flow

97

4.5 Results and Discussion

Time averaged liquid height $\overline{\mathrm{H}}_{\mathrm{L}}$

Figure 4-8 and Figure 4-9 show the mean liquid level measurements performed for various gas and liquid superficial velocities using both an ultrasound system and conductivity probes. In Figure 4-8 in a constant liquid superficial velocity (V_{SL}=0.13m/s) and increasing gas superficial velocity (V_{SL}) from 0.004mls and 2.0mls, the liquid level decreases almost linearly with gas flow velocity as expected. Therefore, it can be deduced that the flow is mostly a smooth stratified flow. In addition, Figure 4-9 shows a similar plot of timed averaged liquid height measured at a constant liquid superficial velocity and increasing gas superficial (V_{SL}= 0.20 m/s) from 0.004mls and 2.0mls. The liquid level, estimated as a function of liquid superficial velocity, and the level keep decreasing but also oscillate with the increasing gas superficial velocity.
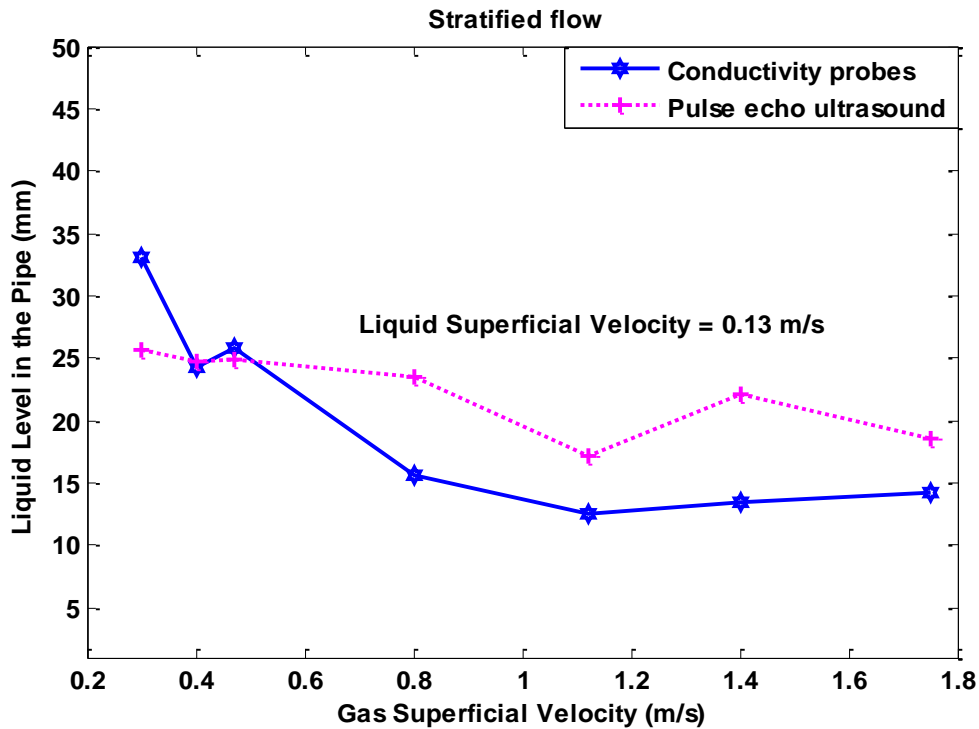
Figure 4-8 Time averaged liquid level for a stratified wavy flow as a function of gas superficial velocity at liquid superficial velocities of $V_{SL} = 0.13\ m/s$
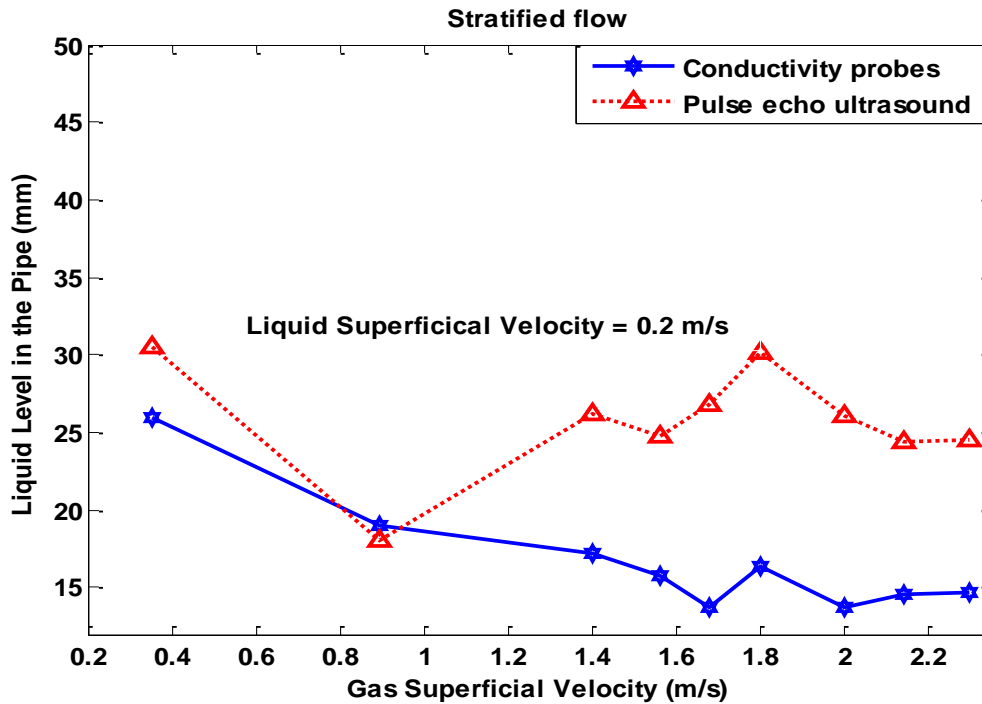
Figure 4-9 Time averaged liquid level for a stratified wavy flow as a function of gas superficial velocity at liquid superficial velocities of $V_{SL} = 0.20 \, m/s$

Moreover, Figure 4-8 and Figure 4-9 show a comparison of the mean liquid levels measured using both the ultrasound sensor and conductivity agreed with each other qualitatively but there is difference in the value which is due to the different sampling duration for the two sensors. The conducticity probes were sampled for a period of 20 seconds but, in contrast, the pulse-echo ultrasound was for 20 milliseconds. This due to the restricted of the memory of required to process the large will be created.

4.6 Summary

In this chapter a pulse echo ultrasonic two-phase flow measurement technique has been set up which uses a single transducer to detect the instantaneous location of the gas/liquid interface in a horizontal pipe. The static test of this technique has shown very good agreement with the geometric measurement of the liquid levels in the pipe and correlation with $R^2 = 0.9938$. Besides, this method has an advantage compared to the conductivity probe technique; it is simpler than other techniques and can be incorporated as a clamp-on on the pipe wall (Chang and Morala, 1990).

We have shown that liquid level measurements of both the pulse-echo system and the conductivity probes technique agreed qualitatively but with some differences quantitatively. This disparity was attributed to mean liquid level measurements being in the whole sampling time used. The conductivity probes were measured for 20 seconds while the present method lasted for 2 seconds. Therefore, the results show the validation of the present method.

5 Ultrasound and Neural network techniques

5.1 Introduction

Multiphase flows occurrences are found in many industrial processes such as petroleum production, power generation, thermal engineering and nuclear reactors. The characteristics used to describe single phase flow, such as turbulence, velocity profile and boundary layer, are not suitable for describing the nature of multiphase flows (Cornelissen et al., 2005). Multiphase flows are categorised into flow regimes; these flows occur both in horizontal and vertical orientations. Flow regimes are developed based on the flow-line geometry and orientation, individual phase flow rates, and component transport properties (density, viscosity and surface tension (Rajan et al., 1993; Thorn et al., 2013). Identification of the flow regimes in multiphase flow is essential both to the efficient operation of the multiphase flow systems and the determination of phase fractions (Arvoh et al., 2012). To group flow regimes according to their topological similarities, several mechanisms of the flow regimes' classifiers or flow regimes' descriptors have been developed over the years. Typical flow regimes in the horizontal pipe flow are: slug, stratified, wavy, elongated bubble and annular flow patterns and in the vertical gas-liquid flow are: the bubbly, slug, churn and annular flows (Falcone et al., 2009). The process of the objective flow regimes' identification from the sensor signals of the flow requires the use of a pattern recognition technique.

The application of pressures fluctuations of the two-phase flow signals and statistical analyses for objective characterisation was pioneered by Drahoš and Čermák (1989). The two-phase flow signals from several pressures transducers have been analysed for features extraction using PSD for generating input variables for the neural network (Kv and Roy, 2012; Sun and Zhang, 2008; Xie et al., 2004). Other sensor signals have been used for flow regime classification using the statistical moment of the analysis, such as conductance probes, (Hernández et al., 2006), and radioactive images (Sunde et al., 2005). It has been found that the pattern recognition of flow regimes using pressure signals is fast enough to be used for online flow regime identification (Kv and Roy, 2012; Xie et al., 2004). However, these transducers are invasive sensors. Hence there

is a need for a non-invasive method of flow regime classification for two-phase flow, such as ultrasound or gamma. In addition, the review of methods of objective flow regime classification have shown that the early methods used mechanistic models or empirical models. The flow patterns of the multiphase flow were identified using equations governing the physics of the fluid developed from the mechanistic models derived from the physics of the fluid. The process of identifying flow patterns using these models have disadvantages as each flow regime has to be examined independently (Ozbayoglu and Ozbayoglu, 2009).

Despite the feasibility of using the pulse-echo ultrasound for flow regime identification, the latter is based on computational models. The computational methods for flow regime identification employed sets of non-linear equations but often the equations are simplified. For practical applications, the simplified equations are not often used because they require prior knowledge of several flow properties, such as pipe diameter and pipe thickness, which degrade over the course of time (Meribout et al., 2010). The method of pulse-echo ultrasound is limited in liquid flow velocity information due to the restriction on the maximum measurable velocity using pulse wave ultrasound by the Nyquist criterion (Evans and McDicken, 2000).

Ultrasound Doppler flow sensors which use continuous waves of ultrasound signals also have a great potential for achieving non-invasive flow velocity measurement. The techniques for using continuous wave ultrasound have existed in the medical ultrasound system. The techniques use frequency shift representing the flow velocities to develop methods to predict multiphase flow regimes (Übeyli and Güler, 2005). In multiphase flow measurement, Kouame et al. (2003) present an application of CWDU velocity measurement to two phase flow in pipes. They proposed the use of frequency resolution techniques to overcome the hindrance to the velocity profile measurement by the presence of coloured noise which introduces a significant obstacle to the classical frequency estimators. Pulse echo ultrasound techniques for two-phase flow measurement have limited liquid velocity information due to the restriction on the maximum measurable velocity using pulse wave ultrasound by the Nyquist criterion

(Evans and McDicken 2000). Also, characteristics of the reflected wave are being influenced by the shape and size of the interface about the ultrasound wave length (Murai et al., 2010).

Artificial Neural Networks are often preferred over statistical methods of pattern recognition because of their fast responses and simplification (Mi et al., 2001a). Also, ANNs have good performance on pattern recognition due to their efficiency and available learning algorithms (Jain et al., 2000). Also, with regard to flow regime classification, ANNs have advantages over other analytical tools such as Expert System and Clustering. Expert Systems require prior information on the flow regime which could affect its objectivity. Similarly, Clustering may not affect performance accurately due to its poor handling of transitional data points (Hu et al., 2011). Usually, the process of NN development is by training the network to recognise the measurement error in training data and then the network tests on another set of data. If the trained network is accurate enough then it is implemented for online measurement for prediction error correction (Liu et al., 2001). More importantly, NNs would offer a non-linear mapping between the ultrasound input signals and the predicted flow regimes. So the use of the ANN avoids the need for calibration of the multiphase flowmeter (Figueiredo et al., 2016).

Seleghim (2010) developed a numerical simulation measurement of interfacial area and volumetric fraction in two-phase flow using acoustic signals and ANNs to investigate the feasibility of the application of the ultrasound system for clamp-on flow measuring systems. They found that the trained ANN models were able to estimate the values of the volumetric fraction and the interfacial area. Similarly, Figueiredo et al. (2016) employed an ultrasonic methodology based on pulse wave ultrasound transducers which operates on the principle of signal attenuation detection. The ultrasound signal attenuation was analysed and incorporated with ANN for flow pattern detection and void fraction measurement. They suggest that the flow regimes' identification in the 2-in pipe was limited to bubbly flow and slug flow only. The technology presented is appropriate for the detection of the GVF and flow regimes' determination in multiphase flow. However, there does not appear to be any consideration of the

flow regimes except for the bubbly flow and slug flow. However, according to the author's knowledge, studies on the two-phase flow regimes classification using a clamp-on continuous wave Doppler ultrasound have not been reported in the open literature.

The main aim of this research was to investigate the feasibility of a non-invasive method of flow regimes classification using an ultrasonic Doppler sensor and NN. A continuous wave ultrasound Doppler sensor employed in this study, has recently been implemented for investigating the velocity characteristics of slug body and film in a two-phase gas-liquid slug flow. The results showed velocity characteristics of the slug flow obtained are in good agreement with other experimental methods (Fan et al., 2013). The present approach is by recording and processing ultrasonic Doppler signals on the flow and then features are extracted using both PSD and WT methods. These features are the inputs for the ANN models which process them for flow regime classification. A multilayer perceptron neural network (MLPNN) with three layers, namely inputs, varying hidden layers and four output neurons, were developed to map the flow regimes. Four numerical outputs selected to represent the flow regimes are as follows: the elongated bubble, slug, stratified flow, and stratified wavy flow (Kandaswamy et al., 2004; Subasi, 2005; Übeyli and Güler, 2005). Despite the ANNs having limitations in that they cannot perform accurately outside the range of the training sets, a combination of several neurons of the ANN will be able to 'learn' and memorise the data's original variability so as to function as an objective flow regime classifier. Therefore, ANNs can still fulfil appropriately the requirement for multiphase flow monitoring processes, such as flow regimes classification and prediction of the individual phase flow rates in multiphase, effectively (Rosa et al., 2010).

5.2 Experimental Setup and Procedures

5.2.1 Two-Phase Flow Test Rig

A horizontal air-water test rig for two-phase flow assessments at the Cranfield University's flow laboratory was used to conduct these experiments. A schematic diagram of the test facility is shown in Figure 3-1. The flow loop

includes a closed loop PVC pipeline of 50mm internal diameter with total pipe length of 21m long. An air compressor provided the air flow and water was pumped into the loop from a storage tank of $2m^3$ capacity using a $40m^3$/hr. water pump. The flow rates of air and water are controlled by regulating hand valves and measured using a turbine gas flow meter (QFG 25B/B/EP1, Quadrina) while the water flow rate is metered with an electromagnetic (EM) flow meter (Altoflux K280/0, Altometer). The measurement section for the two-phase flow is made up of Perspex pipes that allow visualisation of the flow regimes. The clamp-on ultrasound Doppler flow sensor was fixed on the bottom of the pipe.
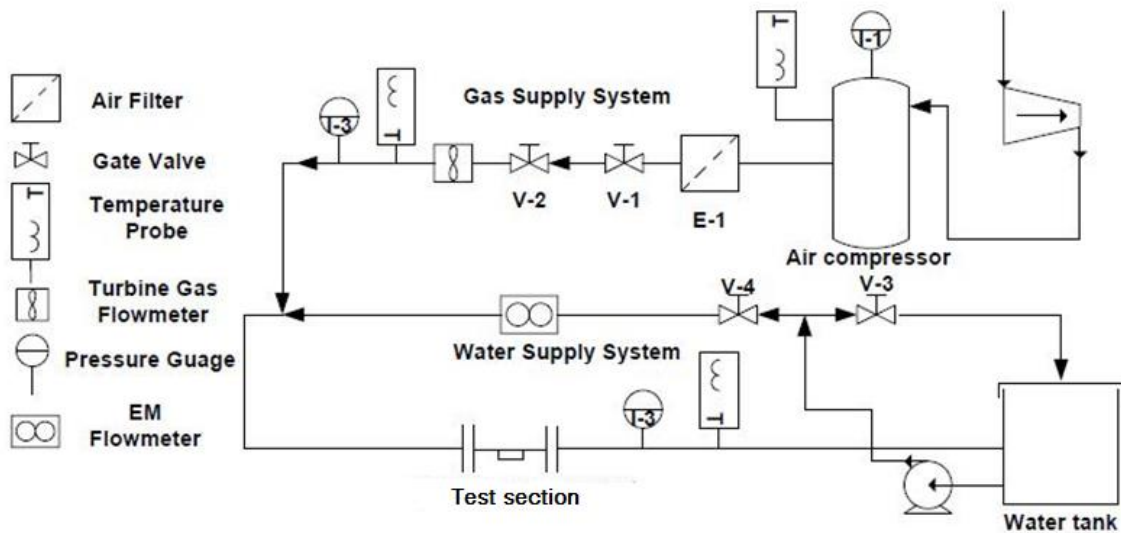
Figure 5-1 part of air-water test rig showing the instruments used in the experiment
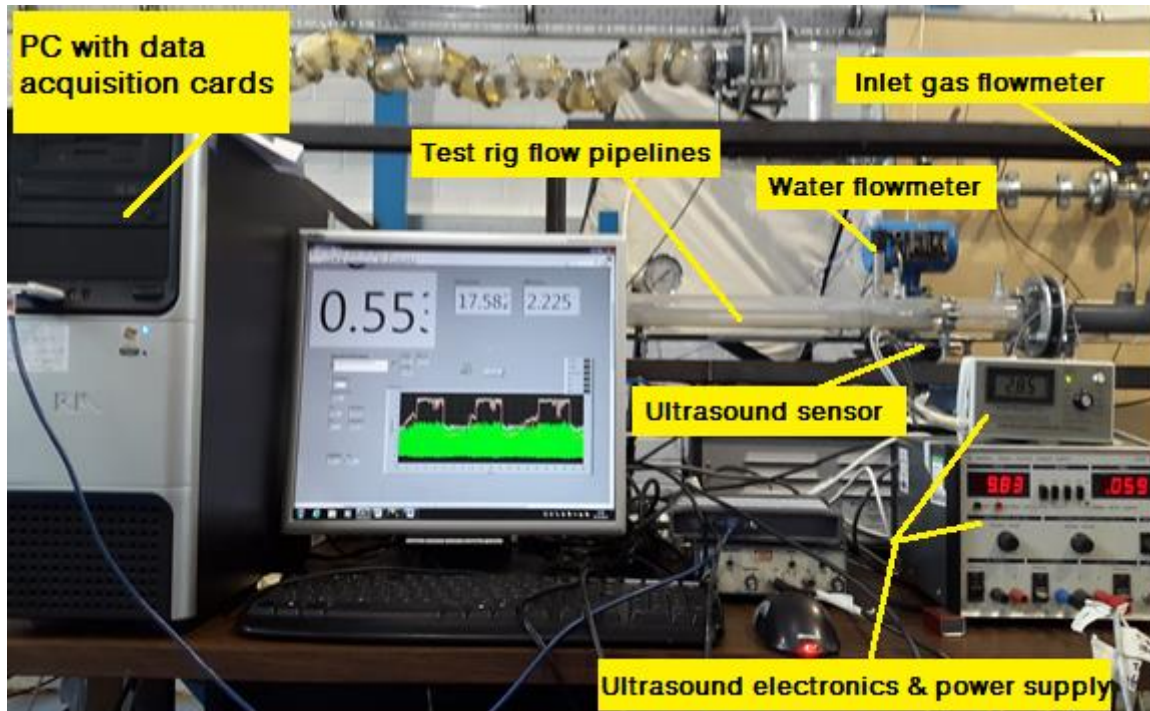
Figure 5-2 The ultrasonic Doppler sensor and its ancillary instruments on the flow test rig

5.2.2 Ultrasonic Doppler senior

The ultrasonic Doppler flowmeter used in this study is a non-invasive fluid flowmeter complete with its sensor, modelled as DFM-2 and manufactured by United Automation Ltd, Southport, UK. This flowmeter is suitable for measuring the flow of any ultrasonic reflective fluid. It measures the frequency shift, processes the signal, computes the flow velocity and gives out digital displays of the flow velocity in feet per second. A green LED shows the strength of the ultrasonic signal reflected back from the flow. It is recommended to be placed on the flow pipe at least ten diameters from bends, valves, tees, so as to prevent measurement errors from swirls, cavitation and turbulent eddies (UAL Ltd). The basic components of the Doppler flow meter system are shown in Figure 5-2. The device measures the Doppler frequency shift of the ultrasonic signals reflected from the scatters or discontinuities, such as bubbles in the flowing liquid. The sensor of the flowmeter is placed at the bottom of the pipe in the 6 o'clock position for the horizontal flow measurement test to avoid attenuation of the signal from gas voids in the upper pipe section. It is important

to have a good bonding between the sensor and the external pipe surface, so a glycerine gel is used for a good coupling which prevents the trapping of air cavities between the pipe surface and sensor. The continuous wave Doppler flow meter has two transducers: one for generating the sound wave and one for receiving the ultrasound reflected by the scatters in the fluids such as air bubbles or particles in the flow.

5.2.3 Measurement principle

The Doppler flowmeter system used in this study has a transducer which has dual piezoelectric ceramic elements. The transducer is excited by the electronic circuit of the flowmeter in continuous mode, the transmitting part of the transducer sends out an ultrasonic signal and the receiving part, to detect the ultrasonic Doppler sensor, provides the output signal. The output signal received is then filtered and amplified by the electronics of the flowmeter. The processed output signal is the Doppler frequency shift signal and it was captured using a data acquisition card (NI-PCI- 6040E) and LabVIEW program controlled sampling frequency of 10kHz for 20 seconds for each data set. The process of development of the flow regimes classification described in a function blocks which various process involved in the system, as shown in Figure 5-3
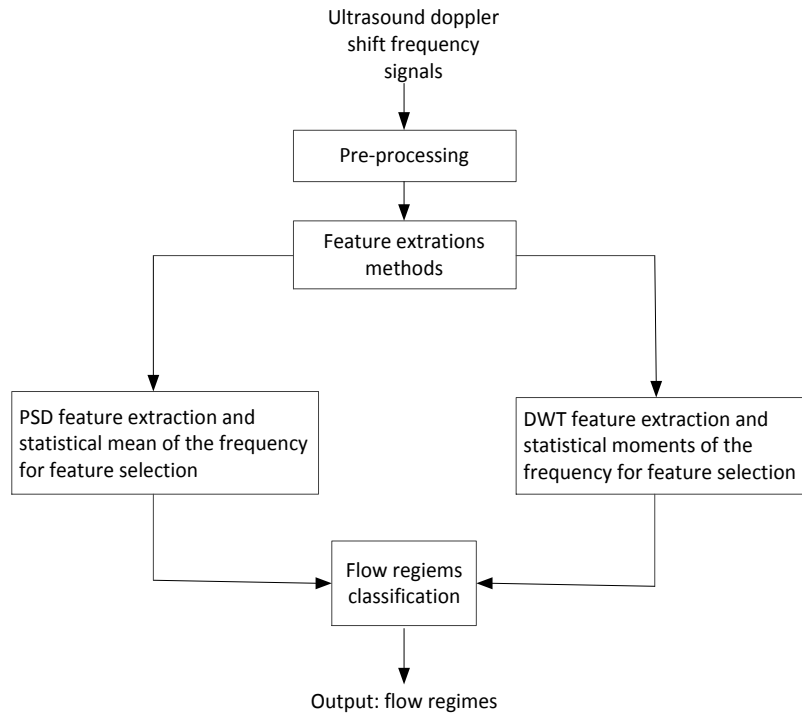
Figure 5-3 functional modules in the flow regime classification system

The relationship between the velocity of the scatters v and the Doppler shift f_d is given in equation (5-1) (Sanderson and Yeung, 2002).

$$f_d = 2f_t \frac{v}{c} \cos \theta \qquad (5\text{-}1)$$

where v = average flow velocity, c = velocity of sound in the fluid, f_d = Doppler shift frequency, θ = angle between ultrasound beam and flow velocity and f_t = ultrasound transmitted frequency.

Usually two transducers are required for Doppler flow meters. However, these two transducers can be made into separate units or one compact unit, as shown in Figure 3-2.

5.2.4 Ultrasonic flow signal data acquisition and Test Matrix

Each of the test data sets of the experiment is created by setting the liquid flow rate to the desired value using a hand operated valve and the flow rate is then measured using the EM flowmeter. First, the signal corresponding to this flow rate is recorded for calibration and air flow is injected into the rig from an air compressor by regulating a valve by hand. The flow of the air supply is varied in

steps, thus generating several, two phase sets in one particular liquid flow rate. The gas flow is measured by the turbine gas flowmeter. Temperature and pressure of the gas at the turbine meter location are recorded for each flow. The superficial gas velocities ranged from 0.05mls to 2.75mls.

All stated superficial gas velocities are at standard conditions (1 bar, average of 22°C). The superficial velocity of the liquid flow was varied between 0.004mls and 2.0mls. The superficial velocities values were calculated as the ratio between the volumetric flow rate of the phase and the cross-sectional area of the pipe. These flow regimes are characterised by distinct phase and velocity differences in the cross section of the pipe. Each of the two-phase flows of the data set's flow regimes was visually observed, identified and recorded for comparison with predicted flow regimes. The total test data sets of the experiment, tabulated as a two-phase test matrix, include the following flow regimes: elongated bubble flow, slug flow, stratified flow and stratified wavy flow. The flow parameters recorded in the experiments are: the initial liquid flow rate, liquid superficial velocities, superficial gas velocities, ultrasonic reflected signals, temperature at the gas flowmeter, temperature at the test section, pressures at both gas and test section. The LabVIEW program was used for controlling the data acquisition at a sampling rate of 10kHz for 20s. The preliminary tests show that this sampling frequency is sufficient as it is more than twice the highest frequency of the Doppler signals.

A four-category classification was chosen for this purpose and the four regimes considered are:

- Stratified flow: when the liquid phase flow is at the bottom and the gas phase is at the top, and the interface of the two flow phases is smooth.
- Stratified wavy flow: this flow occurs under conditions whereby the gas velocity has risen to generate waves on the surface of the liquid.
- Slug flow: in this flow the liquid slugs are separated by the large gas bubbles moving violently downstream of the pipe.
- Elongated bubbly flow: this type of flow occurs when the flow has long gas bubbles and short liquid slugs (Canière et al., 2007; Chang and Morala, 1990):
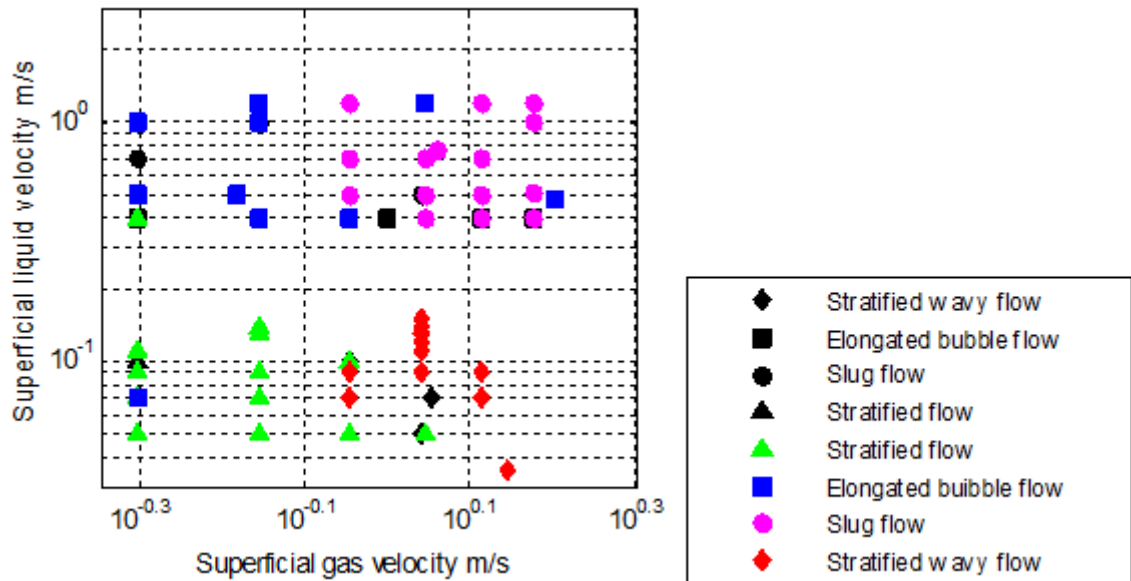
Figure 5-4 Flow regimes map of the present study (black shaded legend test data/ colour shaded legend training data)

5.3 Spectral analyses and Feature Extraction

Spectral analyses techniques are required for the analyses of the signals of two-phase flow to obtain the oscillation period. Two-phase flow signals can be analysed either in the frequency domain, to obtain characteristics of the different flow regimes, or algorithms such as PSD and wavelet transform, which is the time-frequency analysis used. In this work, both PSD and wavelet transform techniques have been applied to two-phase flow signal records of the two-phase signals acquired using an ultrasonic Doppler sensor (Shang et al., 2004). Frequency domain methods using the PSD have been used in analysing two-phase flow to obtain oscillation periods based on the Fourier transform of the signal (Xie et al., 2004). The WTs have the capability of analysing and de-noising the signals to produce the spectrum in the time-frequency domain.

5.3.1 Power spectral density

Frequency domain methods are often used to reveal the distinctiveness in the signal of flow regimes in two-phase flow systems. The PSD is a method of estimating the characteristics of a time-series signal of stochastic process in the

frequency domain that is suitable for detecting the frequency components hidden in the process (Matsumoto and Suzuki, 1984). The application of PSD to time series signals, such as the two-phase flow pressure fluctuation signal, has been studied by several researchers (Santoso et al. 2012; Sun and Zhang 2008; Xie et al. 2004). The PSD is used to produce the characteristics of the two-phase flow signal in the frequency domain which has shown that signals of the flow regime are distinctively different.

FFTs are use in creating the PSD spectrum which assumes that the process signal is stationary. The PSD function $P_x(f)$, of a discrete signal $x(n)$ is the Fourier transform of the autocorrelation sequence $R_x(k)$ of the signal, as shown in equation 5-2 (Xie et al., 2004).

$$P_x(f) = \sum_{-\infty}^{\infty} R_x(k)\, e^{-i2\pi f/f_s} \tag{5-2}$$

The application of the PSD function to a real valued continuous data, the autocorrelation sequence can be approximated by a time-average. However, application of the function to the measurement signal is recorded for a finite time interval, which may present some distortions. As a consequence, a modified form of the PSD called the Welch method is often adopted in these applications. The Welch method subdivides the signal sample into small length N-points overlapping segments and then obtains the periodogram of each of the segments. The power spectrum is estimated by the average of the periodograms (Xie et al., 2004).

The Doppler ultrasonic frequency signals were processed in the MATLAB software package (MATLAB Version: 8.3.0.532) to analyse their spectral contents. Power spectral densities using the Welch method, with segment length of 256 point and Hanning window to alleviate distortions, computes the spectra (Beale et al., 2013), as applied by (Xie et al. 2004). Examples of the power spectra estimates of the samples of the signals are shown in Figures 2-6 and 2-7. It can be seen that the spectrum of the slug flow signal has the highest power on the spectrum. The slug flow ultrasound signal contains higher Doppler frequency shifts as well other the translational than the slug film velocity and the single phase flow. However, the spectrum of the signal of the single phase flow

has produced a higher signal power than both the stratified flow and bubbly flow signals but much less than that of the slug flow signal. The rich ultrasonic shift frequency could be obtained from the single phase flow because the flow pipe was full. Also, in the slug flow, there were intermittent full pipes and in the liquid slugs flow, with a higher velocity than the corresponding single phase flow. The spectrum of the bubbly flow regime is slightly similar pattern to that of slug flow.
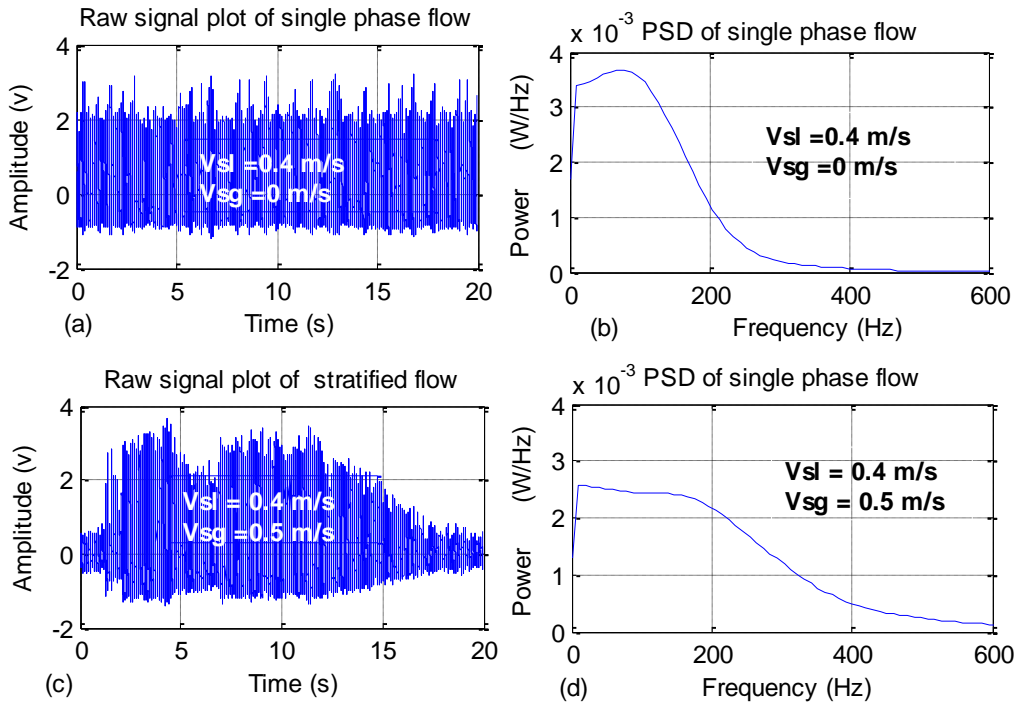
Figure 5-5 Single phase flow and stratified flow of an ultrasonic signal
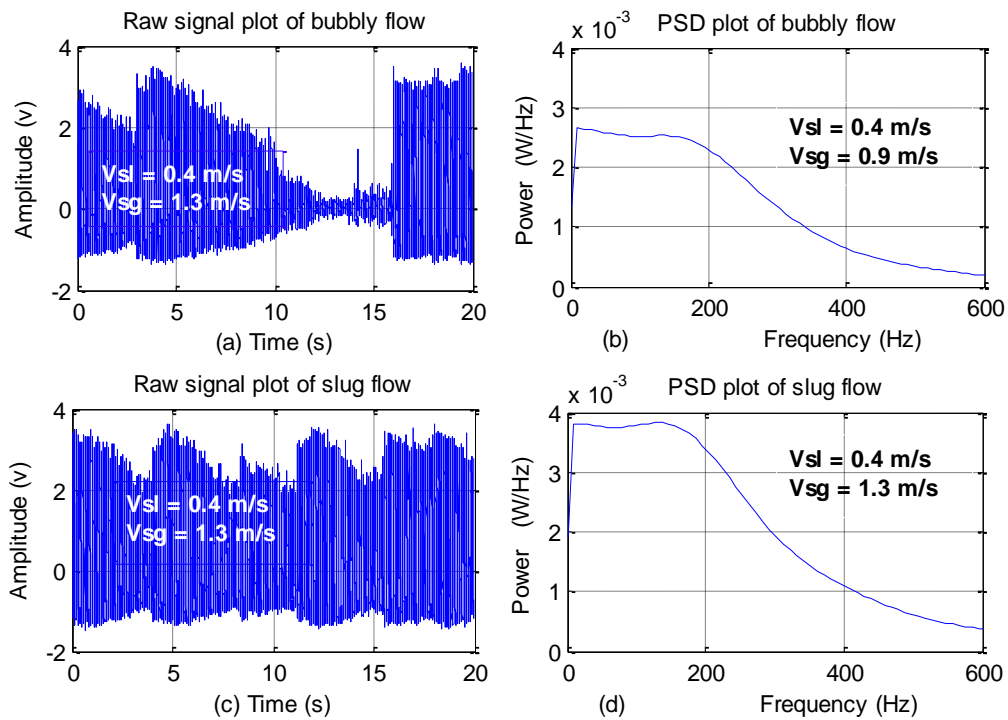
Figure 5-6 Bubbly flow and slug flow of an ultrasonic signal

The principle of extraction of the features from the PSD is based on Parseval's theorem which states that the PSD is the measure of the total energy of the signal if the spectrum is integrated over its entire frequency band. The sampling frequency and length of the signal play an important role in the statistical properties. In the present study, the sampling frequency is chosen to be 10kHz so as to exceed the Nyquist criterion for the signal of the experiment. This can be seen in Figure 5-6 The PSD spectrum produced from the signal recorded by the ultrasonic Doppler sensor effective has a frequency band from 0 - 600Hz. It is obvious that each of the PSD features extracted are distinct and therefore, the PSD feature is a good choice to be used to identify the flow regimes of the gas-liquid flow. As a result, the PSD magnitudes were normalised and their amplitudes corresponded to all data recorded in the frequency range. Each frequency band of the two signals was divided into five bands. The PSDs of the ultrasonic signals are partitioned into 120Hz ranges, as shown in Table 5-1.

Table 5-1 Frequency Band

Ultrasonic signal PSD frequency band		
Band name	Frequency range (Hz)	Average power
B1	0 - 120	$\bar{P}_{B1}$
B2	120 - 240	$\bar{P}_{B2}$
B3	240 - 360	$\bar{P}_{B3}$
B4	360 - 480	$\bar{P}_{B4}$
B5	480 - 600	$\bar{P}_{B5}$

Representative of each flow signal created using a mean value, the frequency bands of the PSD spectrum are computed as $\bar{P}_{B1}, \bar{P}_{B2}, \ \bar{P}_{B3}, \bar{P}_{B4}$, and $\bar{P}_{B5}$ (Matsumoto and Suzuki, 1984). Other properties estimated from the spectrum are the weighted mean of the frequency over the entire band and the variance of the mean frequency (Sun and Zhang, 2008). In total, the five power magnitudes, weighted mean frequency, and variance are used as the features to represent the signal of the flow. The mean spectral power is equation (5-3) and

$$\bar{f} = \frac{\sum_i f_i P_x(f_i)}{\sum_i P_x(f_i)} \tag{5-3}$$

variance of the spectral power is equation (5-4)

$$\sigma_f^2 = \frac{\sum_i (f_i - \bar{f})^2 P_x(f_i)}{\sum_i P_x(f_i)} \tag{5-4}$$

The use of these seven discrete parameters $(\bar{P}_{B1}, \bar{P}_{B2}, \bar{P}_{B3}, \bar{P}_{B4}, \bar{P}_{B5}, \bar{f} \ \& \ \sigma_f^2)$ to represent the signal were first suggested Drahoš and Čermák (1989) and the method has been implemented by many researchers, such as Shaban and Tavoularis (2014) and Xie et al. (2004).

5.3.2 Discrete wavelet transform (DWT)

The idea of signal decomposition using DWT is not new. However, its usefulness lies in its ability to manipulate the wavelet coefficients to identify the characteristics of the signal as distinct from the original time signal (Subasi, 2005). In this work, decomposition of the ultrasound Doppler signal and the

conductance signal from the two-phase flow were carried out using DWT. The procedure for extracting signal features using DWT to represent requires the selection of the wavelet type and level, multiresolution decomposition and selection effective coefficients of the discrete wavelets of the decomposition to represent the signal (Shang et al., 2004).

The DWT of a signal for feature extraction works on the principle of multiresolution signal decomposition in which a signal is filtered using a half band high-pass filter and low-pass filters (Subasi, 2005). There are a number of different wavelets and their levels to choose from for the decomposition of the signals. It is important to select a suitable wavelet type and level to structure the wavelet filter for the decomposition. Wavelet type selection is by either visually inspecting the data for continuity or testing the various types of wavelets with signals and the most efficient one is then selected. If it is a discontinuous type then Harr or sharp or else a smooth wavelet such as Daubechies wavelets is recommended. Daubechies wavelets level 2 was used to compute the wavelet coefficients of the signal in this study (Kandaswamy et al., 2004).

The decomposition of the signals produces approximations and details the levels with different frequency bands by using successive low-pass and high-pass filtering. These detail levels will not lose their information in the time domain (Bendjama et al., 2015). However, useful information can be obtained from the subbands of the dominant frequencies, so statistical measurements of the subbands are representative of these detail levels. The signals of the flow were decomposed continually until all the dominant frequency ranges had been viewed. The signals do not have any useful frequency below 40Hz and that is why the decomposition ended at level 7 which is the level at frequency subbands greater than 40Hz. Therefore, the Doppler signal was decomposed into the detailed coefficients of $D_1 - D_7$ where 1-7 refers to the detailed wavelet coefficient levels: first to seventh and the last approximation is A_7. The ranges of the frequencies' subbands are given in the decomposition The Daubechies wavelet of the order 2(db2) was used to compute the wavelet coefficients of the signal. The computation of the DWT of the coefficient was done using a MATLAB software package (Misiti et al., 1997).

Table 5-2 Ranges of frequency bands in the different wavelet decomposition levels (DWT)

Ranges of frequency bands in wavelet decomposition		
Decomposed signal	Number of samples	Frequency range (Hz)
D_1	100000	2500 - 5000
D_2	50000	1250 - 2500
D_3	25000	625 - 1250
D_4	12500	312.5 - 625
D_5	6250	156.25 - 312.5
D_6	3125	78.125 - 156.25
D_7	1562.5	39.0625 - 78.125
D_8	781.25	19.53125 - 39.0625

For each of the data sets, detailed wavelet coefficients at the first level, second level and up to the seventh level were computed. Importantly, to reduce the size of features extracted from coefficients, statistical measurements were applied to the values of $D_1, D_2, D_3, D_4, D_5, D_6$ and D_7 as implemented in the work of Übeyli and Güler (2005).

Table 5-3 The extracted features of four exemplary ultrasonic records from the four flow regimes

Data set	Extracted features	Wavelet coefficients' subbands (ultrasonic signals)						
		D1	D2	D3	D4	D5	D6	D7
Stratified	Maximum	0.0069	0.0146	0.0328	0.0842	0.2348	0.6549	1.782
	Mean	5.7E-06	3.4E-05	8.9E-05	2.5E-04	6.6E-04	0.0019	0.0054
	Minimum	-0.0104	-0.0146	-0.0259	-0.0684	-0.1908	-0.5353	-1.4834
Bubble	Standard deviation	0.0017	0.002	0.003	0.0063	0.0173	0.0485	0.1365
	Maximum	1.8351	2.7112	4.0595	6.4941	7.3507	7.5821	4.5808
	Mean	1.2E-04	-0.001	-1.9E-04	-0.0064	-0.0045	-0.0024	4.8E-04
Stratified Wavy	Minimum	-1.8178	-2.9443	-4.2209	-6.2225	-7.8911	-8.6795	-5.8672
	Standard deviation	0.1738	0.3981	0.8375	1.4791	1.4709	1.3086	0.9101
	Maximum	0.0069	0.0146	0.0363	0.0891	0.2443	0.6854	1.9266
Slug	Mean	2.6E-06	4.8E-07	1.5E-06	1.5E-06	-3.8E-05	-3.6E-05	-8.8E-06
	Minimum	-0.0069	0.0171	-0.0432	-0.1172	-0.3384	-0.9363	-2.4544
	Standard deviation	0.0017	0.002	0.0031	0.0064	0.0178	0.05	0.1403
	Maximum	2.2339	3.3618	4.7681	6.8243	8.841	9.4888	5.9295
	Mean	0.0011	0.0021	0.0028	-0.016	-0.0193	2.11E-04	0.0036
	Minimum	-2.1424	-3.3179	-4.889	-6.8878	-8.6584	-9.5898	-6.7651
	Standard deviation	0.4739	0.9882	1.9812	3.2405	3.4286	2.3328	1.7116

1. Maximum of the wavelet coefficients in each subband.
2. Mean of the wavelet coefficients in each subband.
3. Minimum of the wavelet coefficients in each subband.
4. Standard deviation of the wavelet coefficients in each subband.

Features 1-3 represent the frequency distribution of the signal and feature 4 the amount of changes in frequency distribution. These are the statistical features used to represent the two-phase flow and as inputs into the neural network for the flow monitoring (Übeyli and Güler, 2005). The wavelet detail coefficients of the signals are distinctly different. Figure 5-7 shows the details of wavelet coefficients corresponding to the D_1 frequency of the two-phase flow.
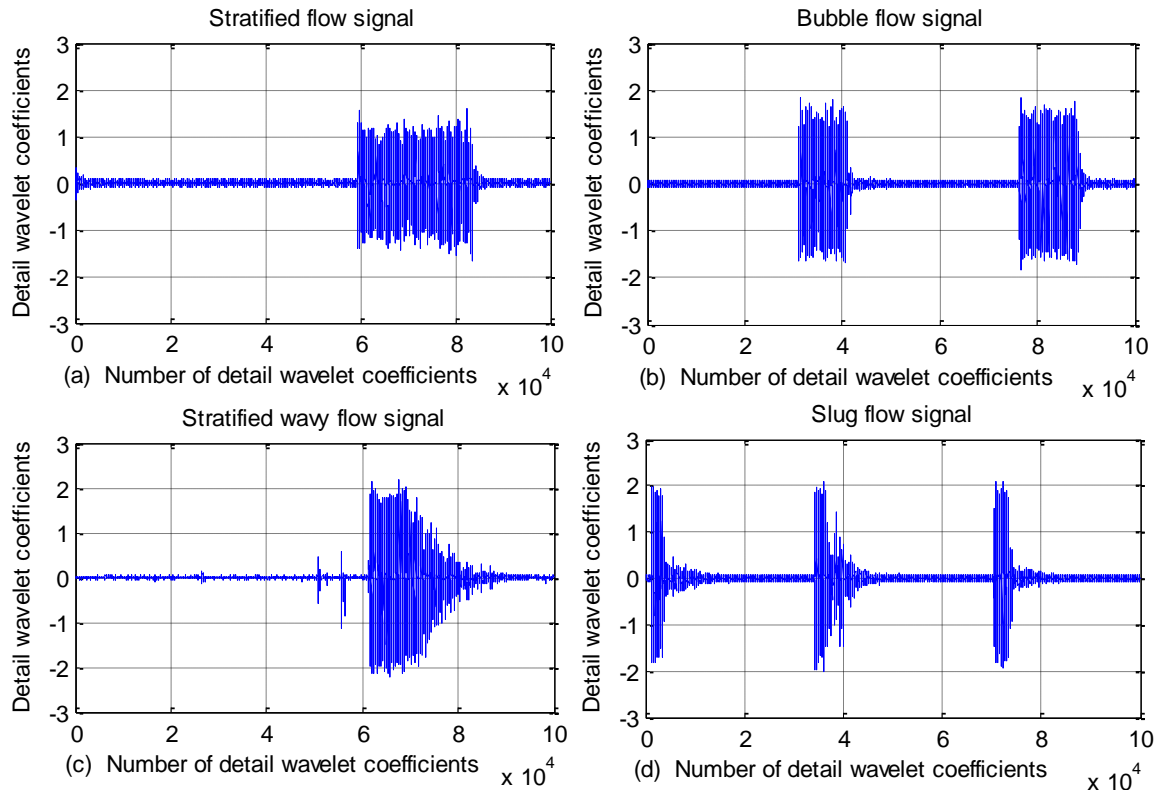
Figure 5-7 The detail wavelet coefficients corresponding to the D1 frequency band of the ultrasonic signals from (a) Stratified flow (b) Bubbly flow (c) Stratified wavy flow and (d) Slug flow regimes

5.4 Multilayer perceptron neural network (MLPNN) model

The MLPNN is a nonparametric technique for conducting various processing techniques for solving function approximation, pattern recognition, classification and estimation problems, and its operation is governed by a set of weights and biases (Übeyli and Güler, 2005). The general structure of the MLPNN with two successive layers is show in Figure 5-8. The structure of the MLPNN model can be represented by equation (5-5). The hidden layer is the unit between the input layer and output layer. Its adjustments are not accessible from outside of the network (Luntta and Halttunen, 1999).

$$y_j = f\left(\sum w_{ji} x_i\right) \qquad (5\text{-}5)$$

where, f is the activation function which transforms the weighted sums of all the input signals on the neurons. The activation function (f) can take many forms

118

such as: threshold functions, or a sigmoidal, hyperbolic tangent or radial basis function. The sigmoidal function is the one chosen for this study.

$$f(\xi) = \frac{1}{1 + e^{-\xi}}$$ (5-6)
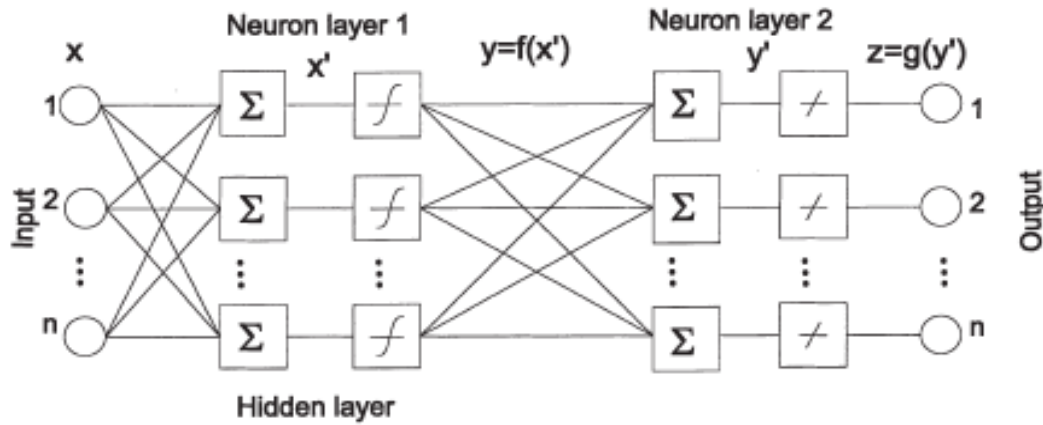
Figure 5-8 Multilayer perceptron neural network (Luntta and Halttunen, 1999)

The performance of an MLPNN can be improved by adjusting the weights of the network to reduce E, which is the difference between the desired output and the actual values of the neurons, as fast as possible.

$$E = \frac{1}{2} \sum_j (y_{dj} - y_j)^2$$ **(5-7)**

where, y_{dj} is the desired value of the output neuron j and is the actual output value whose values can be adjusted and then chosen using the set of targeted outputs.

The flow regimes classification with the ANN is implemented using pattern recognition algorithms. The pattern recognition comprises three steps: 1) data acquisition and pre-processing, 2) data representation or feature extraction, and 3) decision making or pattern classifying. One important aspect of pattern recognition is learning from the training data set (Basheer and Hajmeer, 2000). In this study, the training process consists of the determination of the MLPNN model parameters which are used to validate their quality and ability to classify once the training has been completed (Subasi, 2005). Alternatively, training refers to the process of adjusting and selecting the appropriate weights and biases (Bishop and James, 1993)**.**

5.4.1 Two-phase flow measurement network

Combined neural network design: The combined network algorithm to determine the phase flow superficial velocities comprises five sets of neural network models: N1, N2, N3, N4 and N5. Models N1 to N4 are first level MLPNN which are formed with input (features)-output relationships. The N5 model is the second level of the combined network and uses the outputs of the first level network as the inputs. Each member of the first level network produces two outputs corresponding to the gas-liquid flow velocities and these outputs are concatenated to form a vector for the input of the second level of the combined network. Hence, the combined neural network for the flow velocities training for the four different set of features is extracted.
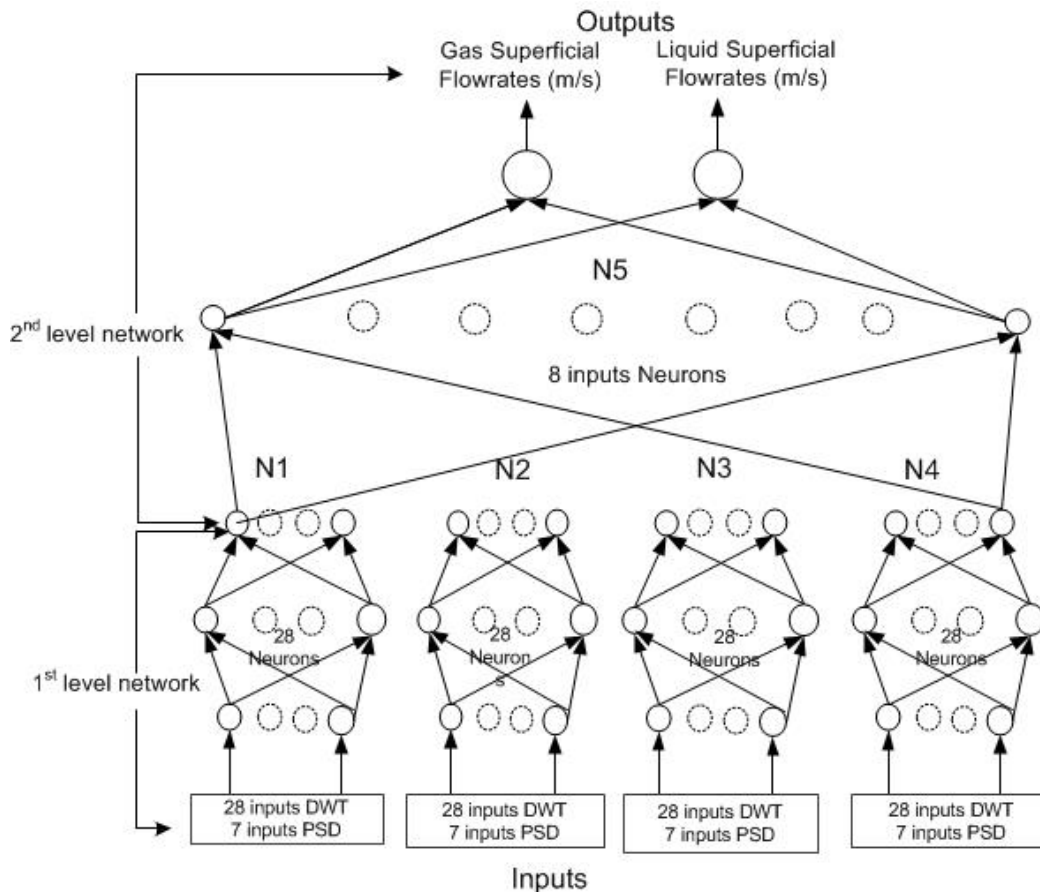
Figure 5-9 A combined neural network topology used for the estimation of liquid and gas superficial flow velocities (Übeyli and Güler, 2005).

5.4.1.1 Neural network training Using DWT features

The DWT applies multiresolution signal decomposition to the flow signals to extract 28 features from the detailed wavelet coefficient from the 47 data sets

for the training. The features from both signals of the ultrasound and conductance sensors are used as the inputs to the first level of the combined neural network (). The corresponding values of the superficial gas and liquid velocities are fed into the network as the outputs for both the first and second levels of the network to train the combined neural network models. Four MLPNN models are set as the first level network and each produces two outputs which the eight inputs for the second level network. The total network models of the combined network are five models, as shown in Figure 5-9. The outputs of the second level are the desired, predicted values of the superficial gas and liquid velocities obtained from the combined network.

During the training, the outputs are repeatedly presented to the networks so as to adjust the weights and biases and this optimises the default weights and biases (). Average performances are taken for the preformed values to establish fitting relationships between the inputs and outputs. Therefore, several network types of back-propagation algorithms and different numbers of hidden layers are tested and their performances are tabulated for the two sensor signals.

Table 5-4 shows the training performance of the ultrasonic signals and Table 5-5 show the performance obtained from the conductance signals.

Table 5-4 Performance of a combined neural network trained using different algorithms (Ultrasonic with DWT)

Algorithms	MAE	MSE	SSE	Rgas	Rliq
LM	0.151	0.057	5.353	0.549	0.958
RP	0.208	0.069	6.481	0.429	0.857
SCG	0.152	0.049	4.628	0.572	0.948
CGB	0.193	0.061	5.759	0.457	0.897
OSS	0.194	0.067	6.267	0.280	0.931
GDX	0.255	0.106	9.939	0.061	0.811
CGB	0.204	0.068	6.352	0.338	0.916
GDM	0.210	0.072	6.795	0.339	0.903
BR	0.057	0.072	5.911	0.588	0.990

Table 5-5 Performance of a combined neural network trained using different algorithms (Conductance signal processed using the DWT)

Algorithms	MAE	MSE	SSE	Rgas	Rliq
LM	0.209	0.096	9.026	0.486	0.763
RP	0.162	0.060	5.608	0.417	0.947
SCG	0.172	0.069	6.530	0.502	0.822
CGB	0.191	0.083	7.817	0.246	0.853
OSS	0.226	0.099	9.284	0.322	0.661
GDX	0.472	0.335	31.481	-0.044	0.526
CGB	0.243	0.091	8.601	0.258	0.732
GDM	0.243	0.113	10.582	0.225	0.553
BR	0.194	0.113	6.011	0.447	0.880

After the extensive training using the DWTs, the MLPNN structure that out-performed in the training for the ultrasonic signal is 28-12-2, and for the conductance signals is 28-28-2. It has been observed that changing the training algorithms. Figure 5-10 shows the results of the best performing models for predicting flow superficial velocities using the features extracted from the signals of the flow using the DWT multi resolution methods (Übeyli and Güler, 2005). It can be seen that the regression coefficient R is 0.96 for the liquid superficial flow velocity while the regression coefficient R of the gas superficial flow velocity is 0.76 (Fan and Yan, 2014; Kandaswamy et al., 2004).
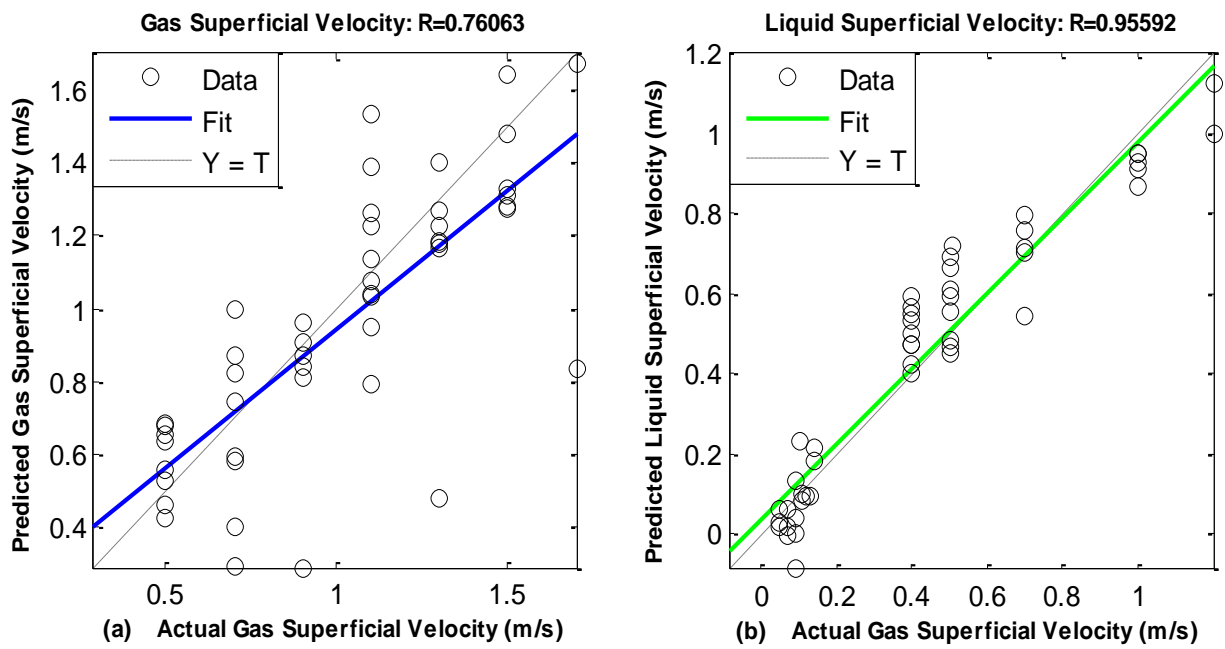
Figure 5-10 Regression plot of the superficial velocities for the combined network training using Ultrasonic with DWT (a) regression of the gas flow (b) regression of the liquid flow
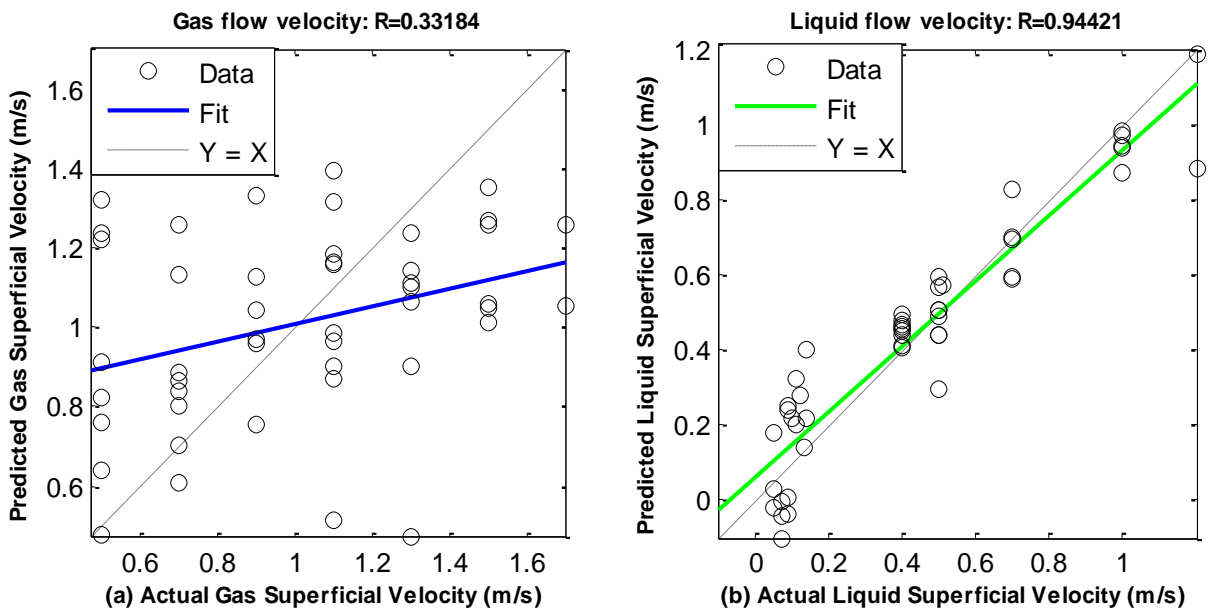
Figure 5-11 Regression plot of the superficial velocities for the combined network training using conductance with DWT (a) regression of the gas flow (b) regression of the liquid flow

5.4.1.2 Neural network training Using PSD features

Similarly, there are a total of seven inputs extracted from the flow signals of both conductance and ultrasonic signals using the PSD to predict the gas–liquid two-phase flow velocities. These seven features $\bar{P}_{B1}$, $\bar{P}_{B2}$, $\bar{P}_{B3}$, $\bar{P}_{B4}$ $\bar{P}_{B5}$, $\bar{f}$ and σ_f^2 are used as inputs for the modelling the combined neural network. Figure 5-11 and Figure 5-12 show the performance of a combined neural network trained using features extracted with the PSD method and different back-propagation algorithms for modelling networks to predict the gas and liquid superficial velocities.

Table 5-6 Performance of a combined neural network trained using different algorithms (ultrasound with PSD 7-12-2)

Algorithms	MAE	MSE	SSE	Rgas	Rliq
LM	0.187	0.079	7.472	0.452	0.871
RP	0.180	0.056	5.220	0.588	0.869
SCG	0.209	0.076	7.157	0.375	0.808
CGB	0.193	0.061	5.757	0.574	0.818
OSS	0.196	0.063	5.919	0.547	0.871
GDX	0.274	0.122	11.440	0.072	0.545
CGB	0.184	0.058	5.459	0.579	0.846
GDM	0.211	0.076	7.114	0.490	0.807
BR	0.174	0.076	4.947	0.602	0.887

Table 5-7 Performance of a combined neural network trained using different algorithms (Conductance with PSD 7-12-2)

Algorithms	MAE	MSE	SSE	Rgas	Rliq
LM	0.227	0.084	7.936	0.722	0.165
RP	0.252	0.137	12.844	0.388	0.115
SCG	0.237	0.091	8.558	0.691	0.047
CGB	0.233	0.088	8.259	0.707	0.143
OSS	0.264	0.105	9.865	0.547	-0.073
GDX	0.311	0.172	16.139	0.056	0.113
CGB	0.304	0.134	12.570	-0.011	-0.054
GDM	0.296	0.126	11.825	0.245	0.130
BR	0.284	0.126	11.216	0.092	0.107
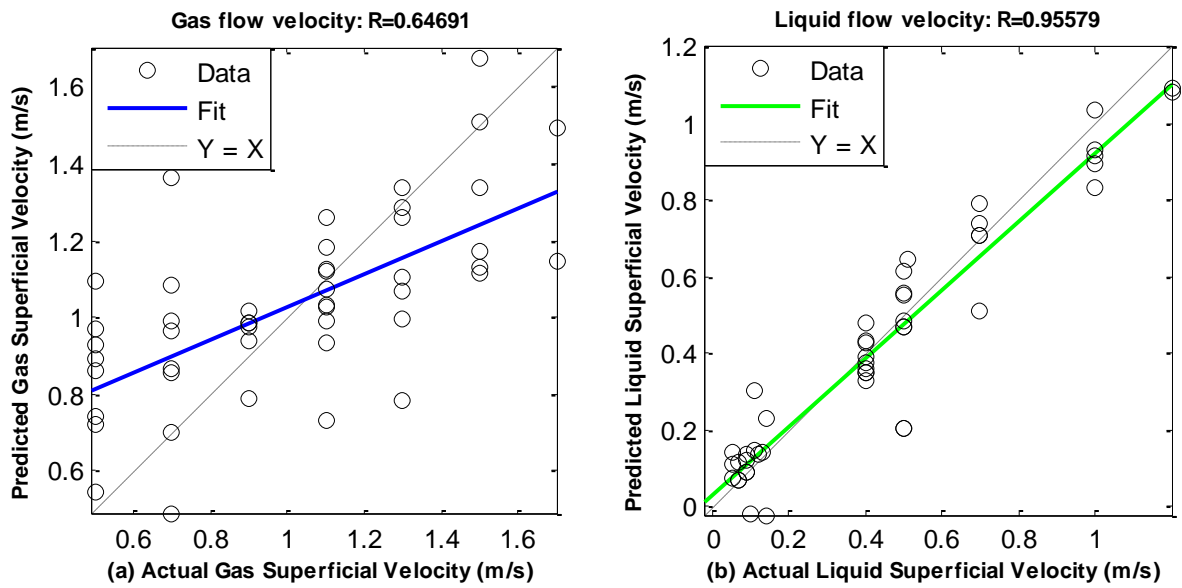
Figure 5-12 Regression plot of the superficial velocities for the combined network training using ultrasound with PSD (a) regression of the gas flow (b) regression of the liquid flow
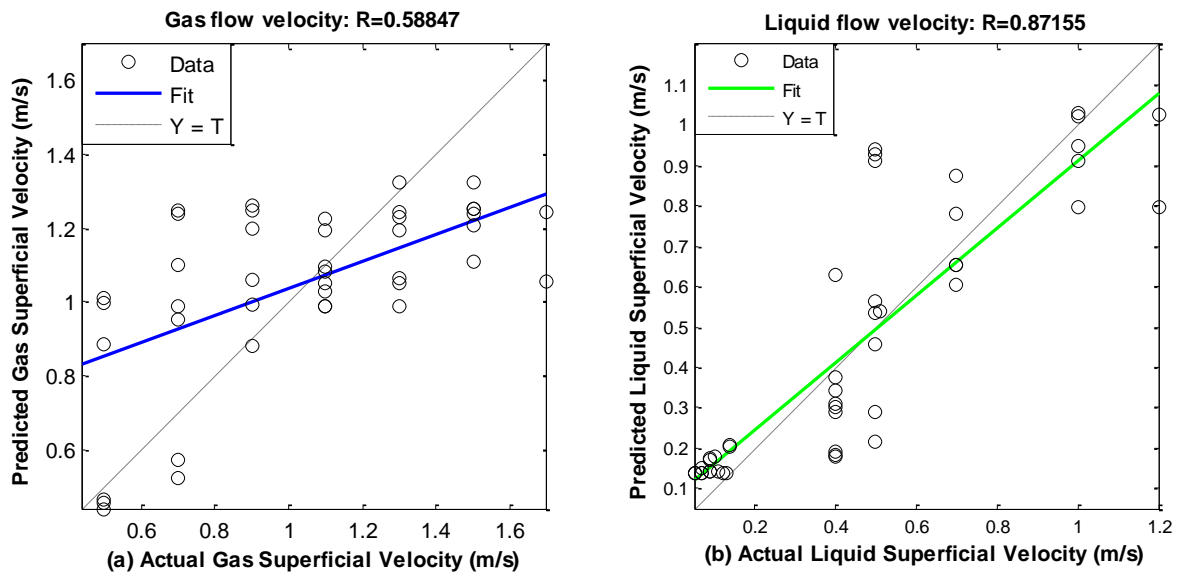
Figure 5-13 Regression plot of the superficial velocities for the combined network training using conductance with PSD (a) regression of the gas flow (b) regression of the liquid flow

5.4.2 Combined neural network models (CMLPNNs)

A combined neural network is a method of improving the performance of the network's predictive accuracy. In designing neural network models, the training data may fail to learn to predict the output accurately, so the network is unable to generalise the concept precisely. The learning system of the network utilises the transformed data to predict the output with greater accuracy. Stack generalisation is a method of combining low level network models into high level neural networks to achieve greater predictive accuracy as introduced by Wolpert (1992). By transforming the data into a suitable form that can enhance the training process, the generalisation minimizes the error rate of the combined network by 'teaching' a second level network whose inputs are the predictions of the first level network but the second is trained with the same target output as the first network.

Multilayer perceptron neural networks were used to form multiple networks and then combined to form a stack generalisation. Figure 5-14 shows the structure of the combined network. The features extracted from the sensors' signals were used as the inputs to the first level network of the combined neural network. After that the outputs of the first level were fed into the second level network as the inputs. The outputs of the second levels are the result of the predicted flow regimes. Both the first and second level neural networks were trained with targeted outputs (Übeyli and Güler, 2005).
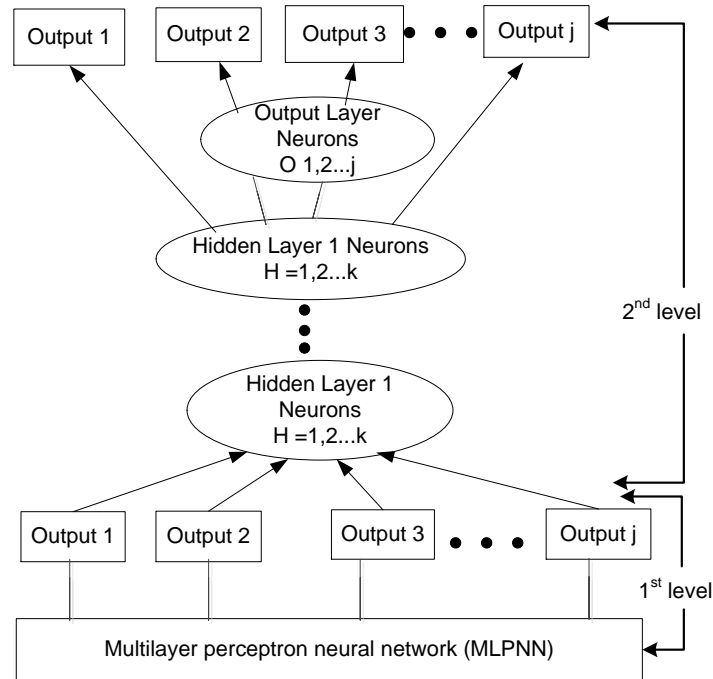
Figure 5-14 A second-level neural network is used to combine the predictions of the first-level neural networks (Übeyli and Güler, 2005)

Multilayer perceptron neural networks were used to form multiple networks and then combined to form a stack generalisation approach to the flow regimes classification. Figure 5-15 shows the structure of the combined network used to predict the targeted flow regimes. Both the first and second level neural networks were trained with targeted superficial flow velocities as the outputs.
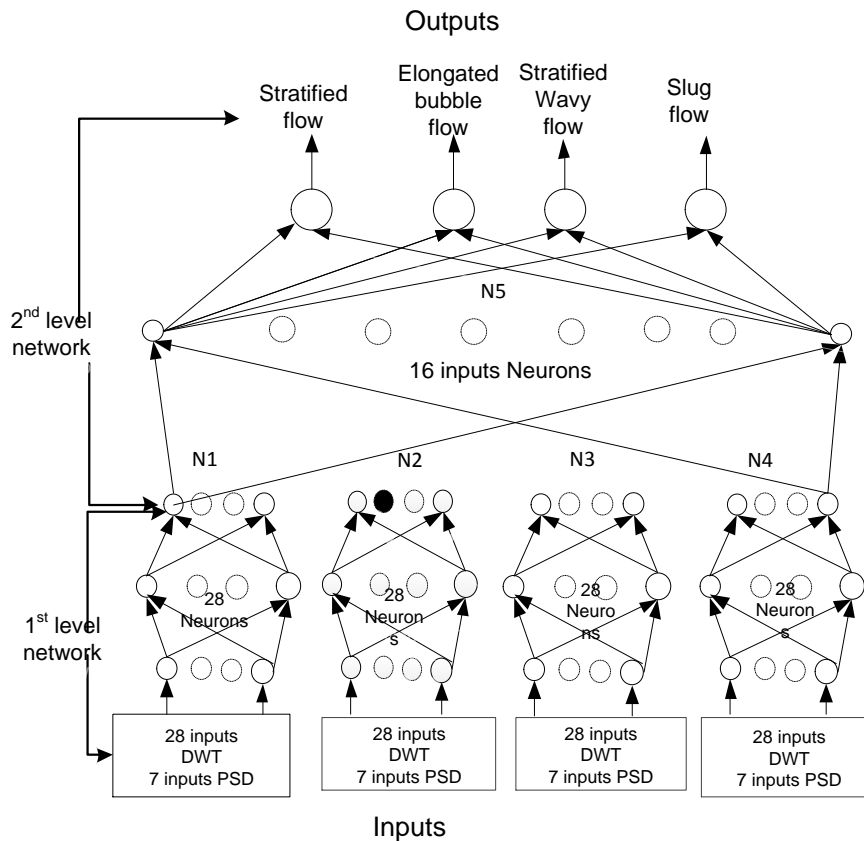
Figure 5-15 A Structure of the flow pattern prediction combined neural network topology (Übeyli and Güler, 2005).

5.4.3 Flow Regime Classification network

Several applications of MLPNN pattern recognition are reported in the literature. It is based on training the neural network to recognise the correct classification for each member of the training data sets. Training the network will be subsequently followed by testing the network to classify the input variables into their correct classes. If the learning process has taught the network the patterns relevant to the test data, then it is expected that the network would classify correctly (Xie et al., 2004).

Flow regime identification using ANN pattern recognition can be implemented by either using a supervised neural network (SNN) or unsupervised neural network (UNN) also known as a self-organising network. The SNN uses feed-forward networks such as multilayer perceptron and Radial-Basis Function networks for pattern recognition in which the back propagation error of the

training algorithm together with information of predefined classes is used to classify the input variables into the specific classes and it does not need; whereas the Kohonen-Network or self-organising map (SOM) used for data feature mapping does not need information about the classes. It uses a network clustering method to group the input variables into several classes that contain similar characteristics (Mi et al., 2001a). The Kohonen Self-Organising Neural Network has been implemented for flow regime classification using measuremnt data points of distinct flow regimes (Cai et al., 1994).

To select the input to the network for the pattern classification, it is essential first to pre-process, balance and normalise the data. The features extracted from the ultrasonic Doppler signal of the flow using both the wavelet method and the PSD methods are pre-processed before presenting them as input variables to the network. As part of the pre-processing of the input data set, data partitioning and balancing are applied to the feature. There several ratios for partitioning the data sets into training, testing and validation. At this moment, there is no mathematical rule for determining the exact sizes of the training, testing and validation data sets. The often used ratios are 60%, 30% and 10% or 65%, 25% and 15% for training, testing and validation respectively (Basheer and Hajmeer, 2000).

Another aspect of preparing the input data is balancing the data sets, which is distributing the training nearly evenly amongst the various classes to annul the effect of networks being biased to over-represented classes. Input data preparation, first balances and then normalises the process to prevent chaos in the network as a result of either the larger numbers overriding smaller ones or the premature saturation of hidden nodes. Normalisation usually confines the data into a uniform range of 0 to 1. A good rule of the thumb is to scale the input variables (z_i) and the output range (λ_2, λ_1) in intervals of the output values which correspond to the function in equation (5-7) (Basheer and Hajmeer, 2000).

$$x_i = \lambda_1 + (\lambda_2 - \lambda_1)\left(\frac{z_i - z_i^{min}}{z_i^{max} - z_i^{min}}\right) \tag{5-8}$$

Statistical analysis of the features plays an important role in selecting the input variables for successful neural network application. Güler and Übeyli (2006)

computed the statistical features (mean, maximum, minimum and standard deviation) to represent the time-frequency features extracted from the Doppler signals using the wavelet transform.

The output of the neural network is the indicator of the flow regimes or classes of classification which are represented with a continuous or binary discrete number. Each of the input variables to the neural network is assigned to the class to which it belongs. Usually, these classes are represented with numerical values. There are two most common representations of the classes: continuous (0.3, 0.5, 0.7, etc.) or discrete (0 and 1 or 0.1 and 0.9). Xie et al. (2004) have implemented the continuous number to represent the output of the neural network to indicate flow regimes. They used continuous numbers (0.3, 0.5, 0.7 and 0.9) to represent the flow regimes: bubbly flow, plug flow, churn-intermittent and slug flow respectively. This technique was supported by their earlier work (Xie et al., 2003). The continuous designation number to represent the output of neural network flow classification methods has been applied by other researchers as well (Sun and Zhang, 2008).

However, due to the importance of the discrete output for extracting rules from trained neural network, Basheer and Hajmeer (2000) have suggested that the continuous variable should be replaced by discrete or binary numbers for representing the output of a neural network classifier. There are methods and algorithms for discretizing the output variables. The discrete or binary number is often modified from (0 and 1) to (0.1 and 0.9) so as to prevent saturation (Basheer and Hajmeer (2000). Also, allocating the targets of 0.1 and 0.9, instead of the common practice of 0 and 1, prevents the outputs of the network from being a directly interpretable posterior (Kandaswamy et al., 2004).

The most frequently used training model in classification problems is back propagation (BP) which is adopted for this investigation and has been in other works (Arubi, 2011; Blaney and Yeung, 2008; Fan and Yan, 2013). The MLPNN has properties such as the ability to learn and transform fewer training set requirements and has fast processing. This is the manner in which the weights can be adjusted, governed by different training algorithms (Übeyli and Güler, 2005). The training tool has functions for performance, magnitude of the

gradient of performance and the number of validation checks. The magnitude of the gradient and the number of validation checks are used to terminate the training. The gradient will become very small as the training reaches a minimum of the performance. If the magnitude of the gradient is less than 1e-5, the training will stop (Beale et al., 2013).

Cross validation in neural network pattern recognition is required to determine the optimum number of hidden units and the model that will perform best on the problem at hand (Bishop and James, 1993; Kandaswamy et al., 2004). The best network model for the flow regime classification is obtained after testing several training algorithms. The performance test of the input data sets is determined by computation of the total classification accuracy and number of training epochs. Total classification accuracy is the number of correctly classified flow regimes/number of total data sets (Übeyli and Güler, 2005).

5.4.4 Flow regimes classifier neural network training and testing

Eighty-six data set measurements on the horizontal two-phase flow are used for this experiment. Sixty-two data sets are used for training the networks and 24 are used for testing the network. Two sets of combined neural network models are developed in a MATLAB software package (MATLAB Version: 8.3.0.532 (R2014a) with neural network toolbox) for classifying the flow regimes of air-water two-phase flow using features from ultrasonic signals of the flow. The inputs to the network are features extracted from the signals of the flow using both PSD and DWTs. The outputs of the combined neural network are (discrete binary) indicators of the four flow regimes: elongated bubble flow, slug flow, stratified flow and stratified wavy flow.

In this training process, the classification scheme of "1-of-C coding method for classification" was adopted to classify the inputs and each member of the data sets belongs to one output of the four flow regime categories. The four predetermined output values are as designated in the following equations: (5-9), (5-10), (5-11) and (5-12). The values are the targets presented to the network as outputs (Subasi, 2005).

$$[0.9 \, 0.1 \, 0.1 \, 0.1 \,] = \text{Elongated bubble flow} \tag{5-9}$$

131

$$[0.1\ 0.9\ 0.1\ 0.1\ ] = \text{ Slug flow} \tag{5-10}$$

$$[0.1\ 0.1\ 0.9\ 0.1\ ] = \text{ Stratified flow} \tag{5-11}$$

$$[0.1\ 0.1\ 0.1\ 0.9\ ] = \text{ Stratified wavy flow} \tag{5-12}$$

Table 5-8 Percentage of flow regimes in the experimental, training and testing data sets

Flow Regime	Exp. Runs	%	Training Runs	%	Testing Runs	%
Elongated bubble flow	20	23.3	14	22.6	6	25
Slug flow	30	34.9	24	38.7	6	25
Stratified flow	20	23.3	14	22.6	6	25
Stratified wavy flow	16	18.6	10	16.1	6	25
Total	86	100	62	100	24	100

The following BP algorithm training algorithms used in the network and their performance for the flow regime identification are examined. The multilayer perceptron has three activation functions for regulating its output: pureline, logsig and tansig). In this study, the sigmoidal function was used throughout due to its properties, such as ranging the output between 0 and 1, non-linear paving the way for complex mappings of the input to the output, and it is also continuous and differentiable (Güler and Übeyli, 2006). Important aspects of the neural network development are architecture and the training process. Several training algorithms and neural network architectures have been tested with different numbers of hidden layer neurons of the network evaluated during the training process.

- Levenberg-Marquardt (LM)
- Scaled Conjugate Gradient (SCG)
- One Step Secant (OSS)
- Resilient Back-propagation (RP)
- Quasi-Newton (BFGS)
- Bayesian Regulation (BR)

Before the fusing of the neural network models, single level neural models were tried out for designing the flow regime classifier but the results were not good

enough. Subsequently, the single levels were integrated into the combined neural network. The neural networks with single layers were found to be superior to the two hidden layers in this experiment. The most efficient configuration for the network with PSD features was 12 neuron hidden layers while that of the DWT features was 28 neurons in the hidden layers.

Combined neural network design: The combined network algorithm to determine flow regimes involves five sets of neural network models: N1, N2, N3, N4 and N5. Models N1, N2, N3 and N4 are the first level MLPNN formed with input (features)-outputs relationships. The N5 model is the second level network of the combined network and it uses the outputs of the first level network as the inputs while using the same outputs as the first level network. Each member of the first level network produces four outputs corresponding to the flow regimes and these outputs are concatenated to form a vector for the input of the second level of the combined network. Hence, the combined neural network for the flow velocities training for the four different set of features is extracted.

5.5 Results and discussion

In this study, horizontal gas-liquid two-phase four flow regimes were classified from ultrasonic Doppler signals processed using ANN. The inputs to the neural network are features obtained from frequency bands of both PSD and DWTs. After the features extracted from the signals, they are normalised. Flow regimes classification models based on feed-forward multilayer perceptron neural network implemented in the MATLAB software package with neural network toolbox. In order improve the performance of the ANN classifier the networks were integrated into two-tier network called combined neural network (Übeyli and Güler 2005). The total number of 85 data sets divided into training and testing sets and 62 data samples used for the training the network and 24 data sets were used for the testing the network.

5.5.1 Feature extractions

The features from the Doppler ultrasound signals of the flow extracted using two methods of features extractions were applied in this study. (1) DWT was for generating the frequency bands by decomposing the Doppler signal and then

applying each of the statistical measures of mean, maximum, minimum and standard deviation to the results of the wavelet transform. (2) Frequency domain spectral analysis of the ultrasonic Doppler signal has been implemented using PSD based on the Fourier transform technique. The PSD spectra were further averaged to be input or representative of the flow in the neural network, as it is necessary to extract statistical moments from the spectra (Xie et al., 2004). Seven frequency bands or levels were obtained from the detailed wavelet coefficients. So, for each of the data set, we obtained 28 features from the seven detailed wavelet coefficient levels and the statistical measure applied to the wavelet levels.

5.5.1 Combined Neural Network for Gas-liquid flow velocities measurement

Twenty-six test data sets used for the combined network were assessed and their results presented as a percentage error deviation from the full scale measurement of both superficial gas and liquid velocities. The superficial velocities' measurements are from the reference EM flowmeter and the turbine gas flowmeter divided by the cross-sectional area of the pipe. All the four feature types investigated in this study were used in testing the performance of the combined neural network.

Figure 5-16 to Figure 5-17 show the performance of the superficial gas and liquid flow velocities' prediction obtained for all the four different types of features used as inputs to the network. The predicted values are presented as how much error deviated as compared to the actual values of the measurement.
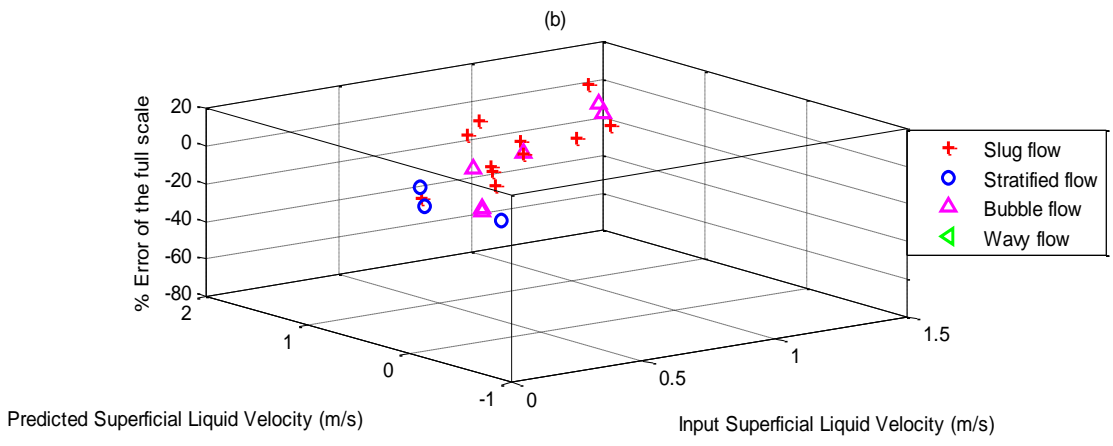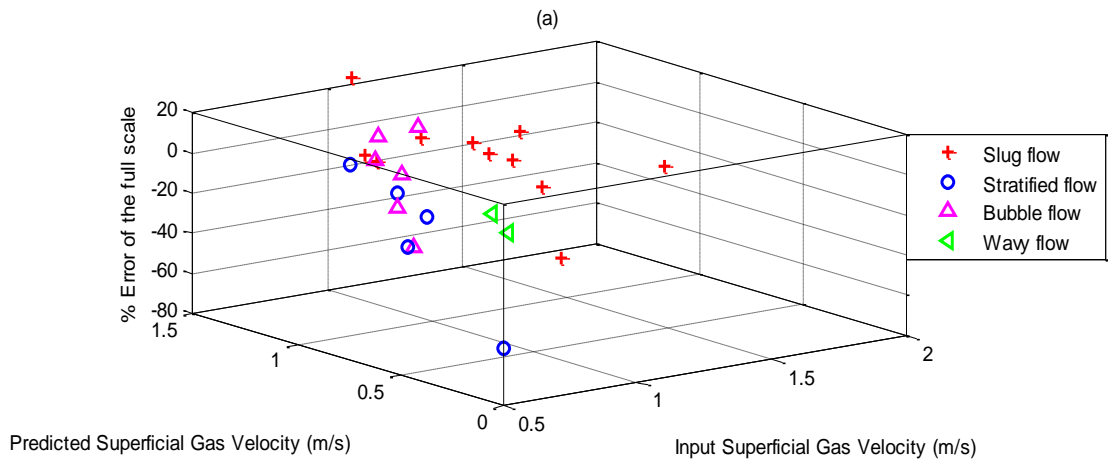
Figure 5-16 Prediction of gas flow and liquid flow velocities for testing the neural network using ultrasonic DWT features
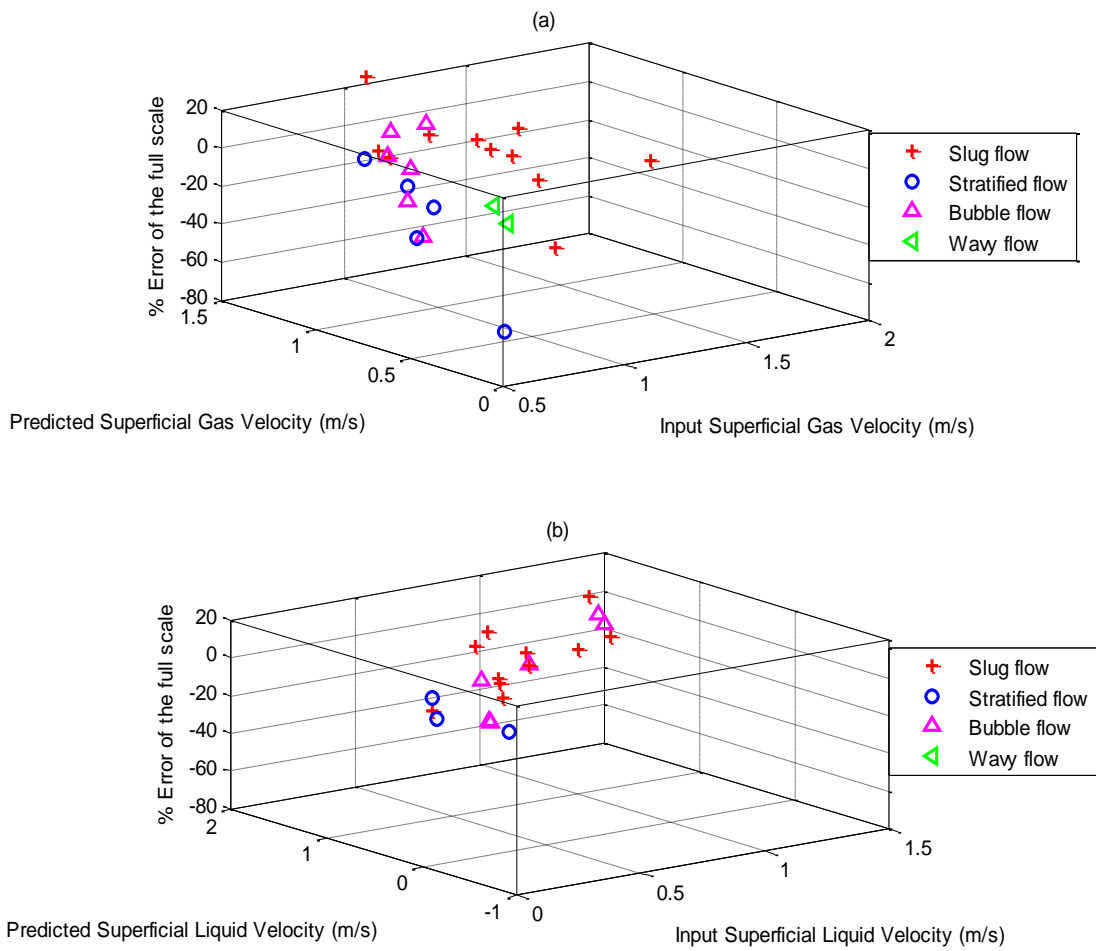
Figure 5-17 Prediction of gas flow and liquid flow velocities for testing the neural network using ultrasonic PSD features
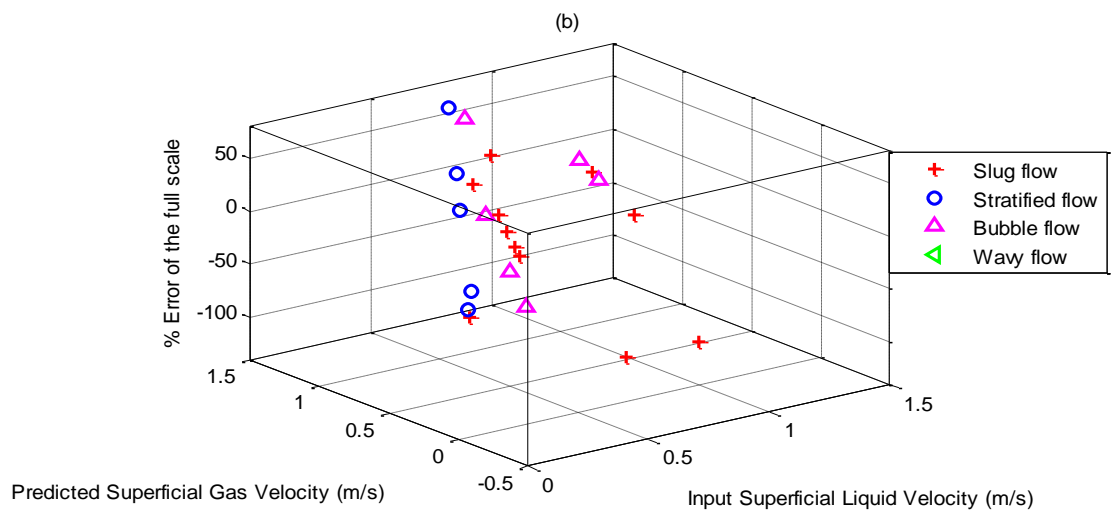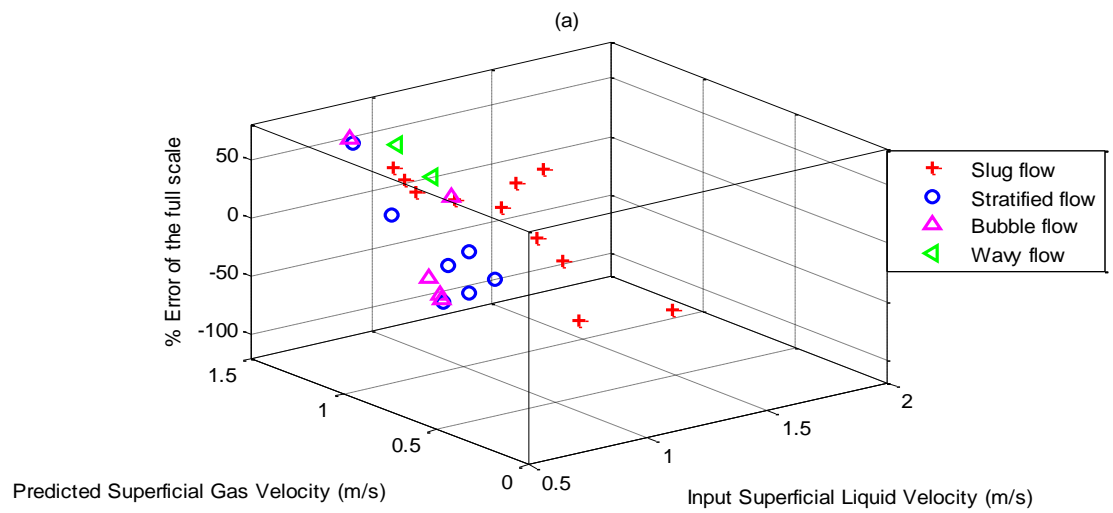
Figure 5-18 Prediction of gas flow and liquid flow velocities for testing the
neural network using conductance DWT features
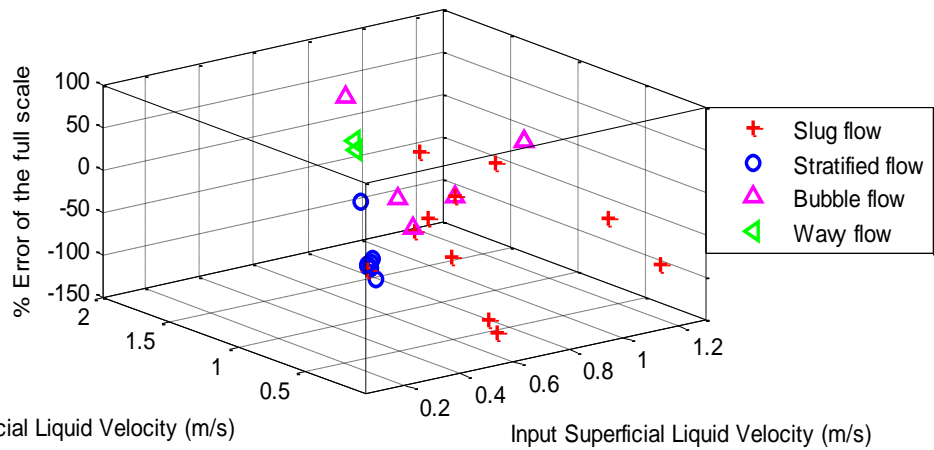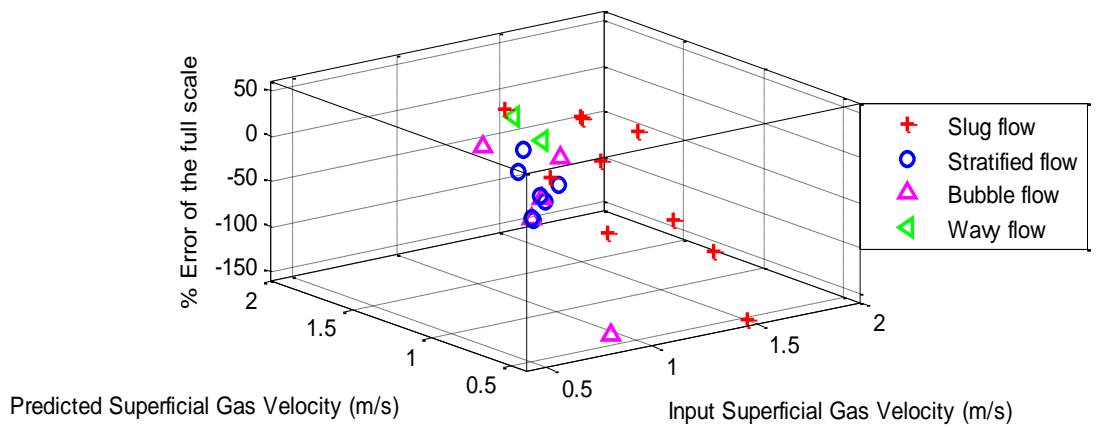
Figure 5-19 Prediction of gas flow and liquid flow velocities for testing the neural network using conductance DWT features

Similarly, the test regression two-phase flow velocity measurement in Figure 5-19, shows the comparisons of the prediction rates of the superficial phase flow velocities within the range of ±10% of the full scale measurement.
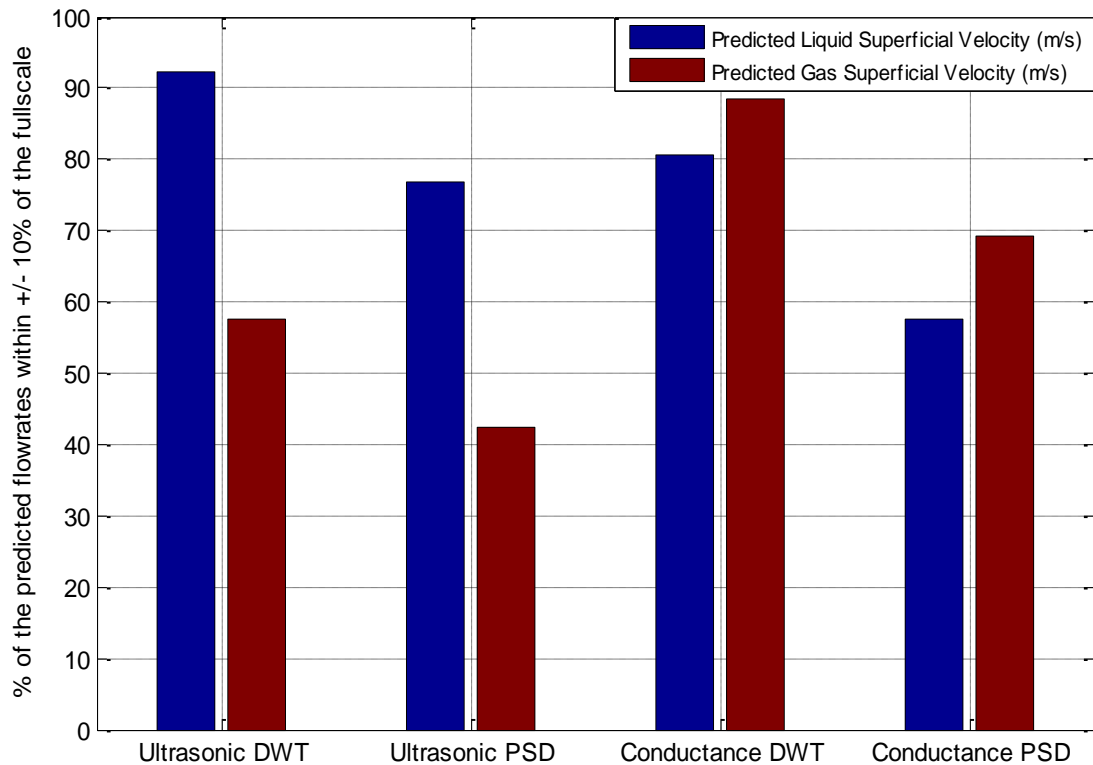
Figure 5-20 Comparison of prediction rates of the four different features inputs

It can be seen that the network used the ultrasonic features extracted by using the DWT method and predicted 92% liquid superficial velocities and 58% gas superficial velocities within ±10% of the targeted values. Moreover, the network used the features extracted from the conductance signal with the DWT method and predicted 81% liquid superficial velocities within ±10% accuracy and 88% gas superficial velocities within ±10% accuracy of the full scale. On the other hand, the features extracted using the PSD method and presented to the network performed lower than the features extracted with the DWT method. The ultrasonic features with the PSD method predicted 77% and 44% full measurement within ±10% for the liquid and gas superficial velocities respectively. In contrast, features extracted from the conductance with the PSD method predicted the gas superficial velocities at 69% which is more accurate than both predictions of the ultrasonic features for the gas superficial velocities. However, the liquid superficial velocities predicted with the conductance features of the PSD method are quite lower than the ultrasonic features.

To sum up, the strength of the ultrasonic signals is in the flow velocity but the strength of the conductance is dependent on the liquid holdup. Also, the features method based on the DWT has been seen to be more effective than the PSD method for both ultrasonic and conductance signals.

In order to appreciate the performance of the network, a linear regression coefficient of the neural network prediction of the test data with ultrasonic DWT features is computed. Figure 5-21 shows the linear correlation coefficient (R) between the network output and target values as measures of network performance. The R value for the liquid superficial velocities is 0.91 and for the gas superficial velocities is 0.50; the closer the value R to 1 the more accurate the prediction results.
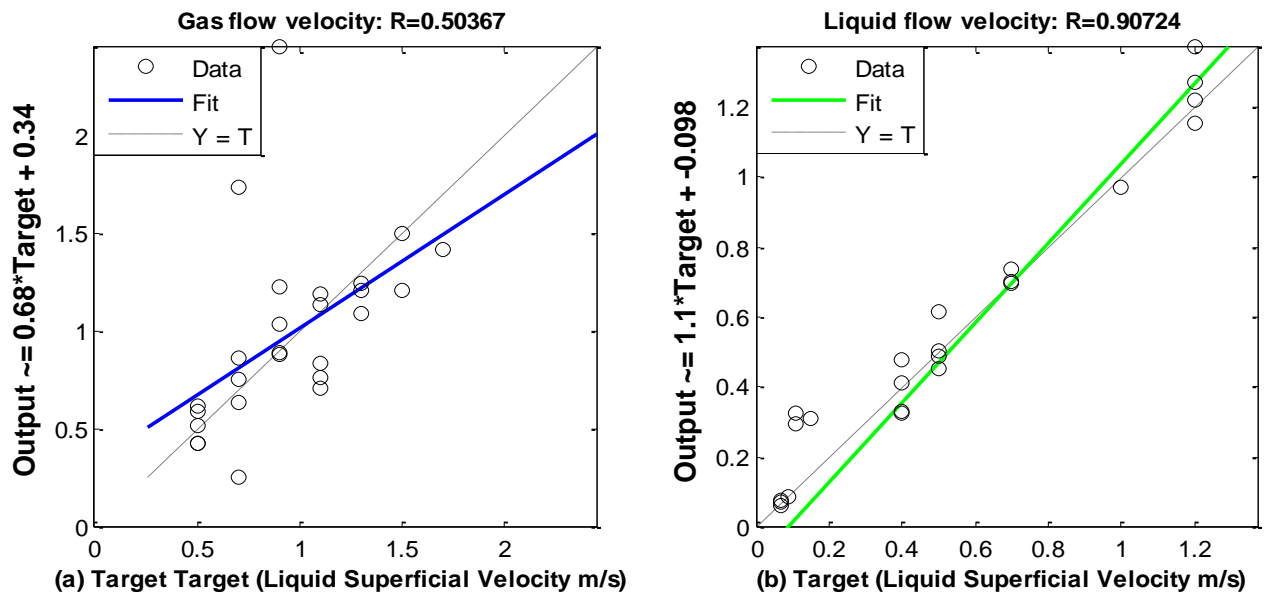
Figure 5-21 Linear correlation coefficient of the outputs of the network tested with ultrasonic DWT features and the target values

5.5.2 Flow regime identification

The testing of the flow regimes classifiers is done using 24 data sets comprising six samples of the four flow regimes. After the flow regime classification neural network has learned the input–output relationship, then the two classifiers, one for each feature vector, are tested with the data sets that the network has not seen before. The classification errors in the testing of new data sets are evaluated and shown in the form of confusion matrices in Figure 5-22 and

Figure 5-23 for the PSD and DWT features respectively. The diagonal cells show the number of data sets that were correctly classified, and the off-diagonal cells show the misclassified data sets. The blue cell in the bottom right shows the total percent of correctly classified cases (in green) and the total percent of misclassified cases (in red). The results show that the PSD trained network has missed three data sets in the classification, while the DWT trained network has misclassified only data point.

Confusion Matrix

	1	2	3	4	
1	**5** 20.8%	**0** 0.0%	**0** 0.0%	**0** 0.0%	100% 0.0%
2	**1** 4.2%	**6** 25.0%	**0** 0.0%	**0** 0.0%	85.7% 14.3%
3	**0** 0.0%	**0** 0.0%	**5** 20.8%	**1** 4.2%	83.3% 16.7%
4	**0** 0.0%	**0** 0.0%	**1** 4.2%	**5** 20.8%	83.3% 16.7%
	83.3% 16.7%	100% 0.0%	83.3% 16.7%	83.3% 16.7%	**87.5% 12.5%**

Output Class / Target Class

Figure 5-22 A confusion plot of the PSD features used in the combined neural network for flow regimes classification showing the classification errors that occurred

Confusion Matrix

	1	2	3	4	
1	**6** 25.0%	**0** 0.0%	**0** 0.0%	**0** 0.0%	100% 0.0%
2	**0** 0.0%	**6** 25.0%	**1** 4.2%	**0** 0.0%	85.7% 14.3%
3	**0** 0.0%	**0** 0.0%	**5** 20.8%	**0** 0.0%	100% 0.0%
4	**0** 0.0%	**0** 0.0%	**0** 0.0%	**6** 25.0%	100% 0.0%
	100% 0.0%	100% 0.0%	83.3% 16.7%	100% 0.0%	**95.8%** **4.2%**

Output Class (vertical axis) / Target Class (horizontal axis)
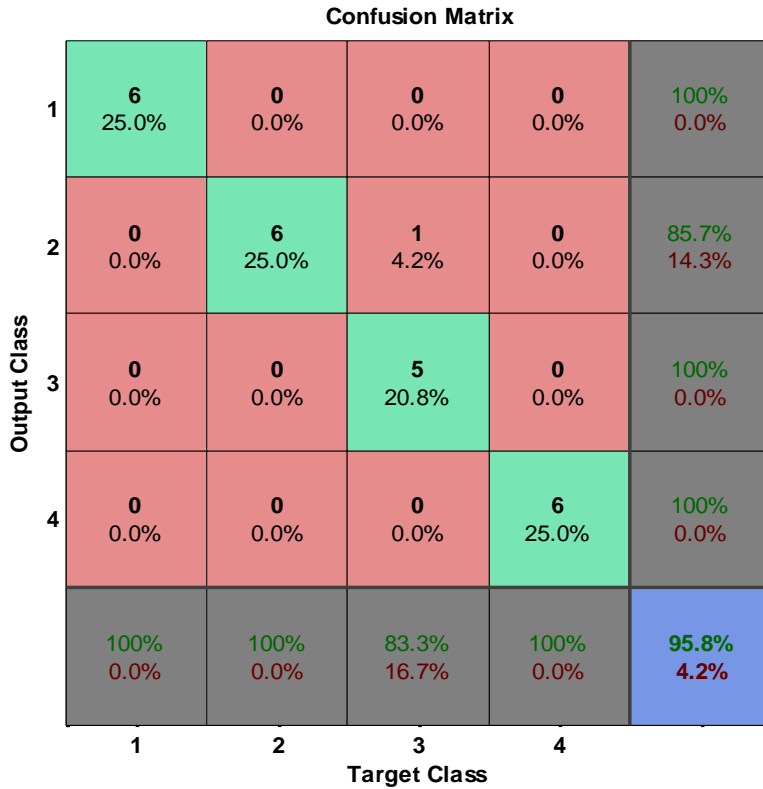
Figure 5-23 a confusion plot of the DWT features used in the combined neural network for flow regimes classification showing the classification errors that occurred

The flow regimes classification performance was evaluated in the form of confusion matrices. A misclassification is said to have occurred when the classifier fails to align a flow regime into the supposedly right group or class. From Figure 5-22 and Figure 5-23, the summary of the classification accuracies of each flow regime and each method of classifier based on the features used in the development of the systems are presented in Table 5-9.

Table 5-9 Classification accuracies for each of the flow regimes and the total accuracy of each classifier

Classifiers	Flow regimes classification values accuracies (%)	
Neural network with PSD features	Elongated bubble flow	100
	Slug flow	85.7
	Stratified flow	83.3
	Stratified wavy flow	83.3
	Total classification accuracy	87.5
Neural network with DWT features	Elongated bubble flow	100
	Slug flow	87.5
	Stratified flow	100
	Stratified wavy flow	100
	Total classification accuracy	95.8

5.5.3 Comparison of Visually Observed and Classified Flow Regimes

Slug flow   Stratified wavy flow

Stratified flow   Bubbly flow
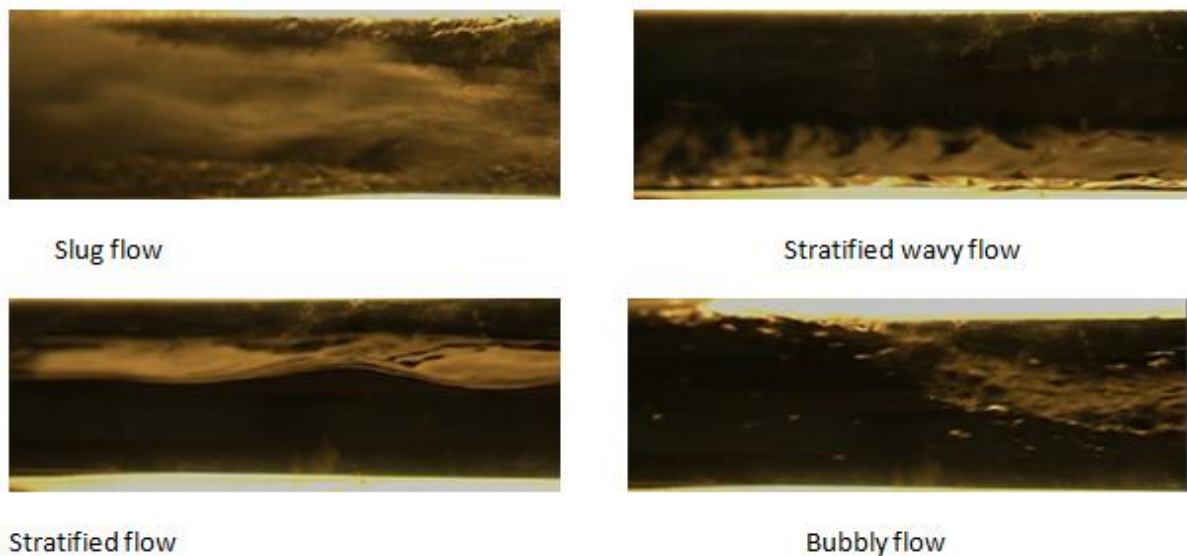
Figure 5-24 Typical flow regimes of the gas-liquid two-phase in a horizontal pipe recorded by a high speed camera

Table 5-10 shows the predicted flow regimes with a classifier using the PSD features which are quite good with only three misclassifications out of the 24 data records. The three misclassified flow regimes are cases no. 7 which is

identified from slug flow to elongated bubble flow, and no. 17 which is also identified from slug flow to elongated bubble flow; the last misclassified regime is number 23 which is from stratified-wavy flow to stratified flow. These misclassified flow patterns are denoted as F for false prediction whereas the successfully classified flow regimes are denoted as T for true. Also, the misclassified flow regimes are very similar to their actual targeted flow regimes. It has been found that only the nearby flow regimes were confused in the neural network, as in the results of other work (Sun and Zhang, 2008).

Table 5-10 Classification performance of 7-16-4 MLPNN Levenberg-Marquardt trained with PSD features

No.	Superficial gas velocity m/s	Superficial water velocity m/s	Observed flow regime	Classified flow regimes with MLPNN
1.	0.5	0.4	Elongated bubble flow	T
2.	0.7	0.4	Elongated bubble flow	T
3.	0.9	0.4	Elongated bubble flow	T
4.	1.0	0.4	Elongated bubble flow	T
5.	1.3	0.4	Elongated bubble flow	T
6.	1.5	0.4	Elongated bubble flow	T
7.	0.5	0.7	Elongated bubble flow	F
8.	0.7	1.0	Slug flow	T
9.	0.9	0.7	Slug flow	T
10.	1.1	0.5	Slug flow	T
11.	1.3	0.7	Slug flow	T

12.	1.5	1.0	Slug flow	T
13.	0.5	0.1	Stratified flow	T
14.	0.5	0.1	Stratified flow	T
15.	0.5	0.1	Stratified flow	T
16.	0.7	0.1	Stratified flow	T
17.	0.7	0.1	Stratified flow	F
18.	0.7	0.1	Stratified flow	T
19.	0.1	0.9	Stratified wavy flow	T
20.	0.1	0.9	Stratified wavy flow	T
21.	0.1	1.1	Stratified wavy flow	T
22.	0.1	1.1	Stratified wavy flow	T
23.	0.1	1.1	Stratified wavy flow	F
24.	0.1	1.3	Stratified wavy flow	T

Similarly, in

Table 5-11, the DWT features from the test data set are applied to the trained neural network. This classifier was able to match all flow regimes except for one in case number no. 18 where it was misclassified from stratified flow to slug flow. Importantly, its overall performance is that it can classify the flow pattern up to 96%. As a result, the combined neural network built using the MLPNN and DWT features has a higher quality of classification than the one trained with PSD features. These results are similar to flow pattern classifications works found in previous studies (Hernández et al., 2006; Sun and Zhang, 2008).

Table 5-11 Classification performance of the 28-10-4 Levenberg-Marquardt selected for DWT features

No.	Superficial gas velocity m/s	Superficial water velocity m/s	Observed flow regimes	Classified flow regimes with MLPNN
1.	0.5	0.4	Elongated bubble flow	T
2.	0.7	0.4	Elongated bubble flow	T
3.	0.9	0.4	Elongated bubble flow	T
4.	1.0	0.4	Elongated bubble flow	T
5.	1.3	0.4	Elongated bubble flow	T
6.	1.5	0.4	Elongated bubble flow	T
7.	0.5	0.7	Slug flow	T
8.	0.7	1.0	Slug flow	T
9.	0.9	0.7	Slug flow	T
10.	1.1	0.5	Slug flow	T
11.	1.3	0.7	Slug flow	T
12.	1.5	1.0	Slug flow	T
13.	0.5	0.1	Stratified flow	T
14.	0.5	0.1	Stratified flow	T
15.	0.5	0.1	Stratified flow	T
16.	0.7	0.1	Stratified flow	T
17.	0.7	0.1	Stratified flow	T
18.	0.7	0.1	Stratified flow	F
19.	0.1	0.9	Stratified wavy flow	T
20.	0.1	0.9	Stratified wavy flow	T
21.	0.1	1.1	Stratified wavy flow	T
22.	0.1	1.1	Stratified wavy flow	T
23.	0.1	1.1	Stratified wavy flow	T
24.	0.1	1.3	Stratified wavy flow	T

5.5.4 Comparison of the Performance of PSD and DWT Features

Performances of the six MLPNN structures trained using six different training algorithms for the flow regimes classification are compared. The comparison is illustrated in Figure 5-25. The training algorithm with a single hidden layer gives the best performing network.

(a) MLPNN structure with PSD features

(b) MLPNN structure with DWT features
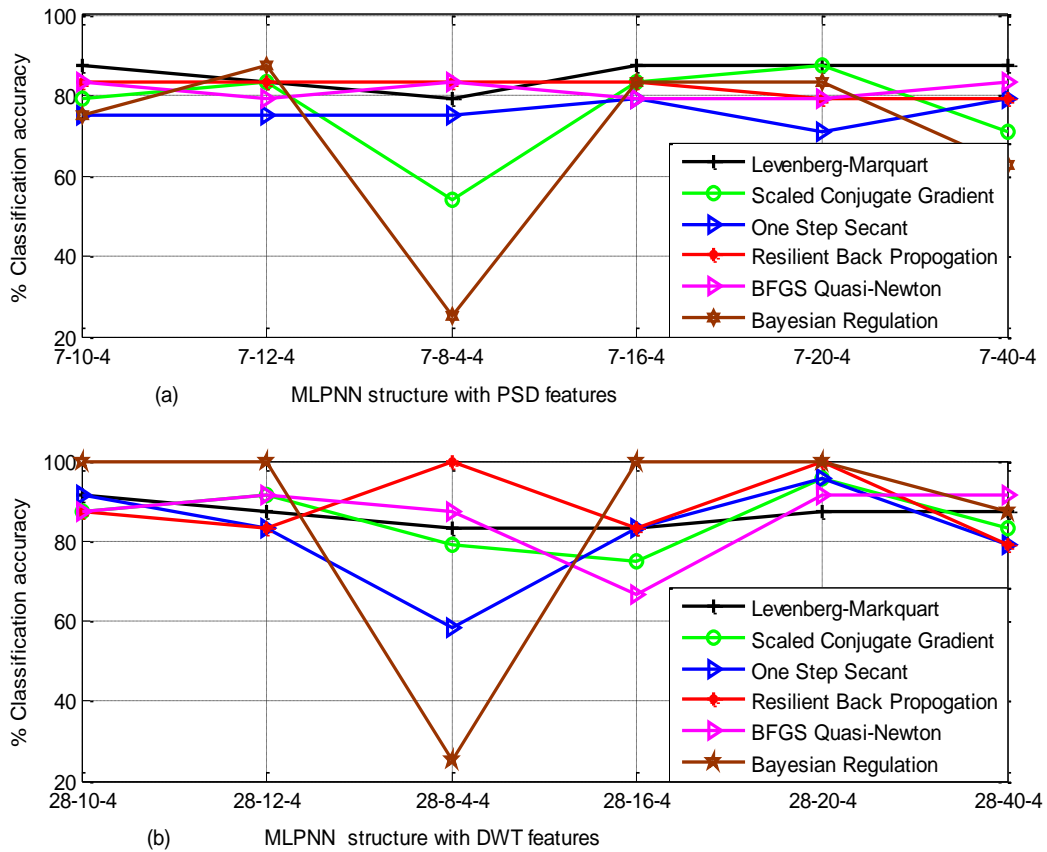
Figure 5-25 Performance of various MLPNN structures and the training algorithms for both (a) Using features trained with PSD extraction (b) Using DWT extracted features.

5.6 Summary

In this paper the development of a clamp-on continuous wave Doppler ultrasound sensor and ANN for gas-liquid two-phase flow regimes classification is performed. The ultrasound signals are processed using the methods of PSD and DWTs for the extraction of input features to the ANN models. A multilayer

perceptron neural network is developed into a combined neural network of two-levels as the classifier and the two methods of feature extractions produced for the network. Comparisons of the performances of the two classifier models are assessed. Four two-phase flow regimes, i.e. slug flow, stratified flow, elongated bubble flow and stratified wavy flow have been classified using the method developed.

The results show that ultrasound signal features of the two phase flow obtained using the DWT performs better for accurate classification compared to the features extracted with PSD methods. The combined neural network models developed for the classification using the PSD features and for the DWT features have accuracies of 87% and 95.6% respectively. In summary, the present study has demonstrated that DWTs feature extraction and the MLPNN classifier has met the industrial requirement of flow regime classification (Sun et al., 2013).

In contrast to the invasive instruments used in other works, this approach is very important for industrial application, given that the sensor used is non-invasive, non-radioactive and is ultrasound technology. Based on the analysis of the experimental results, the proposed method is able provide objective classification of four flow regimes in the horizontal pipe. Other ultrasonic methods reported in the literature employed pulse echo ultrasound plus neural network or subjective methods of flow regimes indemnification (Jha et al., 2013; Figueiredo et al. 2016). The key strengths of the neural network based methods are fast classification and flexible procedure for finding good non-linear solutions.

The continuous wave Doppler sensor is suitable for monitoring flow processes that are ultrasonically reflection fluids, such as crude oil, petrocarbons, oil-gas and oil-water mixtures. Importantly, the sensor can fit well onto existing pipework and it is suitable for both plastic and metallic pipes. However, on horizontal pipes, it is important to mount the sensor at the bottom of the pipe to avoid gas voids in the upper section of the pipe. Poor coupling of the sensor with the pipe, gas voids or bends would tamper with the strength of the signal received. The results of the present study have demonstrated that the proposed

approach of WTs and MLPNN classifier has met the industrial requirements of flow regime classification (Sun et al., 2013).

Further studies are needed in the application of this clamp-on objective flow regime classification system to investigate oil-water two-phase flows, especially for the deployment of this technology to address the requirements of clamp-on ultrasound flow monitoring meter for oil well testing. Also, more studies are recommended on the feasibility of information on the ultrasound Doppler sensor and void fraction measurements, such as the gamma densitometer, which would make the system a complete multiphase flow meter.

6 Data fusion of gamma and ultrasound Doppler sensor

6.1 Introduction

Multiphase flow measurement could be described as a product of the measurement of the flow phase fraction and the measurement of the phase flow velocity. Many techniques have been applied to measure the phase fraction of multiphase flows, such as capacitance, gamma radiation attenuation, neutron attenuation etc. (Rajan et al., 1993). Similarly, conventional single phase flow meters have been applied for measuring fluid velocities of multiphase flows in a mixed, stable and partially separated system (Rajan et al., 1993). For instance, the Venturi meter has been used to measure mixed multiphase flow where the flow is assumed to be 'single phase flow' (Thorn et al., 2013). Also, both vortex shedding and Coriolis meters have been used to measure separated gas-stream and separated oil-water streams respectively (Thorn et al., 2013). If the single phase flow meter were to be combined with a void fraction meter, then the multiphase flow measurement would be complete (Manus et al., 2013).

Energy from radioactive sources, such as $\chi-ray$ and $\gamma-ray$ are applied to measure 1. Gamma ray measurement is commonly known as gamma ray densitometry. In a typical example in an air-water flow, the liquid phase scatters the radiation and it changes at a rate that is equivalent to the amount of water contained in the flow. The energy detected provides data which can be used to reconstruct the void distribution (Dyakowski, 1996). Thorn et al. (1997) describe the operation of a γ-ray densitometer for metering the gas water and oil components of multiphase flow. Two independent measurements are required to determine the values of the components' fractions in three phase flows. This could be accomplished either by a second measurement with the same technique or with another one such as the capacitive technique. The gamma densitometry can be single beam or double as both have application in multiphase flow measurement.

A single beam gamma densitometer is often used for measuring the void fraction of gas-liquid flows in a pipe. The measurement of the void fraction is by correlation between loss of radiation intensity of the test volume and the void

fraction of the fluid. The occurring flow regime in the pipe can be determined from the void fraction and that makes the gamma technique a non-flow regime dependent method (Stahl and von Rohr, 2004). Thorn et al. (2013) reported that the use of dual energy gamma rays for water fraction measurement requires energy sensitive detectors which mean the beam intensity has to be lower. An effective instrument which is based on essentially similar principles as the multi-beam gamma densitometer is the scanning X-ray void fraction meter described by Falcone et al. (2009).

In multiphase flow, ultrasonic techniques have the potential for both phase velocity and phase fraction measurement, although they have not been applied to commercial three-phase flowmeters yet (Thorn et al., 2013). However, the ultrasonic meters' performance is affected by factors such as the number of scatters per unit volume, the distribution of scatters and their velocity profile across the pipe. Also, the ultrasonic attenuation is greatly dependent on the flow regime of multiphase flows and input signal frequency of the transducer (Rajan et al., 1993). Recent developments in other ultrasonic techniques for multiphase flow measurement have progressed considerably.

Usually, the phase fraction and phase velocity measurement are measured with at least two devices or two independent measurements of one device. This approach is achieved by separately metering the phase flow rate and the phase fraction (Tan et al., 2015). Several combinations of two sensors for gas liquid flow measurement have been reported in the literature. Xing et al. (2014) use a combination of ultrasonic e gas flow meter and Coriolis flowmeter for metering gas-liquid two phase flow of low liquid loading. Various models to represent the gas and liquid flow rate, density of mixture flow are used to obtain the coupling models for the two instruments. A theoretical method of data fusion of an electromagnetic (EM) flow meter, electrical resistance tomography (ERT) and two-phase flow models has been developed to improve the accuracy of the EM meter for the measurement of gas-liquid slug flow in a vertical pipe. The feasibility of a two-phase flowmeter was achieved by using a simulation measurement of the averaged velocity, liquid flow rates and gas void fraction. Obviously, this approach requires an invasive sensor and relies on the electrical

conductance of the fluid (Deng, 2011; Xing et al., 2014). Similarly, Meng et al. (2010) present an experimental combination of a liquid (Venturi) flowmeter and ERT sensor for air-water two-phase flow measurement. Three aspects of the flow measurement techniques were acquired with the ERT sensor: the flow regime identification, the void fraction using the conductance signal and void fraction model, and lastly, establishing a mass quality-void fraction correlation from void fraction results. The gas-liquid mass flow rate is measured with the Venturi differential pressure across the tube and the mass quality. Experimental results show the method developed has been accurate within the data tested but both mass quality and fluid flow rate measurement relies on correlations.

In this study, the aim is to use a combination of gamma densitometer and ultrasound Doppler sensor to measure the volume fraction and flow rates of air-water flow, air-oil flow and oil-water flow in a 50mm diameter vertical pipe. The gamma densitometer is set up to measure the area average void fraction at the test section and the ultrasonic Doppler is used to determine the time-average fluid velocity. Both of the sensors are non-invasive and the combination of these two sensors is a good step to estimate quantitatively the volume fraction of oil, water and air mixtures as well as the flow rates of the individual gas, water and oil flow rates.

6.2 Measurement principle

The pictures of the gamma densitometer and ultrasound instruments and the three two-phase flows measured are shown in Figure 6-7. The gamma source used in this study is Caesium-137 and its ancillary equipment is manufactured by Neftemer® for a multiphase clamp-on flowmeter. The Caesium has gamma energy of 662 keV and the linear absorption coefficient is 8.6 m^{-1}. The absorption of a narrowed or collimated beam of the gamma of initial intensity I_0 (Photon/m$^{2\text{-sec}}$) is given equation (6-1). The method of measurement of the two-phase flow with gamma is calibrated by first determining the gamma count rates for single phase water flow and air only in the pipe for every test series (for instance I_L and I_G, respectively, for the liquid and gas phases in a gas-liquid two-phase flow). Single phase flow calibration is to ensure that densities of the

respective flows are recorded both for calibration and the determination of the volume fractions according to the equations (Falcone et al. 2009; Fischer 1994).

$$I = I_0 exp^{(-\mu z)} \tag{6-1}$$

where $-\mu$ is the linear absorption coefficient; z the distance travelled through the absorbing medium, the intensity I of the gamma beam received at the detector. Sensor responses of the gamma densitometer to the three two-phase flows are shown in Figure 6-1 and Figure 6-2

6.2.1 Gamma densitometer measurement principle
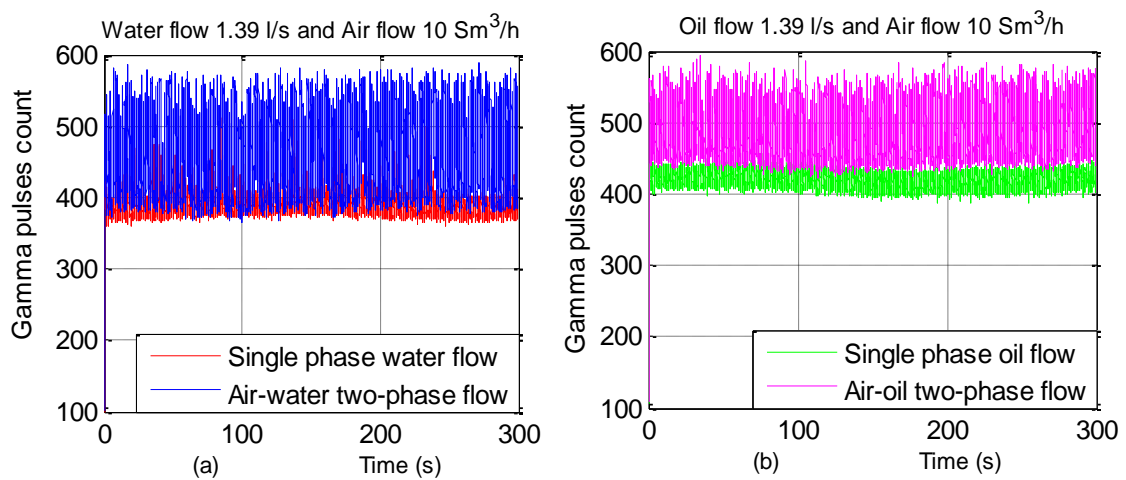
Figure 6-1 Air-water mixture response and air-oil response to gamma pulses
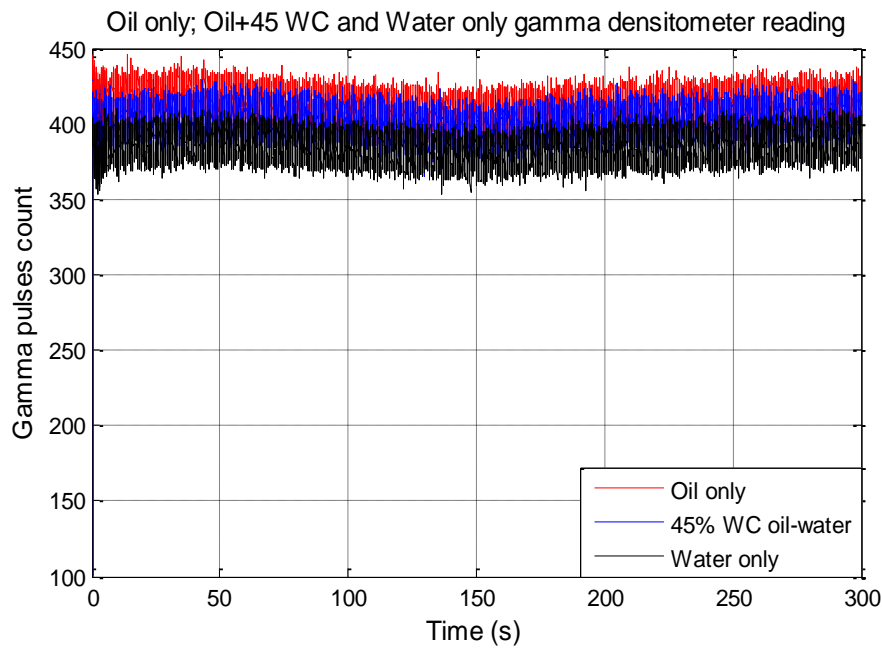
Figure 6-2 oil-water two-phase flow response to oil only, water and oil-water emulsion flows

The void fraction of the flow is calculated using equation (6-2)

$$\alpha_G = l_n(\frac{I_{GL}}{I_L})/l_n(\frac{I_G}{I_L})$$

(6-2)

Similarly, the liquid fraction can be obtained using equation (6-3)

$$\alpha_L = l_n(\frac{I_{GL}}{I_G})/l_n(\frac{I_L}{I_G})$$

(6-3)

where I_L and I_G are the intensities recorded with the channel full of liquid and gas, respectively and α_G, α_L, ρ_{GL}, ρ_G, and ρ_L are: gas volume fraction, liquid volume fraction, gas-liquid density, gas density and liquid density respectively. Gas-liquid ratio or void fraction

The phase fraction can be determined using equation (6-4)

$$\alpha_G = (\rho_{GL} - \rho_L)/(\rho_G - \rho_L)$$

(6-4)

In gas-liquid flow, the equation gives the void fraction (namely the fraction of the gas phase in the channel). For the assessment of the air-liquid two-phase, we employ two models based on no slip between the gas phase and liquid phase and also the homogeneous models. The slip model was required to estimate

155

the gas mass quality from the void fraction measurement while the homogeneous model is to estimate the gas-liquid mixture density. The slip model based on the void fraction is given in equation (6-5) and is based on Lockhart and Martinelli (1949).

$$\alpha_g = \frac{1}{1 + \left(\frac{1-x}{x}\right)\left(\frac{\rho_g}{\rho_l}\right)}$$ (6-5)

The homogeneous model is given as:

$$\rho_{gl} = \left(\frac{x}{\rho_g} + \frac{1-x}{\rho_l}\right)^{-1}$$ (6-6)

The homogeneous model considers the two-phase flow as though it is a single phase flow. The mass quality of the gas flow x is calculated from the measurement of the void fraction and equation (6-6). The slip ratio, S is given as

$$S = 0.28 \left(\frac{1-x}{x}\right)^{-0.36} \left(\frac{\rho_g}{\rho_l}\right)^{-0.64} \left(\frac{\mu_l}{\mu_g}\right)^{0.07}$$ (6-7)

and

the density of the mixture $\rho_{gl} = \alpha_g \rho_g + (1 - \alpha_g)\rho_l$ (Oddie and Pearson, 2004) where α_g is the volumetric void fraction of the gas-liquid mixture, and ρ_g and ρ_l denote the densities of the gas phase and liquid phase, respectively (Xing et al., 2014).

$$\rho_{gl} = \alpha_g \rho_g + (1 - \alpha_g)\rho_l$$ (6-8)

Therefore, the models described can be used to estimate the flow rates of the gas flow and liquid flow using equations:

$$S = W_g/W_l$$ (6-9)

The liquid mass flow rate is given as W_l

$$W_l = \rho_{gl} Q_{lultra}(1 - \alpha_g)$$ (6-10)

Hence, the gas mass flow rate W_g

$$W_g = S * W_l \qquad \text{(6-11)}$$

Equations (6-9), (6-10) and (6-11) were employed to calculate the gas and liquid flow rates. It can be seen that the term, $\rho_{gl}Q_{l.ultra}$, is the two-phase measured with the ultrasound Doppler sensor.

The phase fraction can be determined using equation (6-12)

$$\alpha_G = (\rho_{GL} - \rho_L)/(\rho_G - \rho_L) \qquad \text{(6-12)}$$

6.2.2 Ultrasonic Doppler flow measurement method

The continuous wave Doppler ultrasound sensor used in this experiment was viewed through an X-ray image which is shown in Figure 6-7. A sinusoidal beam of ultrasound is emitted by the piezoelectric transducer placed on the outside wall of the pipe flow. The fluid flowing through pipe has scatterers (bubbles or particles) which reflected the incident ultrasound beam. The receiving piezoelectric transducer collects the backscattered ultrasound beam and then it is converted into an electrical signal. The received ultrasound is from a point scatters that has been shifted in frequency from the incident ultrasound by an amount of frequency shift, Δf (Brody et al., 1974). The CW Doppler flowmeter can be applied for average flow measurement in two ways:

1. Doppler flowmeter for measuring the full-pipe (true) average flow which is independent of the velocity profile. It is based on the following assumptions:
   a. There is homogeneous distribution of the scatterers in the fluid
   b. A uniform beam is focused across the flow pipe
2. Average flow velocity of a small portion of the pipe can also be computed with a Doppler flowmeter by estimating the average flow velocities of homogeneous particles in the small region of the pipe which is assumed be occupied and illuminated by an ultrasound beam (Brody et al., 1974).

The frequency shift can be computed from the classical Doppler shift formula as

$$\Delta f = 2\frac{v}{c}f_t \cos\theta \qquad \textbf{(6-13)}$$

where:

v particle flow velocity

c speed of sound

f_t transmitted carrier frequency

θ transducer orientation angle

The scattering of the ultrasound by the particles in the flow is a random phenomenon and as such the process of the scattering is described using statistical analysis. As a result, the ultrasound flowmeter is described as a stochastic process and it is being simplified using the statistical measurement for calculating the flowmeter estimates (Brody et al., 1974).
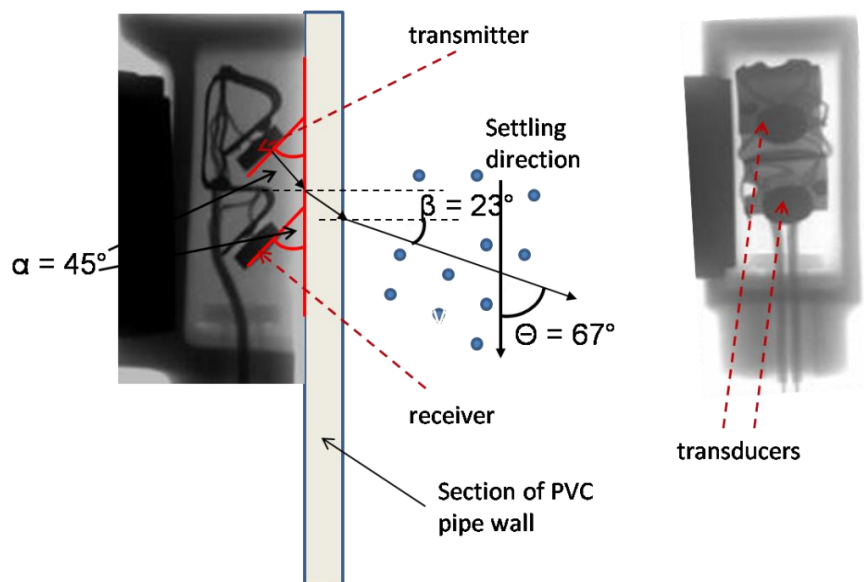
Figure 6-3 X-ray image of ultrasonic transducer

The measurement signal from the ultrasound sensor was acquired using a digital signal acquisition card (NI PCI) and the sampling and acquisition was controlled using the LabVIEW program at a sampling frequency of 10kHz. The average velocity of the flow is directly proportional to the mean frequency derived from the spectrum of the shift frequency.

The velocity of sound of the gas-liquid mixture is used in the present test. It can be illustrated from the linear interpolation of the velocity of sound in air and water and the phase of the mixture (Huang et al., 2013).

$$c_{GL} = c_G(1 - \alpha_L) + (c_L\alpha_L) \qquad (6\text{-}14)$$

Then, the averaged velocity of the gas-liquid mixture is given as:

$$v = \frac{c_{GL}f_d}{2\,f_t\cos\theta} \qquad (6\text{-}15)$$

The Doppler flowmeter equation for single phase flow is used to measure the velocity of the two-phase flow with the ultrasound Doppler flowmeter. For the two-phase flow, the single phase flow Doppler flowmeter equation is modified as described by Huang et al. (2013).

$$v = \frac{c_{GL}f_d}{2\,f_t\cos\theta} \qquad (6\text{-}16)$$

where $c_{GL} = c_w(1 - \alpha) + c_g\alpha$.

The ultrasound signal of the flow for both single and two-phase varies according to the flow conditions at the test centre. As a result, every data point has a unique fluctuation of the ultrasound signal. However, it is usually not easy to see any difference between varies ultrasound signals of the data. In order to visualise the differences of the ultrasound signal, a typical value from each of the three two-phase flows were analysed using PSD. Figure 6-4 toFigure 6-6 show the type of PSD plots of the air-water flow, air-oil flow and oil-water flow respectively.
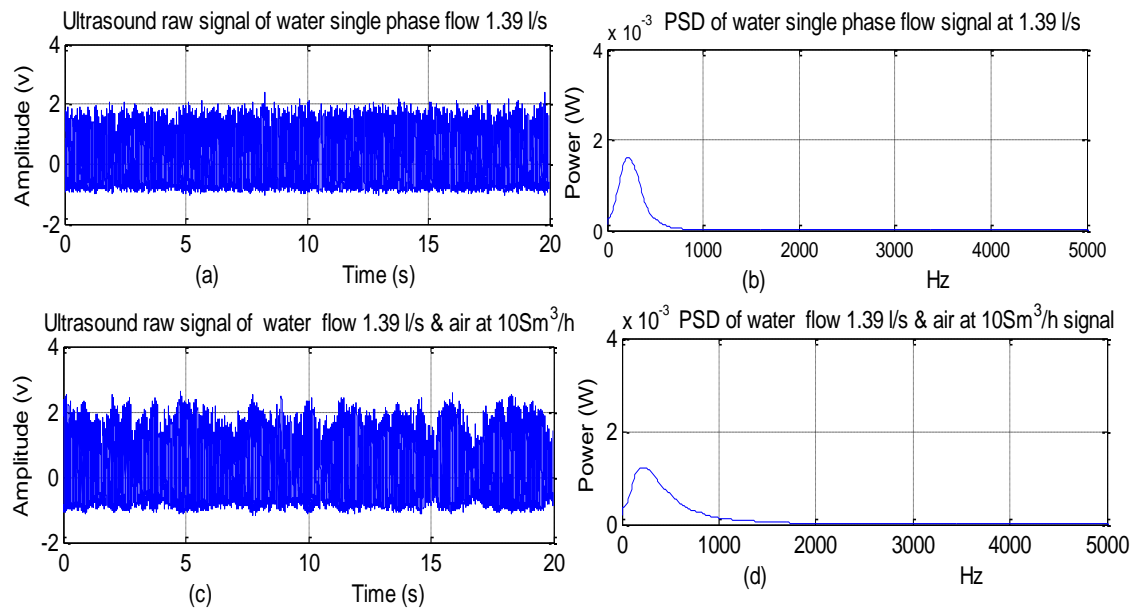
Figure 6-4 Typical ultrasonic flow sensor signals and their corresponding PSD distributions under single phase water flow and air-water flow: (a) Single phase ultrasound signals, (b) PSD distributions, (c) Air-water two-phase flow, and (d) PSD distribution.
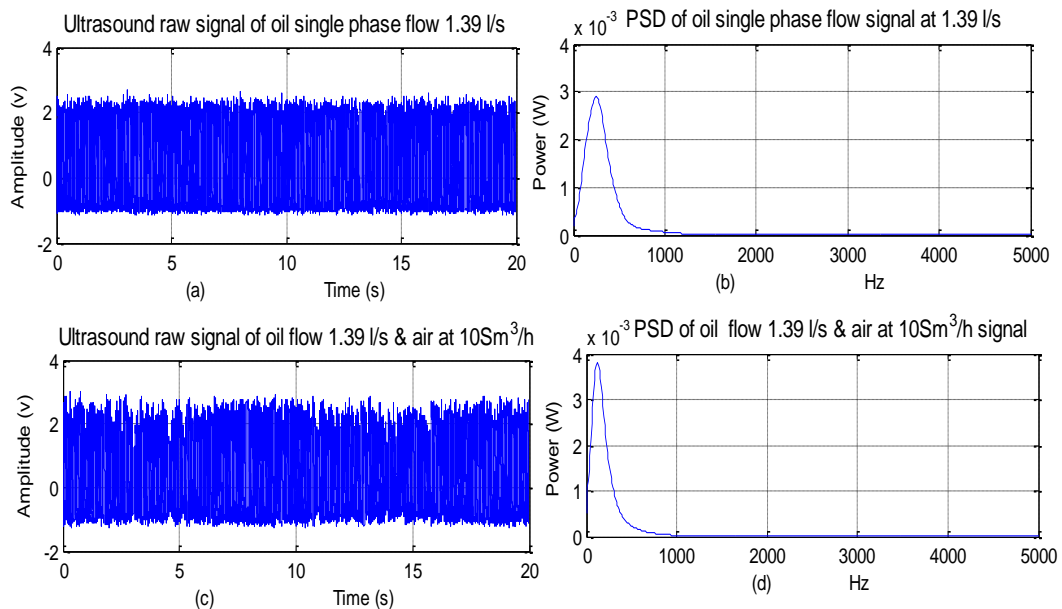
Figure 6-5 Typical ultrasonic flow sensor signals and their corresponding PSD distributions under single phase water flow and air-oil flow: (a) Single phase ultrasound signals, (b) PSD distributions, (c) Air-oil two-phase flow, and (d) PSD distribution.
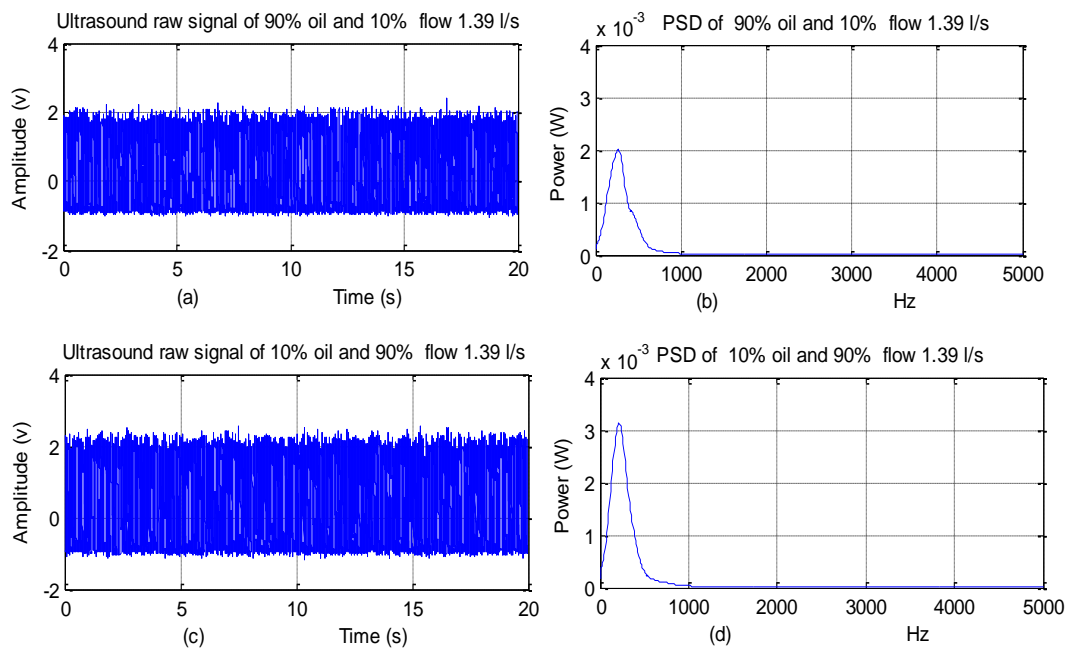
Figure 6-6 Typical ultrasonic flow sensor signals and their corresponding PSD distributions under single phase water flow and oil-water flow: (a) 10% water-cut oil-water phase ultrasound signals, (b) PSD distributions, (c) 90% water-cut oil-water two-phase flow, and (d) PSD distribution.

The differences in the PSD plots of the two-phase flows are evidence that the ultrasound signal can be analysed for flow regime identification in all the three two-phase flows.

6.3 Experimental set up and procedures

Three sets of two-phase flows: air-water, air-oil and oil-water were carried out in the three phase (air-water-oil) flow test facility. The test measurement instruments are shown in Figure 6-7. The gamma densitometer was used for measuring the phase fraction and density of the phase flow, while the ultrasound sensor was used for measuring flow velocity. The two instruments' measurement values are combined for measurement of the flow rates of individual phases in each of the two-phase flows investigated.

(a) Air-water flow   (b) Air-oil flow   (c) Oil-water flow
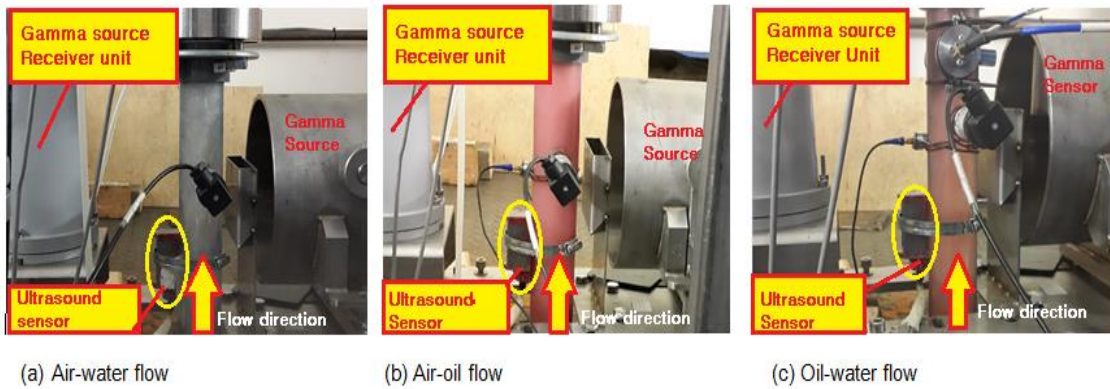
Figure 6-7 Concept meter in the flow test section showing the combined instrument and three types of the two-phase flows tested

Two ultrasound sensors clamped on the test section of the vertical pipeline

Acquired ultrasound waveforms

Ultrasound data acquisition PC

Pulser/receiver   PicoScope
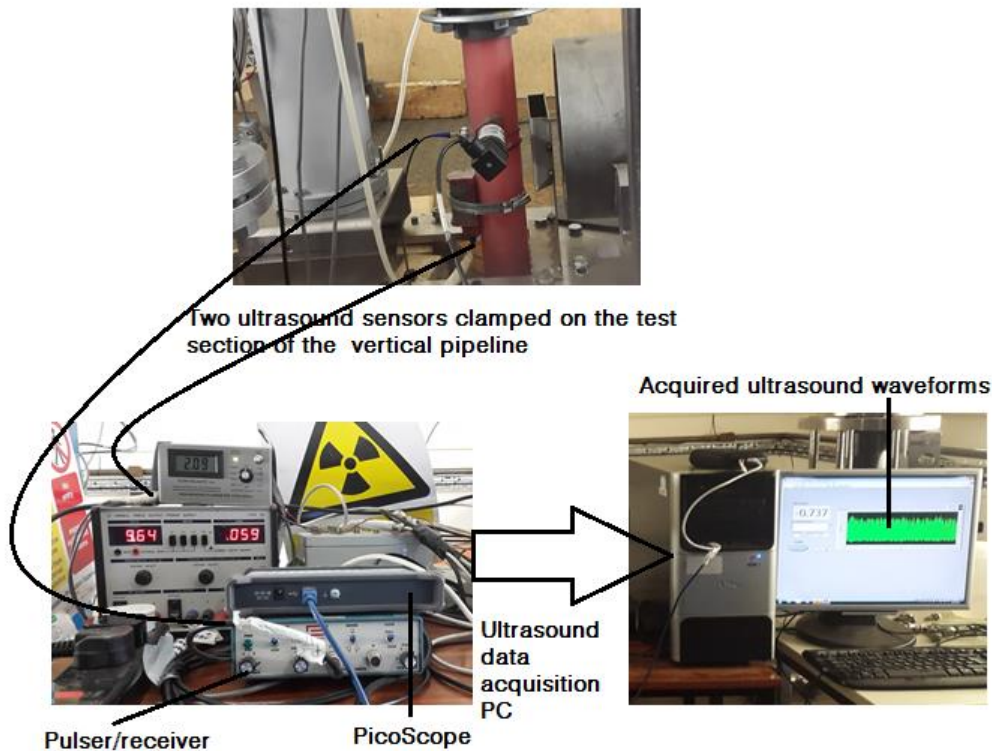
Figure 6-8 Setup of the PC with the ultrasound sensors and its data acquisition

6.3.1 Test Matrices

The flow rates of water and air, air and oil, and oil-water were varied so that a wide range of void fraction and water-cut is generated for investigation of the vertical two-phase flows measurement. Figure 6-9 shows the test matrix of the air-water flow and air-oil flow which were plotted on the gas-liquid two-phase

162

vertical flow map of Taitel et al. (1980). It can be seen that there are five flow patterns in the vertically upward gas-liquid two-phase flow. The test data points investigated in this study contain flow patterns, mainly slug flow, churn flow, and annular flow, for both air-water flow and air-oil flow. In vertical flows, for example, at the end of the vertical pipeline from the reservoir to the well head, the flow regimes that could be observed in gas-liquid two-phase vertical flow are shown in the Figure 2-2. For high liquid superficial velocities, bubbly flow is the prominent flow regime. But as superficial gas velocity increases, the multiphase flow regime will change from bubbly-slug-churn-annular (Cornelissen et al., 2005; Rajan et al., 1993).

6.3.2 Experimental procedure

Three different types of two-phase flows, i.e. air-water, air-oil and water-oil, were tested in the experiment on the 52mm riser of the three phase facility. The test rig operates on a blowdown principle in which high-pressure air is introduced into the system at the starting up of the rig operation and maintained at 1 bar (g) throughout the operating session. This pressure is required to facilitate the smooth operation by enabling the centrifugal pumps to maintain constant flow rates. The desired flow rates of air, water and oil are all set using the Delta V control systems and measured with their respective flowmeters before the flows are introduced into the rig. There are three independent individual inlets for each of the air, water and oil, which are distributed into by using the valve manifold section of the rig. The valve manifold allows for the selection of the pipeline and what fluid is to be supplied for conducting the experiment (Brini Ahmed, 2014).

6.3.2.1 Test matrices of Vertical Flow Experiments

Experiments for the air-water two-phase flow tests were conducted by setting the flow rate of the water at a certain amount (1, 2, 3, 5 7, 10m^3/h) and then varying the flow rates of the air for seven different values (5, 10, 20, 50, 100, 150, 200Sm^3/h) for each of the water flow rates. Therefore, air-water flow tests were conducted for 42 different two-phase flow test points.

163

The superficial gas velocities of the gas flows were calculated based on the condition at the test section, i.e. by considering the effect of pressure and temperature on the gas flow at the test location. Both the water flow and gas flow were introduced into the flow line at the valve manifold of the and the two flows travelled 40m horizontally before rising up to the test section at the riser top. The superficial gas (air) velocity at the test section (riser top) is calculated according to equation (6-17).

$$U_{sg} = \frac{Q_g}{A_p} = \frac{P_{std}.T_t}{P_t.T_{std}} . \frac{Q_{std}}{A_p}$$
(6-17)

where:

$A_p =$		Cross-sectional area of the pipe
$P_{std} =$		Average pressure at standard conditions
$P_t =$		Average pressure at the test section
$Q_g =$		Gas volume flow rate at the test section
$Q_{std}=$		Volume flow rate at standard conditions
$T_{std}=$		Temperature at standard conditions
$T_t=$		Temperature at the test section

Table 6-1 Air-water flow test matrix

		QW (m3/h)						
			1	2	3	5	7	10
		Kg/s	0.28	0.56	0.83	1.39	1.94	2.78
Air-water flow	QG (m3/h)	0	√	√	√	√	√	√
		5	√	√	√	√	√	√
		10	√	√	√	√	√	√
		20	√	√	√	√	√	√
		50	√	√	√	√	√	√
		100	√	√	√	√	√	√
		150	√	√	√	√	√	√
		200	√	√	√	√	√	√

Similarly, the air-oil two-phase flow was tested in the same manner as the air-water flow. The main difference between the air-water and air-oil is on which of the liquid pumps was selected and which valve manifold was open for the liquid to flow into the rig.

Table 6-2 Air-oil flow test matrix

		QW (m3/h)						
			1	2	3	5	7	10
		Kg/s	0.28	0.56	0.83	1.39	1.94	2.78
Air-water flow	QG (m3/h)	0	√	√	√	√	√	√
		5	√	√	√	√	√	√
		10	√	√	√	√	√	√
		20	√	√	√	√	√	√
		50	√	√	√	√	√	√
		100	√	√	√	√	√	√
		150	√	√	√	√	√	√
		200	√	√	√	√	√	√

Finally, the experiment is on testing the flow rates of oil-water two-phase flow. Table 6-2 shows the test matrix of the oil-water flow tests. Both the oil and water were stored and supplied to the rig from the same capacity tanks of 12.5m3. The liquid flows were passed through each centrifugal pump and then metered for mixing with each at the valve manifold which is 40m upstream of the riser base. The superficial velocity of the water flow was calculated using equation **(6-18)**.

$$U_{sw} = \frac{Q_w}{1000.A_p} \tag{6-18}$$

where:

$Q_w =$ Water flow rates (l/s)

$A_p=$ Cross-sectional area of pipe (m^2)

Similarly, the oil superficial velocity can be calculated using equation (6-19).

$$U_{so} = \frac{Q_o}{\rho_o . A_p}$$

(6-19)

where:

$Q_w =$ Water flow rates (l/s)

$A_p =$ Cross-sectional area of pipe (m2)

$\rho_o =$ Density of oil (kg/m3)

Table 6-3 Oil-water test matrix

		QW (m3/h)								
		0	10	20	30	45	60	75	90	100
		Kg/s	0.28	0.56	0.83	1.39	1.94	2.78		
Oil-water flow	QO (m3/h)	0	√	√	√	√	√	√	√	√	√
		5	√	√	√	√	√	√	√	√	√
		10	√	√	√	√	√	√	√	√	√
		20	√	√	√	√	√	√	√	√	√
		50	√	√	√	√	√	√	√	√	√
		100	√	√	√	√	√	√	√	√	√
		150	√	√							

6.3.3 Data acquisition system

Four independent computers with data acquisition and control software were used to measure and collect the test data in this experiment. 1) A PC with process management software (Delta V). Delta V coordinates the fully automated operation of the rig and some of its function is for setting test points by controlling the flow rates of the liquid and gas and real-time monitoring of the operation of the test rig. 2) A PC with data acquisition and a control LabVIEW program was acquiring and storage of the readouts from the reference

instrumentations, such as the Coriolis flowmeter, pressure transducers. 3) The entire gamma densitometer set up is the Neftemer flowmeter which was controlled by a separate PC together with signal processing unit. 4) The fourth PC with data acquisition software is for acquiring signals of the flow using the two ultrasonic sensors: Ultrasonic Doppler flowmeter and Ultrasound pulse echo measurements (Blaney, 2008; Fischer, 1994; Oddie et al., 2003).
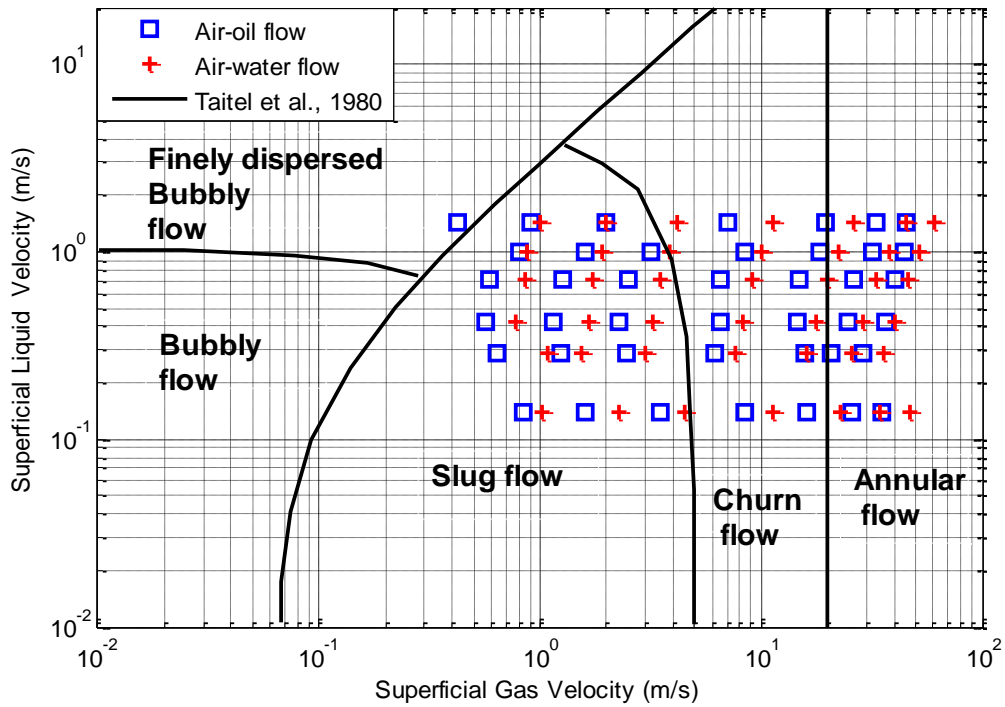
Figure 6-9 Flow regime map showing the matrix of gas-liquid data collected

Similarly, the oil-water upward vertical flow map produced by Flores et al. (1999) was used to classify the test matrix. In Figure 6-10, it can be seen that there are six different types of flow regimes existing on the vertical oil-water flow.
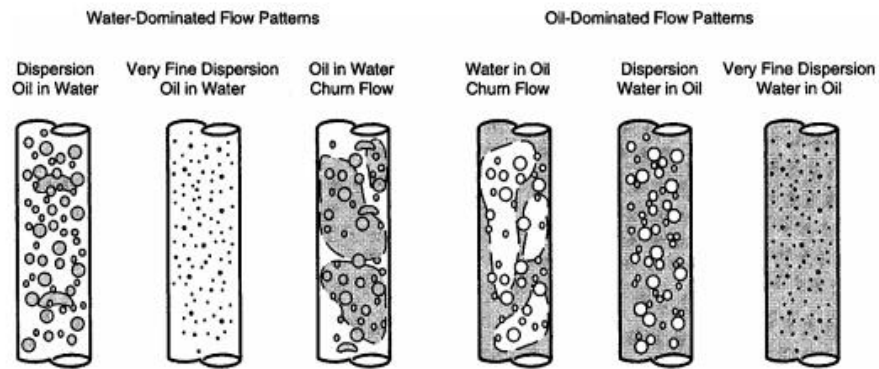
Figure 6-10 Examples of the vertical upward oil-water flow regimes (Flores et al., 1999)
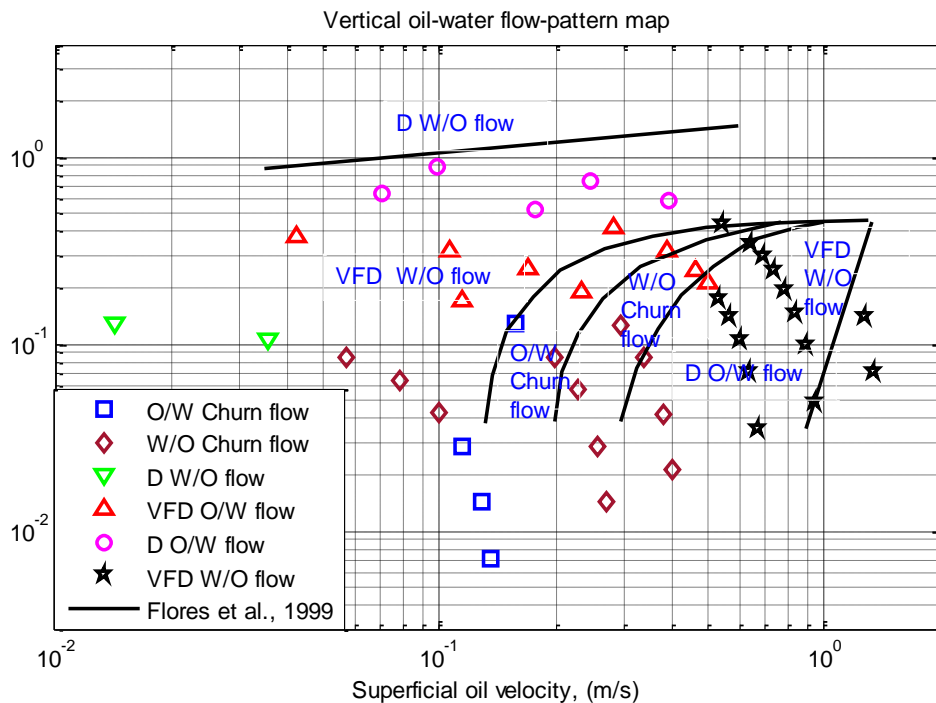
Figure 6-11 Flow regime map showing the matrix of oil-water data collected

6.4 Results and discussion

Data from three different types of two-phase flow: air-water, air-oil and oil-water flows were extracted from the gamma densitometer measurement and ultrasound Doppler sensor for measurement of the flows' velocity. The liquid flow rates tested ranged from 1 m^3/h to 10 m^3/h (0.28 to 2.8kg/s) for both water and oil. Air flow rates ranged from 5 Sm^3/h to 200 Sm^3/h (GVF 20% to 91%). Void fraction and liquid fraction are measured with the gamma

densitometer and the liquid velocity was estimated using FFT to obtain the averaged shift frequency. The Doppler ultrasound sensor used for measuring the liquid flow of the air-water flow is from the ultrasonic Doppler flowmeter whose liquid flow velocity ranged from 0 to 20ft/s (0 to 6m/s). The average flow velocity of the fluid is proportional to the averaged shift frequency. Different symbols were used to represent the void fractions and liquid fractions to identify the dependencies of the liquid flow rate on other phase fractions. Averaged values of the measured parameters were plotted against the measurement obtained from the reference sensors (Whitehouse et al., 1991).

The performance of the combined measurement of the gamma densitometer and ultrasonic Doppler flow sensors was compared to the actual time-averaged values calculated from the measurements of the gas, water and oil injected. The tests results are presented as air-water flow, air-oil flow and oil-water flow respectively.

6.4.1 Air-water two-phase flow measurement

The gas void fraction in the air-water flow was measured using the gamma densitometer from the changes to the gamma pulses count by the variation of the gas and liquid at the test section. Figure shows the result of the measured void fraction against the calculated one. It can be seen that all the data test points' results are within ±10% of the calculated ones which illustrates the applicability of the gamma densitometer for void fraction measurement. This result agrees with other experimental measurements of void fraction using a gamma densitometer (Zhao et al., 2013).
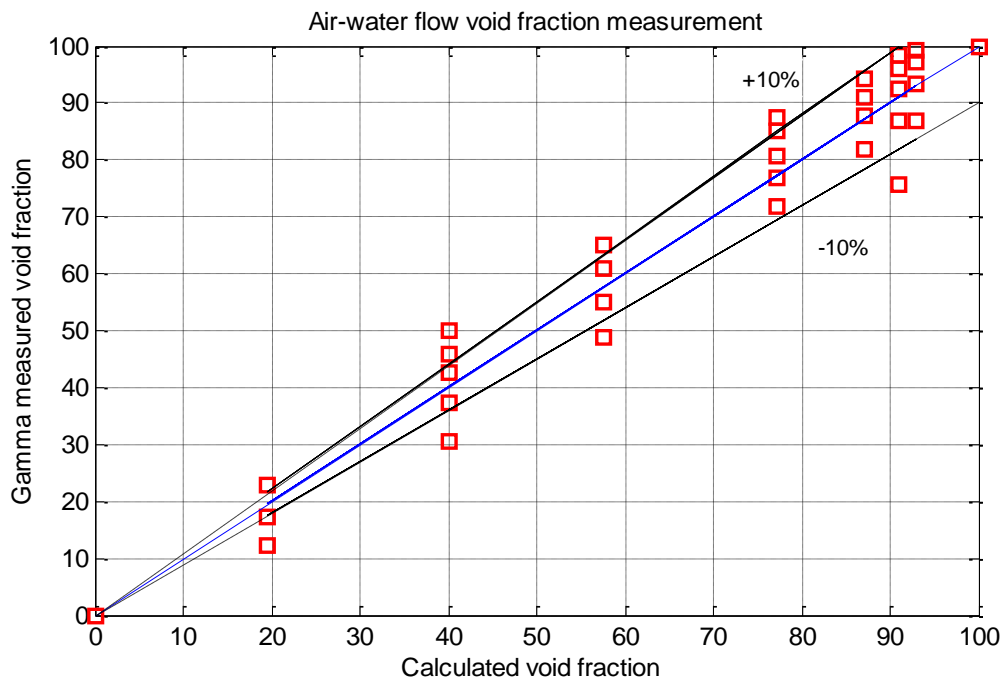
Figure 6-12 Comparison of air-water flow void fraction measured and calculated using the input conditions

The measurement of the void fraction provided an opportunity to measure gas and liquid phase flow rates from total flow velocity measured with the ultrasonic Doppler.

$$Q_w = (1 - \alpha_g)Q_{us} \tag{6-20}$$

$$Q_g = \alpha_g * Q_{total} \tag{6-21}$$

where the flow (Q) is in m^3/s and the void fraction, α_g is the void fraction. It is assumed that the Q_{us} is the total flow of the gas and liquid, then

$$Q_{us} = Q_{total} = v_m A_{pipe} \tag{6-22}$$

That is because if the void fraction at the flowmeter location is known, then the liquid and gas flow rates can be computed using the total volumetric flow using equations (6-20) and (6-21) (Whitehouse et al. 1991).

Figure 6-13 shows the results of the total flow measured by the ultrasound Doppler compared with the reference inlet liquid flow. It can be seen that flow velocity measured by the ultrasound is higher than the reference flow velocity.

Measured velocity is overestimated which illustrates that the gas flow has an effect on the flow measured by the ultrasound flow sensor.
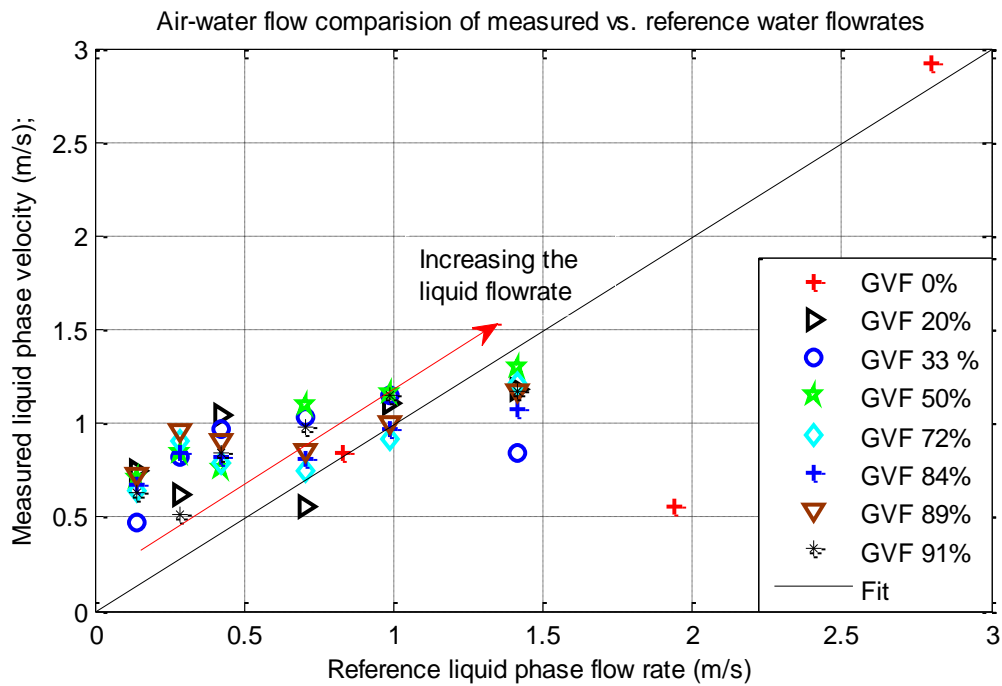
Figure 6-13 Ultrasound measured flow vs. reference liquid flow velocity of air-water flow

in order to obtain the velocity of the liquid water phase only the velocity from the total flow measured by the ultrasound sensor was multiplied with the fraction of the liquid in the flow. Liquid water phase flow velocities were plotted versus the reference input liquid velocities in Figure 6-14. It can be seen that the measured velocities did not correlate with the reference flow velocity at the higher void fraction and higher flow rates (higher Reynolds number). However, outside the higher Reynolds number, the measured liquid velocity is within the range of ±10%. This range of accuracy is good for industrial application.
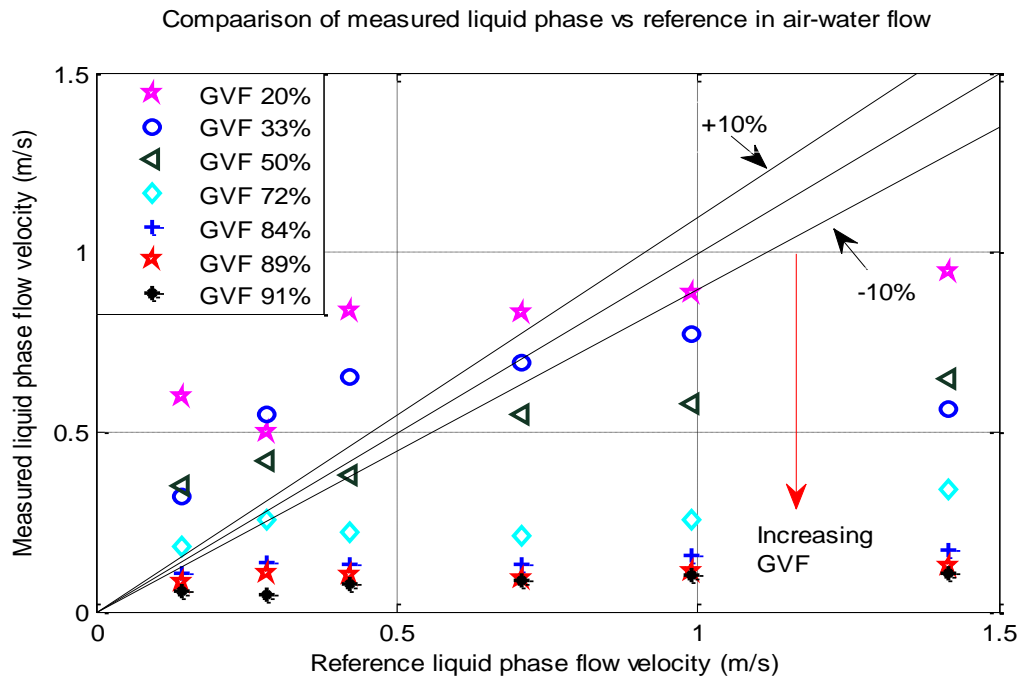
Figure 6-14 Comparing the ultrasound measured liquid phase velocity with the reference input flow velocity

The combination of ultrasound sensor and gamma densitometer signals of the flow were then investigated for measurement of the gas flow rates in the air-water as the void fraction of the gas has been measured successfully with the densitometer. The gas flow rate of the two-phase was calculated using a slip model.

The coupling models of the slip ratio model based on the models of Lockhart and Martinelli (1949) were used for calculating the gas flow rates. The void fraction measurement of the two-phase flow was used for calculating the gas quality, x, (Xing et al., 2014). The gas-quality function, x, was calculated for each of the void fractions with equation 6-22:

$$\alpha_g = \frac{1}{1 + \left(\frac{1-x}{x}\right)\left(\frac{\rho_g}{\rho_l}\right)S} \qquad \textbf{(6-23)}$$

where *S* is the slip ratio and is ratio of the gas flow velocity to the liquid velocity. Therefore, the product of the slip, *S* and the measured liquid flow phase flow

rates were used for calculating the gas flow rates of the two-phase. The combination of the two models, in effect, has made the combination of the gamma densitometer and ultrasound Doppler measurement as two-phase flowmeter.
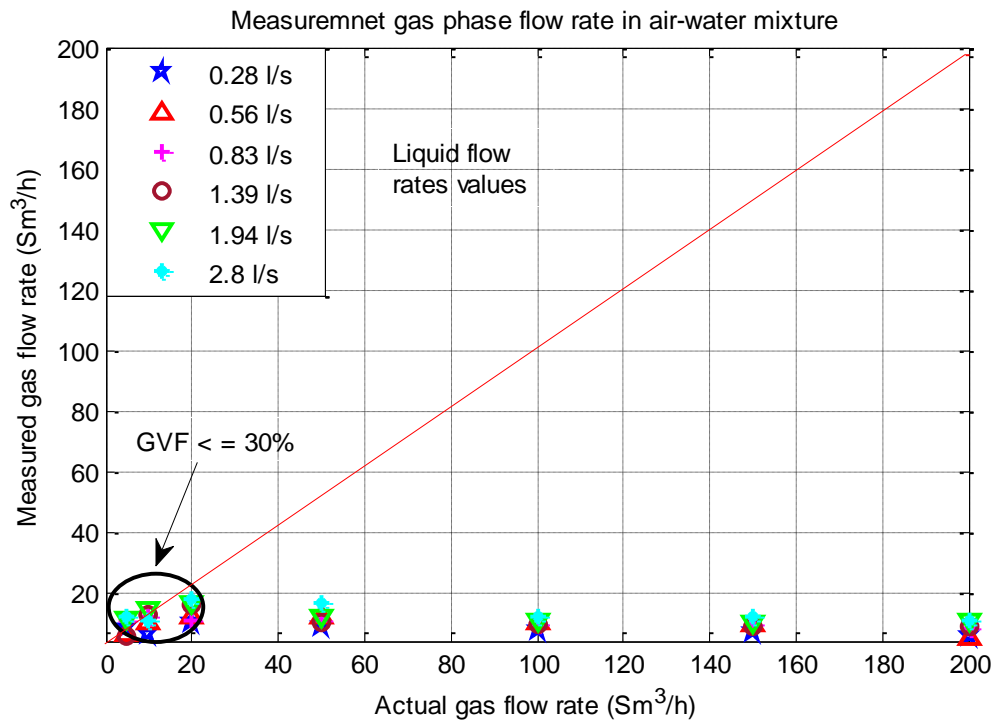
Figure 6-15 Gas flow rate measurement compared with reference measurement based on the input conditions

Figure 6-16 Comparison of the ultrasound measured gas phase velocity with the reference input flow velocity

Data tests for the air-water have the GVF starting from 20% up to 91%. It is certain that the gas flow has profound effect on the transmission and reception of the ultrasound signals. As a result, the gas flow rate determined from a combination of the sensors measurement and the models did not give accurate results. Figure 6-15 and Figure 6-16 show the results of the gas flow rates measured and the comparison of the measured gas flow with the reference gas flow respectively. It can be seen from both figures that the method developed using the combined ultrasound Doppler and gamma densitometer is only able to estimate flow at low Reynolds numbers (low gas and low liquid flow). It can be seen that the error between the measured and the reference ranged from less than 5% up to as high as 450%! It was also found that the gas flow limits the propagation of the ultrasound into the liquid flow. Thereby, the gas flow is preventing the measurement of the liquid flow in the event of high gas flow (Huang et al., 2013).

6.4.2 Air-oil two-phase flow measurement

In this section, data obtained from the gamma densitometer and the ultrasound Doppler flow sensor on air-oil two-phase and the results obtained are presented. The data presented in Figure 6-17 show the averaged void fraction of the air-oil flow measured with the gamma densitometer and compared with the void fraction calculated based on the input conditions of the flow. The air-oil flow void fraction measured is slightly less accurate than those of the air-water flow measured above. In the air-oil flow, only a few of the data points are within the range of ±10%.
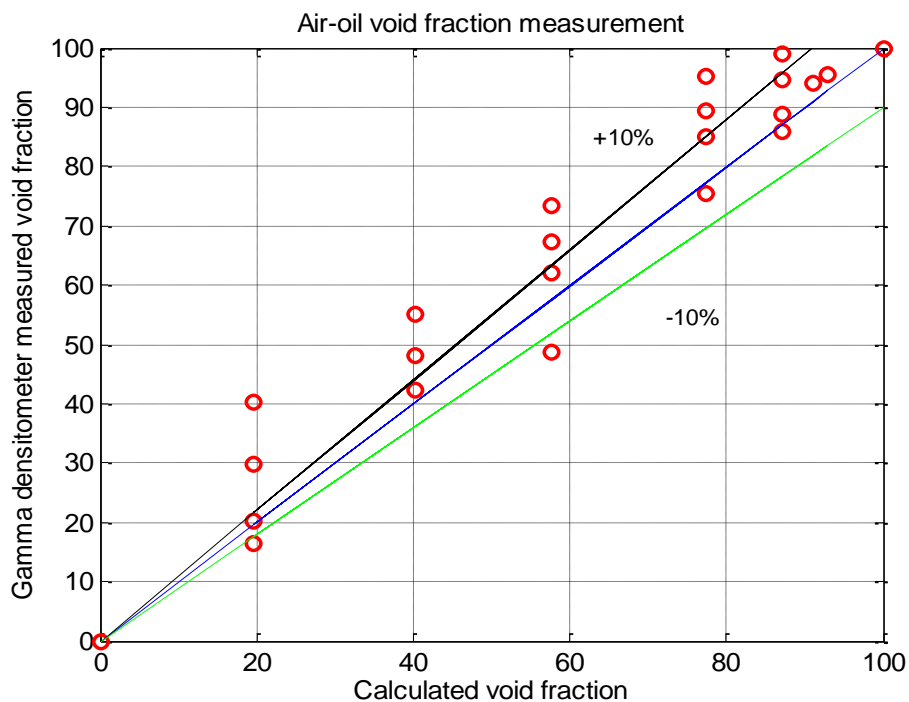
Figure 6-17 Comparison of air-oil flow void fraction measured and calculated using the input conditions

Similarly to the air-water flow above, the air-oil flow was also measured with the ultrasound Doppler flow sensor and the gamma densitometer to estimate the liquid flow rate and the liquid and gas individual phase fractions. The total flow velocity of the air-oil flow was estimated with the ultrasound Doppler sensor and the result was compared with the input liquid (oil) flow velocity. Figure 6-18 shows the comparison of the estimated liquid flow measured by the ultrasound sensor and the reference oil input velocity. It can be seen that the measured liquid velocity by the ultrasound is underestimated when compared with the

reference. Also, it is clearly illustrated that there is a connection between the underestimation of the liquid flow velocity and the increase in the gas void fraction.
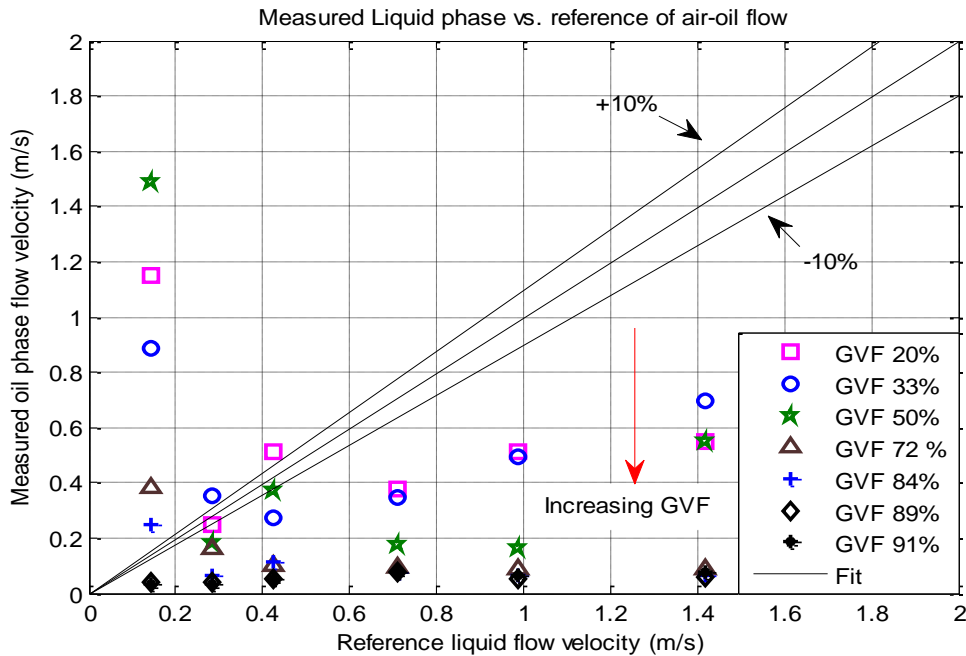
Figure 6-18 Comparison between experimental and reference liquid input velocity

Also, the fraction of the oil flow in the air-oil flow was estimated using the gamma densitometer and the total liquid flow velocity measured with ultrasound was multiplied with the oil fraction to obtain the velocity of the liquid phase only. The result of the comparison between the liquid oil flow velocity measured and the reference liquid flow is illustrated in Figure 6-19. It can be seen that the combined measurement of the gamma densitometer and ultrasound Doppler works best at low Reynolds numbers of the flow, i.e. low flow rate with high GVF and low GVF with high flow rate.
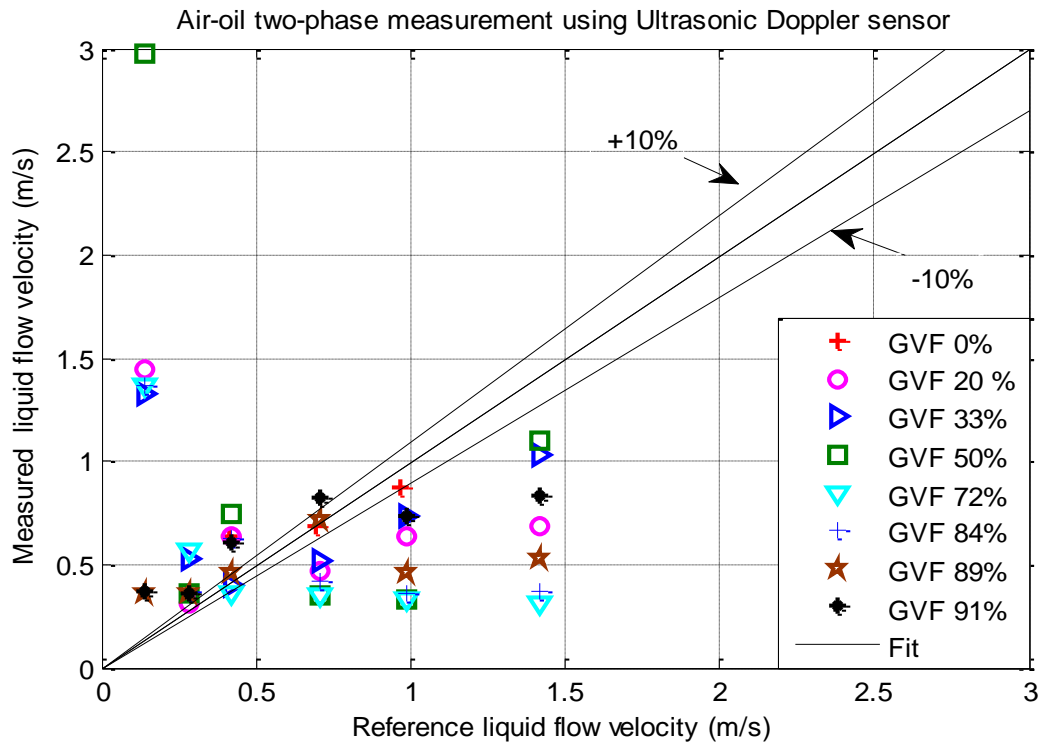
Figure 6-19 Comparison of the liquid phase velocity measured with combined instruments and the reference liquid (oil) of the input.

Similarly, the air flow rate of the air-oil two-phase is also determined from the combined measurement of the gamma densitometer and ultrasound Doppler sensor. In order to obtain the gas flow rate, two different models were used. Slip models were used to calculate the gas mass fraction or quality. A homogeneous model of gas-liquid two-phase flow was used for the estimation of the gas-liquid mixture density by substituing the values of the gas fraction in the model. The results of the gas flow rates measurement are plotted in Figure 6-20. The results of the comparison of the measured and reference gas flow rates show that the method developed can measure gas flow with small with when the GVF is less than 20%. At the low Reynolds, similarly to the air-water flow, the gas flow can be determined within the range of ±10%.
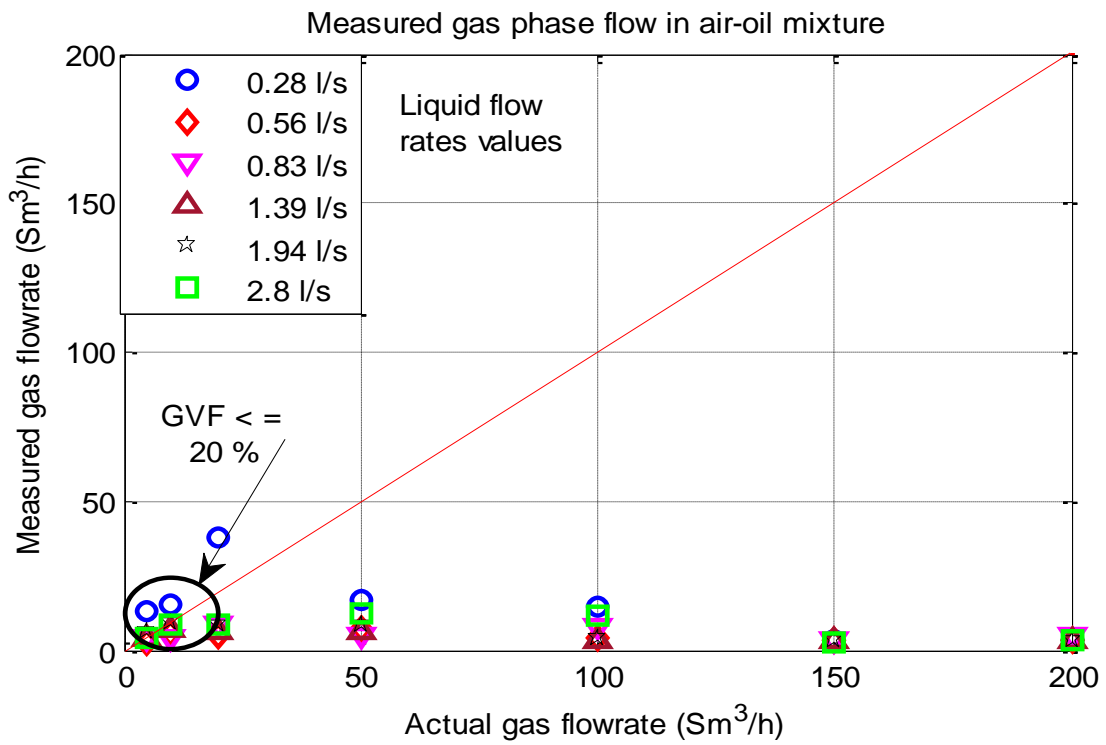
Figure 6-20 Gas flow rate measurement compared with reference measurement based on the input conditions in air-oil two-phase flow

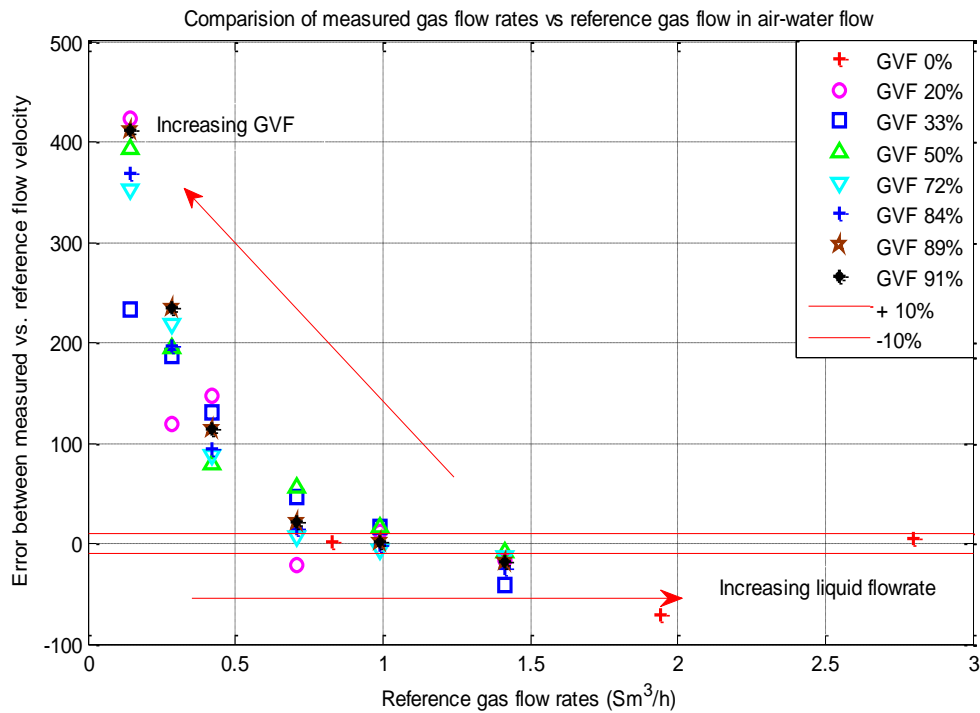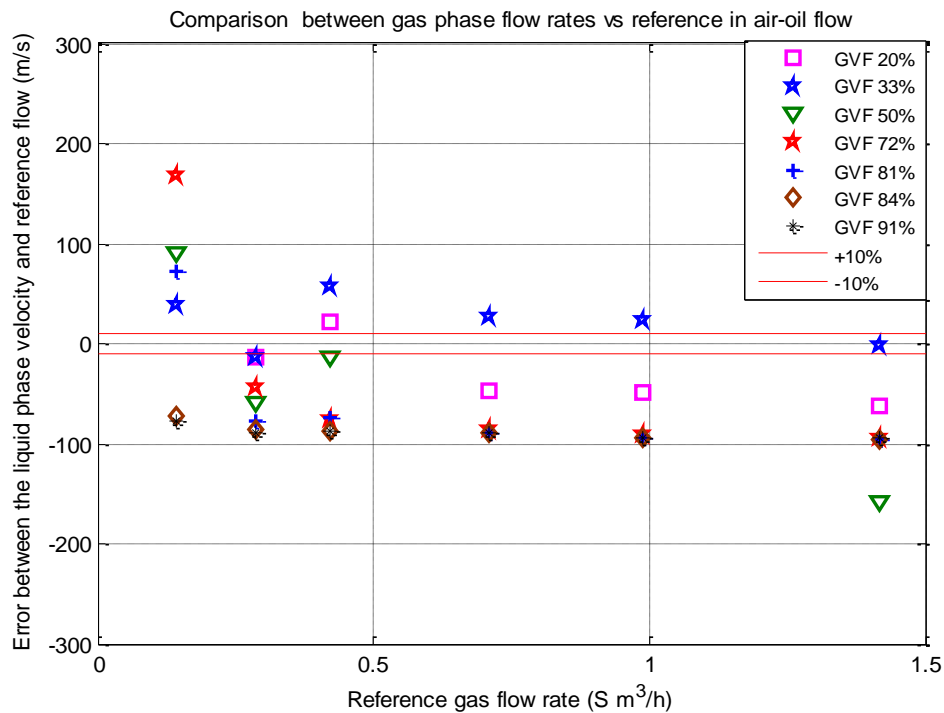**Figure 6-21** Comparison of the ultrasound measured gas phase velocity with the reference input flow velocity

The error between the measured gas flow rates in the air-oil flow and the reference gas flow rates is plotted in Figure 6-21. In the same way as the air-water flow, the gas flow rates error ranged from 5% to up 200%. This large error is attributed to the fact that high gas flow rates attenuate the penetrative strength of the ultrasound signal.

6.4.3 Oil-water two-phase flow measurement

Before the determination of the liquid phase fraction and liquid phase velocities using the combined measurements of the gamma densitometer and ultrasound in the oil-water flow, we estimated both the water-cut and density of each oil-water data point. The water-cuts measured were compared with those calculated based on the input conditions of the flow, as shown in Figure 6-22. It can be seen that most of the measured water-cut agrees with the calculated water-cut with ±10% uncertainty.
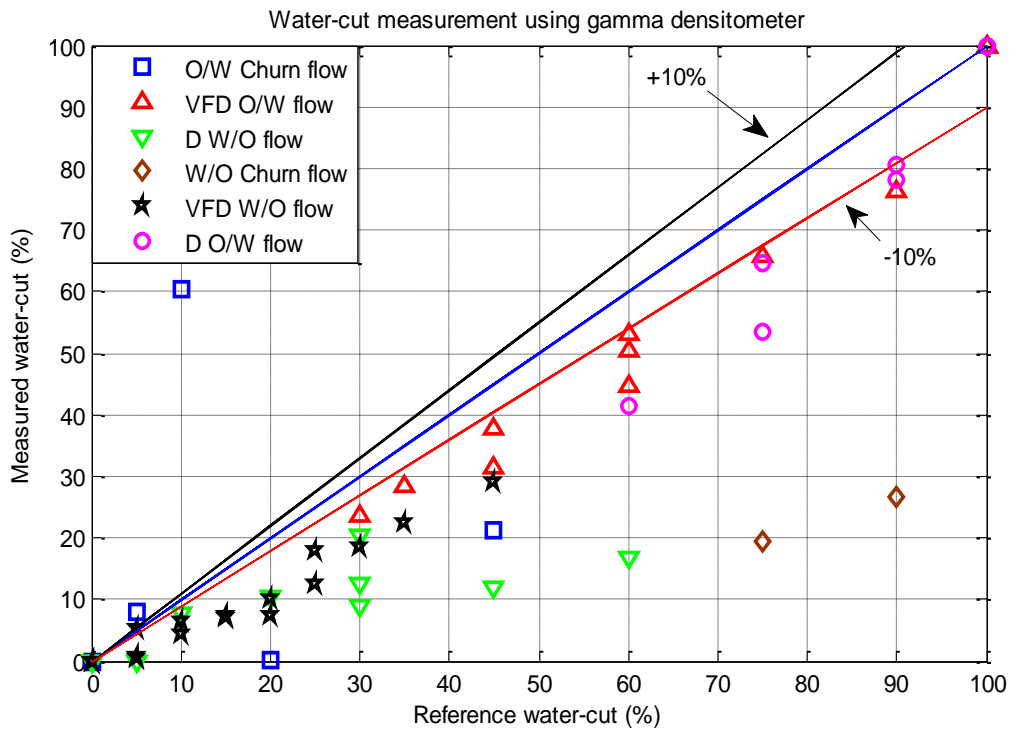
Figure 6-22 Comparison between experimental and calculated water-cut of the oil-water flow

The overall density of the oil-water flow estimation is plotted in Figure 6-23 where it is seen that the density measurement is in good agreement with the reference. Densities of all the data points are with the range of ±5%. The oil-continuous part of the plot shows a much higher accuracy than the water dominated region of the graph. This deviation is caused by changes in the phase and flow composition which affected the accuracy of the mean gamma pulses estimated, as the flow changes from oil flow only at the beginning to water only at the tail end of the plot, and oil and water have different rates of absorption rate for the gamma radiation.
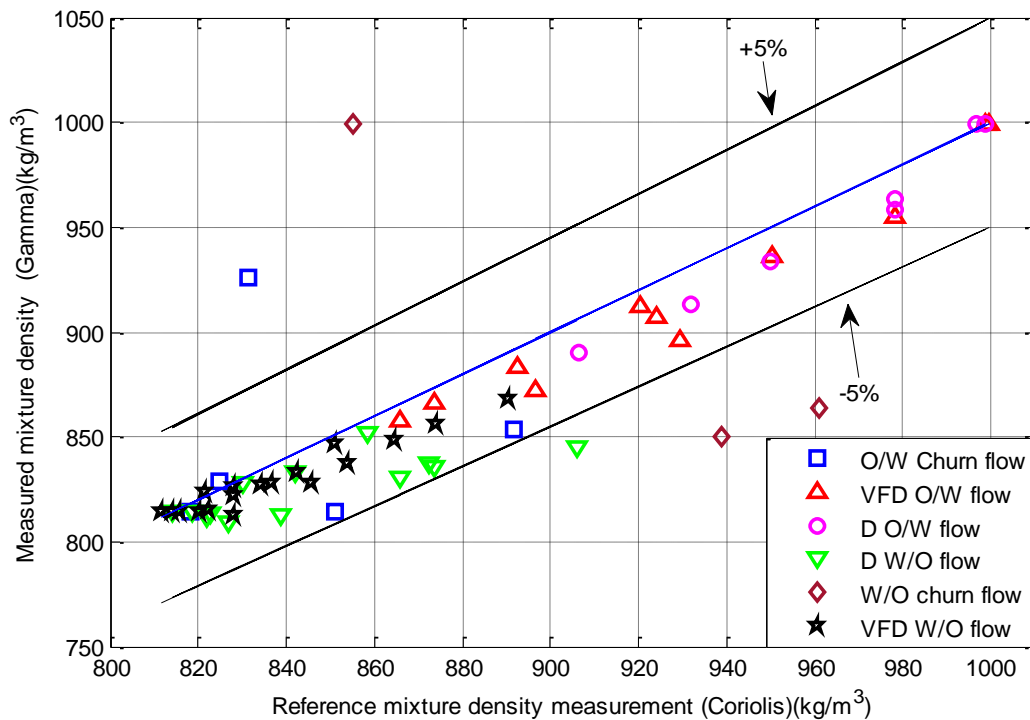
Figure 6-23 Oil-water two-phase flow density estimation compared with the reference density measurement

The next analysis of the oil and water measurement is the flow rate estimation of the individual oil phase and water phase flows in the oil-water flow. The total flow velocity of the two-phase oil-water was estimated using the ultrasound Doppler sensor. As the speed of sound in oil and water is different, we used a mixture of sound speed for the two-phase. The mixture sound velocity was calculated for each data point based on the fraction of each phase in the data. A similar strategy of estimation of sound speed in a two-phase flow has been applied in the work of Huang et al. (2013).

$$c_{mix} = c_{oil}(1 - \alpha_w) + c_w \tag{6-24}$$

After the mixture sound speeds are estimated, and then averaged, a flow velocity measurement using the Doppler flow technique was applied to obtain the velocity of the emulsion flow.

The flow rate estimation for the oil phase flow is plotted in Figure 6-25, while the flow rate estimation of the water phase flow is plotted in Figure 6-26. It can be

seen from both of the individual phase flow estimates obtained, that using the combined instruments measurement is underestimating the reference mass flow rates of each phase flow.
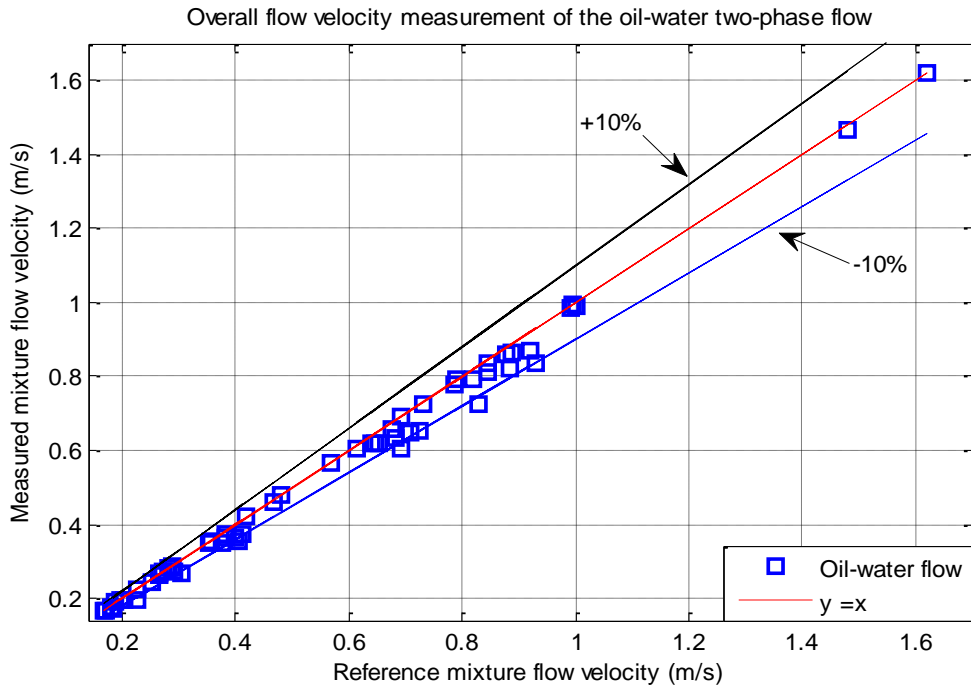
Figure 6-24 Overall oil-water flow measurement against the flow velocities
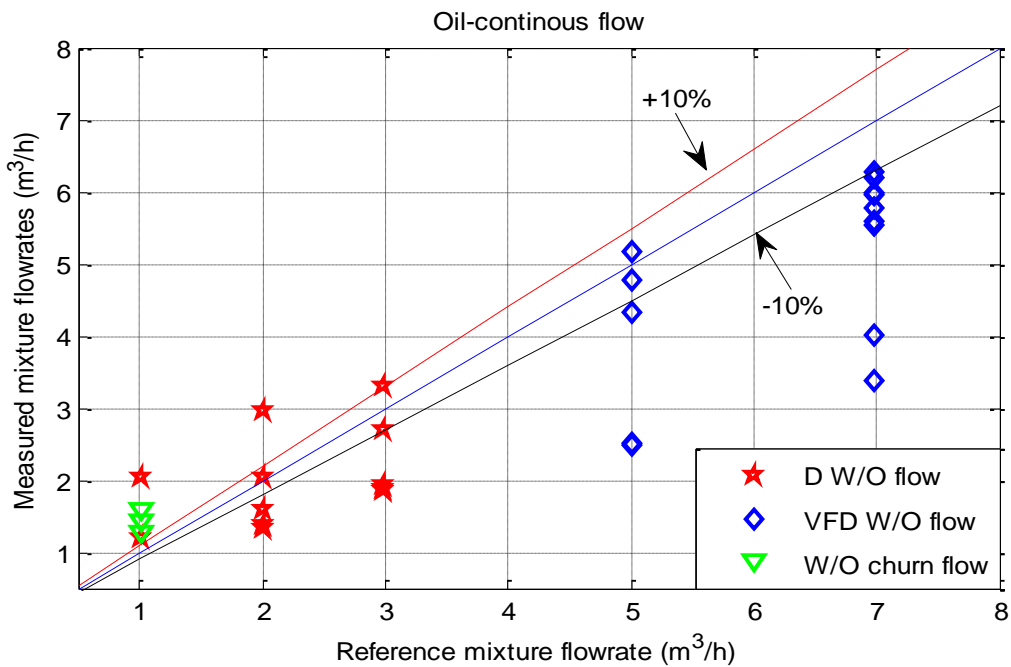
Figure 6-25 Oil phase flow velocity estimation and reference oil phase flow
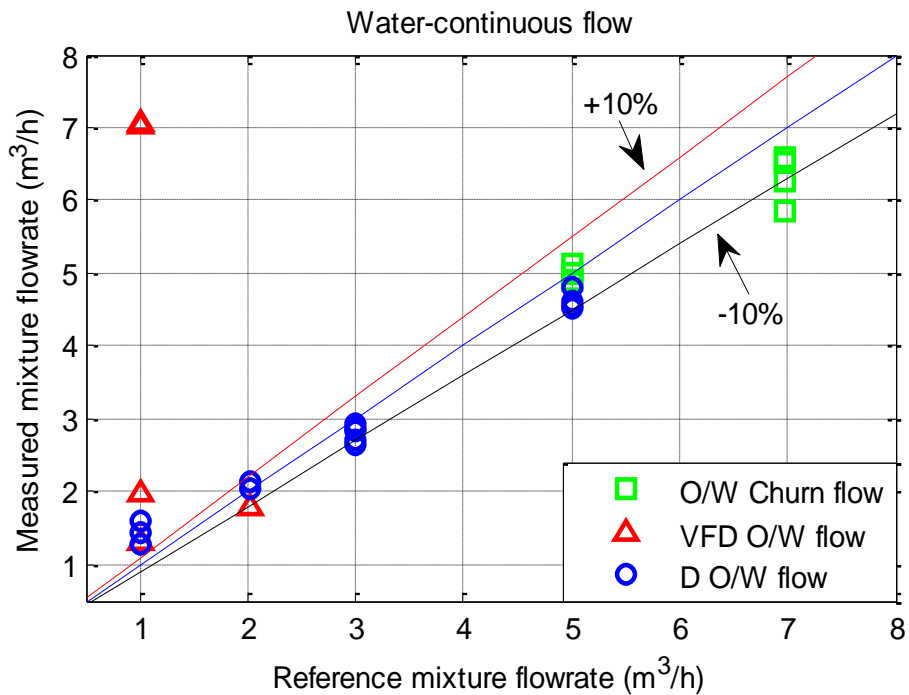
Figure 6-26 Water phase flow velocity estimation and reference oil phase flow

The main reason for this error in the estimate is assumed to be as a result of the changing flow regimes, as there are six different flow regimes in oil-water vertical flow. The measurement could be due to the fact that the flow regime was not considered, because test data points were computed based on classification of their water volume fraction. As a result, the method developed from the combination of the gamma densitometer and ultrasound Doppler sensor underestimated the flow rates.

The changes in the water volume fraction of the oil-water flow mixture causes changes in the sound speed in the mixture. Consequently, the velocity of fluid changes as the content of the flow changes, even if the total mixture mass flow rates remain the same. Figure 6-27 shows the changes in the mixture velocities due to changes in the water volume fractions. The plot clearly illustrates that the higher the water content, the higher flow the velocity and this trend applies to the four test data points investigated.
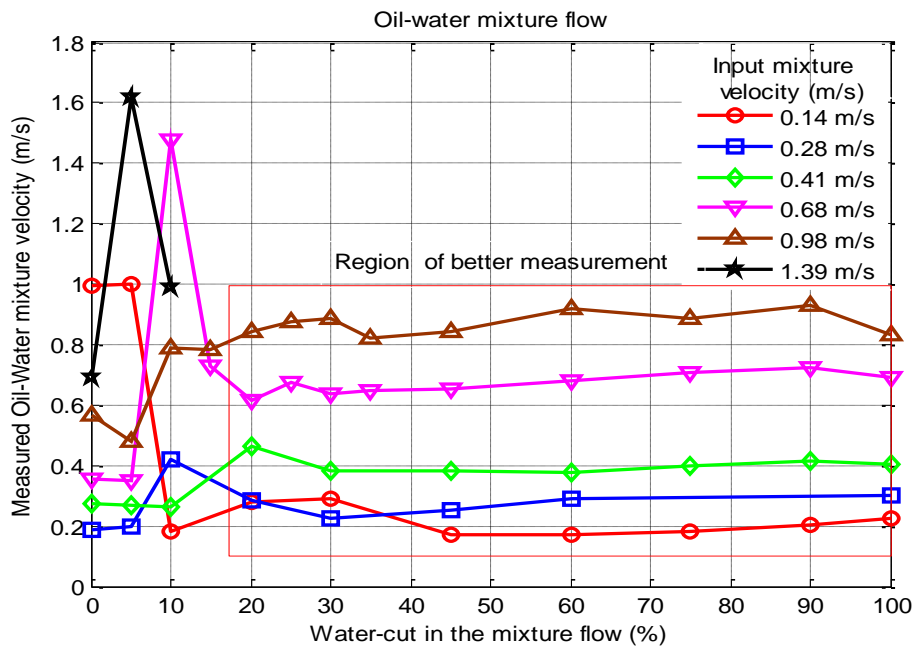
Figure 6-27 Variation of the oil-water mixture velocities due to changes in the water-cut of the oil-water two-phase

In Figure 6-27, it can be seen that the mixture velocities rose sharply in between zero water-cut and 15% (WC 15%) and then steadily increased in line with the increase in water volume fraction. This spontaneous increase in the flow velocities is due to the relatively about 20% difference in densities between water and oil. However, no definite summary can be made other than the sound in water is higher than in oil and it was the result of the increases in the velocities of the higher water-cut flows.

6.5 Summary

In this study, a new approach to measuring the flow rates of three types of two-phase flows: air-water flow, air-oil flow and oil-water, using ultrasonic Doppler sensor and gamma densitometer, has been investigated. Both the ultrasound sensor and the gamma densitometer are clamped on devices and hence they are ideal tools for the development of non-invasive multiphase flow measurement.

Both the air-water and air-oil flows are treated as gas-liquid two-phase flow and the same methods are developed for the individual liquid flow rates and individual gas flows. The liquid flow rates were determined by the product of the

liquid fraction determined with the gamma densitometer and liquid flow velocity estimated from the ultrasonic signal of the two-phase flow. It has been found that liquid phase velocity can be determined with good accuracy, especially for the flow data points within the low Reynolds ranges. The gas flow rates estimation was based on the combination of the sensor's measurement and the two slip and homogeneous models. The slip model was required to estimate the gas mass quality from the void fraction measurement while the homogeneous model estimates the gas-liquid mixture density.

This work presents an investigation of two-phase gas-liquid and liquid-liquid emulsion flow using a combination of two non-invasive sensors to determine individual phase's volume fractions and flow rates. The methodology developed here can be further improved by incorporating the effect of flow regimes into the measurement approaches adopted.

7 Conclusions and recommendations

7.1 Conclusions

This thesis has presented investigations into the capabilities of the two types of ultrasound Doppler sensors: continuous wave Doppler sensor and pulse-echo ultrasounds to conduct measurements of two-phase multiphase flow in both horizontal and vertical pipe orientations. The results have demonstrated that ultrasound waveforms reflected from the flow in the pipe can be manipulated to detect slug flow parameters. The ultrasound signals can be processed to generate features such as inputs to neural network models for pattern recognition techniques of two-phase flow measurement, and coupling of the ultrasound measurement with gamma densitometer for the measurement of two-phase flow rates. Both the ultrasound continuous wave sensor and pulse-echo transducer were installed non-invasively. The non-invasive setup was proposed to develop a technique and method for the clamp-on multiphase flowmeter. However, there are challenges encountered in the analysis of the waveforms which include attenuation of the ultrasound waveforms by the gas flow, which thus limits the reliability of the measurement systems developed into two-phase with reasonable amounts of gas fraction, such as in the slug flow.

The findings of the investigation include estimations of the hydrodynamic parameters of air-water flow. Slug flow can be achieved using the non-invasive ultrasound and processing of the ultrasound waveforms of the slow using HHT techniques. Then, neural network models were developed for classification of the flow regimes of the two-phase flow with reasonable accuracy and to predict gas flow rates and liquid flow rates. Moreover, the ultrasound sensor measurements were coupled with the gamma densitometer measurements to obtain the flow rates of the oil continuous flow and water continuous flow of the oil-water two-phase flow, and measurement of gas flow rates and liquid flow rates in air-water and air-oil two-phase flow. Finally, a high frequency pulse-wave ultrasound Doppler sensor was utilised in the pulse-echo mode to determine film thickness in both vertical and horizontal flow pipes. These capacities of the technology developed have extended the application of the

ultrasound sensor use in the industry from the original function as a flow velocity measurement sensor to two-phase flow measurement.

7.1.1 Application of continuous wave ultrasound Doppler

The determination of the hydrodynamic parameters of the two-phase slug flow, such as slug frequency, slug lengths and elongated bubble velocity, is important for many design calculations in pipe and petroleum industry downstream equipment. The parameters are often measured with invasive or light dependent instruments which are not good enough for field operations. In this study, experimental measurements of air-water flow on a horizontal flow pipe were conducted with a clamp-on (non-invasive) ultrasound Doppler sensor to determine slug flow hydrodynamic parameters. The HHT is applied to the ultrasound signals to investigate a non-invasive measurement of the parameters of the two-phase slug flow. The clamp-on ultrasonic sensor measurement is validated by a synchronised measurement of the slug flow parameters using a pair of flush mounted conductivity probes. The application of acontinuous wave ultrasound Doppler sensor's ability to measure the parameters of the multiphase flow was enhanced with the use of the HHT signal processing method. In addition, the HHT technique is shown to be more accurate than FFT for extracting the Doppler shift frequency from the ultrasound waveforms for the estimation of average flow velocity.

7.1.2 Application of pulse echo ultrasound
In addition, the pulse-echo methods have the capability of measuring two-phase flow parameters in both temporal and spatial resolution. Therefore, they have the potential for pattern recognition of two-phase flow for the quantitative characterisation of flow regimes by plotting the instantaneous level as a function of time series.

7.1.3 Ultrasound and neural network techniques
The feasibility of the pattern recognition technique using the continuous wave Doppler ultrasound and neural network was investigated on the 2-inch horizontal air-water flow test rig. The ultrasound sensor is a single unit clamp-on device and the ultrasound signals were acquired and processed using both

PSD and DWT to generate the representative feature of the data set. These features are used as the input to the neural network models and trained to predict new data set features which are not seen by the network. The method was implemented for both flow regime classification and the prediction of the flow rates of the gas and liquid flow. Flow regimes studied, including slug, elongated bubbly, stratified and stratified wavy were first visually identified and then the neural network was developed from the ultrasound signal to objectively classify them.

The results show that the methodology is suitable for a non-invasive flow regime classification using ultrasound signals. The features extracted using DWTs is much better than those extracted using the PSD. The efficacy of the flow regimes classification method was assessed numerically. A few and infrequent misclassifications were observed in the process but those inaccuracies were misread as the flow regimes of nearest flow patterns. This makes the methodology proposed and developed for the flow regime classification reliable and of significance for field deployment. However, further studies are recommended to investigate the methodology for vertical flows and improvements in the accuracy of the prediction of flow rates.

7.1.4 Data Fusion of Gamma and ultrasound sensor

A new approach to the experimental study of air-water, air-oil and oil-water two-phase flows in a vertical pipe has been conducted to investigate a non-invasive multiphase flow metering using a combination of measurements from ultrasound Doppler sensor and gamma densitometer. Gas phase and liquid phase flow rates were computed with the measurements from the instruments and the use of a slip model and a homogeneous model. The methodology proposed here was aimed at the development of a clamp-on multiphase flow metering system. The flow phase fractions were computed from the gamma pulses counted across the flow of the fluids. The flow velocity was measured with the ultrasound sensor, using the FFT method of extracting the shift frequencies of the reflected ultrasound signals. The measurement of the mean velocity was calculated by estimating the mean frequency of the frequency

shifts using the time averaged maximum frequency Doppler of the ultrasound waveforms.

Generally, the results obtained for the gas flow rates and liquid flow rates were good, particularly for the flow conditions with low gas void fraction (GVF <40%). The flow conditions with higher GVF have caused considerable errors in the measurement of the flow velocities and this was attributed to the attenuation of the ultrasound signals by the gas flow. On the other hand, the measurement flow velocity and the flow volumetric rates are much better for oil and water flow. The flow rates determined for all the data sets in the region of the water-continuous flow regimes of oil-in-water churn (O/W Churn), dispersed oil-in-water (D O/W) and very finely dispersed oil-in-water flow, are all measured within the uncertainty of ±10%.

The key challenges encountered in this experiment were the inaccuracies in the gas-liquid flow rates measurements at higher GVF and oil-water flow rate inaccuracies at very low water-cut. Therefore, further study and improvement on the models and signal processing of the ultrasound signals are recommended.

7.2 Recommendations for further study

The four applications of ultrasound technology for multiphase flow measurement explored in this thesis have shown better development of the technology and demonstrated its potential for industrial application in both vertical and horizontal pipe flow orientations. However, there is room for improvement in all the four applications proposed in this study.

7.2.1 Application of continous wave ultrasound Doppler

In this chapter, an ultrasonic continuous wave Doppler sensor was applied to gas-liquid two-phase flow to measure flow rates and monitor the parameters of the two-phase flow regimes. The results are compared with models developed from experimental methods in the literature. Further investigation will be carried out to determine the inhibitor of these test points.

7.2.2 Application of pulse echo ultrasound

Two pulse echo transducers methods have been used on either of the horizontal and vertical pipe flows. The first, a wet transducer of 1 MHz centre frequency was used for measuring liquid thickness by pulse echo methods to develop ultrasonic method of liquid level measurement in the horizontal air-water flow. This method was found to be suitable for finding liquid height in the pipe and it can be extended to flow regime classification as well. The second transducer was a 7.5 MHz centre frequency clamp-on sensor which uses operation principle similar to the previous 1 MHz transducer for the pulse echo ultrasound technique. The second sensor was used for determining the liquid thickness of both oil and water in the vertical flow. However, it is found to be unsuitable in the current setting as the high frequency ultrasound signal being generated by the transducer were strongly attenuated by the gas flow.

7.2.3 Ultrasound and neural network techniques

In order to develop the technology further or to apply the methodology on different types of fluid, further feature extraction training is required. Since the response of the ultrasound is affected by the gas flow by attenuation of the ultrasound waveforms, as a result the strength of the ultrasound is higher in the flows with low gas content. Therefore, it recommended that a combination of the ultrasound sensor and another sensor would provide the features in both phases of two-phase for ultrasound signal. Then it is expected that the prediction of the gas flow rates would be accurate and the prediction of liquid flow rates could also be enhanced. Another interesting aspect that could be taken into account is the online measurement of the multiphase flow in real time. In this study, both the process of the flow regimes classification and prediction of the gas flow rates and liquid flow rates were conducted offline using MATLAB. The neural network models developed could be integrated in the LabVIEW programs to implement online multiphase flow monitoring. The benefits of the online measurements cannot be overemphasised.

7.2.4 Data fusion of Gamma and ultrasound sensor

The data acquisition of the experiments is conducted using four independent computers to collect the test data in this experiment – PCs with process management software (Delta V). Delta V coordinates the fully automated operation of the rig and some of its function is for setting test points by controlling the flow rates of the liquid and gas, and real-time monitoring of the operation of the test rig. One of the PCs is for the ultrasound Doppler sensor, gamma densitometer and one for reference instrumentation on the test rig. Therefore, one of the improvements that could be undertaken for the future work of this study is to develop a mechanism in which all the different sensors can be operated using a single PC and to synchronise the data acquisition.

Another challenge encountered in the study is the issue of measurement of flow with high GVF. As low void fraction data were measured accurately, it is desirable to improve on that. Flow rates of the data set with high GVF were estimated inaccurately and the author believes that by instruction of flow pattern information into the current measurement method, there will also be improvement in the estimation of the gas flow rates as well as the liquid flow rates at higher GVF.

Most techniques need further development, despite some success having been achieved in MFM applications. The most significant improvements that could be undertaken for the future work of this study is to develop a mechanism in which all the different sensors can be operated using a single PC and to synchronise the data acquisition.
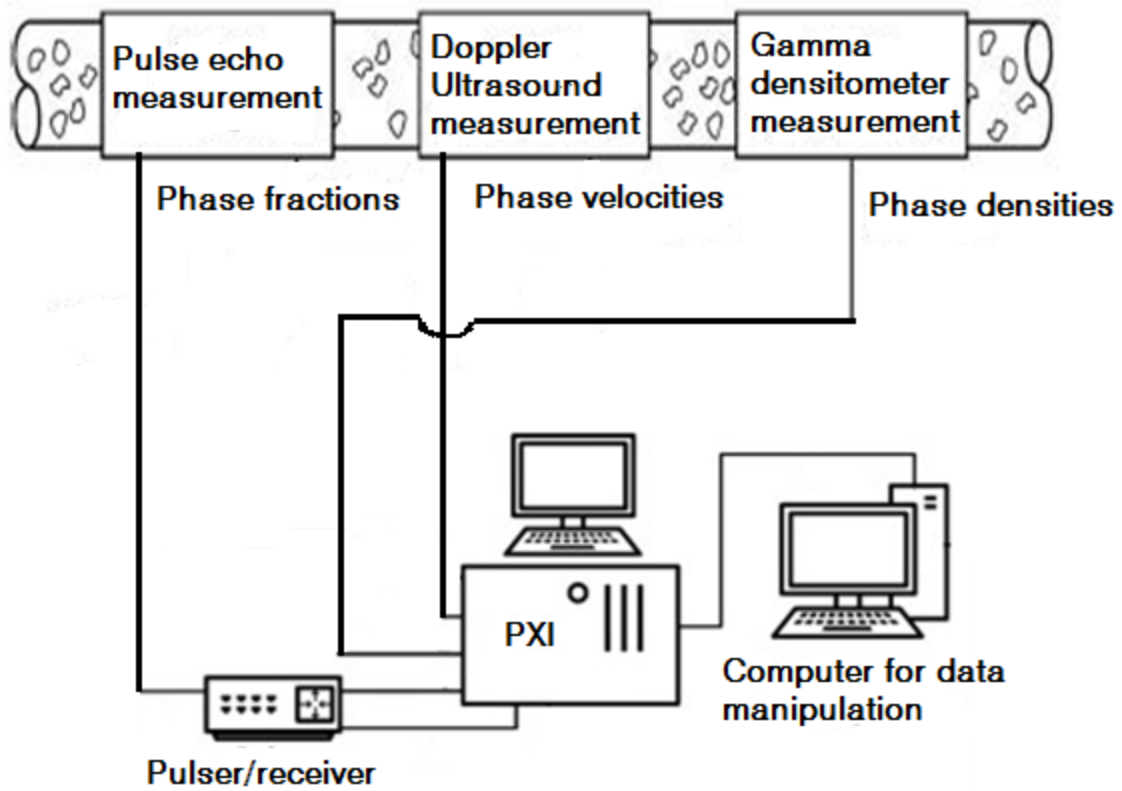
Combination of the three clamp-on sensors for
multiphase flow measurement

Figure 7-1 Instruments setup for the proposed future work of combining all the three sensors in a single PC for synchronised data acquisition and analyses

8 REFERENCES

Açikgöz, M., Franca, F. & Lahey Jr, R.T., 1992. An experimental study of three-phase flow regimes. *International Journal of Multiphase Flow*, 18(3), pp.327–336.

Afanasyev, V. et al., 2009. Multiphase Fluid Samples: A Critical Piece of the Puzzle. , pp.30–37.

Al-Lababidi, S., 2006. Multiphase flow measurement in the slug regime using ultrasonic measurement techniques and slug closure model.

Amin, A. et al., 2005. Subsea Development from Pore to Process As oil companies step out into deeper waters , operators may discover that finding. *Oilfield Review*, pp.4–17.

Andreussi, P., Di Donfrancesco, A. & Messia, M., 1988. An impedance method for the measurement of liquid hold-up in two-phase flow. *International Journal of Multiphase Flow*, 14(6), pp.777–785. Available at: http://www.sciencedirect.com/science/article/pii/0301932288900742.

Arvoh, B.K., Hoffmann, R. & Halstensen, M., 2012. Estimation of volume fractions and flow regime identification in multiphase flow based on gamma measurements and multivariate calibration. *Flow Measurement and Instrumentation*, 23(1), pp.56–65.

Baker, D.W., 1970. Pulsed ultrasonic Doppler blood-flow sensing. *Sonics and Ultrasonics, IEEE Transactions on*, 17(3), pp.170–184.

Banerjee, S. & Lahey Jr, R.T., 1981. Advances in two-phase flow instrumentation. In *Advances in Nuclear Science and Technology*. Springer, pp. 227–414.

Barber, W.D., Eberhard, J.W. & Karr, S.G., 1985. Measurements Using Doppler Ultrasound. , (3).

Basheer, I.A. & Hajmeer, M., 2000. Artificial neural networks : fundamentals , computing , design , and application. *Journal of Microbiological Methods*, 43, pp.3–31. Available at: http://www.sciencedirect.com/science/article/pii/S0167701200002013.

Bendjama, H. et al., 2015. Selection of Wavelet Decomposition Levels for Vibration Monitoring of Rotating Machinery. In *The Ninth International*

Conference on Advanced Engineering Computing and Applications in Sciences ADVCOMP 2015. Nice, France: IARIA XPS Press, pp. 96–100.

Blaney, S., Clamp-on Multiphase Flow Metering School of Engineering Phd Thesis.

Blaney, S., 2008. *Gamma radiation methods for clamp-on multiphase flow metering*. Cranfield University.

Bonnet, J.C. & Tavlarides, L.L., 1987. Ultrasonic technique for dispersed-phase holdup measurements. *Industrial & Engineering Chemistry Research*, 26(4), pp.811–815.

Brini Ahmed, S.K., 2014. A study of gas lift on oil/water flow in vertical risers. , 41(January), pp.2013–2014.

Brody, W.R. & James, D., 1974. CW Doppler Ultrasonic Flowmeter. , (3), pp.183–192.

Brody, W.R., Meindl, J.D. & James, D., 1974. Theoretical analysis of the CW doppler ultrasonic flowmeter. *IEEE transactions on bio-medical engineering*, 21(3), pp.183–192. Available at: http://www.ncbi.nlm.nih.gov/pubmed/4277736.

Cai, S. et al., 1994. Neural network based objective flow regime identification in air-water two phase flow. *The Canadian Journal of Chemical Engineering*, 72(3), pp.440–445.

Canière, H. et al., 2007. Horizontal two-phase flow characterization for small diameter tubes with a capacitance sensor. *Measurement Science and Technology*, 18(9), pp.2898–2906.

Carvalho, R.D.M. d. et al., 2009. Application of the ultrasonic technique and high-speed filming for the study of the structure of air–water bubbly flows. *Experimental Thermal and Fluid Science*, 33(7), pp.1065–1086.

Case, M. et al., 2013. ULTRASONIC BLOOD FLOW SENSING USING DOPPLER VELOCIMETRY. *International Journal on Smart Sensing and Intelligent Systems*, 6(4), pp.1298–1316.

Chakraborty, S. et al., 2009. Void fraction measurement in two-phase flow processes via symbolic dynamic filtering of ultrasonic signals. *Measurement Science and Technology*, 20(2), p.23001.

Chang, J.S. & Morala, E.C., 1990. Determination of two-phase interfacial areas by an ultrasonic technique. *Nuclear Engineering and Design*, 122(1–3), pp.143–156. Available at: http://www.sciencedirect.com/science/article/pii/002954939090203A.

Christmann, H.A. et al., 1990. Real-time DSP system for ultrasonic blood flow measurement. In *Circuits and Systems, 1990., IEEE International Symposium on.* IEEE, pp. 2045–2048.

Christopher, D.A. et al., 1996. A HIGH-FREQUENCY CONTINUOUS-WAVE DOPPLER ULTRASOUND SYSTEM FOR THE DETECTION OF BLOOD FLOW IN THE MICROCIRCULATION. *Medicine*, 22(9).

Chun, M.H., Lee, S.K. & Park, J.R., 1984. Parametric effects on the liquid-film-thickness measurement by an ultrasonic method. *Transaction of American Nuclear Society*.

Cobbold et al., 1983. Influence of Beam Profile and Degree of Insonation on the CW Doppler Ultrasound Spectrum. *Sonics and Ultrasonics, IEEE Transactions on 30.6*, (6), pp.364–370.

Corneliussen, S. et al., 2005. Handbook of multiphase flow metering. *Norwegian Society for Oil and Gas Measurement (NFOGM), Revision*, 2.

Deng, X. et al., 2011. Theoretical study of vertical slug flow measurement by data fusion from electromagnetic flowmeter and electrical resistance tomography. *Flow Measurement and Instrumentation*, 22(4), pp.272–278.

Ding, H. et al., 2007. Hilbert–Huang transform based signal analysis for the characterization of gas–liquid two-phase flow. *Flow Measurement and Instrumentation*, 18(1), pp.37–46. Available at: http://www.sciencedirect.com/science/article/pii/S0955598607000040 [Accessed October 13, 2015].

Dong, X. et al., 2015. Oil-water two-phase flow velocity measurement with continuous wave ultrasound Doppler. *Chemical Engineering Science*, 135(92), pp.155–165. Available at: http://dx.doi.org/10.1016/j.ces.2015.05.011.

Drahoš, J. & Čermák, J., 1989. Diagnostics of gas—liquid flow patterns in chemical engineering systems. *Chemical Engineering and Processing:*

Process …, 26, pp.147–164. Available at: http://www.sciencedirect.com/science/article/pii/025527018990007X.

Dyakowski, T., 1996. Process tomography applied to multi-phase flow measurement. *Measurement Science and Technology*, 7(3), p.343.

Eren, H., 1998. Accuracy in real time ultrasonic applications and transit-time flow Meters. *IMTC/98 Conference Proceedings. IEEE Instrumentation and Measurement Technology Conference. Where Instrumentation is Going (Cat. No.98CH36222)*, 1, pp.568–572.

Evans, D.H. & McDicken, W.N., 2000. *Doppler ultrasound: physics, instrumentation, and signal processing*, Wiley Chichester.

Exploration, B., 1994. Multiphase Design Manual. *BP Exploration*. Available at: https://www.scribd.com/doc/237635019/BP-Multi-Phase-Design-Manual-pdf.

Falcone, G., Hewitt, G.F. & Alimonti, C., 2009. *Multiphase Flow Metering: Principles and Applications*, Elsevier Science.

Fan, S. et al., 2013. Velocity characteristics of slug body and film for two-phase gas-liquid slug flow using ultrasonic techniques. *8th International Conference on Multiphase Flow ICMF 2013, Jeju, Korea, May 26 - 31, 2013*, pp.1–5.

Fan, S. & Yan, T., 2014. Two-phase air-water slug flow measurement in horizontal pipe using conductance probes and neural network. *IEEE Transactions on Instrumentation and Measurement*, 63(2), pp.456–466.

Figueiredo, M.M.F. et al., 2016. The use of an ultrasonic technique and neural networks for identification of the flow pattern and measurement of the gas volume fraction in multiphase flows. *Experimental Thermal and Fluid Science*, 70, pp.29–50. Available at: http://dx.doi.org/10.1016/j.expthermflusci.2015.08.010.

Filletti, E.R. & Seleghim jr, Paulo, 2010. Nonintrusive measurement of interfacial area and volumetric fraction in dispersed two-phase flows using a neural network to process acoustic signals—A numerical investigation. *International Journal for Numerical Methods in Biomedical Engineering*, 28(1), pp.72–86. Available at:

http://onlinelibrary.wiley.com/doi/10.1002/cnm.1494/full.

Fischer, C., 1994. Development of a metering system for total mass flow and compositional measurements of multiphase/multicomponent flows such as oil/water/air mixtures. *Flow Measurement and Instrumentation*, 5(1), pp.31–42.

Flores, J. et al., 1999. Characterization of Oil–Water Flow Patterns in Vertical and Deviated Wells. *SPE Production & Facilities*, 14(2), pp.5–8.

Fossa, M., Guglielmini, G. & Marchitto, A., 2003. Intermittent flow parameters from void fraction analysis. *Flow Measurement and Instrumentation*, 14(4), pp.161–168.

Gonzalez A, S.R., Murai, Y. & Takeda, Y., 2009. Ultrasound-based gas–liquid interface detection in gas–liquid two-phase flows. *Advances in chemical engineering*, 37, pp.1–27.

Güler, İ. & Übeyli, E.D., 2006. A recurrent neural network classifier for Doppler ultrasound blood flow signals. *Pattern Recognition Letters*, 27(13), pp.1560–1571.

Hedrick, W.R., Hykes, D.L. & Starchman, D.E., 1995. *Ultrasound physics and instrumentation*, Mosby St. Louis.

Henry, M. et al., 2013. Coriolis mass flow metering for three-phase flow: A case study. *Flow Measurement and Instrumentation*.

Henry, M., 2001. On-line compensation in a digital Coriolis Mass Flow meter. *Flow Measurement and Instrumentation*, 12(2), pp.147–161. Available at: http://www.sciencedirect.com/science/article/B6V38-43854NV-7/2/ce8c78f86de85e72ba25c5b77becd67a.

Hernandez, L. et al., 2006. Fast classification of two-phase flow regimes based on conductivity signals and artificial neural networks. *Measurement Science and Technology*, 17(6), p.1511.

Hernández, L. et al., 2006. Fast classification of two-phase flow regimes based on conductivity signals and artificial neural networks. *Measurement Science and Technology*, 17(6), pp.1511–1521.

HISTAND, M.B., Miller, C.W. & MCLEOD, F.D., 1973. Transcutaneous measurement of blood velocity profiles and flow. *Cardiovascular research*,

7(5), pp.703–712.

Hu, H.L. et al., 2011. Identification of Gas–Solid Two-Phase Flow Regimes Using Hilbert–Huang Transform and Neural-Network Techniques. *Instrumentation Science & Technology*, 39(2), pp.198–210. Available at: http://www.tandfonline.com/doi/abs/10.1080/10739149.2010.545852.

Huang, N.E. et al., 1998. The empirical mode decomposition and the Hilbert spectrum for nonlinear and non-stationary time series analysis. In *Proceedings of the Royal Society of London A: Mathematical, Physical and Engineering Sciences*. The Royal Society, pp. 903–995.

Huang, N.E. & Wu, Z., 2008. a Review on Hilbert-Huang Transform : Method and Its Applications. *October*, 46(2007), pp.1–23. Available at: http://rcada.ncu.edu.tw/reference010.pdf.

Huang, S. et al., 2013. Issues of a Combination of Ultrasonic Doppler Velocity Measurement with a Venturi for Multiphase Flow Metering. In *18th Middle East Oil & Gas Show and Conference (MEOS)*.

Huang, Z. et al., 2005. Gas–oil two-phase flow measurement using an electrical capacitance tomography system and a Venturi meter. *Flow Measurement and Instrumentation*, 16(2), pp.177–182.

Jain, a. K., Duin, R.P.W. & Mao, J., 2000. Statistical pattern recognition: a review. *IEEE Transactions on Pattern Analysis and Machine Intelligence*, 22(1), pp.4–37. Available at: http://ieeexplore.ieee.org/ielx5/34/17859/00824819.pdf?tp=&arnumber=824819&isnumber=17859\nhttp://ieeexplore.ieee.org/xpls/abs_all.jsp?arnumber=824819.

Jha, D.K. et al., 2013. Classification of Two-Phase Flow Patterns by Ultrasonic Sensing. *Journal of Dynamic Systems, Measurement, and Control*, 135(2), p.24503.

Jin, N.D. et al., 2003. Characterization of oil/water two-phase flow patterns based on nonlinear time series analysis. *Flow Measurement and Instrumentation*, 14(4), pp.169–175.

Kandaswamy, A. et al., 2004. Neural classification of lung sounds using wavelet coefficients. *Computers in biology and medicine*, 34(6), pp.523–537.

Available at: http://www.sciencedirect.com/science/article/pii/S0010482503000921.

Keeton, P.I.J. & Schlindwein, F.S., 1997. Application of wavelets in Doppler ultrasound. *Sensor Review*, 17(1), pp.38–45.

Kossoff, G., 2000. Basic physics and imaging characteristics of ultrasound. *World journal of surgery*, 24(2), pp.134–142.

Kouame, D. et al., 2003. High Resolution Processing Techniques for Ultrasound Doppler Velocimetry in the Presence of Colored Noise. Part II: Multiplephase Pipe-Flow Velocity Measurement. , 501(1).

Kulkarni, A.A. et al., 2001. Application of multiresolution analysis for simultaneous measurement of gas and liquid velocities and fractional gas hold-up in bubble column using LDA. *Chemical Engineering Science*, 56(17), pp.5037–5048. Available at: http://www.sciencedirect.com/science/article/pii/S0009250901001919.

Kumara, W.A.S., Halvorsen, B.M. & Melaaen, M.C., 2010. Single-beam gamma densitometry measurements of oil–water flow in horizontal and slightly inclined pipes. *International Journal of Multiphase Flow*, 36(6), pp.467–480.

Kv, S. & Roy, B.K., 2012. An Intelligent Flow Measurement Technique using Ultrasonic Flow Meter with Optimized Neural Network. *International Journal of Control and Automation*, 5(4), pp.185–196.

Liu, R.P. et al., 2001. A neural network to correct mass flow errors caused by two-phase flow in a digital coriolis mass flowmeter. *Flow Measurement and Instrumentation*, 12(1), pp.53–63. Available at: http://www.sciencedirect.com/science/article/pii/S0955598600000455.

Luntta, E. & Halttunen, J., 1999. Neural network approach to ultrasonic flow measurements. *Flow Measurement and Instrumentation*, 10(1), pp.35–43.

Mahadeva, D. V, Baker, R.C. & Woodhouse, J., 2008. Studies of the accuracy of clamp-on transit time ultrasonic flowmeters. In *Instrumentation and Measurement Technology Conference Proceedings, 2008. IMTC 2008. IEEE*. IEEE, pp. 969–973.

Mandhane, J.M., Gregory, G.A. & Aziz, K., 1974. A flow pattern map for gas—liquid flow in horizontal pipes. *International Journal of Multiphase Flow*,

1(4), pp.537–553.

Matani, A., Oshiro, O. & Chihara, K., 1996. Doppler signal processing of blood flow using a wavelet transform. *Japanese journal of applied physics*, 35(part 1), pp.3131–3134.

Matsumoto, S. & Suzuki, M., 1984. Statistical analysis of fluctuations of froth pressure on perforated plates without downcomers. *International Journal of Multiphase Flow*, 10(2), pp.217–228.

Meng, H. et al., 2012. Time-Frequency Analysis of Hilbert Spectrum of Pressure Fluctuation Time Series in a Kenics Static Mixer Based on. *Brazilian Journal of Chemical Engineering*, 29(01), pp.167–182.

Meng, Z. et al., 2010. Air–water two-phase flow measurement using a Venturi meter and an electrical resistance tomography sensor. *Flow Measurement and Instrumentation*, 21(3), pp.268–276.

Meribout, M. et al., 2010. A Multisensor intelligent device for real-time multiphase flow metering in oil fields. *Instrumentation and Measurement, IEEE Transactions on*, 59(6), pp.1507–1519.

Messer, M., 2005. PULSED ULTRASONIC DOPPLER VELOCIMETRY FOR MEASUREMENT OF VELOCITY PROFILES IN SMALL CHANNELS AND CAPPILARIES by PULSED ULTRASONIC DOPPLER VELOCIMETRY FOR MEASUREMENT OF VELOCITY PROFILES IN SMALL CHANNELS. , (December).

Mi, Y., 1998. *Two-phase Flow Characterisation Based on Advanced Instrumentation, Neural Network and Mathematical modelling*. Purdue University.

Mi, Y., Ishii, M. & Tsoukalas, L.H., 2001a. Flow regime identification methodology with neural networks and two-phase flow models. *Nuclear Engineering and Design*, 204(1), pp.87–100.

Mi, Y., Ishii, M. & Tsoukalas, L.H., 2001b. Investigation of vertical slug flow with advanced two-phase flow instrumentation. *Nuclear Engineering and Design*, 204(1), pp.69–85.

Misiti, M. et al., 1997. *Wavelet toolbox. For use with MATLAB.*, Natick, MA: The MathWorks Inc.

Molla, M.K.I. et al., 2006. Empirical mode decomposition analysis of climate changes with special reference to rainfall data. *Discrete Dynamics in Nature and Society*, 2006, pp.1–17. Available at: http://www.hindawi.com/journals/ddns/2006/045348/abs/.

Morriss, S.L. & Hill, A.D., 1991. Measurement of Velocity Profiles in Upwards Oil/Water Flow Using Ultrasonic Doppler Velocimetry. In *SPE Annual Technical Conference and Exhibition*.

Morriss, S.L. & Hill, A.D., 1993. Ultrasonic imaging and velocimetry in two-phase pipe flow. *Journal of energy resources technology*, 115(2), pp.108–116.

Murai, Y. et al., 2010. Ultrasonic detection of moving interfaces in gas–liquid two-phase flow. *Flow Measurement and Instrumentation*, 21(3), pp.356–366.

Ngo, J., 2013. *HILBERT-HUANG TRANSFORM ANALYSIS FOR SNOW AND ICE COVER DATA OVER THE NORTHERN HEMISPHERE AND TIBETAN PLATEAU*. San Diego State University. Available at: http://www.google.co.uk/url?sa=t&rct=j&q=&esrc=s&frm=1&source=web&cd=1&ved=0CCAQFjAAahUKEwig--2Zx7_IAhVCQBoKHTiEDQ0&url=http://sdsu-dspace.calstate.edu/bitstream/handle/10211.10/5034/Ngo_Jazlynn.pdf?sequence=1&usg=AFQjCNEEVIPLUGK-y04rjPwM5MURO0mcIw&sig2=a.

Nguyen, V.T., Euh, D.J. & Song, C.-H., 2010. An application of the wavelet analysis technique for the objective discrimination of two-phase flow patterns. *International Journal of Multiphase Flow*, 36(9), pp.755–768.

Oddie, G. et al., 2003. Experimental study of two and three phase flows in large diameter inclined pipes. *International Journal of Multiphase Flow*, 29(4), pp.527–558.

Oddie, G. & Pearson, J.R.A., 2004. Flow-Rate Measurement in Two-Phase Flow. *Annual Review of Fluid Mechanics*, 36(1), pp.149–172.

Oddie, G. & Pearson, J.R.A., 2004. Flow-rate measurement in two-phase flow. *Annu.Rev.Fluid Mech.*, 36, pp.149–172.

Ozbayoglu, E.M. & Ozbayoglu, M. a., 2009. Estimating Flow Patterns and

Frictional Pressure Losses of Two-Phase Fluids in Horizontal Wellbores Using Artificial Neural Networks. *Petroleum Science and Technology*, 27(2), pp.135–149.

Poesio, P., 2008. Experimental determination of pressure drop and statistical properties of oil-water intermittent flow through horizontal pipe. *Experimental Thermal and Fluid Science*, 32(8), pp.1523–1529. Available at: http://www.sciencedirect.com/science/article/pii/S0894177708000502 [Accessed October 13, 2015].

Rahammohan, A. et al., 2014. Insights into Multiphase flow through Ultrasound Doppler. In *32 nd International North Sea Flow Measurement Workshop*. pp. 1–21.

Rajan, V.S. V, Ridley, R.K. & Rafa, K.G., 1993. Multiphase flow measurement techniques--A review. *Journal of Energy Resources Technology;(United States)*, 115(3), pp.151–161. Available at: http://energyresources.asmedigitalcollection.asme.org/article.aspx?articleid =1413270.

Romero, C.H. et al., 2012. Experimental Determination of Hydrodynamic Parameters of Air-Water Two-Phase Slug Flow in Horizontal Pipes. In *ASME 2012 Fluids Engineering Division Summer Meeting collocated with the ASME 2012 Heat Transfer Summer Conference and the ASME 2012 10th International Conference on Nanochannels, Microchannels, and Minichannels*. American Society of Mechanical Engineers, pp. 1211–1218.

Roosnek, N., 2000. Novel digital signal processing techniques for ultrasonic gas flow measurements. *Flow Measurement and Instrumentation*, 11(2), pp.89–99.

Rosa, E.S. et al., 2010. Performance comparison of artificial neural networks and expert systems applied to flow pattern identification in vertical ascendant gas–liquid flows. *International Journal of Multiphase Flow*, 36(9), pp.738–754. Available at: http://dx.doi.org/10.1016/j.ijmultiphaseflow.2010.05.001.

Safvi, A.A., 1996. *Measurement of fluid flow using the ultrasound time domain correlation technique in a flow phantom and in guinea pigs*. Urbana

Campaign: University of Illinois. Available at: www.brl.uiuc.edu/Downloads/Safvi-MS.../AmjadSafvi-MS-Thesis.pdf.

Sanderson, M.L. & Yeung, H., 2002. Guidelines for the use of ultrasonic non-invasive metering techniques. *Flow Measurement and Instrumentation*, 13(4), pp.125–142.

Santoso, B. et al., 2012. The Identification of Gas-liquid Co-current Two Phase Flow Pattern in a Horizontal Pipe Using the Power Spectral Density and the Artificial Neural Network (ANN). *Modern Applied Science*, 6(9), pp.56–67. Available at: http://www.ccsenet.org/journal/index.php/mas/article/view/20121.

Sato, Y. et al., 2002. Signal processing for advanced correlation ultrasonic velocity profiler. In *Third International Symposium on Ultrasound Doppler Methods for Fluid Mechanics and Fluid Engineering (EFPL), Lausanne*.

SATOMURA, S., 1957. Ultrasonic Doppler Method for the Inspection of Cardiac Functions. *THE JOURNAL OF THE ACOUSTICAL SOCIETY OF AMERICA*, VOLUME 29,(NOVEMBER,).

SCHMITT, P. et al., 2012. Ultrasonic wave interaction with air-water boundary layer. In *8th International Symposium on Ultrasonic Doppler Methods for Fluid Mechanics and Fluid Engineering*. Dresden, Germany.

Schneider, F., Peters, F. & Merzkirch, W., 2005. Ultrasound Cross-Correlation Flow Meter: Analysis by System Theory and Influence of Turbulence. In *Fluid Mechanics of Flow Metering*. Springer, pp. 129–148.

Shaban, H. & Tavoularis, S., 2014. Measurement of gas and liquid flow rates in two-phase pipe flows by the application of machine learning techniques to differential pressure signals. *International Journal of Multiphase Flow*, 67, pp.106–117. Available at: http://www.sciencedirect.com/science/article/pii/S0301932214001608.

Shang, Z. et al., 2004. An investigation of two-phase flow instability using wavelet signal extraction technique. *Nuclear Engineering and Design*, 232(2), pp.157–163.

Sleutjes, B., 2006. *Characterization of the blood velocity waveform in the common femoral artery*. Eindhoven University of Technology Radboud

University Nijmegen Medical Center.

Smallwood, R.H. & Dixon, P., 1986. An electronic Doppler signal generator for assessing continuous-wave ultrasonic Doppler flowmeters. *Physical Science, Measurement and Instrumentation, Management and Education - Reviews, IEE Proceedings A*, 133(2), pp.104–108.

Stahl, P. & von Rohr, P.R., 2004. On the accuracy of void fraction measurements by single-beam gamma-densitometry for gas–liquid two-phase flows in pipes. *Experimental Thermal and Fluid Science*, 28(6), pp.533–544.

Stolojanu, V. & Prakash, A., 1997. Hydrodynamic measurements in a slurry bubble column using ultrasonic techniques. *Chemical engineering science*, 52(21), pp.4225–4230.

Subasi, A., 2005. Automatic recognition of alertness level from EEG by using neural network and wavelet coefficients. *Expert Systems with Applications*, 28(4), pp.701–711.

Sun, Z. & Zhang, H., 2008. Neural networks approach for prediction of gas–liquid two-phase flow pattern based on frequency domain analysis of vortex flowmeter signals. *Measurement Science and Technology*, 19(1), p.15401.

Sun, Z.Q., Shao, S. & Gong, H., 2013. Gas-liquid Flow Pattern Recognition Based on Wavelet Packet Energy Entropy of Vortex-induced Pressure Fluctuation. *Measurement Science Review*, 13(2), pp.83–88. Available at: <Go to ISI>://WOS:000318150800006.

Sunde, C., Avdic, S. & Pázsit, I., 2005. Classification of two-phase flow regimes via image analysis and a neuro-wavelet approach. *Progress in Nuclear Energy*, 46(3-4), pp.348–358. Available at: http://linkinghub.elsevier.com/retrieve/pii/S0149197005000302.

Taitel, Y., Bornea, D. & Dukler, A.E., 1980. Modelling flow pattern transitions for steady upward gas-liquid flow in vertical tubes. *AIChE Journal*, 26(3), pp.345–354.

Takeda, Y., 1991. Development of an ultrasound velocity profile monitor. *Nuclear Engineering and Design*, 126(2), pp.277–284.

Takeda, Y., 1986. Velocity profile measurement by ultrasound Doppler shift

method. *International Journal of Heat and Fluid Flow*, 7(4), pp.313–318.

Tan, C. et al., 2015. Characterization of oil–water two-phase pipe flow with a combined conductivity/capacitance sensor and wavelet analysis. *Chemical Engineering Science*, 134, pp.153–168. Available at: http://linkinghub.elsevier.com/retrieve/pii/S0009250915003073.

Thorn, R., Johansen, G.A. & Hammer, E.A., 1997. Recent developments in three-phase flow measurement. *Measurement Science and Technology*, 8(7), p.691.

Thorn, R., Johansen, G.A. & Hjertaker, B.T., 2013. Three-phase flow measurement in the petroleum industry. *Measurement Science and Technology*, 24(1), p.12003.

Übeyli, E.D. & Güler, İ., 2005. Improving medical diagnostic accuracy of ultrasound Doppler signals by combining neural network models. *Computers in biology and medicine*, 35(6), pp.533–554.

Ux, L.-A., Leonard, D. & Green, R.G., 1985. A pulsed ultrasound transducer system for two component flow. *Journal of Physics E: Scientific Instruments*, 18(7), p.609.

Vedapuri, D., 2001. Design ofa Clamp-on Ultrasonic Flow Meter for Wet Gas Pipelines. *PhD thesis, Ohio State University*, (June 2001).

W.M.D Wright, 2011. Anlytical Methods Ultrasonic Techniques. In P. F. Fox & P. L. H. McSweeney, eds. *Enclyclopedia of dairy sciences*. Amsterdam: Elsevier, c2011, pp. 206–209.

Wada, S., Kikura, H. & Aritomi, M., 2006. Pattern recognition and signal processing of ultrasonic echo signal on two-phase flow. *Flow Measurement and Instrumentation*, 17(4), pp.207–224. Available at: http://www.sciencedirect.com/science/article/pii/S0955598605001081.

Whitehouse, J.C. et al., 1991. MEASUREMENT OF TWO-COMPONENT FLOW USING ULTRASONIC FLOWMETERS (U). In *American Society Mechanical Engineers Winter Annual Meeting*. Atlanta, GA.

Wolpert, D.H., 1992. Stacked generalization. *Neural Networks*, 5(2), pp.241–259.

Xie, H. & Wang, Z., 2006. Mean frequency derived via Hilbert-Huang transform

with application to fatigue EMG signal analysis. *Computer methods and programs in biomedicine*, 82(2), pp.114–20. Available at: http://www.sciencedirect.com/science/article/pii/S0169260706000472 [Accessed October 17, 2015].

Xie, T., Ghiaasiaan, S.M. & Karrila, S., 2004. Artificial neural network approach for flow regime classification in gas–liquid–fiber flows based on frequency domain analysis of pressure signals. *Chemical Engineering Science*, 59(11), pp.2241–2251. Available at: http://www.sciencedirect.com/science/article/pii/S0009250904001381.

Xie, T., Ghiaasiaan, S.M. & Karrila, S., 2003. Flow Regime Identification in Gas / Liquid / Pulp Fiber Slurry Flows Based on Pressure Fluctuations Using Artificial Neural Networks. *Industrial and Engineering Chemistry Research*, 42, pp.7017–7024.

Xing, L. et al., 2014. A combination method for metering gas–liquid two-phase flows of low liquid loading applying ultrasonic and Coriolis flowmeters. *Flow Measurement and Instrumentation*, 37, pp.135–143.

Xu, L.A. et al., 1988. The pulsed ultrasonic cross-correlation flowmeter for two-phase flow measurement. *Journal of Physics E: Scientific Instruments*, 21(4), p.406.

Yamanaka, G., Kikura, H. & Aritomi, M., 2002. STUDY ON THE DEVELOPMENT OF NOVEL VELOCITY PROFILE MEASURING METHOD USING ULTRASOUND TIME-DOMAIN CROSS-CORRELATION. In *Papers of the Third International Symposium on Ultrasonic Doppler Methods for Fluid Mechanics and Fluid Engineering Co-organized by EPFL and PSI*.

Yang, W., 2006. Sensors and instrumentation for monitoring and control of multi-phase separation. *Measurement and control*, 39(6), pp.178–184.

Ye, Y., Si-liang, M.W. & Qi, Y., 2008. Detection and estimation of Doppler signal using HHT marginal spectrum. *2008 9th International Conference on Signal Processing*, 1, pp.199–202. Available at: http://ieeexplore.ieee.org/lpdocs/epic03/wrapper.htm?arnumber=4697103.

Zhai, L.-S. et al., 2013. The ultrasonic measurement of high water volume

fraction in dispersed oil-in-water flows. *Chemical Engineering Science*.

Zhao, Y., Bi, Q. & Hu, R., 2013. Recognition and measurement in the flow pattern and void fraction of gas-liquid two-phase flow in vertical upward pipes using the gamma densitometer. *Applied Thermal Engineering*, 60(1-2), pp.398–410. Available at: http://dx.doi.org/10.1016/j.applthermaleng.2013.07.006.

Appendix A

A.1 Instrumentation and data acquisition

Details of the instrumentation and metering system of the air-water rig are shown in Table_Apx 1. The water flow meter is in the supply flow line adjacent to the meeting point of air and water. The gas flow meter connected to the one-inch pipe air flow supply and the meter has a flow range of 6 – 60m^3/hr. Pressure and temperature of the air is measured at the air flow meter so as to determine the actual flow rates of air flow into the rig. The method of the data acquisition is described in section A.1.3.

Table_Apx 1 Equipment used in the horizontal two-phase experimental setup

	Equipment	Range
Air flow rate	Turbine gas flow meter Quadrina (QFG 25B/EP1)	Range: 6~60m^3/hr
Water flow rate	Electromagnetic flow meter Altometer (Altoflux K280/0)	Accuracy: 1% Range: 0-4.524 m^3/hr
Temperature sensors	Tgh: Temperature at the gas inlet (Type T thermocouple wire) Tm: Temperature at the test section (Type T thermocouple wire)	Calibrated range: 0~50°C
Pressures sensors	Pgh: Pressure transducer at the gas inlet (Druck PMP1400) Pm: Pressure transducer at the test section (Druck PMP1400)	Accuracy: 0.15% typical, 0.25% maximum Range: 0~6bar(g)
Water Holdup	Conductance probes Conductivity probes ring A and B	0-5 v
Water flow velocity	Ultrasonic transducer (United Automation Ltd DFM-2)	Frequency: 500kHz 1% repeatability Range 0-20 ft/s
Data	National Instruments DAQ card (NI PCI-	Resolutions: 12bits

	acquisition MIO-16E-4)	Maximum sampling rate (single-channel scanning): 500kS/s

Table_Apx 2 Continued from previous Table_Apx 1

Quantity	Equipment	Specifications
Pulsed wave ultrasonic sensors	1 MHz Panametrics NDT A303S 7.5 MHz	Frequency: 1MHz Nominal element size: 13mm Frequency: 7.5 MHz Nominal element size: 8 mm
Pulser/Receiver	Panametrics-NDT 500 PR (Waltham, MA)	PRF: 500~5000 Pulsers/second Pulse: negative impulse Bandwidth : 25 MHz (Low:-125Vpeak, rise time $7nS$ High: -250Vpeak, rise time $10\,nS$)
PC oscilloscopes	PicoScope 5444B	Up to 1 GS/s real-time sampling Up to 512 MS buffer memory Analogue bandwidth: 50MHz Up to 512 MS buffer memory Resolution: 8 to 16 bits

A.1.1 Electromagnetic flow meter (EM flowmeter)

The electromagnet of the electromagnetic flowmeter was powered by a 220v AC voltage supply from the mains. **Figure 3-1** shows the electromagnetic flowmeter used in this research. It was manufactured by Krohne Altimeter (Alto flux K280/0). It has two pairs of electrodes made of non-corrosion-resistive and non-magnetic material which are installed as flush mounted along the inner wall of the flowmeter. It was fitted in the pipeline with the use of flanges from either end of the flowmeter.

The present electromagnetic flowmeter was installed at a distance of 45 diameters from the water tank and at 360 diameters to the test section which was located at 18m downstream of the EM flowmeter. The water flow rate is

measured before the air and water mixed at the upstream of the test section. The EM flow meter has a range of 0-4.524 m³/ hr. The output signal range of the EM flowmeter was scaled up to the discharge flow range of the water pump for the data acquisition. Current output range of the EM flow meter is 4-20 mA, discharge flow rate 0-12.54 l/s and a 250 Ω resistor was connected at the output leads of the EM flowmeter. The current range was converted into voltage range (1-5v) by using the resistor. So the slope of the EM flowmeter is the ratio of the flow rate span and output voltage span.

$$slope = \frac{maximum\ flowrate - minimum\ flowrate}{maximum\ voltage\ outoput - minimum\ voltage\ ouptut} = \frac{12.54}{4} \ \frac{l}{s}/v$$

Slope = 3.135 l/s/v.

The total flow rate of the EM flow meter, Q, in the data acquisition is given by:

$$Q = 3.135(V - 1) * \frac{3600}{1000} \ m^3/hr$$

where V is the output voltage of the EM flowmeter.

A.1.2 Conductivity probes

The conductivity probes used for the measurement of the liquid holdup in the two-phase flow are based on the impedance method. This principle has been applied for continuous monitoring of the liquid holdup in both experimental and industrial settings. Details of the techniques have been described by Andreussi et al. (1988) and Fossa et al. (2003). In the present study, the conductance probes are a pair of non-intrusive probes, ring electrodes fitted into the flow pipe in a flush mounted setup. The liquid holdup of the water can be measured with the probe in the resistance term of the impedance (Andreussi et al., 1988).

The conductance probes were set to give a voltage high reading of (5V) for full pipe area and a low level voltage (0V) for the empty pipe section between the electrodes. The relationship between the voltage output and volume of water in the pipe is non-linear and requires a static calibration (Andreussi et al., 1988). Figure A-1 shows the setup of the two ring-type conductance probes, spaced at a distance of 186.5mm, used for liquid holdup measurement. These probes' electrodes operated with a sinusoidal voltage of ±400mV at frequencies of 7 and 13kHz respectively.
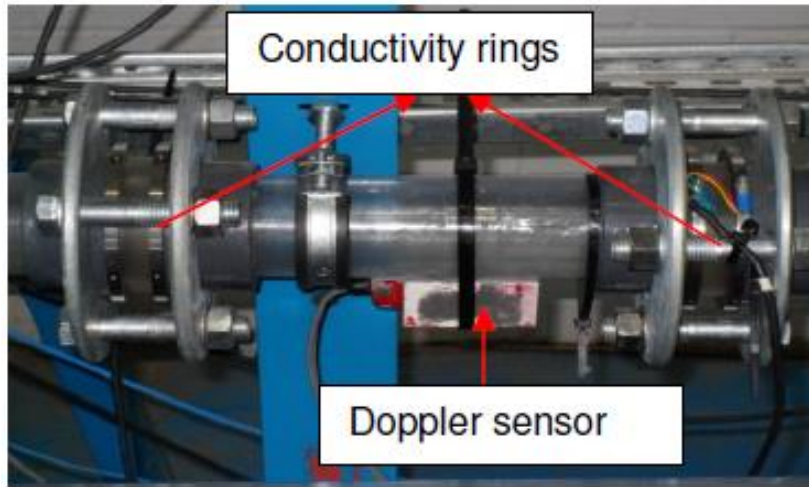
Figure A-1 Setup of conductivity probes and ultrasound Doppler flowmeter's sensor

The probes were first calibrated for the holdup measurement by serially introducing known volumes of water into a horizontally placed section of the pipework, which contains the conductance probes. Every volume of water introduced into the short test section and the corresponding voltage reading resulting from the electrical impedance of the volume of water was recorded. The normalised liquid holdup was calculated using equations **(3-1)** and normalised voltage was calculated using equation **(3-2)**

$$Normalised\ Holdup = \frac{volume\ of\ water\ poured\ into\ the\ pipe}{volume\ of\ full\ pipe\ section} \quad \textbf{(3-1)}$$

$$Normalised\ voltage \quad \textbf{(3-2)}$$
$$= \frac{Voltage\ readings\ for\ volume\ of\ water\ in\ the\ pipe\ section}{voltage\ reading\ of\ full\ pipe\ section}$$

Figure A-2 Shows the calibration curve for the normalised hold-up and normalised voltages with 1 being a full pipe and 0 equals an empty pipe.
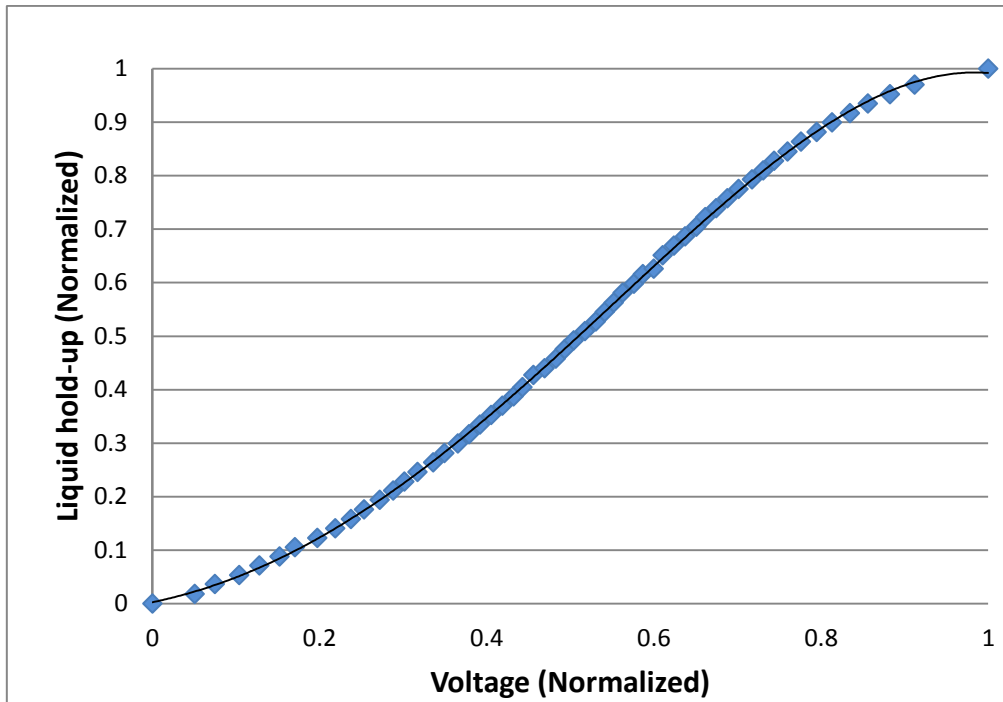
Figure A-2 shows the calibration curve for the normalised hold-up and normalised voltages with 1 being a full pipe and 0 equals empty pipe. The calibration curve was obtained by means of the methods described in detail (Andreussi et al., 1988; Fan and Yan, 2014; Fossa, 1998).

A.1.3 Test matrix of the horizontal test experiments

Table_Apx 3 shows the test matrix which covers the volumetric air flow rate from 3.5m^3/h to 12m^3/h and volumetric water flow rate from 0.4m^3/h to 8.5m^3/h. Over 77 tests were performed which covered four flow regimes in the horizontal pipeline. All stated superficial gas velocities are at standard conditions (1 bar, average of 22°C). The experimental test matrix values are generated by fixing a value of the superficial water velocity and varying instep the gas superficial velocities by using the gas flow control valve of the rig.

Table_Apx 3 Air-water horizontal flow test matrix

Air-water flow	Q_W (m³/h)	0.35	0.49	6.36	0.78	0.92	1.06	2.83	3.53	4.95	7.07	8.48
	V_{LG} (m/s)	0.05	0.07	0.9	0.11	0.13	0.15	0.4	0.5	0.7	1	1.2
Q_G (m³/h)	V_{SG} (m/s)	√	√	√	√	√	√	√	√	√	√	√
3.53	0.5	√	√	√	√	√	√	√	√	√	√	√
4.95	0.7	√	√	√	√	√	√	√	√	√	√	√
6.36	0.9	√	√	√	√	√	√	√	√	√	√	√
7.78	1.1	√	√	√	√	√	√	√	√	√	√	√
9.19	1.3	√	√	√	√	√	√	√	√	√	√	√
10.60	1.5	√	√	√	√	√	√	√	√	√	√	√
12.02	1.7	√	√	√	√	√	√	√	√	√	√	√

A.1.4 Data acquisition systems

The data acquisition of the air-water flow measurement using the ultrasonic Doppler flowmeter was conducted using the instrumentation on the rig and the LabVIEW data acquisition card system installed on the PC running Windows 7. Each of these instruments is connected to the PC via the data acquisition–Card. However, the pulse echo ultrasound sensor signals of the flow were acquired using the PicoScope (PC-based oscilloscope). The PicoScope was used for receiving the ultrasound signal of the two-phase flow from the Pulser/receiver

which is used in sending and receiving signal from the ultrasonic pulse echo transducer. The measurement data for both sensors were collated for the appropriate test points.

A.1.5 LabVIEW DAQ system

Data collection on the air-water horizontal rig comprises all the instruments on the rig except that of the pulse echo ultrasound which was collected using a LabVIEW program written exclusively for the data acquisition. The data acquisition system comprises the sensors, signal condition units for each sensor, Rack-Mounted Terminal/Connector Block (NI BNC 2090), analogue to digital converter (ADC), LabVIEW program and a PC. The signal conditioning unit receives analogue voltage from the instruments and then smooths and stabilises into DC voltages equivalent to the measured variable. Different sensors have different signal conditioning units. The ADC is based on the data acquisition card (NI PCI-MIO-16E-4) and LabVIEW program (version 10). The rack-mounted terminal connector interfaces the BNC connectors of each signal conditioning units' physical channel with the ADC unit. Table_Apx 4 shows the physical channels on the rack terminal used for each instrument.

The data acquisition output then processes the corresponding digital signal of each of the instruments according to the prior calibration, in the correct engineering units, of the quantity measured. The LabVIEW program, running on the PC running Windows 7, samples the data from the instruments at 10kHz for 20 seconds, which displays the engineering unit values, and stores the raw data for further processing. The raw data voltage signals are converted into engineering units of the corresponding instruments in the LabVIEW program using equation **(8-3)**

$$MV_{EU} = K(V - V_0) \qquad\qquad \textbf{(8-3)}$$

where:

$MV_{EU} =$ The measured quantity in engineering units

$K =$ The gain of the instrument (obtained from the calibration chart)

$V =$ The signal output of the instrument

$V_0 =$ The signal output of the instrument at zero input

Table_Apx 4 Data acquisition channels for the LabVIEW program

Instrument	Description	Signal range (v)	Physical channel
Cond 1	Conductance probe 1	0-10	Dev1/ai0
Cond 2	Conductance probe 2	0-10	Dev1/ai1
EM	EM flowmeter output signal	0-5	Dev1/ai6
Pgh	PMP 1400 2.5 bar(a)	0-5	Dev1/ai7
Pm	PMP 1400 2.5 bar(g)	0-5	Dev1/ai8
Tgh	Type T thermocouple	0-5	Dev1/ai9
Tm	Type T thermocouple	0-5	Dev1/ai10
Ultrasound	Ultrasound Doppler signal	-5-5	Dev1/ai2
Um	Ultrasound flowmeter output signal	-5-5	Dev1/ai4
Vgas	Turbine gas flowmeter output signal	0-5	Dev1/ai5

Appendix B Air-water-oil 3-phase flow experiments

A second set of experiments were conducted in the three phase test rig; the rig has two loops of different pipe diameters of 52mm and 102mm pipelines. The 52mm diameter was the pipeline used for conducting this study. Figure B-1 shows a schematic diagram of the three phase rig. The rig is a high capacity automated control test facility and has four main sections: the fluid supply and measurement, test area, the three separation and the valves' manifolds. The pipeline of the rig is made up of NB schedule 10 stainless steel. It has a total length of 50.5m which consists of a 40m horizontal line connected to a 10.5m high riser.
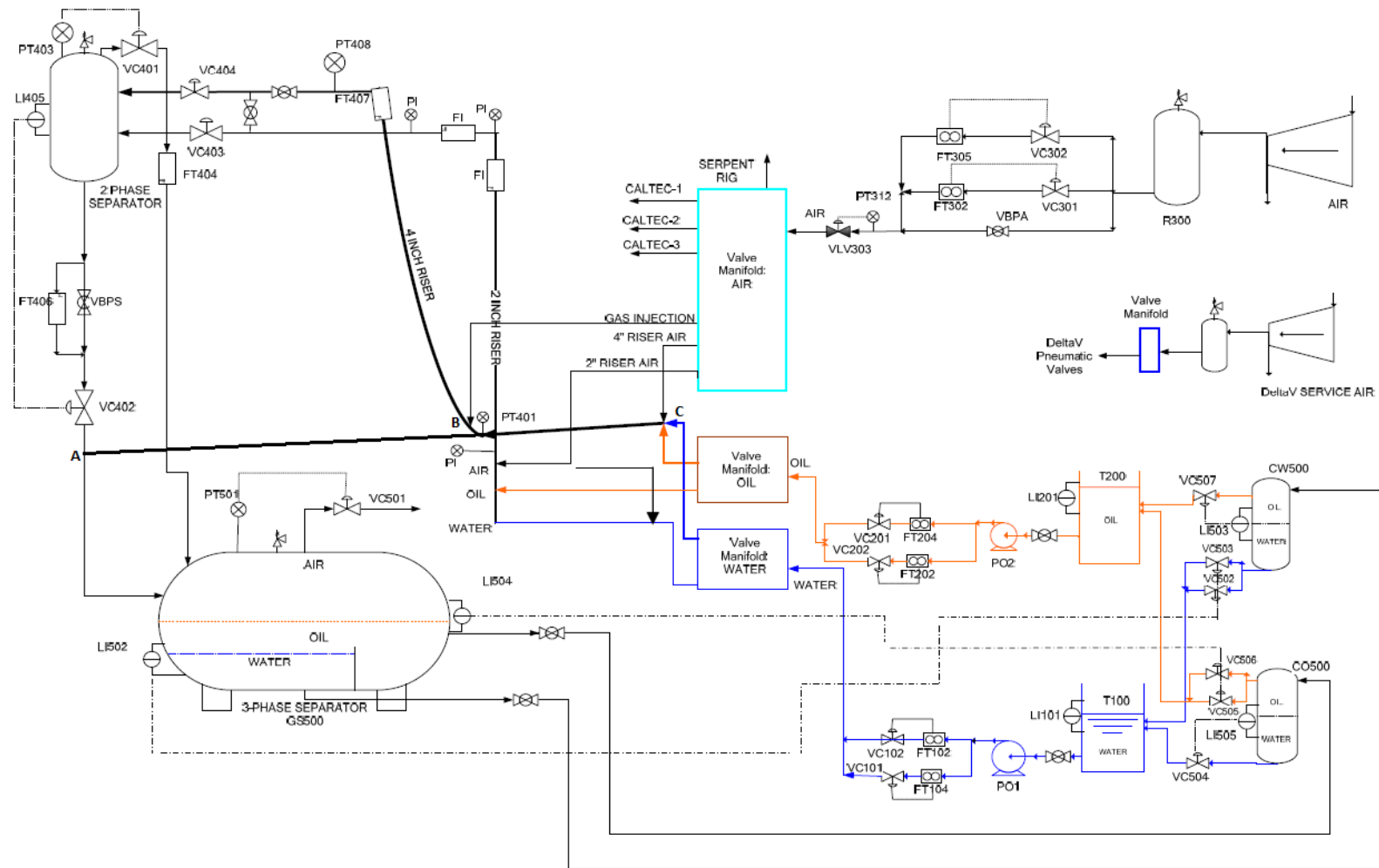
Figure B-1 Three-phase flow rig diagram

B.1.1 Experimental fluids

The fluids supplied into the rig are gas (air) and liquids (oil and water). The air supply into the rig is from two identical compressors (Atlas Copco Elektronikon GA75 compressors C01 and C02) which are connected in parallel. The compressors have a combined maximum capacity of air flow rate of $1410m^3/h$ at 7 bar (g). The air flow from the compressors is fed into a receiver tank of $2.4m^3$ capacity which serves as a buffer between the rig and compressors. The buffer tank is required to prevent fluctuation of the air supply flow. The air from the receiver tank is measured by two Mass ProBar flowmeters and then passes through a bank of air filters before being supplied to the rig. The bank of air filters is for air treatment which removes impurities and dirt, and also regulates the air temperature. Air flow to the rig is measured using automated control valves located at the upstream of the Mass ProBar flowmeters. The automated control valves are managed using process systems management software (Delta V Emerson process management). Metering of the air flow into the rig is done with two Rosemount Mass flowmeters, one for lower flow rates (0-$120Sm^3/h$) and the other for higher flow rates (120-$4250Sm^3/h$) and regulation of the air flow rates into the rig is carried using the DeltaV (Blaney, n.d.; Brini Ahmed, 2014).

Figure B-2 Air supply filtering and metering system of the three phase rig

B.1.2 Liquid flow supply

Water is supplied into the rig from a reservoir tank with $12.5m^3$ capacity (T100) and the oil is supplied from a reservoir tank with $12.5m^3$ capacity (T200).

Similarly, water and oil are both pumped into the flow loop by using two identical multistage Grundfos CR90-5 pumps (P01 and P02 respectively). Each of the pumps has a capacity of 100m^3/h at 10 bar (g). Oil is dielectric oil (Rustlick EDM-250). The oil is non-hazardous with a density of 815kg/m^3 and a viscosity of about 7.2mPa at 21^{0}C.

In addition, the measurement of the liquid flow rates of both oil and water is metered in two categories. The water flow rate is metered with a Rosemount 8742 Magnetic flowmeter in the lower flow rate range (0-1kg/s) and in the higher flow rate, a Foxboro CFT50 Coriolis meter with a range of (up to) 10kg/s. Similarly, the oil flow rate is also metered in two ranges: the lower flow rate is with a Micro Motion Mass flow meter (0-1kg/s) and the higher oil flow rate is by using a Foxboro CFT50 Coriolis meter with a range of (up to 10kg/s).
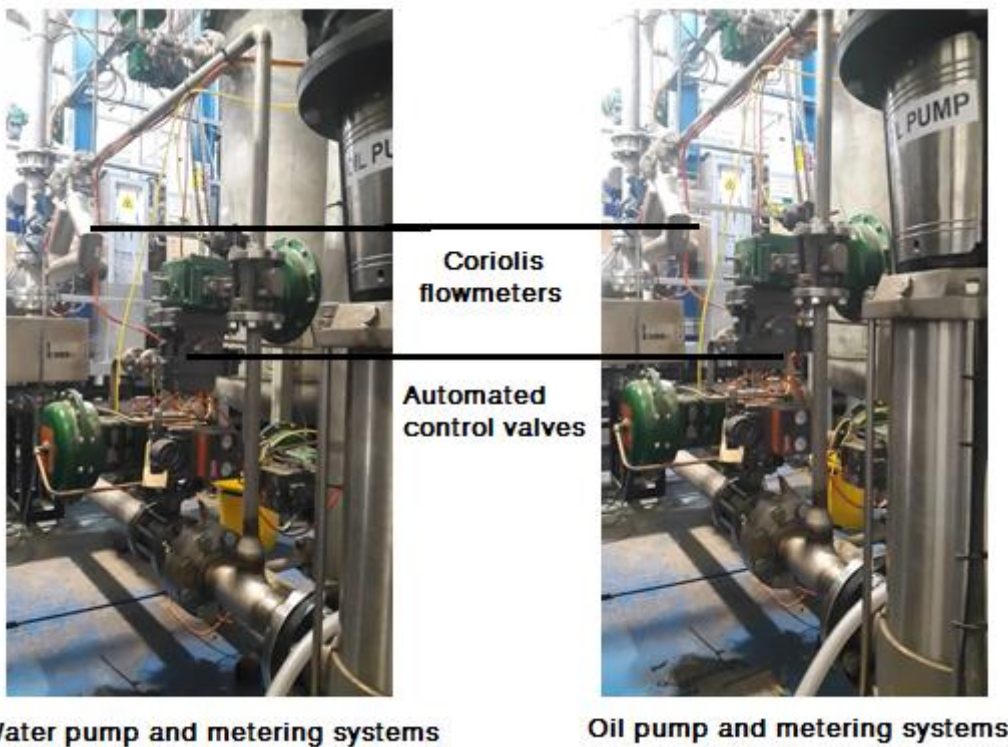

Water pump and metering systems   Oil pump and metering systems

Figure B-3 Oil flow pump and water flow pump photos

B.2 Three-phase rig instrumentation and data acquisition

The rig has instrumentations provided for the measurement of fluid pressure, differential pressure, fluid temperature, water flow and gas flow, and a single beam gamma densitometer was used for each of the flows.

B.2.1 Vertical flow test section
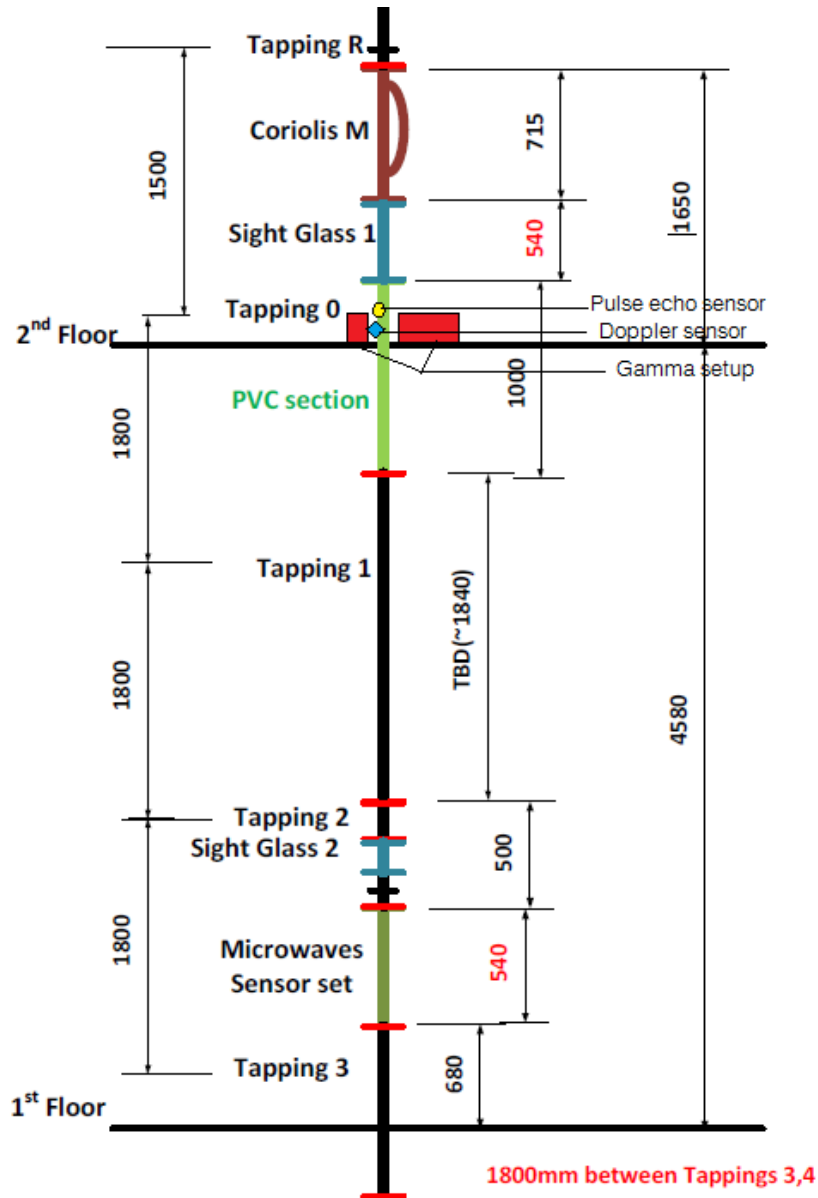
B.2.2 Pressure transducers

Four flush mounted pressure transducers are installed along the riser pipeline section of the rig. A pressure transducer is installed at the test section to facilitate estimation of the real time gas flow rate of the test section. The pressure transducers are all Druck PMP 1400 0-2.5 bar (g), with an accuracy of

+/-5%. Each of these transducers is individually pre-calibrated and the output of the pressure transducers' calibration shows a linear relation between the pressure and voltage output of the transducer. In addition to the pressure transducer at the test, the other three transducers are installed and spaced along the riser pipeline at positions of 5.4m, 3.6m and 1.8m from the riser base. The measurements from the pressure transducers are included in the LabVIEW data acquisition system.

B.2.3 Coriolis flow meter

A Coriolis mass flowmeter (Endress and Hauser Promass 83F) is installed at the top of the riser 8.03m from the riser base. The Coriolis meter is used for measuring the fluid density. The output of the Coriolis is also included in the data acquisition of the reference instrumentation LabVIEW program. The measurement principle of the Coriolis mass flow meter is that the vibrating tubes, which are in line with the flow direction, vibrate in response to the flow. The vibration of the tube is managed by an electronic system. The density of the flow is calculated from the frequency of the vibration of the tubes while the flow rate is calculated from the phase difference in the vibration of the opposite tubes of the Coriolis meter. The Coriolis meter can be as accurate in it smeasurement as 0.2% (Manus, 2001).

B.2.4 Gamma densitometer

This is a commercial available single beam gamma densitometer (Neftemer Flowmeter Ltd) for multiphase flow measurement. It was installed at 8.0m above the riser base of the 2-inch line of the three phase facility. The measurement of the flow is across the test section of the riser. The gamma densitometer uses a Caesium isotope ($^{137}C_s$) with radioactivity of a half-life of 30.1 years which is the most frequently used gamma source for conventional gamma-ray densitometers (Kumara et al., 2010). The half-life span is long enough for the practical application of the meter. The instrument has an in-built, microprocessor based, self-calibration that stabilises the pulse count in the event of losses. Therefore, it does not need continuous recalibration (Fischer,

1994). The absorption of a narrowed or collimated beam of the gamma, of initial intensity I_0 (Photon/m$^{2\text{-sec}}$), is given in equation **(1-4)**.

The method of measurement of the two-phase flow with gamma starts with the calibration of the densitometer by first determining the gamma count rates for single phase water flow and air only in the pipe for every test series (for instance I_L and I_G, respectively, for the liquid and gas phases in a gas-liquid two-phase flow). This is to ensure that the densities of the respective flows are recorded for calibration and for the determination of the volume fractions according to equation **(1-4)** (Falcone et al., 2009; Fischer, 1994).

$$I = I_0 exp^{(-\mu z)} \qquad\qquad \textbf{(1-4)}$$

where $-\mu$ is the linear absorption coefficient; z the distance travelled through the absorbing medium, the intensity I of the gamma beam received at the detector.

The gamma densitometer comprises a gamma source and its lead-filled stainless steel casing, which prevents the gamma radiation from escaping to the surroundings, a collimator that narrows and focuses the beam of the gamma source, and the gamma detection unit. The source and detector are arranged diametrically opposite to each other and this allows the densitometer to be used in measuring the average flow parameters to be measured across the whole pipe diameter (Kumara et al., 2010). The detector unit consists of scintillation crystals, photomultiplier tube and electronic circuit for amplification of the signal from the photomultiplier.
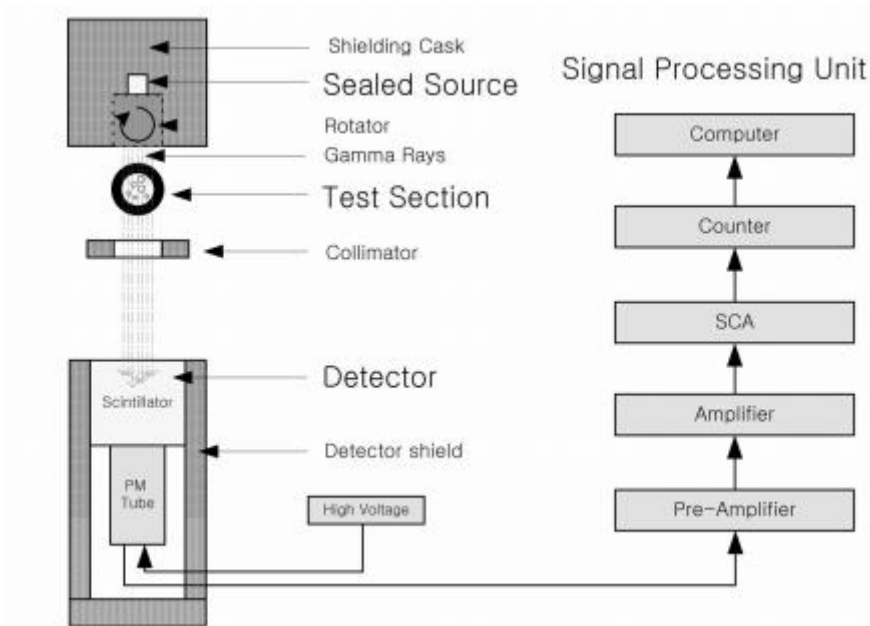
Figure B-4 Schematic diagram of a single-beam gamma densitometer (Park and Chung, 2007)

The gamma densitometer system comprises an encased Caesium-137 source, a scintillator and data processing unit. The Caesium source is in a cylindrical lead-filled shielding cask with an open and close source window shutter handle. A lead collimator or beam narrower is used to direct the gamma source beam and the scintillator. Figure B-5 shows the gamma densitometer setup installed on a vertical pipeline. The data processing unit performs the pulse counting from the scintillator and it consists of a pre-amplifier, amplifier, a PLC controller and Neftemer flowmeter software. The gamma densitometer was designed as a clamp-on flowmeter and it is controlled by the Neftemer flowmeter software at a sampling frequency of 250Hz.

The single beam gamma densitometer systems have two advantages over multi-beam systems (Chan, 1990): 1) the source strength is lower and this helps in reducing the shielding requirement and thus, a single beam gamma densitometer is portable and flexible. 2) With the single beam systems, data interpretation is simpler and straightforward. This allows for application of the densitometer for objective flow regime identification.
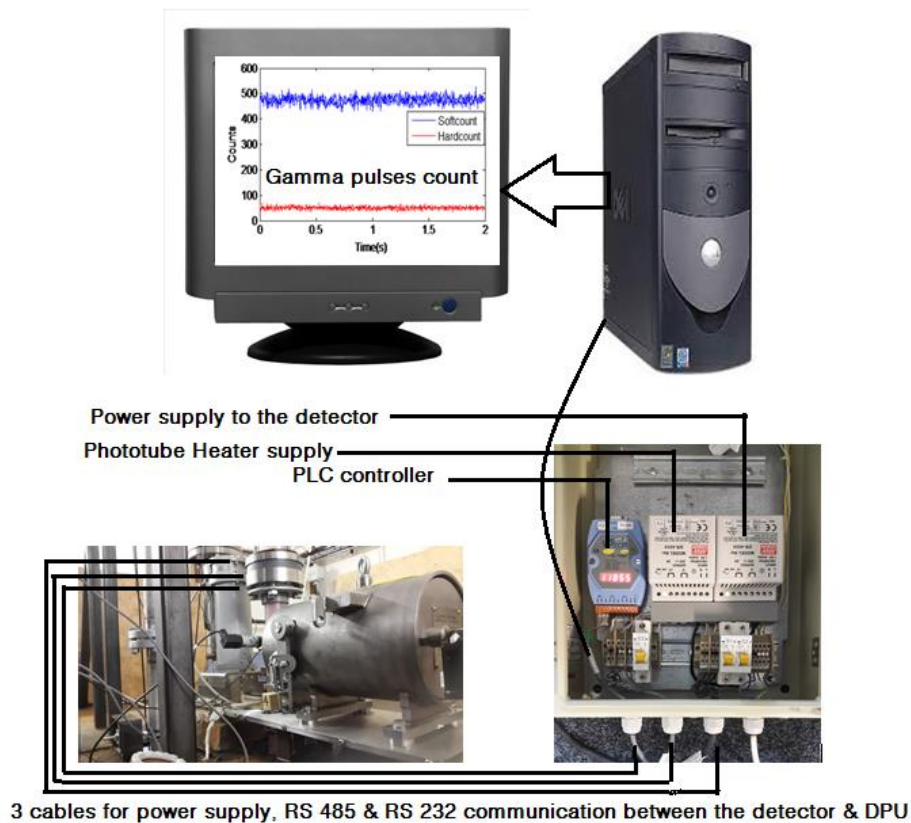
Figure B-5 Pictorial diagram of the gamma densitometer setup

B.2.5 PC with Delta V

A process management software has been developed by Emerson Process Systems (Delta V) for the automated monitoring of gas and liquid inlet flow conditions, including flow rates, static pressures, temperature, density, reservoirs and tanks' liquid levels. Delta V enables us to set the input water, and gas and oil flow rates, and operates the appropriate pumps and valves. The sensor signals from these process parameters are transmitted into the Delta V via Profibus and Fieldbus signal transmission systems. Process parameters transmission and recording with the Delta V is at a frequency of 1Hz and process operations history are also recorded for future reference. The controllers of the Delta V can be used to set the flow rates of both gas and liquid by inputting the desired flow rates in the Graphical User Interface of the metering area of the Delta V. A detailed description of the three phase rig and Delta V were previously presented by Yeung and Lao (2013).

B.2.6 PC with LabVIEW for reference instrumentation

A PC running Windows XP professional was used for controlling the instrumentation used for the reference measurement of flow, pressure, density and temperature. Signals from the instruments are acquired using the LabVIEW program written to perform controlled data acquisition systems. The instruments: Coriolis mass flowmeters, temperature transducers and pressure transducers, are distributed along the test line of the rig. The output voltages from the instruments are acquired using National Instruments E-series card PCI-MIO-16E-4 data acquisition (DAQ) board. The DAQ board was connected to the instruments via National Instruments BNC-2090 connector and then controlled with the LabVIEW program. The LabVIEW program comprises three features for DAQ, viewing and saving on the disk storage device. The stored information was originally read from the channel of the DAQ kit as output voltages and then converted into their respective engineering values based on the calibration result of each instrument. The data were stored as a text file. The recording and saving of the data in this experiment was done with 100Hz scan rate, 100Hz sampling rate and five minutes test duration.

B.2.7 PC with Neftemer Flowmeter Software

Gamma densitometer pulse count rates of the flows were collected using the Neftemer DAQ and time series pulse count rates visualisation with the software 'Chastotomer' installed in a PC. The Chastotomer communicates with the controller in the data processing unit (DPU) of the gamma system. The key part of the gamma densitometer DPU is the programmable logic controller (PLC) ICP 1-7188D which processes the gamma count rates at the rate of 250Hz, communicates with the gamma detector via an RS-485 and transmits to the PC also through an RS-232 serial port. The Chastotomer was used for facilitating the pulses count rate display and saving in the form of two counts of Hard count and Soft count in "dat" filing systems. Figure B-6 illustrates the flow information between the gamma source and the controller of the DPU. The saved gamma pulses count rates taken from the flow processes are exported into the MATLAB environment for offline processing.
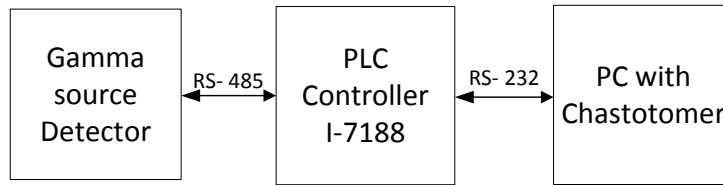
Figure B-6 Schematic diagram of the Neftemer flowmeter

B.2.8 PC with Ultrasonic sensors

Using a 0.5-MHz CW Doppler system (DMF-2 UAL), the Doppler signals from the two-phase signal of the vertical test rig were recorded for approximately 20s (enough time for the flow regime profile to pass through the test section). The recordings sampled the frequency at 10kHz digitized using a 12-bit ADC (National instruments E-series card PCI-MIO-16E-4 data acquisition board) and were stored on a hard disk of a PC running Windows 7. The range of the Doppler flowmeter was to 0-6m/s (0-20ft/s). Also a pulse echo ultrasound transducer was used to characterise the two-phase flow in the pipe. The ultrasound sensors were attached axially and five centimetres apart to the outside of the pipe in the test section. The ultrasonic Doppler flowmeter signal was acquired with a LabVIEW program, while the ultrasound pulse echo signal was acquired using PC-based oscilloscope, namely a PicoScope.